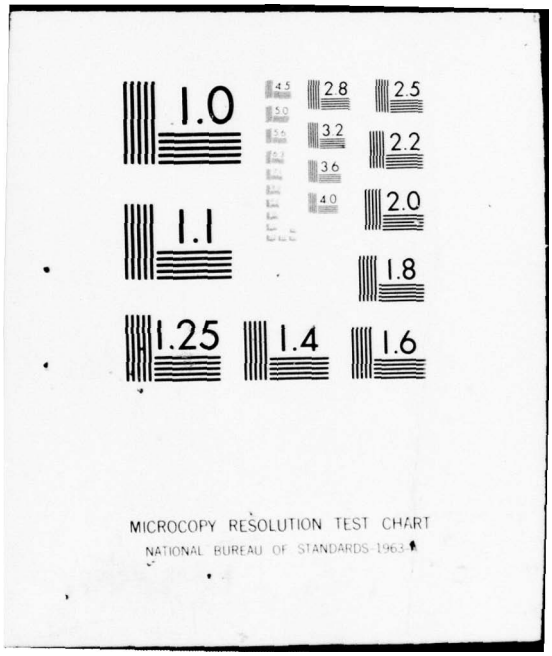
AD-A052 141 NOTTINGHAM UNIV (ENGLAND) DEPT OF INORGANIC CHEMISTRY F/G 7/2
HDA CORROSION CHEMISTRY.(U)
DEC 77 C C ADDISON, N LOGAN AFOSR-74-2709

UNCLASSIFIED AFRPL-TR-77-65 NL

1 OF 4
AD
A052141




1.0
1.1
1.25
1.4
1.6
1.8
2.0
2.2
2.5
2.8
3.2
3.6
4.0
4.5
5.0
5.6
MICROCOPY RESOLUTION TEST CHART
NATIONAL BUREAU OF STANDARDS-1963-A

AFRPL-TR-77-65 AFOSR-74-2709

HDA CORROSION CHEMISTRY FINAL SCIENTIFIC REPORT, 1 MAY 1974 - 30 APRIL 1976

AD A052141

THE UNIVERSITY OF NOTTINGHAM
DEPARTMENT OF INORGANIC CHEMISTRY
UNIVERSITY PARK, NOTTINGHAM, ENGLAND NG7 2RD

AUTHOR: CYRIL CLIFFORD ADDISON
NORMAN LOGAN

DDC RECEIVED APR 3 1978 F

DECEMBER 1977

DDC FILE COPY

APPROVED FOR PUBLIC RELEASE;
DISTRIBUTION UNLIMITED

PREPARED FOR:
EUROPEAN OFFICE OF AEROSPACE RESEARCH & DEVELOPMENT
LONDON, ENGLAND

AIR FORCE ROCKET PROPULSION LABORATORY
DIRECTOR OF SCIENCE AND TECHNOLOGY
AIR FORCE SYSTEMS COMMAND
EDWARDS AFB, CALIFORNIA 93523

NOTICES

When U. S. Government drawings, specifications, or other data are used for any purpose than a definitely related government procurement operation, the Government thereby incurs no responsibility nor any obligation whatsoever, and the fact that the Government may have formulated, furnished, or in any way supplied the said drawings, specifications or other data, is not to be regarded by implication or otherwise, or in any manner licensing the holder or any other person or corporation, or conveying any rights or permission to manufacture, use or sell any patented invention that may in any way be related thereto.

FOREWORD

This report covers work sponsored by the Air Force Rocket Propulsion Laboratory, Edwards Air Force Base, California under AFOSR Grant 74-2709. The period of performance was 1 May 1974 through 30 April 1976. During this period, Lt. S. G. Wax (LKDP), Lt. E. Bishop (LKDP), and Lt. R. G. Butts (LKDP), in turn, provided technical direction and administrative functions for AFRPL.

The work was performed by the Department of Inorganic Chemistry, The University of Nottingham, England. Professor Cyril C. Addison was the principal investigator, and Norman Logan was the joint research supervisor.

This report has been reviewed by the Information Office/XOJ and is releasable to the National Technical Information Service (NTIS). At NTIS it will be available to the general public, including foreign nations. The report has been reviewed and is approved for publication.

Rodney G. Butts

Rodney G. Butts, 1st Lt., USAF
Project Manager

Forrest S. Forbes

Forrest S. Forbes, Chief
Propellants Section

FOR THE COMMANDER

Edward E. Stein

Edward E. Stein, Deputy Chief
Liquid Rocket Division

UNCLASSIFIED

SECURITY CLASSIFICATION OF THIS PAGE *(When Data Entered)*

REPORT DOCUMENTATION PAGE	READ INSTRUCTIONS BEFORE COMPLETING FORM
1. REPORT NUMBER: AFRPL-TR-77-65	2. GOVT ACCESSION NO. / 3. RECIPIENT'S CATALOG NUMBER
4. TITLE *(and Subtitle)*: HDA CORROSION CHEMISTRY.	5. TYPE OF REPORT & PERIOD COVERED: Final Scientific Report. 1 May 1974 - 30 April 1976.
	6. PERFORMING ORG. REPORT NUMBER: AFOSR-74-2709
7. AUTHOR(s): Author: Cyril Clifford Addison, Norman Logan	8. CONTRACT OR GRANT NUMBER(s): AFOSR-74-2709B
9. PERFORMING ORGANIZATION NAME AND ADDRESS: Department of Inorganic Chemistry, University of Nottingham, University Park, Nottingham NG7 2RD, U.K.	10. PROGRAM ELEMENT, PROJECT, TASK AREA & WORK UNIT NUMBERS: 62302F, 623058 RC/CC 621000
11. CONTROLLING OFFICE NAME AND ADDRESS: Air Force Rocket Propulsion Laboratory/LK, Edwards AFB, California 93523	12. REPORT DATE: December 1977
	13. NUMBER OF PAGES: 364
14. MONITORING AGENCY NAME & ADDRESS *(if different from Controlling Office)*: EOARD, Box 14, FPO New York 09510	15. SECURITY CLASS. *(of this report)*: UNCLASSIFIED
	15a. DECLASSIFICATION/DOWNGRADING SCHEDULE

16. DISTRIBUTION STATEMENT *(of this Report)*

APPROVED FOR PUBLIC RELEASE; DISTRIBUTION UNLIMITED

17. DISTRIBUTION STATEMENT *(of the abstract entered in Block 20, if different from Report)*

DDC RECEIVED APR 3 1978 F

18. SUPPLEMENTARY NOTES

19. KEY WORDS *(Continue on reverse side if necessary and identify by block number)*

HDA Corrosion products
Metal corrosion rates

20. ABSTRACT *(Continue on reverse side if necessary and identify by block number)*

An experimental procedure for the detection of phase separation in HNO_3 - N_2O_4 mixtures by electrical conductivity measurements has been developed. This method has also been used to investigate the influence of $Fe(NO_3)_3 \cdot 1.5N_2O_4$ and KNO_3 on the two-phase boundary of the HNO_3 - N_2O_4 phase diagram in the acid-rich region. The two-phase boundary is not greatly influenced by these additives.

DD FORM 1 JAN 73 1473 EDITION OF 1 NOV 65 IS OBSOLETE

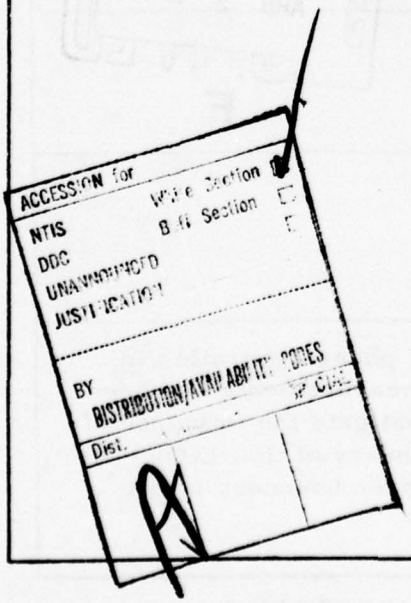
UNCLASSIFIED

SECURITY CLASSIFICATION OF THIS PAGE *(When Data Entered)*

406860

The corrosion products produced by reaction of iron, chromium, nickel, 321 stainless steel, and aluminium with HDA have been identified. They consist essentially of metal nitrate hydrates. The chemistry of these products has been investigated in depth, including a study of their reactions with HF in HDA solution. The rates of corrosion of 321 stainless steel by various HNO_3/N_2O_4 mixtures have been measured, and correlated with the solubility of the corrosion products.

Rates of corrosion of 321 steel in uninhibited, standard and modified HDA are in the approximate ratio 600:6:1. In the presence of HF, the rate increases with N_2O_4 content. Oxygen, fluorine and phosphorus (but not nitrogen) have been identified, by electron spectroscopy, of the steel surface after immersion. Corrosion products formed by iron, chromium, and aluminium in modified HDA consist of complex fluoride-phosphates, but nickel nitrate hydrate in HDA does not react with PF_5. All experiments indicate that the major factor controlling corrosion rates is the solubility of corrosion products in HDA.



FINAL SCIENTIFIC REPORT

TABLE OF CONTENTS

Section		Page
1.	INTRODUCTION	3
2.	THE HNO_3 - N_2O_4 PHASE SYSTEM	4
2.1	Electrical conductivity measurements	4
2.2	Experimental procedure	6
2.3	Additives	8
2.4	References	11
3.	CORROSION STUDIES WITH UNINHIBITED HDA	12
3.1	Preliminary Experiments	12
3.2	The effect of N_2O_4 concentration and temperature on corrosion rate	19
3.3	Factors related to corrosion rates	27
3.4	Conclusions	37
3.5	References	39
4.	CORROSION RATES IN INHIBITED HNO_3 - N_2O_4 MIXTURES	40
4.1	Introduction	40
4.2	Corrosion using polypropylene containers	40
4.3	Corrosion experiments using Teflon containers	47
4.4	Spectroscopic studies of steel surfaces exposed to inhibited HDA	56
4.5	Discussion	67
4.6	References	73
5.	CORROSION PRODUCTS OF STEELS WITH 100% HNO_3 AND HDA	74
5.1	Introduction	74
5.2	The reaction of 321 stainless steel with 100% HNO_3 and HDA	76
5.3	The reaction of mild steel and iron with 100% HNO_3 and HDA	78
5.4	The reaction of nickel with HDA	126
5.5	The reaction of chromium and hexacarbonylchromium (0) with HDA	146
5.6	References	159
6.	CORROSION PRODUCTS OF ALUMINIUM WITH 100% HNO_3 AND HDA	160
6.1	The reaction of metallic aluminium with 100% HNO_3 and HDA	160
6.2	Some properties of $Al(NO_3)_3 \cdot 6H_2O$	169
6.3	The solubility of $Al(NO_3)_3 \cdot 6H_2O$ in HNO_3/N_2O_4 mixtures	180

TABLE OF CONTENTS (Cont'd)

Section		Page
6.4	Reactions of aluminium nitrate tetra- and hexa-hydrates with N_2O_4 and HDA	185
6.5	The reaction of $AlCl_3$ with HDA	186
6.6	Single crystal X-ray investigation of the Al/HDA solid product	188
6.7	References	194
7.	REACTIONS OF HF WITH METAL CORROSION PRODUCTS IN HDA AND RELATED STUDIES	195
7.1	Introduction	195
7.2	Reaction of HF with Fe/HDA corrosion products	195
7.3	Reaction of $FeF_3 \cdot 2H_2O$ with HNO_3/N_2O_4 mixtures	198
7.4	The reaction of HF with Chromium/HDA corrosion products	199
7.5	The reaction of HF with Nickel/HDA corrosion products	205
7.6	The reaction of Al/HDA corrosion products with HF	208
7.7	References	219
8.	SOME CHEMISTRY OF PHOSPHORUS PENTAFLUORIDE IN HNO_3 AND HDA	220
8.1	Preparation and manipulation of phosphorus pentafluoride	222
8.2	The reaction of phrosphorus pentafluoride with 100% HNO_3 and HDA	225
8.3	Reactions of orthophosphoric acid with metal nitrate hydrates and metals in HDA	243
8.4	Reactions of phosphorus pentafluoride with metal nitrate hydrates and metals in HDA	255
8.5	References	277
9.	THE EFFECT OF PF_5 IN INCREASING THE CORROSION RATE OF MILD STEEL IN HDA	278
APPENDIX A	Concentration Data From Corrosion Studies with Uninhibited HDA	A-286
APPENDIX B	Experimental Techniques	B-341
	References	B-356
Nomenclature		357

1. INTRODUCTION

The Agena propulsion system has been in operation since 1957. To date, several engine modifications and propellant changes, including a change from IRFNA (Inhibited Red Fuming Nitric Acid) to HDA (High Density IRFNA). HF (Hydrogen Fluoride) is added to both of these oxidizers as a corrosion inhibitor.

Despite the pressence of HF as an inhibitor, HDA is highly corrosive and a significant amount of corrosion products are associated with it. This results in a large pressure drop as the materials build up on the feed system filters. In addition, the finer corrosion products which pass through the filter begin to deposit in the small orifices of the system. Unfortunately, preliminary filtration appears to be only a partial solution. There is evidence to suggest that the gelatinous material which escapes filtration is saturated with soluble corrosion products. Thus only the precipitated excess is filtered. A change in state between the gelatinous and crystaline material has also been observed. Little else is known about the chemistry, solubility, or conglomeration of the corrosion materials found in HDA. To insure the future reliability of HDA as an oxidizer, and to determine the effect of the fluoride ion (present in the corrosion inhibitors of HDA) on the chemistry of the corrosion products of HDA, this program (AFOSR Grant 2709, "HDA Corrosion Chemistry") was initiated by the Air Force Rocket Propulsion Laboratory.

The initial emphasis of the work was focussed toward a) a phase study of N_2O_4 - HNO_3 mixtures, and b) an investigation of the corrosion products of HDA. As the work developed, emphasis was increasingly directed toward the identification and control of corrosion products.

2. THE HNO_3 - N_2O_4 PHASE SYSTEM

The work on this system involved a quantitative study of the influence of dissolved corrosion products from 347 stainless steel or 6061 aluminium on the phase separation in High Density Acid (HDA), containing 52.7 - 57.4 wt% HNO_3 and 44 ± 2 wt% N_2O_4. The presence of two liquid phases could be responsible for flow irregularities, particularly if one of these phases is of high viscosity as a result of a high concentration of dissolved corrosion product. For any given amount of corrosion product in solution, it is important to determine the exact liquid composition at which a second phase appears. Preliminary work was therefore carried out to determine the best method for detection of phase separation in HNO_3 - N_2O_4 mixtures. Of the various approaches tried, changes in electrical conductivity was found to provide a sensitive and accurate method (section 2.1).

In an earlier contract (F61052-70-C-0035) on N_2O_4 flow decay, the corrosion product responsible for flow decay in steel systems, the compound $Fe(NO_3)_3 \cdot 1.5N_2O_4$, was found to be virtually insoluble in N_2O_4 but highly soluble in HNO_3. It appeared to have a profound effect on the miscibility of HNO_3 with N_2O_4, particularly on the N_2O_4 - rich side of the phase diagram[1]. In anticipation that this or closely related compounds will result from the corrosion of steel by HDA, a quantitative investigation of phase separation from HNO_3 - rich mixtures in the presence of $Fe(NO_3)_3 \cdot 1.5N_2O_4$ was performed using the electrical conductivity technique. In order to compare the influence of a simple ionic nitrate, some parallel investigations with KNO_3 were also carried out.

2.1 Electrical conductivity measurements

The HNO_3 - N_2O_4 phase diagram was investigated using the conductivity cell and burette unit illustrated in Figure 2-1.

When phase separation occurs at a fixed temperature in a system of two partially miscible liquid components (e.g. $HNO_3 + N_2O_4$)[2], the composition of the phases separating out remains constant over the entire two-phase region

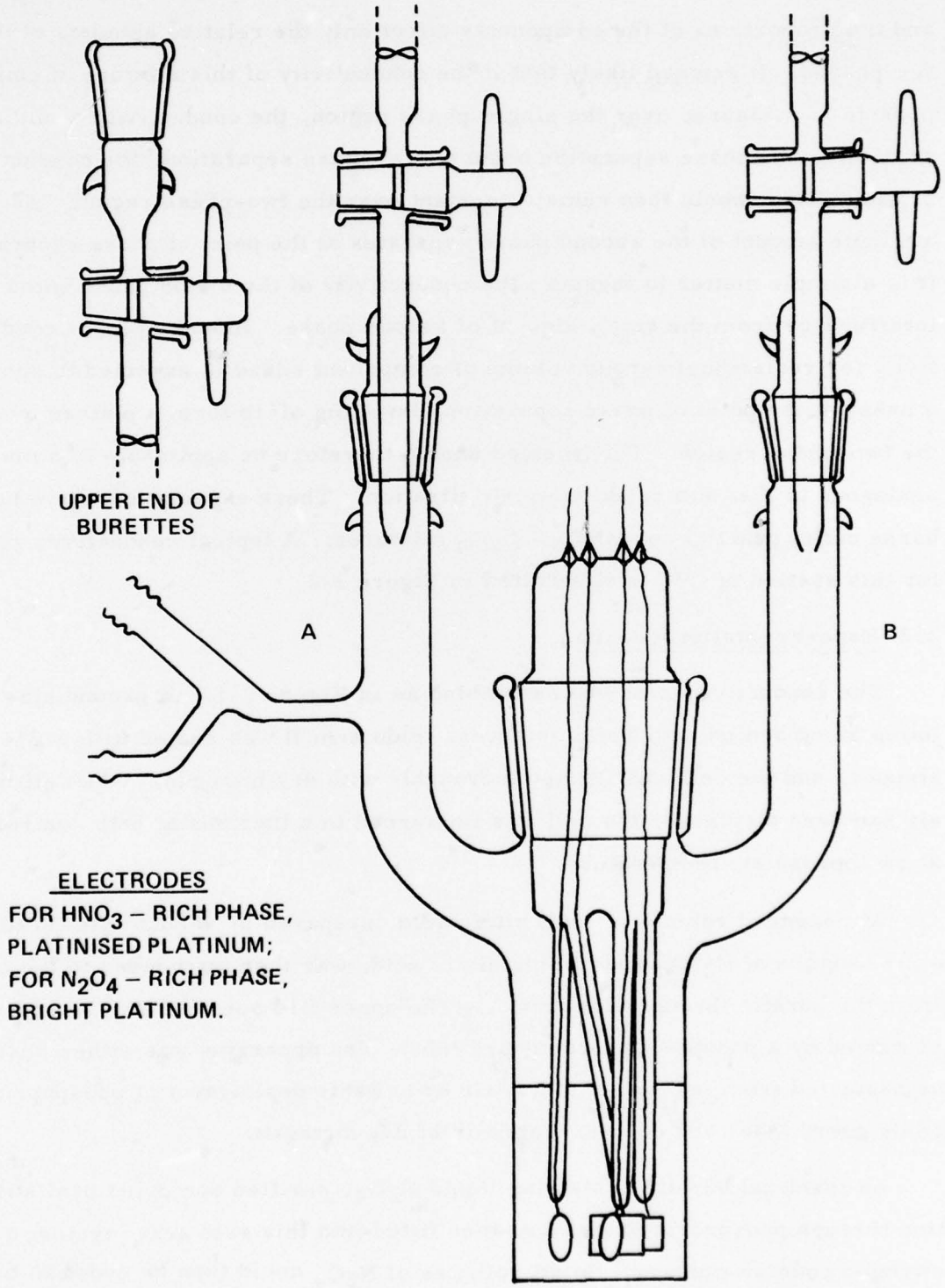


Figure 2-1. Conductivity Cell

and the proportions of the components affect only the relative amounts of the two phases. It seemed likely that if the conductivity of this mixture of components is measured over the single-phase region, the conductivity would change smoothly until phase separation occurs. On phase separation, the conductivity of each phase should then remain constant over the two-phase region. As only a minute amount of the second phase separates at the point of phase separation, it is a simple matter to measure the conductivity of the major phase without interference from the small amount of second phase. Hence a plot of conductivity (or resistance) versus volume of component added is expected to show a break at the point of phase separation, levelling off to form a plateau over the two-phase region. This method should therefore be applicable in a manner analogous to that of a conductimetric titration. These expectations have been borne out in practice for HNO_3 - N_2O_4 mixtures. A typical conductivity plot for this system at 0^oC is illustrated in Figure 2-2.

2.2 Experimental procedure

The conductivity cell was assembled as in Figure 2-1, all ground glass joints being sealed with Teflon sleeves. Side arm B was sealed with a B14 stopper, and the cell was flushed thoroughly with dry nitrogen. When all moist air had been displaced, the cell was immersed in a thermostat bath controlled at an appropriate temperature.

A measured volume of 100% nitric acid, prepared by vacuum distillation of a 2:1 mixture of H_2SO_4 and fuming nitric acid, was then introduced to the cell from the burette through side arm A. The upper B14 socket of the burette was protected by a phosphoric oxide guard tube. The apparatus was either sealed or protected from ingress of moist air by suitable deployment of phosphoric oxide guard tubes and counter-currents of dry nitrogen.

An identical burette containing liquid N_2O_4, purified and dried by distillation through phosphoric oxide, was then fitted into this side arm, against a nitrogen counter-current. Small volumes of N_2O_4 could then be added to the

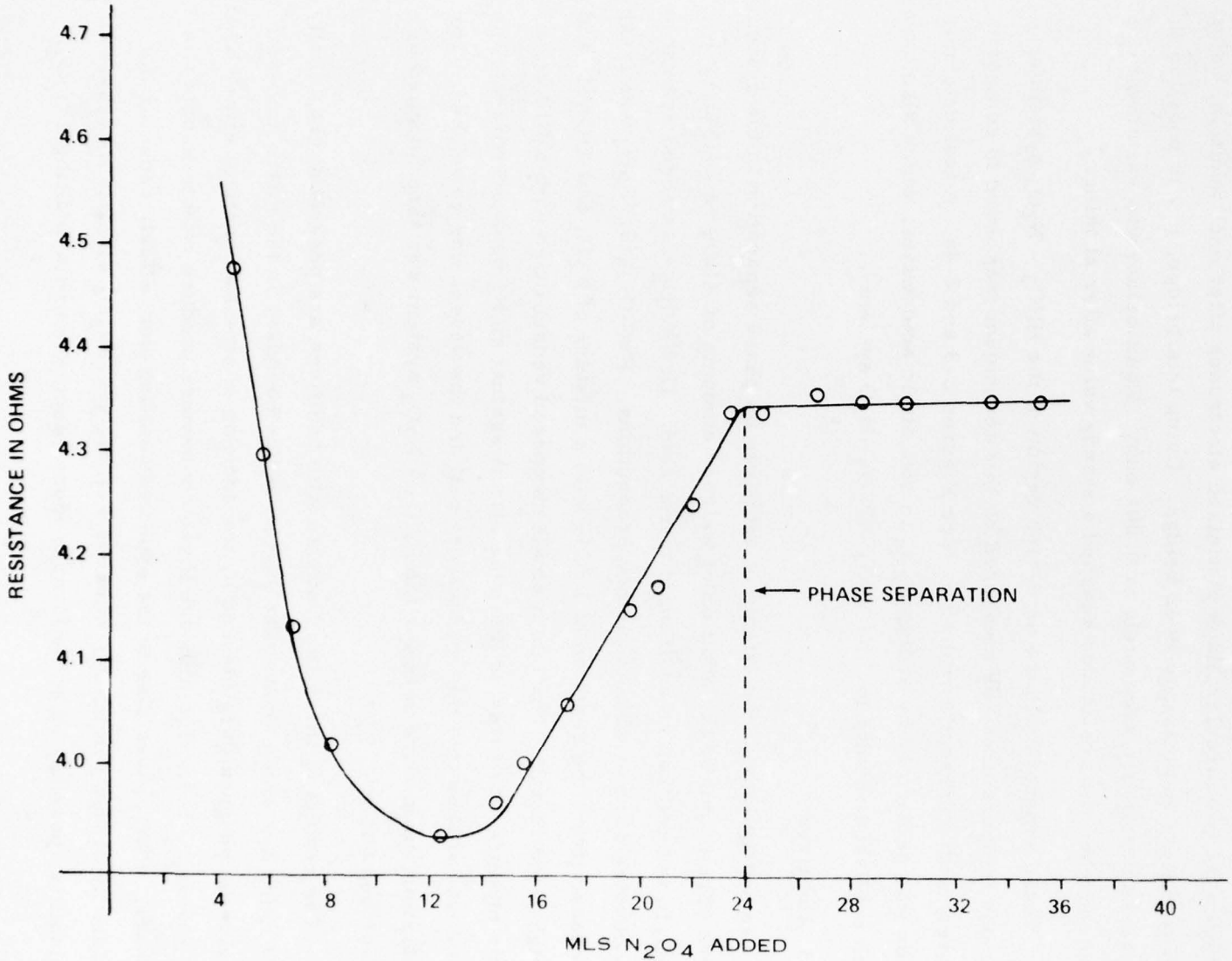


Figure 2-2. Typical Conductivity Plot; N_2O_4 Added to HNO_3 at Constant Temperature ($0^{\circ}C$)

cell, the pressure of N_2O_4 above the liquid in the sealed burette being sufficient to force liquid out. The resistance of the HNO_3 + N_2O_4 mixture was measured between the two circular black platinised electrodes after each addition, using a Wayne Kerr Autobalance B642 bridge. Using this bridge, it was possible to measure resistance accurately to 0.001 ohm. Equilibrium was assumed to be attained when the resistance reached a steady value after shaking.

Phase separation in the acid-rich region of the HNO_3 - N_2O_4 system at various temperatures, as measured by this technique, was found to compare closely with published results[2,3] (see Figures 2-3 and 2-4). A test determination was performed by adding N_2O_4 to 96% nitric acid-water, which also agreed with published results for the N_2O_4 -HNO_3 -H_2O system[3].

2.3 Additives

Investigations of the effects of additives on phase separation in the system were carried out by the addition of weighed amounts of KNO_3 or $Fe(NO_3)_3 \cdot 1.5\ N_2O_4$ to the cell before addition of nitric acid. Dry KNO_3 was added against an N_2 counter-current without further precautions. $Fe(NO_3)_3 \cdot 1.5N_2O_4$ was freshly prepared (from the reaction of $FeCl_3$ with a mixture of N_2O_4 and EtOAc)[1] and weighed out in a dry-box into a small stoppered vessel fitted with a B14 cone. This mixture was inserted into side arm A against an N_2 counter-current, the solid was shaken into the conductivity cell and the vessel was reweighed. The "titration" procedure used for the HNO_3 - N_2O_4 system was then followed as described above.

The results of these experiments with additives are presented graphically in Figure 2-4 which shows that the two-phase boundary in the nitric acid-rich region is not greatly influenced by the addition of small amounts of either KNO_3 or $Fe(NO_3)_3 \cdot 1.5N_2O_4$, although these compounds produce effects in opposite senses. KNO_3 gives rise to the expected "salting-out" effect, reducing the solubility of N_2O_4 in HNO_3, whereas $Fe(NO_3)_3 \cdot 1.5N_2O_4$ actually increases this solubility, possibly by some form of loose association with additional N_2O_4.

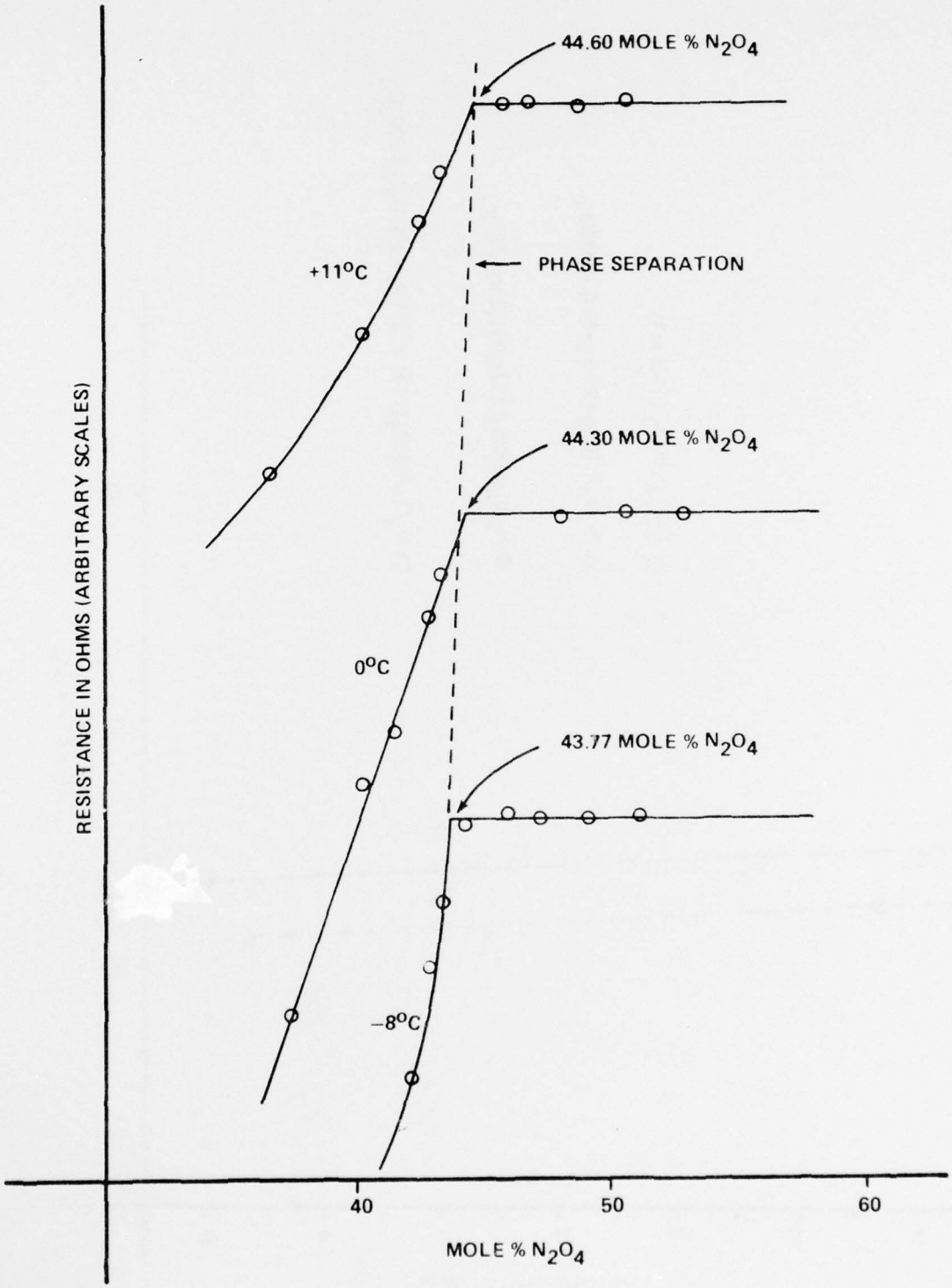


Figure 2-3. Conductivity Plots Showing Effect of Temperature on Phase Separation in the HNO_3-N_2O_4 System

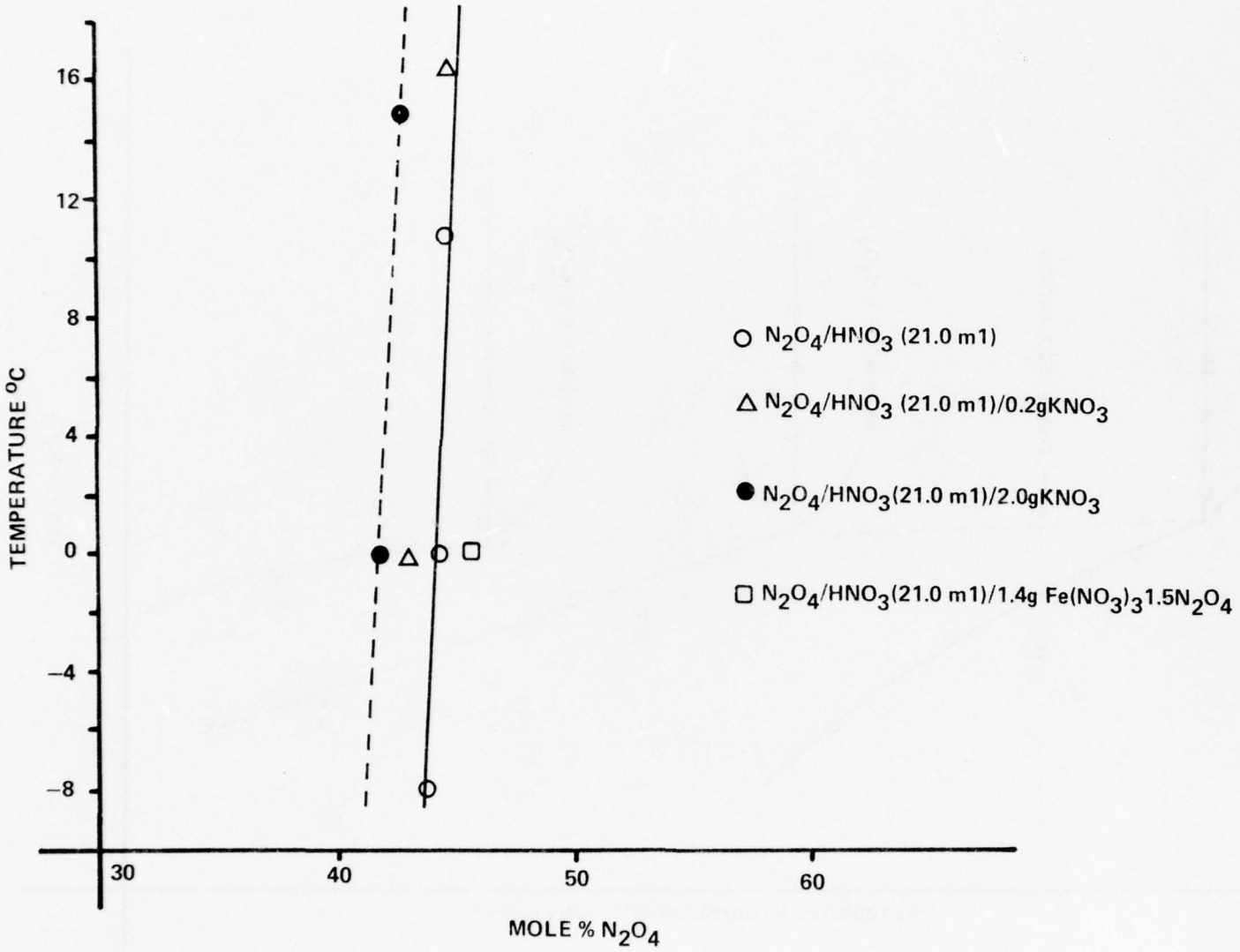


Figure 2-4. Effect of Additives on the HNO_3-N_2O_4 Phase Diagram

Since the effect of added salts on the HNO_3 - N_2O_4 phase boundary was relatively small, the phase study of HNO_3 - N_2O_4 mixtures was discontinued at this point, and emphasis was placed on the corrosion products of HDA.

2.4 References

1. Flow Decay, University of Nottingham, Department of Chemistry, Final Report AFRPL-TR-72-84, (June 1972).
2. G. W. Elverum and D. M. Mason, J. Phys. Chem., 60, 104 (1956).
3. A. Klemenc and T. Spiess, Monatsch., 77, 216 (1947).

3. CORROSION STUDIES WITH UNINHIBITED HDA

The corrosion rate of iron or steel in uninhibited HDA was determined in order to obtain values against which the effect of inhibitors could be compared. N_2O_4/HNO_3 mixtures of varying composition were used covering the full relevant range (0 to 55% N_2O_4 in HNO_3).

It was desired to obtain the rate of corrosion under conditions which would most closely resemble the conditions encountered during the storage of the oxidizer in propellant tanks. The corrosion rates are measured from graphs (Appendix A) of weight loss per unit area versus time and the graphs are, in general, found to have the S-shape shown in Figure 3-1. The weight loss per unit area values are based entirely on the quantity of metal in solution, as found by analysis.

The experimental results (fully tabulated and plotted in Appendix A) show a considerable decrease in corrosion rate by uninhibited HDA as the concentration of N_2O_4 is increased (Figure 3-2). Corrosion rates were also found to increase rapidly with increasing temperature, but experiments on the variations in corrosion rate when the specimens were stirred in the liquid were inclusive.

The experimental techniques used for the research are described in Appendix B.

3.1 Preliminary Experiments

These experiments were carried out to determine the best experimental routine to be used, and in particular to find the temperature range within which sufficient corrosion products were formed to permit accurate analysis of the solution.

The steel was turned on a lathe into cylindrical samples approximately 15mm. diameter by 20mm. The iron used was 'Specpure' iron rod. Metal samples were immersed in liquid contained in glass, round bottomed, 250 ml Quickfit flasks fitted with B24 stoppers, and temperature controlled where necessary using a methcol bath.

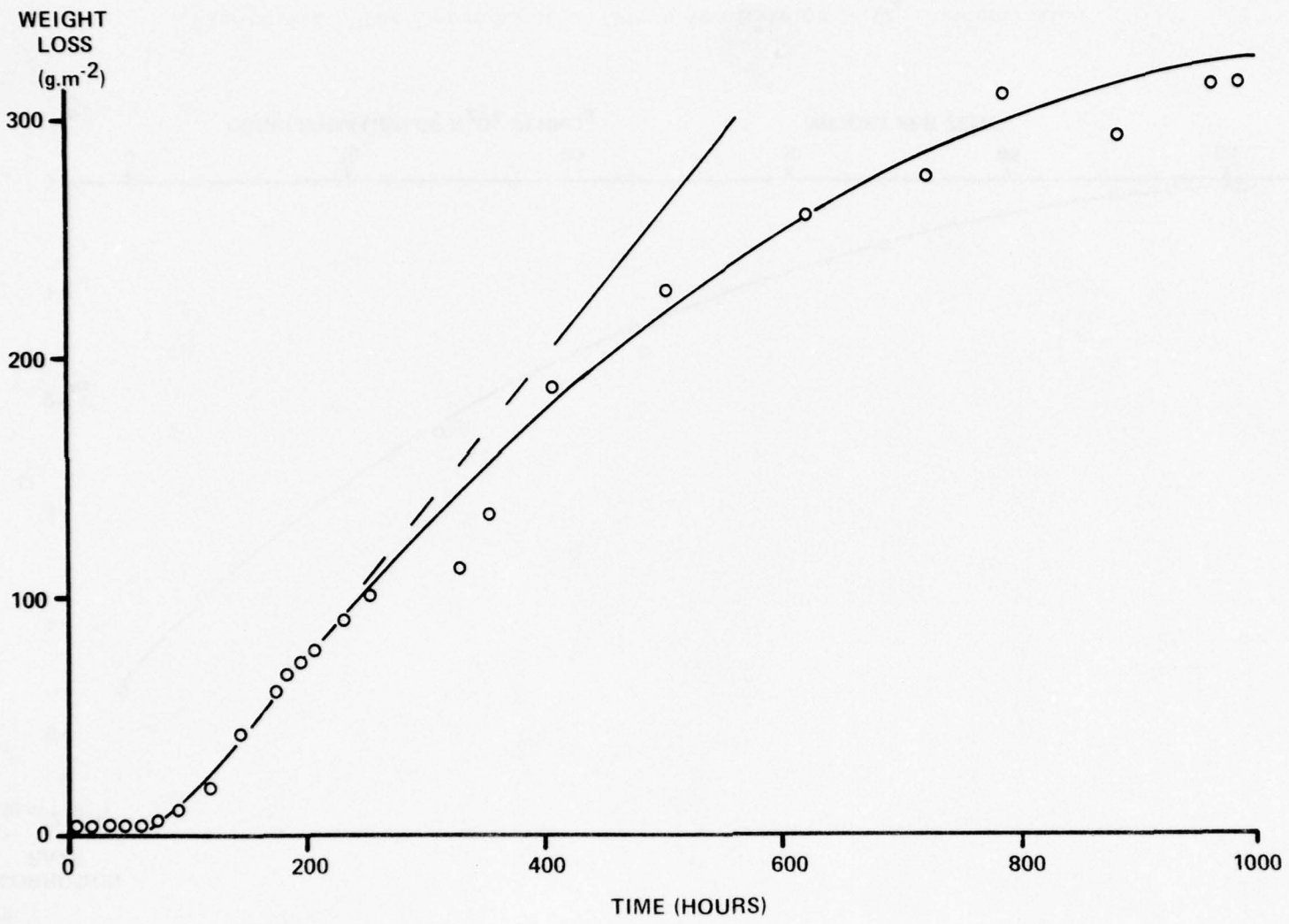


Figure 3-1. Weight Loss Curve for an Unstirred Specimen of 321 Stainless Steel in 34% N_2O_4/HNO_3 at 20°C (Expt 10)

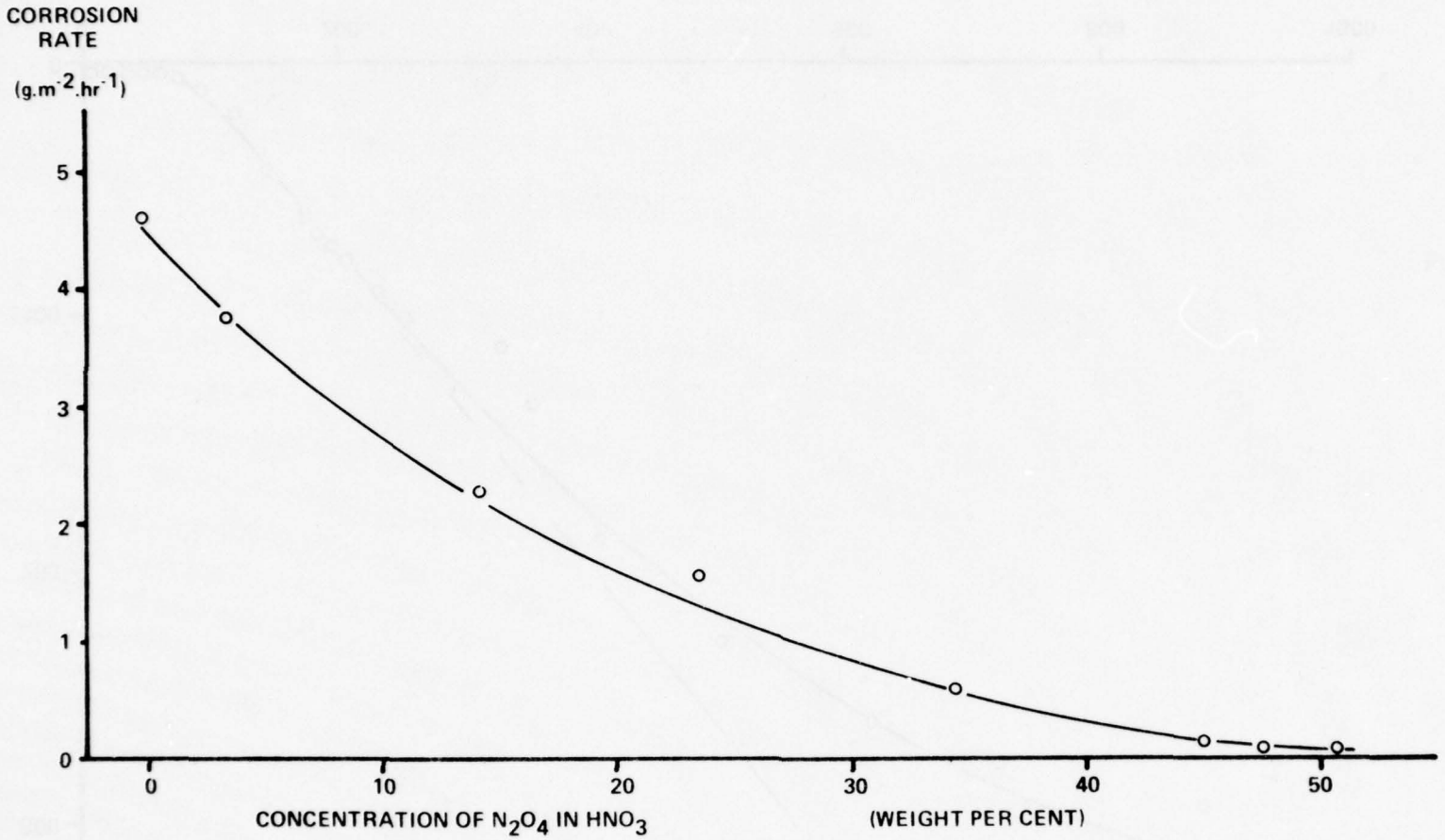


Figure 3-2. The Dependence of Corrosion Rate on N_2O_4 Concentration

(a) Experiment 1, 321 Stainless Steel in Uninhibited HDA at $0^{o}C$ (not stirred)

Throughout the duration of the experiment (2 months), there was no visible sign of reaction. The steel sample retained its original lustre and there was no colouration of the surrounding liquid to indicate dissolved metal. Analysis of the liquid showed that throughout the experiment the chromium and nickel concentrations did not reach a measurable value, and that the iron concentration did not rise above 100 ppm. The line (Appendix A, Figure A-1) which fitted the data points best gave an induction period of 204 hrs. and a rate of weight loss of $0.0226 g.m^{-2}.hr^{-1}$.

(b) Experiment 2, 321 Stainless Steel in Uninhibited HDA at $22^{o}C$ (not stirred)

The steel sample developed a black colouration almost immediately. After 24 hrs. this colouration deepened to cover the sample completely. After seven days, the HDA developed a steadily darkening greenish colouration, and became opaque after about 2 weeks. There was no intergranular corrosion at any stage during the experiment. The results, based on analysis of Fe, Cr, and Ni in the solution, are shown in Appendix A, Figure A-2. A series of five samples, (one per day), were taken approximately 18 weeks after the start of the experiment. These showed that the metal concentrations had stabilised at 3200, 600 and 500 ppm of iron, chromium and nickel respectively. Taken together with the results in Figure A-2, this indicates that these levels would have been attained approximately 6 weeks after the start of the experiment. No corrosion products precipitated at any stage, and the liquid was homogeneous throughout. Analysis of the liquid over the first 800 hours (Figure A-2) showed that after a short induction period of about 60 hours, the concentrations of all three metals rose steadily. The rate of weight loss was $1.092 g.m^{-2}.hr^{-1}$.

(c) Experiment 3, 321 Stainless Steel in Uninhibited HDA at O°C (stirred, 200 r.p.m.)

Observation of the sample during the experiment was not possible in this case due to the nature of the apparatus (Figure 3-3), which was immersed in a thermostat bath at O C. However, after the experiment was terminated it was found that the sample had developed a black colouration, though there had been no intergranular corrosion. There was no colouration of the liquid above the sample. The results are shown in Figure A-3. They are rather erratic, but indicate that the corrosion rate is increased by rapid stirring of the metal sample (compare Section 3.1 (a)).

(d) Experiment 4, Pure iron in Uninhibited HDA at 22°C (not stirred)

This reaction proceeded visibly quicker than reactions of steel with uninhibited HDA. The sample developed a black colour after only three hours, but the HDA above the sample never developed the green colour which is characteristic of its reaction with steel. This suggests that the colouration is due to the presence of chromium or nickel in solution. However, the HDA did undergo a progressive deepening in colour due to the presence of iron compounds in solution. At no time during the experiment did the liquid become opaque. After four days, intergranular corrosion was observed; appreciable quantities of the metal were deposited as a black powder on the bottom of the flask.

Analysis of the liquid (Appendix A, Figure A-4) showed that there was no measurable induction period and the iron concentration rose uniformly throughout the experiment. The calculated rate of weight loss was $3.692 g.m.^{-2} hr^{-1}$.

(e) Experiment 5, 321 Stainless Steel in N_2O_5/HNO_3 (25 wt% N_2O_5) at O°C (not stirred)

This reaction produces the fastest corrosion of 321 stainless steel by a nitric acid medium observed. The steel sample lost its lustre after only 4 hours, and the initially colourless solution turned green within one day. The solution quickly became opaque, and a white reaction product precipitated after

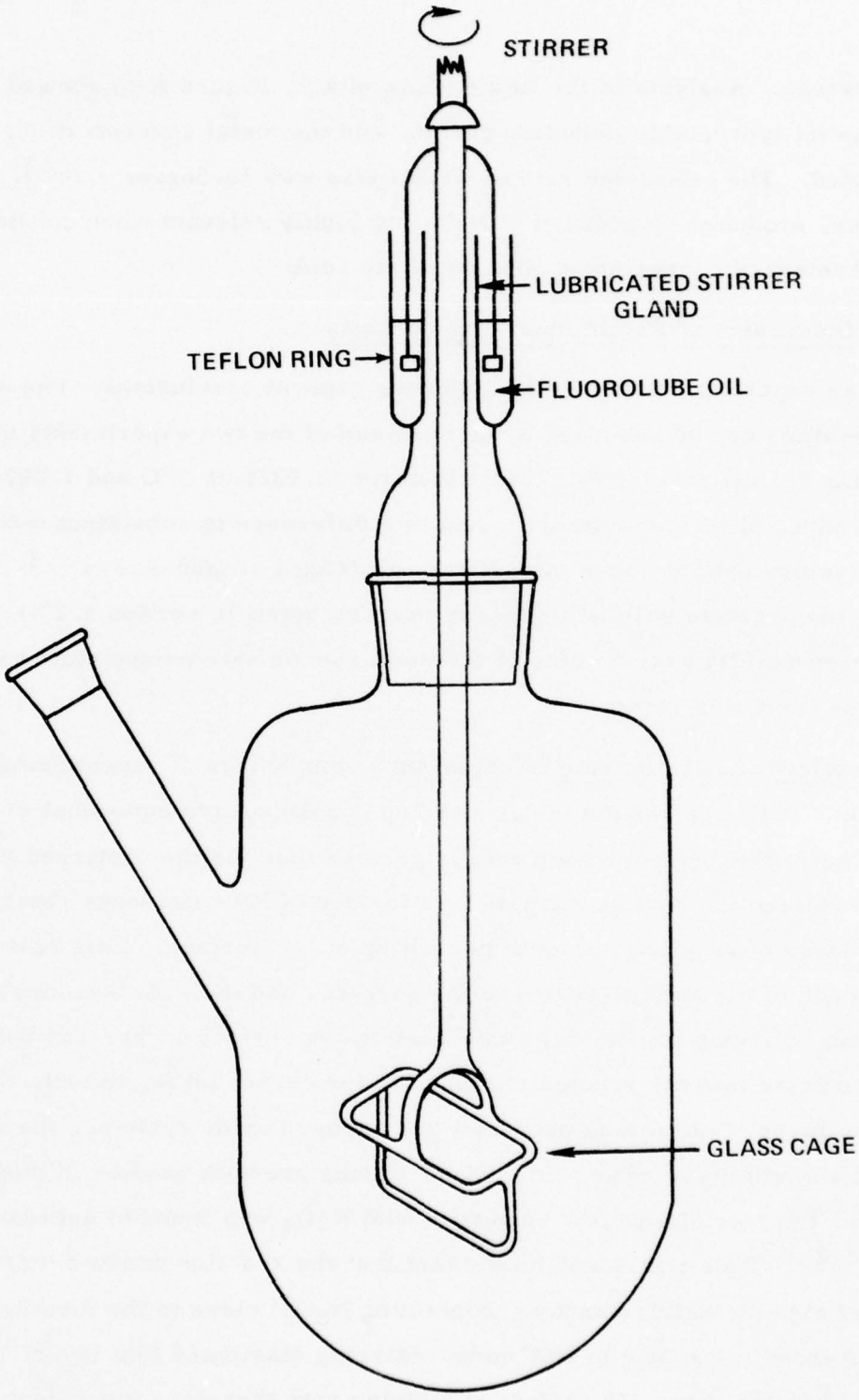


Figure 3-3. Stirring Apparatus

about 2 weeks. Analysis of the liquid (Appendix A, Figure A-5) showed that there was no appreciable induction period, and the metal concentrations rose as expected. The calculated rate of weight loss was 10.86g.m^{-2}.hr^{-1}. This high value, produced by addition of N_2O_5, is highly relevant when considering the mechanism of corrosion by HDA or nitric acid.

(f) Discussion of Preliminary Experiments

These experiments lead to the following general conclusions: The effect of temperature can be assessed by comparison of the two experiments described in Sections 3.1 (a) and 3.1 (b). The two rates (0.0226 at 0^oC and 1.092g.m^{-2}.$hr.^{-1}$ at 22^oC) differ considerably, and this difference is consistent with temperature factors usually found in systems involving nitrogen oxides [1,2,3]. The effect of temperature will be discussed in more detail in section 3.2(b), but the preliminary results gave a guide to the most appropriate temperatures for comparison of corrosion rates.

The effect of stirring rate is shown by a comparison of experiments 3.1(a) and 3.1(c). Although results under stirring conditions are somewhat erratic, it would seem that the corrosion rate is greater than for the unstirred reaction. Increase in reaction rate on stirring is a feature of heterogeneous reactions where a layer of reaction products is built up at the surface. This restricts the approach of the active species to the surface, and the rate becomes diffusion controlled. Stirring breaks down this restricting surface layer, and the present results indicate that the species responsible for corrosion is, in fact, restricted by the layer of corrosion products. In nitrogen oxide systems, the reverse case can sometimes be observed. Thus, during previous studies in these laboratories, the rate of reaction of metals with N_2O_4 was found to decrease with stirring.[1,2,3] This was based on the fact that the reaction product (NO) formed a layer of high dielectric constant (containing N_2O_3) close to the metal surface which enhanced the supply of NO^+ ions. Stirring dissipated this layer, thus reducing reaction rate. The effect of stirring rate therefore gives useful

evidence on the mechanism of corrosion, and was examined more carefully later in the work. The preliminary experiments indicate that NO^+ may not be the attacking species. This leaves two candidates, the proton, H^+ and the nitronium ion NO_2^+. In aqueous media, the proton mechanism is revealed by the liberation of hydrogen, but in uninhibited HDA, any hydrogen produced will be instantaneously oxidized. The NO_2^+ mechanism has been postulated for the N_2O_4/HNO_3 system by Beskov, Kochetkova, and co-workers[4,5] on the basis of figures showing that the reactivity of HNO_3 towards steels is mirrored by the "N_2O_5 content." Preliminary experiment 3.1.(e) was therefore set up to determine the reactivity of N_2O_5 towards steel. The reaction shows that the NO_2^+ ion is indeed highly reactive towards steel and in fact this experiment shows the highest rate of reaction among the preliminary experiments, even though the reaction took place at 0^oC. The effect of corrosion on the surface of the steel was similar in all respects to that described by Berl and Saenger[6], and the characteristic pattern of intergranular corrosion depicted by them was also observed. Thus the preliminary experiments indicate a mechanism involving the NO_2^+ ion, produced by ionisation of nitric acid as follows:

$$2HNO_3 \rightarrow NO_2^+ + NO_3^- + H_2O$$

and that the N_2O_4 acts merely as an inert diluent.

In the preliminary experiments, the separate concentrations of chromium, nickel, and iron which collect in solution as corrosion products were not reported, but the "weight loss" values represent a sum of the three analytical values. It is relevant to note, however, that the relative concentrations of these three metals in solution are, very broadly, similar to the relative amounts in the solid metal. This illustrates the well-known difference between the reactivity of a metal in pure form and its reactivity when present as a component in an alloy. In the pure state, chromium is less reactive towards uninhibited HDA by an order of magnitude than iron or nickel, but when alloyed with iron and nickel, its reactivity towards uninhibited HDA is very similar.

3.2 The Effect of N_2O_4 Concentration and Temperature on Corrosion Rate

3.2 (a) The Effect of N_2O_4 Concentration (Experiments 6 through 24 and 26)

Each of the samples had an initial induction period after which it developed a black colour. After the induction period, the constituent metals (iron, chromium, and nickel) began to dissolve, and as the reaction progresses, the rate slowly decreases giving rise to the shape of the curve as shown in Figure 3-1. The reaction rates used in Figure 3-2 are taken as the initial reaction rate immediately following the induction period, as illustrated by the line AB in Figure 3-1. The corrosion rate and induction period observed in each of these experiments is given in Table 3-1. Each of these experiments used specimens of 321 stainless steel of similar size. In each case, specimens were immersed in approximately 150ml. of uninhibited HDA contained in a 250ml. flask.

The effect of increasing the tetroxide content of an uninhibited N_2O_4/HNO_3 mixture is clearly to decrease the corrosion rate of steel immersed in that mixture. This appears at first sight to be in direct conflict with effects observed in the operation of liquid oxidant propulsion systems[7], namely that corrosion rate increases with increasing tetroxide content. However, in operational studies, inhibited HDA is used, and it is of considerable interest that the different corrosion mechanisms which are presumably involved in inhibited and uninhibited HDA respond quite differently to changes in N_2O_4 concentration.

Figure 3-4 shows logarithmic plots of corrosion rate versus nitric acid concentration at four temperatures. In a simple system, these graphs should give straight lines but in this case they do not; this is no doubt due to the complicating effect of diffusion processes. However, the reaction orders which can be taken from the graph are always greater than two. This would seem to add weight to the assumption made in section 3.1(f) that the nitronium ion NO_2^+

Table 3-1. Rates and Induction Periods from the Concentration and Temperature Studies

Experiment No.	Composition of Mixture (wt % N_2O_4)	Temperature (^oC)	Corrosion ($g.m^{-2}hr^{-1}$)	Induction Period (hours)
13	0 (Pure HNO_3)	14.9	2.66	85
14	15.44	14.9	1.90	105
15	32.63	14.9	0.545	185
16	46.37	14.9	0.159	142
6	0	20.5	4.61	40
7	3.51	20.5	3.74	35
8	14.36	20.5	2.36	50
9	23.21	20.5	1.64	45
10	34.64	20.5	0.593	73
11	44.82	20.5	0.239	82
26	48.72	20.0	0.169	87
12	51.05	20.5	0.0977	55
17	0	27.3	5.39	40
18	14.21	27.3	3.51	45
19	31.04	27.3	1.68	45
20	42.91	27.3	0.826	62
21	0	31.0	7.78	25
22	15.20	31.0	4.22	33
23	29.61	31.0	2.62	57
24	43.44	31.0	1.02	22

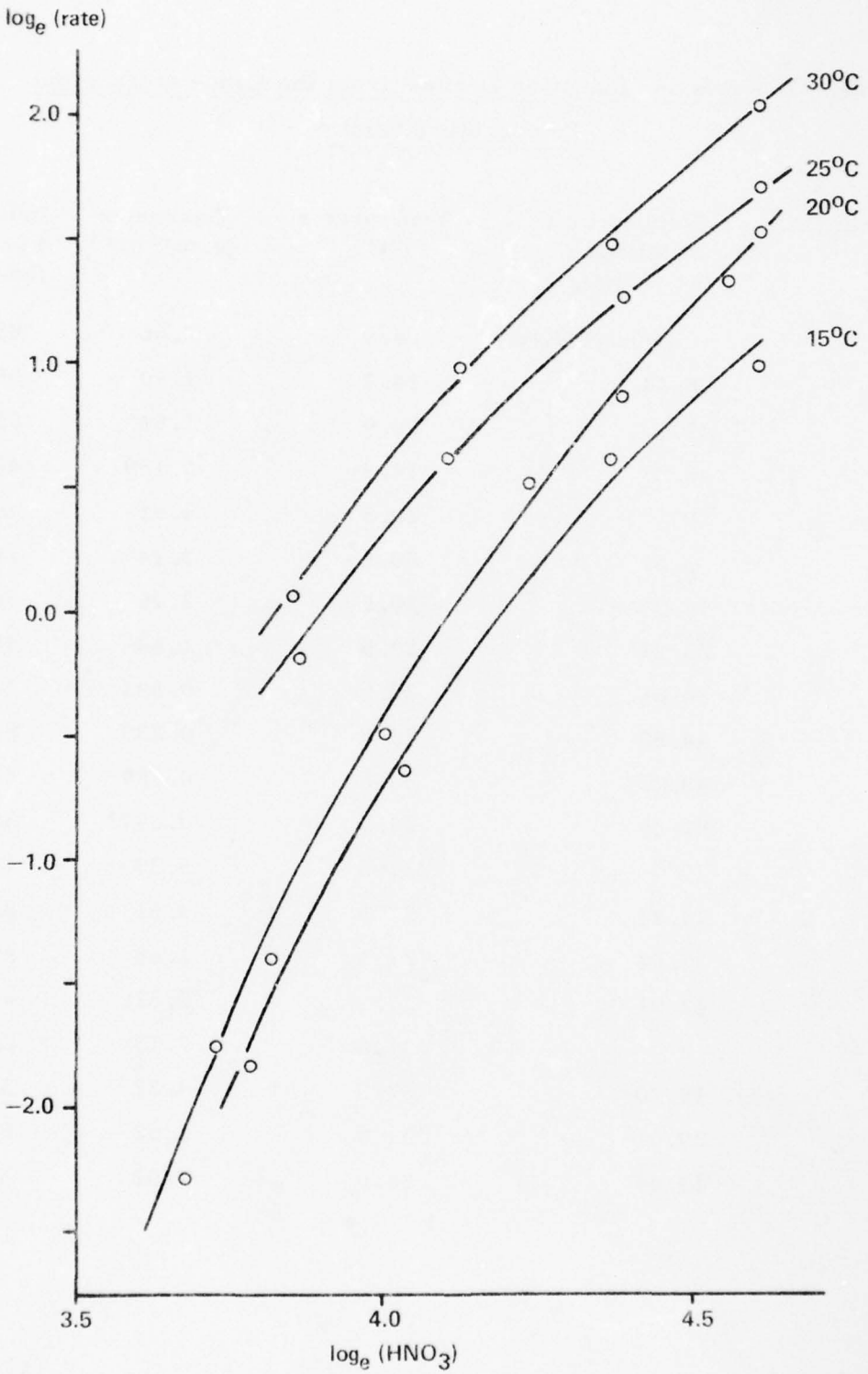


Figure 3-4. The Dependence of Corrosion Rate on Nitric Acid Concentration

is the active species, since the order of reaction is expected to be at least 2 with respect to nitric acid from consideration of the equilibria

$$2HNO_3 \rightleftharpoons N_2O_5 + H_2O \qquad \& \qquad N_2O_5 \rightleftharpoons NO_2^+ + NO_3^-$$

3.2(b) The Effect of Temperature

Corrosion rate increases rapidly with increase in temperature, and the results are summarised in Figure 3-5 which relates to uninhibited HDA. Similar curves have been obtained for mixtures containing 30% and 14% N_2O_4 and for pure nitric acid. All four curves are roughly exponential, as expected by consideration of the Arrhenius Law

$$\text{Rate} \propto \exp\left(\frac{E_A}{RT}\right)$$

In plotting graphs of rate versus temperature, care was taken to eliminate any effects due to variation in composition. This was achieved by plotting a rate versus composition curve for each separate temperature, and reading off the rates at the nominal compositions 14%, 30%, and 44% N_2O_4.

The apparent Arrhenius Activation Energy, can be obtained from the results by plotting the natural logarithm of the corrosion rate against the reciprocal of the absolute temperature. The gradient of this line gives the value of $E_{A/R}$, and hence the activation energy E_A. The Arrhenius Plots are shown in Figure 3-6 and the values of the activation energies are given in Table 3-2. These values do not constitute activation energies for a single process; the system is not stirred, and the rate of reaction is therefore diffusion controlled. Indeed the magnitude of the activation energies[1,8] (all over 4 k. cal) indicates that processes other than simple electron transfer play a significant part.

Activation energies vary with the composition of the mixture. The most likely interpretation is that there is a basic chemical process (the transfer of an electron from NO_2^+ to the metal surface) having a constant activation energy, and a diffusion process whose activation energy varies according to the composition of the mixture.

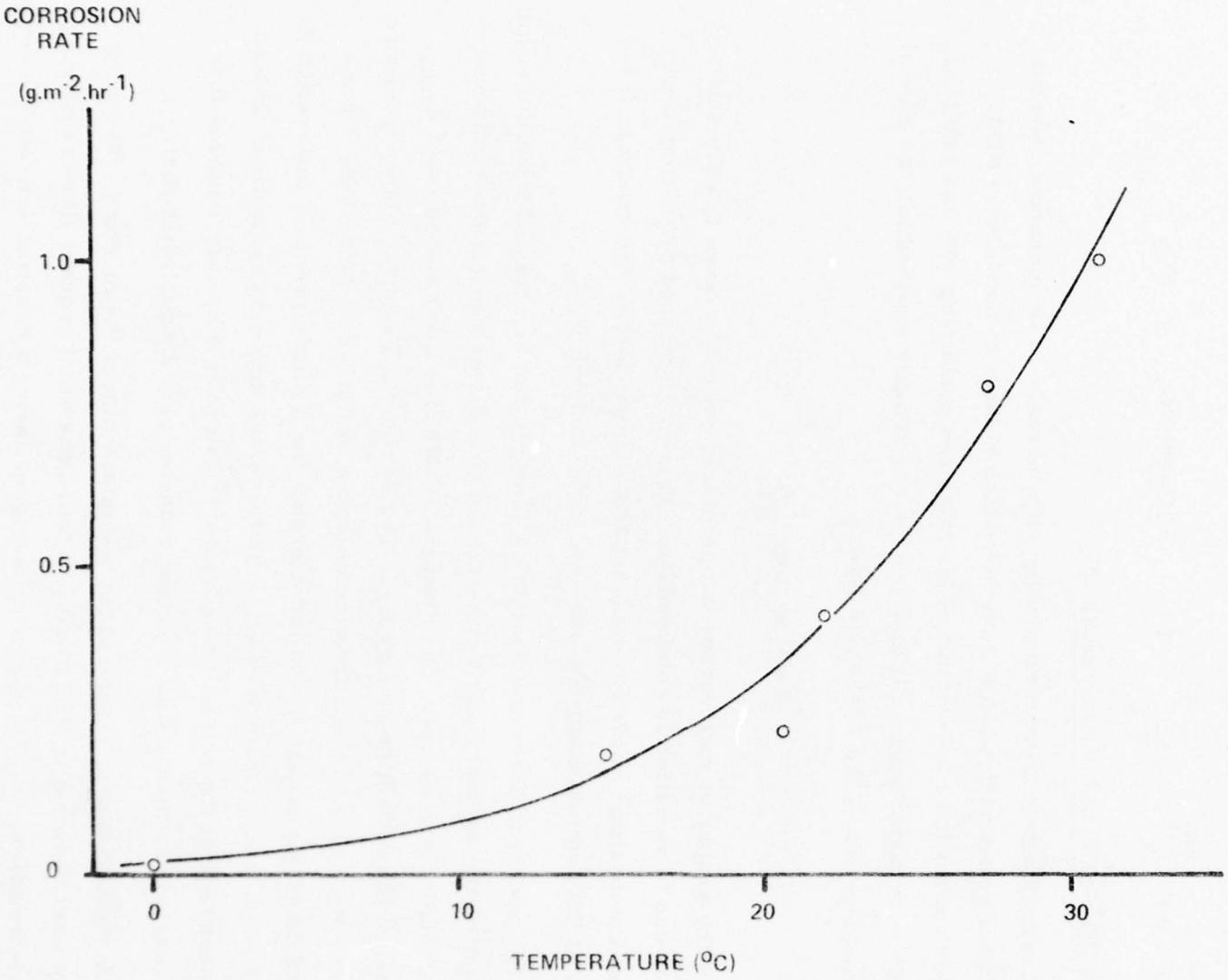


Figure 3-5. The Effect of Temperature on Corrosion Rate in HDA

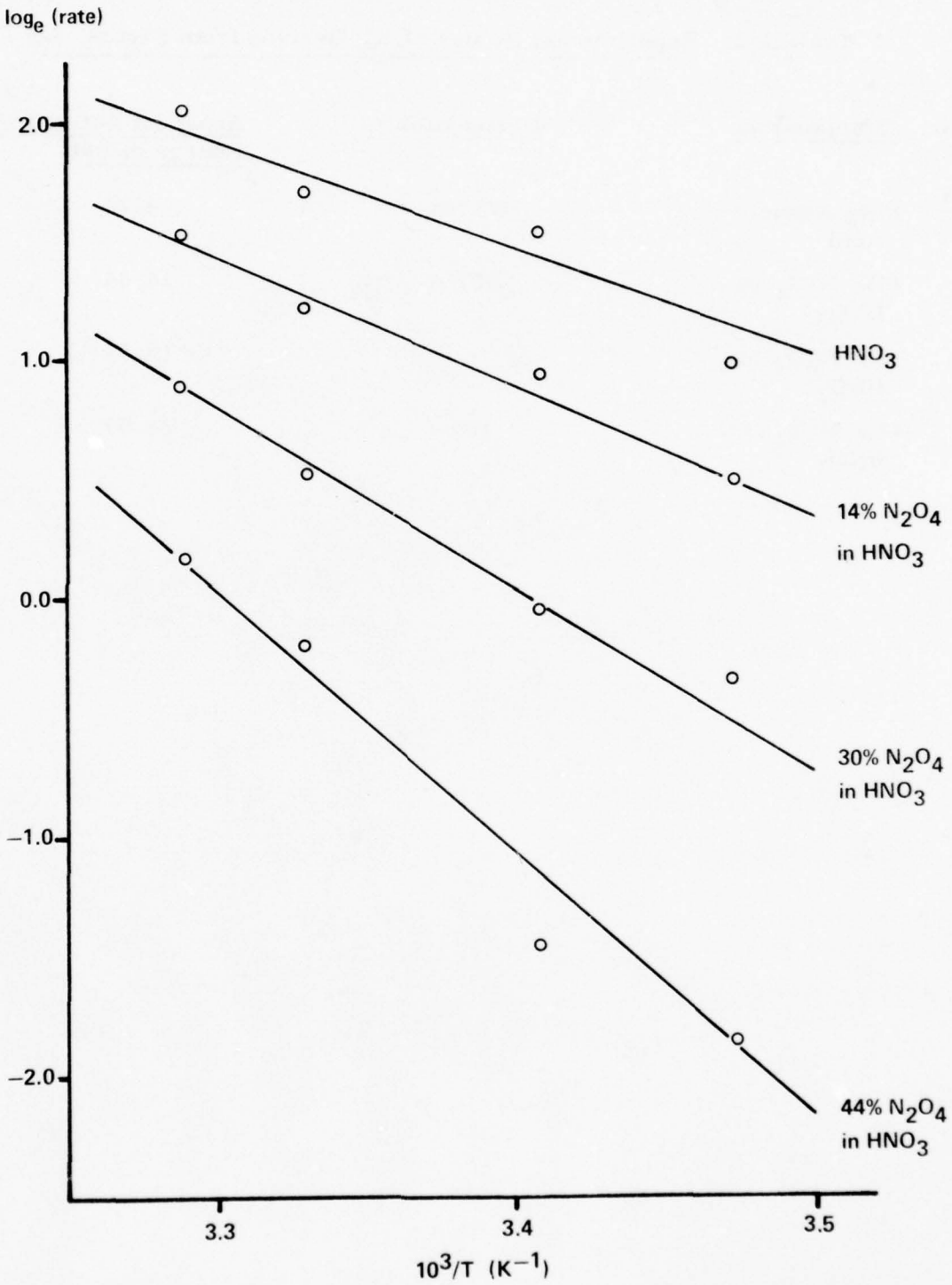


Figure 3-6. The Dependence of Corrosion Rate on Temperature

Table 3-2. Experimental Values of E_A Derived from Figure 3-5

Composition	Designation	Apparent Activation Energy (k. cal)
Pure Nitric Acid	WFNA	9.76
14% N_2O_4 in HNO_3	RFNA	14.84
30% N_2O_4 in HNO_3	-	18.37
44% N_2O_4 in HNO_3	HDA	24.99

3.3 Factors Related to Corrosion Rates

(a) The Surface film

The black film which forms on the surface of the steel specimen during the induction period was at first thought to be a visual effect only, resulting from the roughing of the steel surface in HDA to give a black appearance. This was supported by the fact that the so-called film was insoluble in water and resisted attempts to remove it from the surface by abrasion. This was also supported indirectly by examination of the powder taken from the surface of mild steel, after immersion in HDA, which was found to be composed largely of iron powder, containing oxygen in trace quantities only.

Finally, some of the material responsible for the black colour on the surface was removed, and studies to date suggest that it may be a discrete compound. Only very small quantities have been available, but preliminary atomic absorption analysis indicates that the compound may be rich in chromium. From X-ray powder photography the film is amorphous. Infra-red spectra have been obtained from three different samples (Figure 3-7 and Table 3-3). In spite of the different treatments which the samples received, and the small quantities available, the spectra show some common features (e.g. the presence of coordinated water and possibly nitrate) which suggest that the black film formed when 321 steel is immersed in HDA may be a consistent product.

(b) The induction period

In all experiments involving 321 steel, irrespective of the composition of the HNO_3/N_2O_4 mixture, an induction period is observed. This is the period, immediately following the immersion of steel in the acid, during which corrosion is negligible. The induction period may extend over several days (see expts. 1-12) but is then followed by corrosion at its maximum rate. A number of isolated observations may be collected together to give some picture of the process which is occurring during this period.

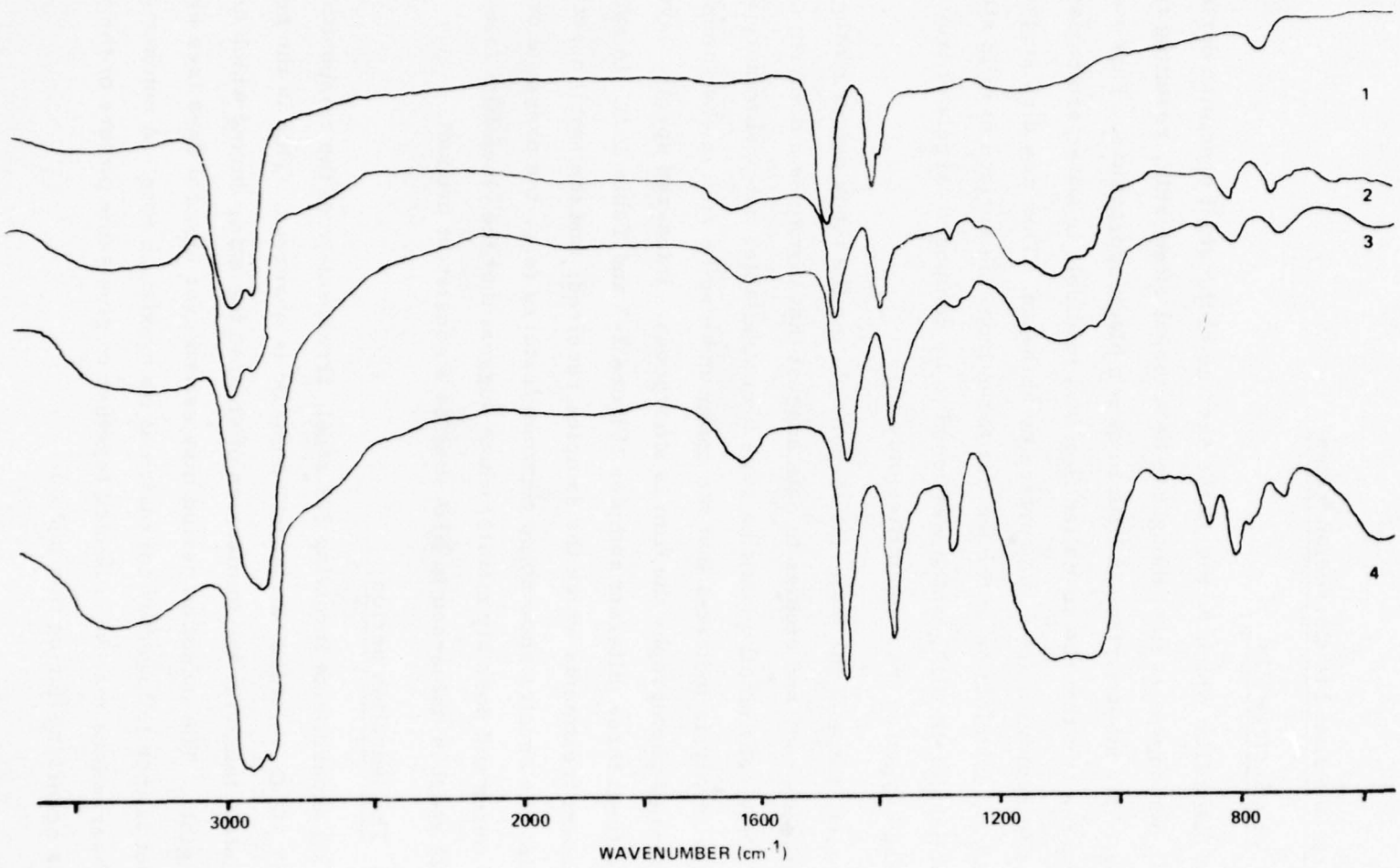


Figure 3-7. Infra-Red Spectra of the Surface Film

Table 3-3. Description of Infra-Red Spectrum Shown in Figure 3-7

Spectrum No.	Description and Treatment
1	Blank of nujol between AgCl windows.
2	Nujol mull of film sample taken from 321 stainless steel immersed in HDA for 1000 hrs. at 35°C. Steel specimen was washed with HDA and film removed in dry conditions.
3	Nujol mull of film sample taken from 321 stainless steel immersed in HDA for 500 hrs. at 20°C. Steel specimen washed with N_2O_4 and film removed in air.
4	Nujol mull of film sample taken from 321 stainless steel immersed in HDA for 1000 hrs. at 20°C. Steel specimen washed in water and acetone and film removed in air.

1. Using iron alone (in the form of mild steel, expt. 4) reaction occurs immediately, and there is no induction period. The latter therefore results directly from the fact that the exposed steel surface contains several metals (e.g. Fe, Cr and Ni.).

2. Some hardening is inevitably produced in the production of a metal surface, but we have no evidence that in the case of steel the induction period has any purely mechanical origin of this sort.

3. As explained under (a) above, a surface film develops during the induction period, and it seems that corrosion does not begin until this film is fully established.

It seems clear, then, that the fresh steel surface is unable to react with the acid, but that during the induction period, the surface becomes activated, and that this occurs through the agency of the black surface film. Put in chemical terms, the metal atoms in the alloy matrix have less chemical reactivity than they would have in the case of the pure metals, so that for example, the transfer of an electron to the NO_2^+ in the acid medium from the Fe atom in iron is possible, but the same transfer from any one of the metal atoms in the steel surface is not possible. During the induction period, some other (and much slower) reaction takes place, which has the effect of loosening the metal-to-metal bonding in the metal surface and the production of a thin surface film. We therefore define "activation" of the surface in these nitric acid systems as the formation of a film through which the transfer of electrons from the metal surface to NO_2^+ can now take place. As soon as the film has developed to the stage where this is possible, corrosion at its maximum rate occurs, and is only slowed down by the accumulation of metal salts in the liquid.

An experiment (No. 26) was carried out to determine whether the activation of a steel surface is in any way connected with the presence of reaction products in solution. A quantity of HDA was divided into two 150 ml. samples. A specimen of 321 stainless steel was immersed in the first 150 ml. sample of HDA.

The specimen had an induction period of 87 hours, after which the corrosion proceeded at an initial rate of 0.17g.m.$^{-2}$hr^{-1}. After 264 hours, when the corrosion rate was still appreciable the steel specimen was removed from the liquid, washed with HDA, and immersed in the second 150 ml. sample of HDA (expt. 27). After an induction period of only 18 hours the specimen corroded rapidly, at a rate of 1.3g.m^{-2}hr^{-1}, i.e. at a rate about seven times greater than in the initial experiment. This is consistent with discussion above. Once the activating surface film had been formed, in the first HDA sample, it persisted in the second HDA sample, which accounts for the very small induction period. The corrosion products in solution are involved only in the subsequent corrosion rates; in the second run we have created ideal conditions for corrosion, i.e. an activated surface together with the complete absence of corrosion products in solution in the HDA, which accounts for the very high corrosion rate.

(c) Separation of precipitates

In experiments involving steel turnings immersed in nitric acid, precipitation of a green solid was observed (Section 5.2) and this was identified as the compound $Ni(NO_3)_2 \cdot 2H_2O$. During some extended rate experiments (3000 hrs.) at 15°C, the green crystalline precipitate of $Ni(NO_3)_2 \cdot 2H_2O$ was again observed to separate from nitric acid solution, and also from 14% N_2O_4 in HNO_3.

The formation of the precipitate appeared to have no effect on corrosion reaction, and was first noticed after about 2500 hrs. Both solutions gave precipitates at about 1200 - 1300 p.p.m. of nickel. Since the solubility of $Ni(NO_3)_2 \cdot 2H_2O$ in the 14% N_2O_4 mixture is much higher than in nitric acid, there is no immediate correlation between the nickel concentration when precipitation occurs, and the solubility of $Ni(NO_3)_2 \cdot 2H_2O$ when present alone in the liquid (Figure 5-21). Presumably the iron and chromium salts also present exert some influence on precipitation of the nickel compound.

(d) The shape of corrosion-time curves, and the key role of nickel

There are some general comments which are relevant at this stage, since they form the background against which inhibitor action should be considered.

The corrosion rates (expt. 1-12) show an S-shape which becomes more pronounced as N_2O_4 content of the medium increases. This is due to an initial induction period, followed by more rapid corrosion, but as the metal content of the liquid increases the corrosion rate decreases. In the limiting case of 50% N_2O_4 (expt. 12) the levelling-off is virtually complete, and the corrosion rate eventually becomes almost negligible. It is believed that this reflects some form of "saturation" of the liquid, but it now becomes necessary to attempt a definition of the term "saturation" in a system in which three metals with widely different solubilities, are involved.

The solubilities of $Fe(NO_3)_3 \cdot 2H_2O$ and the corresponding chromium compound in nitric acid alone, and in mixtures containing up to 50% N_2O_4 are considerable, and much higher than any concentration achieved during these corrosion experiments. There is therefore no question of saturation by iron or chromium occurring in these experiments. However, $Ni(NO_3)_2 \cdot 2H_2O$ has a lower and clearly defined solubility (Figure 5-21), and crystallises readily from the solution, and it is reasonable to believe that corrosion is a solution process, the rate of which follows the nickel content of the solution. Thus, when corrosion becomes negligible, as in expt. 12 the solution is saturated with respect to nickel. Thereafter, some precipitation of the nickel compound may occur (perhaps due to temperature changes), and some corrosion then occurs to restore the nickel content of the solution. This is supported by a qualitative experiment in which a piece of nickel metal was left in contact with a sample of HDA for some days. It was then replaced by a steel specimen, which was then observed for signs of corrosion. The specimen showed an induction period of 12 days, whereas (expt. 11) a similar steel specimen in untreated HDA had an induction period of only 3 days.

This interpretation cannot presently be put on a fully quantitative basis due to lack of solubility data. The solubility of the nickel compound varies widely and in an unusual way with N_2O_4 content of the medium (Figure 5-21), and this must be taken into account. The extent of the salting-out effect produced by the presence of the iron and chromium salts in solution has not yet been measured. But this should decrease the solubility of the nickel compound in solution, and may well account for the levelling-off in corrosion rate curves at nickel concentrations which are lower than the known saturation values in the absence of iron and chromium salts.

This general postulate is also relevant to what is occurring at the metal surface. In an alloy of three metals (i.e. steel) the metals are not able to react independently. The inter-metallic bonding is such that when a stage is reached at which one of the metals (i.e. nickel) is no longer able to dissolve, the surface reaction of the iron and chromium also ceases, and corrosion no longer occurs.

This interpretation is also consistent with the results of expt. 4, in which pure iron was allowed to react with HDA. Here the corrosion curve was not S-shaped; corrosion continued at a constant rate because of the extremely high solubility of the iron corrosion product, and the absence of nickel. Again, it will be shown in a later Chapter that compounds (such as PF_5) which act as efficient corrosion inhibitors with respect to steel, have no inhibiting effect on the corrosion of mild steel, where only iron reactions are involved.

(e) The Surface/volume Ratio

These experiments support the belief (which has developed from industrial experience on the storage of liquid propellants) that the volume of liquid used has a direct influence on corrosion rates. This is illustrated by comparison of two experiments (6 and 25) for which the essential details are given in Table 3-4.

Table 3-4. Influence of Surface/volume ratio on corrosion of 321 steel in nitric acid at 20°C.

	Expt. 6	Expt. 25
Initial rate ($g.m^{-2}.hr^{-1}$)	4.61	21.0
Volume of acid used (ml.)	122.3	400.0
Surface area of specimen (cm^2)	14.17	13.05
Surface/volume ratio cm^{-1}	0.116	0.0326

The two experiments were virtually identical except for the volume of acid; when this was increased threefold, the maximum corrosion rate was increased fourfold. The effect is readily interpreted in terms of the concentration of reaction products in the liquid. The larger the available volume, the lower will be the concentration set up by solution of a given quantity of metal, so that a higher corrosion rate will be maintained.

It was not attempted to set up experiments to determine the effect of surface/volume ratios in liquids of different composition, though this would be a worth-while exercise. On the basis of the arguments outlined above, it is the nickel concentration which is likely to be the most important factor. In any quantitative study, it must be remembered that it is the chemical potential of the dissolved metal, rather than its simple concentration, which is significant. In the present context, the chemical potential refers to the extent to which the actual concentration approaches the saturation value. Since the latter can vary with the amount of iron or chromium salts present and with the composition of the liquid, it is clear that the conversion of concentration into chemical potential depends upon the other components in the liquid mixture.

(f) The Effect of Stirring

In all experiments (except expt 3) discussed in this Chapter, the metal and liquid have been static, and therefore resemble most closely the conditions met with in the storage of liquid propellants. Under these conditions the soluble corrosion products will collect near the surface, and there will be a concentration gradient at right angles to the surface. Stirring should disperse the excess of corrosion products, and it was desired to examine the effect this would have on corrosion rates. It will be remembered (see (b) above) that the transfer of a corroded metal specimen to a fresh sample of HDA produced a large increase in rate. Again, if the reaction products have an influence on the attacking species in the liquid (as with the Zn/N_2O_4 reaction[1]) their dispersion may actually decrease reaction rates. The question of stirring was mentioned briefly in Sections 3.1(c) and 3.1(f); no firm conclusions could be made from the preliminary experiments; therefore, the stirring effect was examined more closely.

The first experiment (No. 25) was set up using nitric acid alone, at 20°C, using the apparatus shown in Figure 3-8. The specimen was stirred with the stirring rod as illustrated at approximately 90 rpm using an electric motor. Since Teflon is self lubricating there was no need to use any sophisticated stirrer gland since the stirring rod fitted tightly into the Teflon stopper and provided an adequate seal. Sampling was carried out through the short side arm, and temperature control was by means of the thermostat jacket built into the apparatus.

The acid was introduced to the unstirred specimen, which was then left to corrode (and thus to form the activating surface film) for 187 hours before stirring was commenced. The results of the experiment are shown in Figure 3-9. During the initial unstirred period, there was an induction period of about 20 hours, followed by a maximum corrosion rate of 21.0 $g.m^{-2}hr^{-1}$ after 50 hrs. The reaction then slowed down gradually, to a rate of about 14 $g.m^{-2}hr^{-1}$ at the end of this period. Stirring was then commenced, and the corrosion rate increased to 27.5 $g.m^{-2}hr^{-1}$.

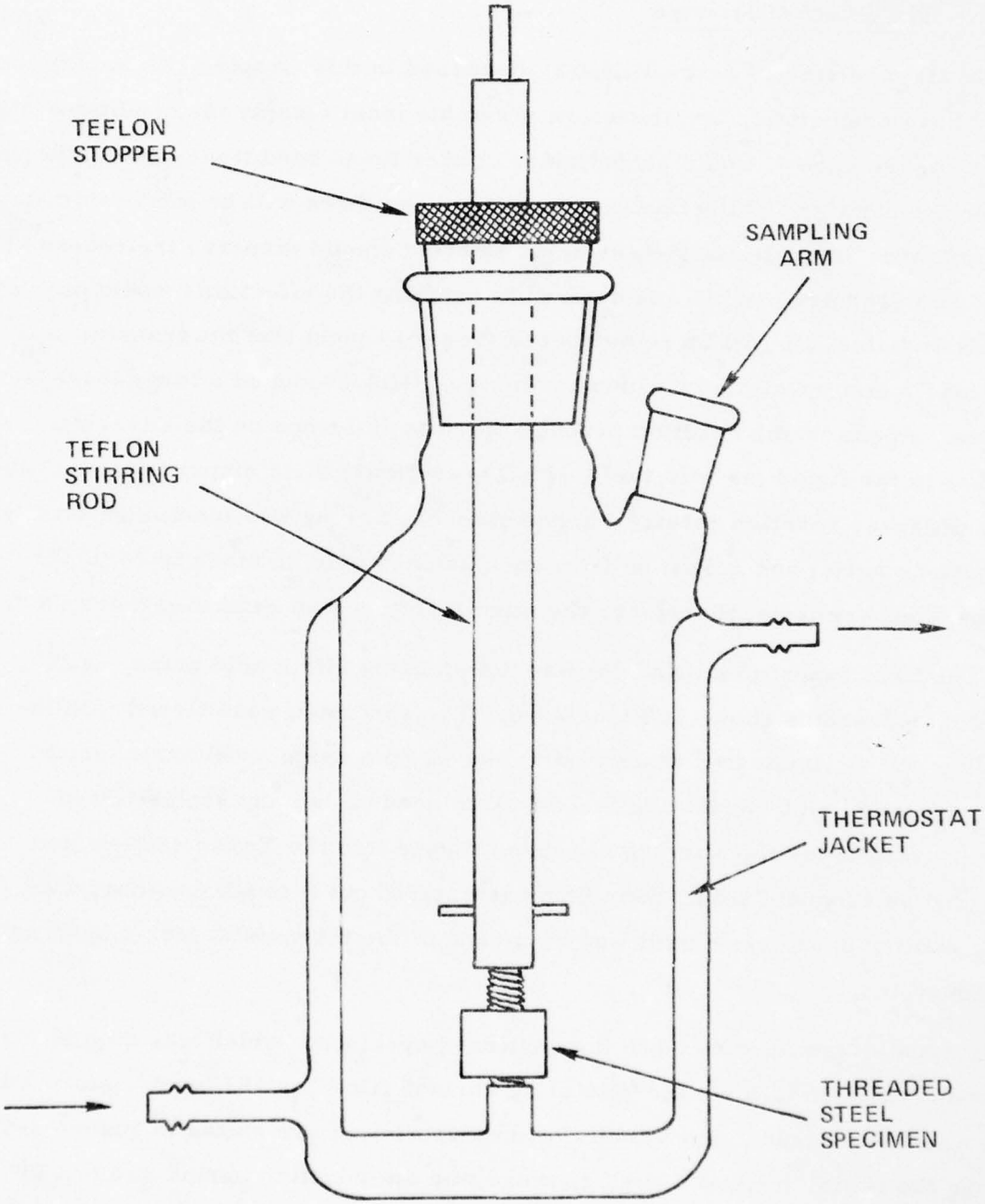


Figure 3-8. Stirring Apparatus

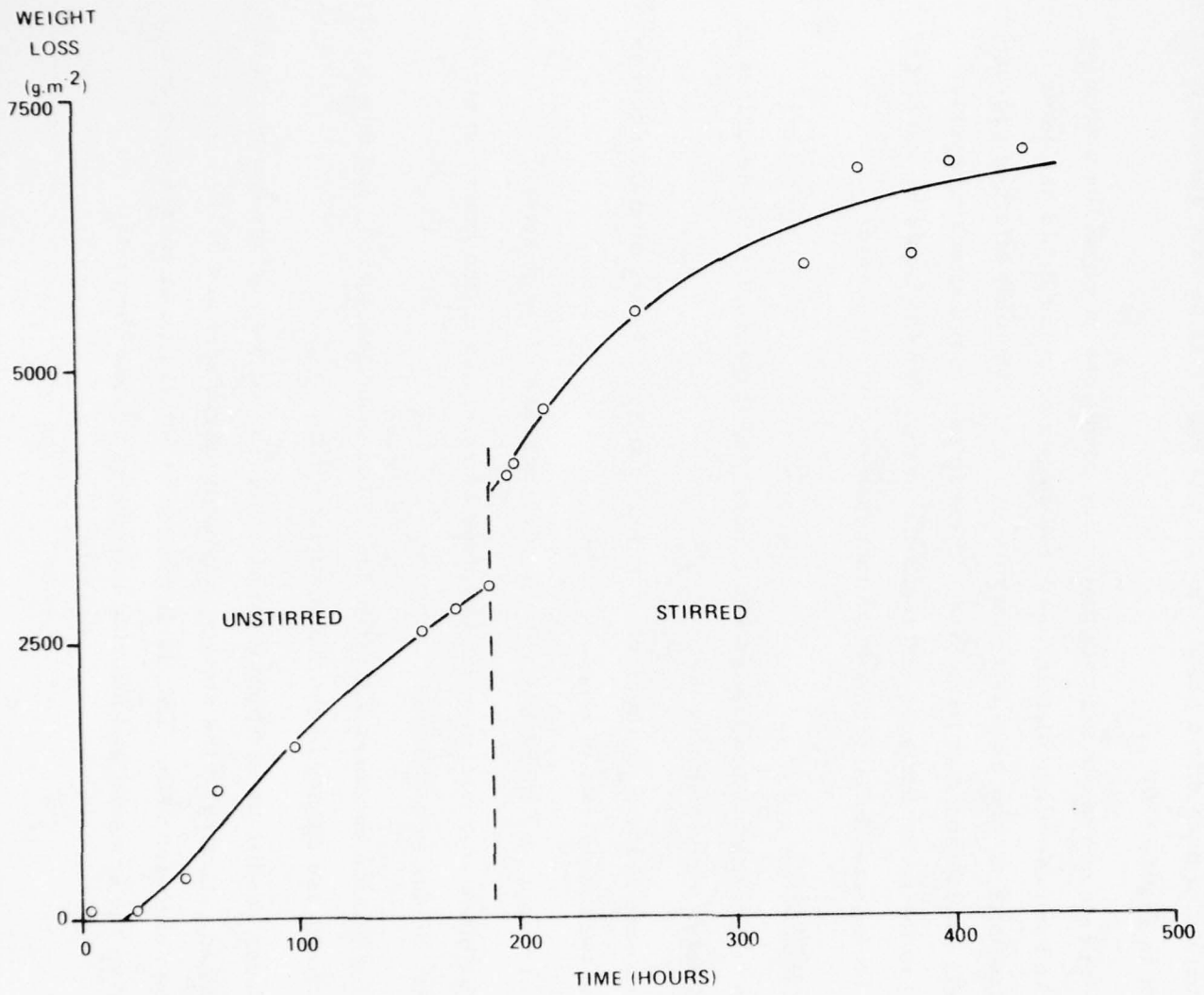


Figure 3-9. Weight Loss Curve for a Specimen of 321 Stainless Steel in 100% Nitric Acid at 20°C (Expt 25)

A second experiment (which is still running at the time of preparation of this report) has been set up which is identical with Expt. 25 except that HDA is used instead of pure nitric acid. The results appear to be very similar to those present in Figure 3-9.

Both sets of results indicate that under conditions in which the activating film has been established, stirring of the specimen in the liquid has some effect, but introduces no new chemistry into the system. The only effect of corrosion products would appear to be to hinder the diffusion of the attacking species (NO_2^+) to the metal surface, and their dispersion into the liquid by stirring would be expected to give rise to an increase in corrosion rate.

3.4 Conclusions

So far as uninhibited liquids are concerned, the experiments described in this Chapter would indicate that:

1. Increase in the N_2O_4 content of uninhibited N_2O_4/HNO_3 mixture decreases the corrosion rate of steel.
2. Corrosion rate increases rapidly with increase in temperature.
3. The black colouration which develops on steel during the induction period may be due to a discrete compound.
4. The surface becomes activated during the induction period, and this occurs through the agency of the black surface film.
5. Under conditions in which the activating film on the surface has been established, stirring of the steel specimen in nitric acid and in HDA increases the corrosion rate. This is attributed to dispersion of corrosion products from the surface, and stirring introduces no new chemistry.

6. In experiments of long duration, the compound which eventually precipitates from HDA is pure $Ni(NO_3)_2 \cdot 2H_2O$, and the precipitate contains no iron or chromium.

7. Nickel is the key element which dominates corrosion rates. The solubility of $Ni(NO_3)_2 \cdot 2H_2O$ depends upon N_2O_4 content and Fe and Cr concentration in solution, but corrosion becomes much slower when the solution is saturated with the nickel compound.

8. The ratio surface area of metal/volume of liquid influences both the extent and rate of corrosion.

3.5 References

1. C. C. Addison and J. Lewis, J. Chem. Soc., 1951, 2833.

2. C. C. Addison, J. Lewis and R. Thompson, J. Chem. Soc. 1951, 2838.

3. C. C. Addison and J. Lewis, J. Chem. Soc., 1951, 2843.

4. I. P. Mukanov, S. D. Beskov and L. I. Kochetkova, Z. Prikl. Chem., 1960, 33, 2084.

5. S. D. Beskov, Y. D. Sova and L. I. Kochetkova, Z. Prikl. Chem., 1967, 40, 330.

6. E. Berl and H. H. Saenger, Monatsh. Chem. 1929, 53, 1036.

7. Personal Communication to Professor C. C. Addison during visit to Bell Aerospace, Buffalo, 1974.

8. T. H. James, J. Amer. Chem. Soc. 1943, 65, 39 and references therein.

4. CORROSION RATES IN INHIBITED HNO_3 - N_2O_4 MIXTURES

4.1 Introduction

A number of experiments were carried out to obtain quantitative corrosion information on inhibited N_2O_4/HNO_3 systems in contact with 321 stainless steel, which were compared with the corrosion data obtained from uninhibited systems. In this report, "Standard" HDA refers to HDA inhibited by HF, and "Modified" HDA refers to HDA inhibited by PF_5.

In considering the existing knowledge of the behaviour of HF and PF_5 inhibited N_2O_4/HNO_3 systems, there was one issue which appeared to be of prime importance. In uninhibited systems, the rate of corrosion of stainless steel decreases with increasing N_2O_4 content (Chapter 3). However, experience in the storage of inhibited HDA (Bell Aerospace Co.) indicates that the corrosion increases with increasing N_2O_4 content and that although HF was successful in inhibiting red fuming nitric acid (14 wt% N_2O_4) it was not adequate when used with HDA (44 wt% N_2O_4). Efforts to resolve this apparently contradictory evidence are reported in this Chapter, and a direct comparison of the effect of HF and PF_5 as inhibitors has been made.

In addition to obtaining the quantitative corrosion results mentioned above, a study of the surfaces of stainless steel samples exposed to inhibited HDA, including an investigation using electron spectroscopy for chemical analysis (ESCA) has been made. This is described later in this chapter.

4.2 Corrosion using polypropylene containers

The inclusion of fluorine-containing inhibitors ruled out the use of the standard glassware apparatus used in the work on uninhibited liquids, and our first experiments on inhibited HDA were carried out in vessels made from polypropylene.

(a) Experimental

Polypropylene showed considerable resistance to attack from uninhibited HDA. Furthermore, as commercial aqueous solutions of HF are often supplied in polypropylene, it seemed reasonable to expect that short duration experiments with inhibited HDA might be possible using standard (300 ml. capacity) polypropylene containers with screw-on lids fitted with Teflon seals. This proved to be the case. In practice it was possible to store inhibited HDA in these containers at 25°C for up to 7 weeks; however, deterioration of the polypropylene appeared to occur on longer storage.

Inhibited HDA was made up by measuring out the required amount of cooled HDA into the containers. The inhibitor was then added to the form of a frozen solid contained in a short length of FEP tube. This tube was initially connected to the all-Kel-F/FEP vacuum line and evacuated to a pressure of 10^{-6}mm. The required amount of HF or PF_5 was then condensed into the tube and frozen using liquid nitrogen. Argon gas was then allowed into the line, the tube was disconnected, and the argon gas was immediately added to the cool HDA in order to provide protection from atmospheric moisture during the short period of exposure.

In each of these experiments, two discs of 321 stainless steel, each 15 mm in diameter and 2.5mm thick, were immersed in 50ml. of HDA containing 0.6 wt% of inhibitor, as per propellant specification. Corrosion rates were obtained by withdrawing one ml. of solution at intervals and analysing for metal by atomic absorption (see Appendix B.2).

(b) Comparison of corrosion rates of 321 steel by uninhibited, standard and modified HDA at 25°C

The observed corrosion rates are shown in Fig. 4-1 and Fig. 4-2. Fig. 4-1 indicates the marked difference in corrosion rates between uninhibited and standard HDA. Fig. 4-2 shows the superiority of PF_5 over HF as an inhibitor. For

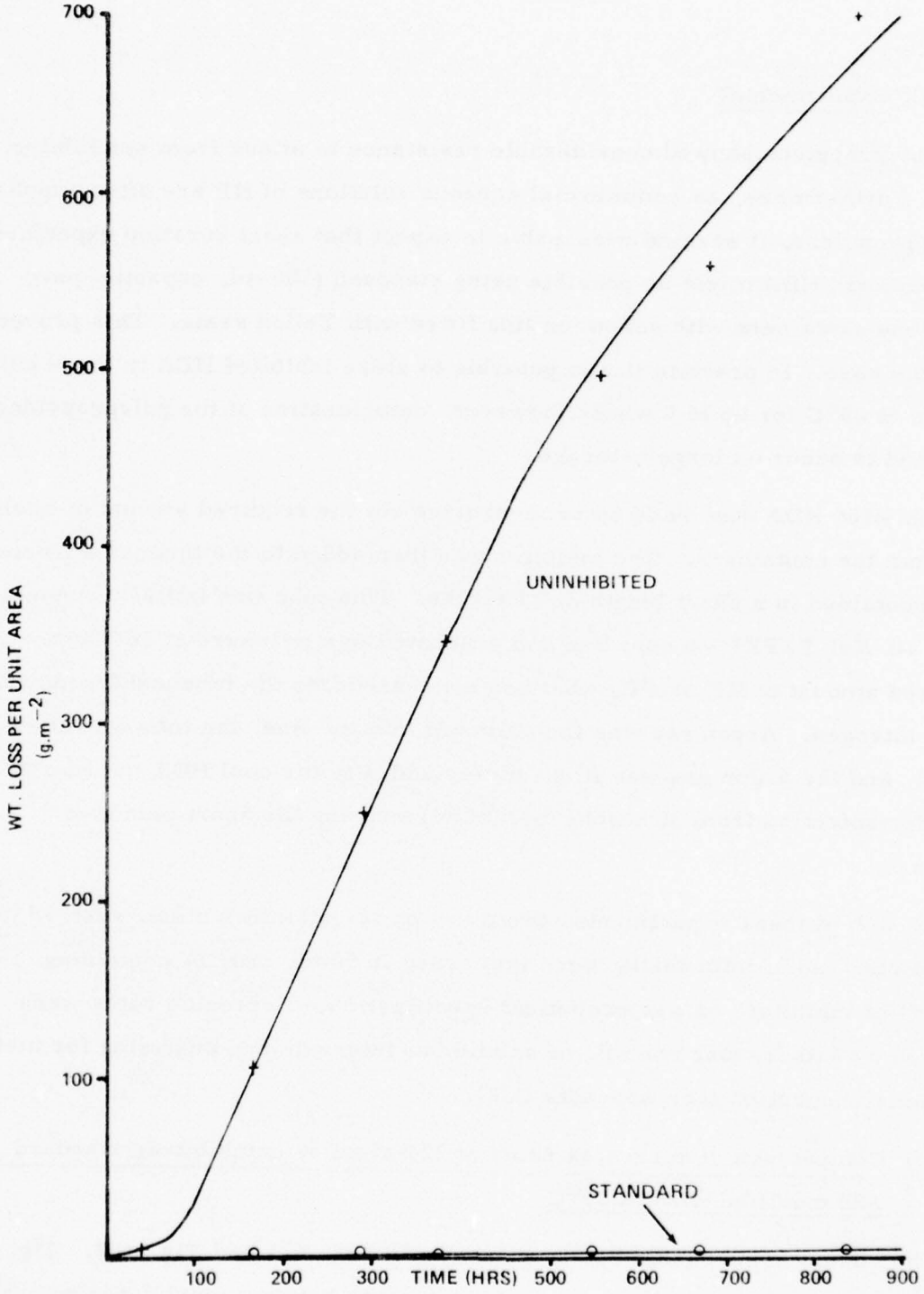


Figure 4-1. Corrosion of 321 Steel by Uninhibited and Standard HDA at 25°C (Polypropylene Vessels)

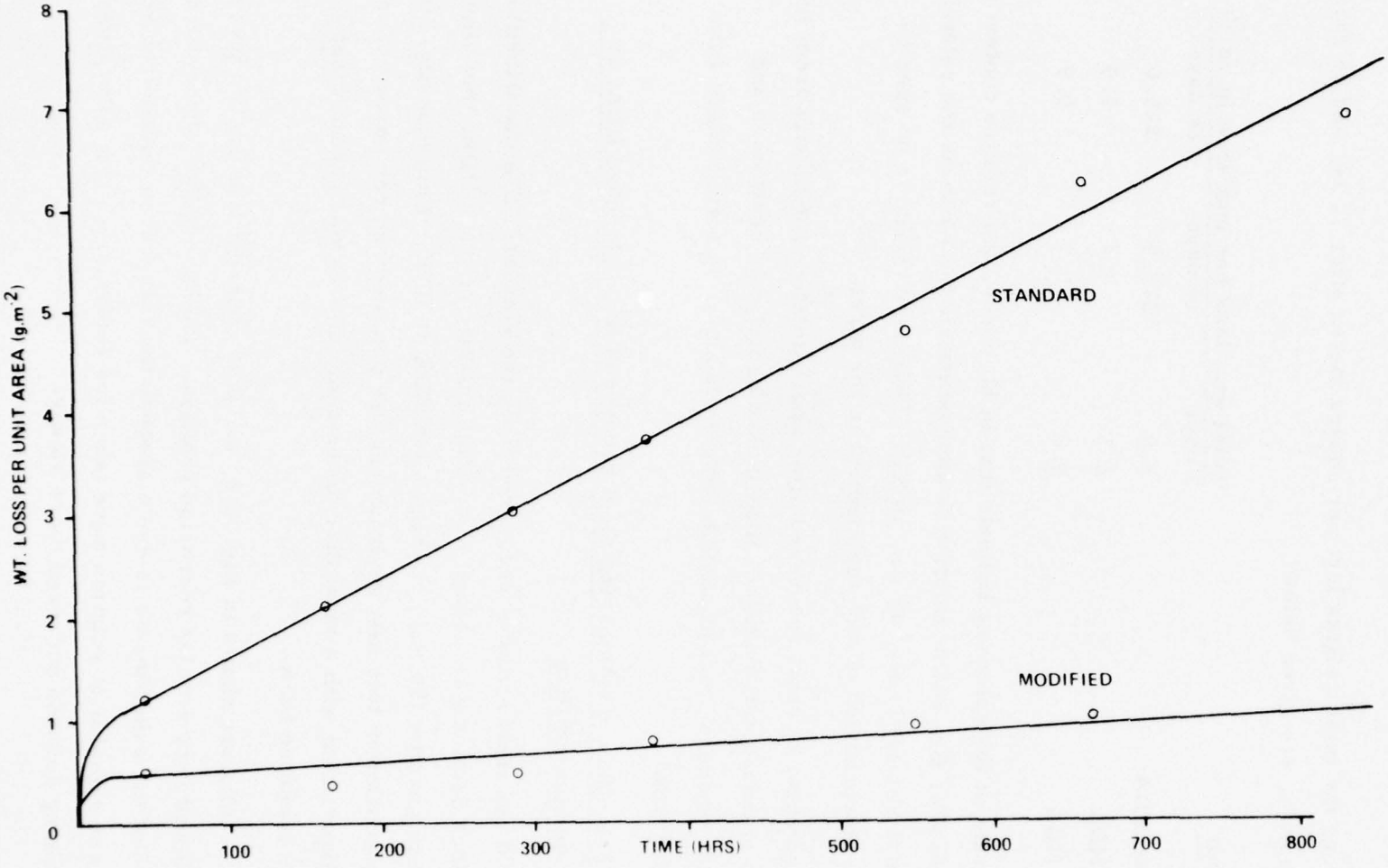


Figure 4-2. Corrosion of 321 Steel by Standard and Modified HDA at 25°C (Polypropylene Vessel)

comparison, the total weights lost per square metre after 7, 14, and 28 days in each system, are given below

System	Total wt. loss per unit area ($g.m^{-2}$)		
	7 days	14 days	28 days
Uninhibited HDA	3.9	275.0	575.0
Standard HDA	2.1	3.4	5.9
Modified HDA	0.6	0.7	0.9

Analysis of the solutions indicate that in all cases, the relative content of each metal (Fe, Cr, Ni) in solution is approximately the same as the relative content in the steel (71 Fe, 18 Cr, 10 Ni). Therefore, there is no specific inhibition or corrosion of any one element in the steel.

The samples of steel recovered after approximately 1000 hours from inhibited (both standard and modified) HDA looked completely unattacked and unchanged, whereas steel in uninhibited acid is known to form a black film within a few days.

(c) The effect of immersing steel recovered from standard HDA, in uninhibited HDA

One of the steel samples recovered from the standard HDA described in the previous Section was washed in a small quantity of fresh HDA, then immersed in a further quantity (50 ml.) of uninhibited HDA at 20°C. Consequently, its rate of corrosion in this new environment was obtained and compared with a control experiment with a steel disc of the same dimensions but not treated previously in inhibited HDA.

The results are shown in Fig. 4-3, and it is apparent that the two pieces of steel followed very similar corrosion profiles. The divergence of the two curves at the end of the experiments is due merely to the fact that in the control experiment fewer samples of solution were taken for analysis, so that saturation of the remaining solution occurred more slowly.

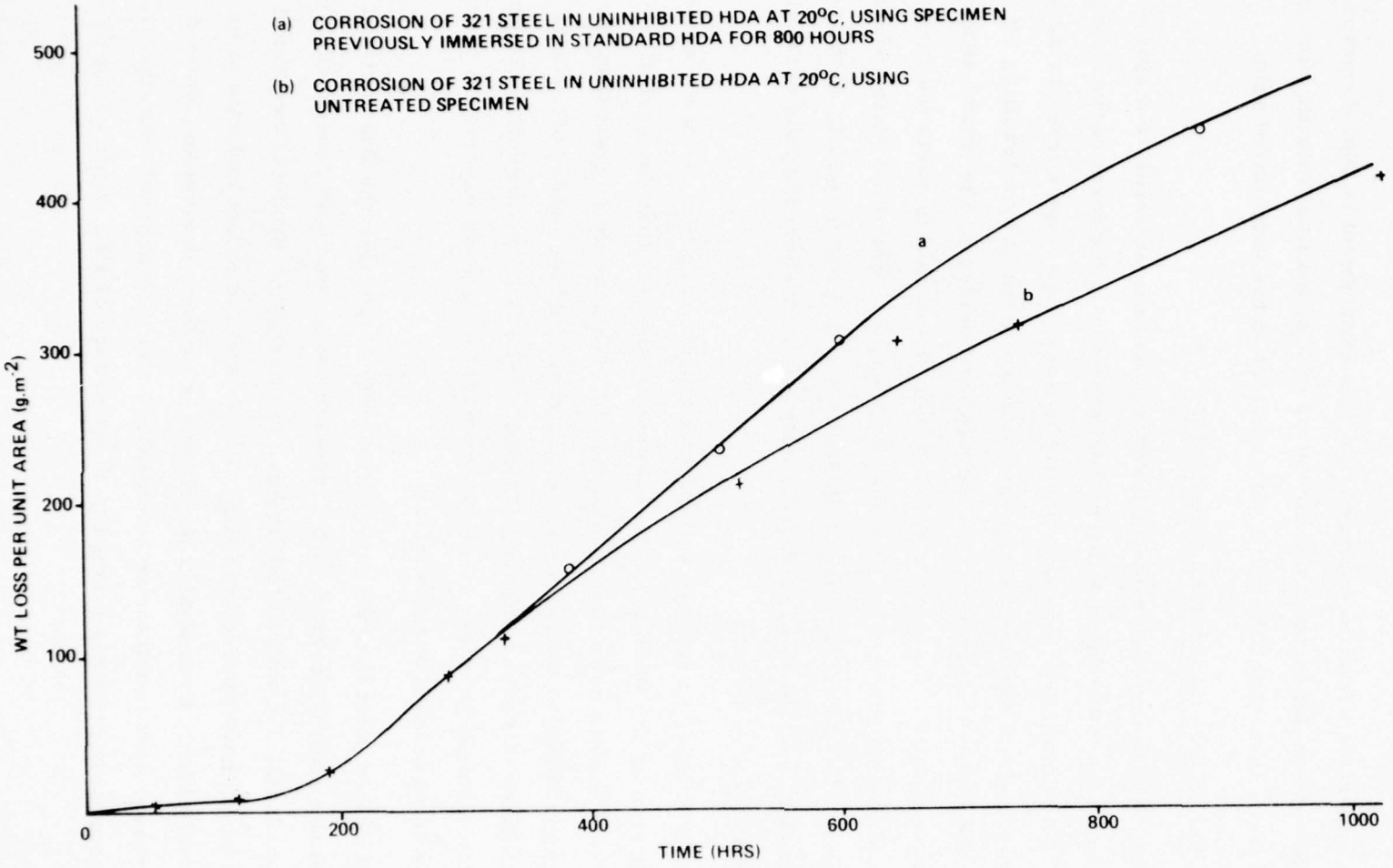


Figure 4-3. Comparison of Steel Previously Treated in Standard HDA and Steel not Treated in Standard HDA in Uninhibited HDA

The important result to emerge from this experiment is that if corrosion inhibitors were to act through the formation of a protective fluoride film on the steel surface, then such films are not resistant to the uninhibited acid.

(d) The shape of corrosion rate curves

Apart from the considerable difference in corrosion rates, a major difference between the uninhibited and inhibited systems is the form of the reaction profile. The uninhibited reaction profile is a typical s-type curve having an induction period, a period of steady corrosion, followed by a levelling off as the solution approaches saturation. In the inhibited systems, the initial attack is rapid, but quickly falls off and a constant corrosion rate is observed for the duration of the experiment (in this case 800 hours). The main factor which is considered to be responsible for this effect is the low solubility of the corrosion product. Thus saturation is rapidly attained whereupon the corrosion rate is greatly diminished.

The other obvious interpretation, that a protective film is produced on the metal surface by the inhibitor, is weakened by the fact that any such film which may form is broken down in uninhibited acid. This would suggest that any such film is more likely to consist of a chemisorbed fluoride layer rather than a resistant layer of some compound. Again, there is no preferential dissolution of any one element from the steel, which might have been expected if molecular fluorides were formed at the surface.

It is at this point that we can conveniently emphasise the link between that aspect of the work concerned with corrosion rates, and that concerned with corrosion products. In uninhibited liquids, the corrosion products are metal nitrates which have appreciable solubilities, and the extent and rate of corrosion is relatively high. Presumably the fluorides or their derivatives formed when HF is present have much lower solubilities, and it is probable that the solubilities of corrosion products formed in the presence of PF_5 would be lower still.

4.3 Corrosion experiments using Teflon containers

In view of the valuable and informative experiments conducted in polypropylene vessels, work on inhibited systems was expanded. There is no reason to believe that polypropylene containers are unsatisfactory for any but the most protracted experiments, but it seemed worthwhile to prepare a new apparatus in the most resistant material (i.e. Teflon), and to develop a design which would minimise loss of vapour, and thus loss of inhibitor, during sampling.

(a) Experimental

The resulting design, constructed entirely of Teflon, Kel-F and FEP is shown in Fig. 4-4.

Sampling of the solution is achieved by connecting a length of FEP tube to the valve. When the valve is opened, the solution rises up into the tube due to the internal vapour pressure in the vessel. When the liquid level in the tube reaches a fixed mark corresponding to ca. 2ml of liquid, the valve is closed, the solution is poured into a small pre-weighed polyethylene sample bottle and the bottle is quickly stoppered and re-weighed. The sample bottle is then opened, and the solution allowed to degas overnight before being diluted with triply distilled water prior to analysis by atomic absorption. A final weighing of the diluted acid enables the overall dilution factor (allowing for degassing) to be found. The metal concentrations in aqueous solution, and in the original HDA, can then be calculated.

After sampling, the sample tube is disconnected from the valve, and both are washed with Inhibisol and blown dry. The open end of the valve is then sealed to prevent ingress of foreign matter.

It may be noted that this process results in a small quantity of solution remaining isolated in the valve and delivery tube. As this is not able to mix with the bulk solution it is necessary to purge this liquid before the next sample is withdrawn. This is done either by expelling approximately 2 ml. of liquid

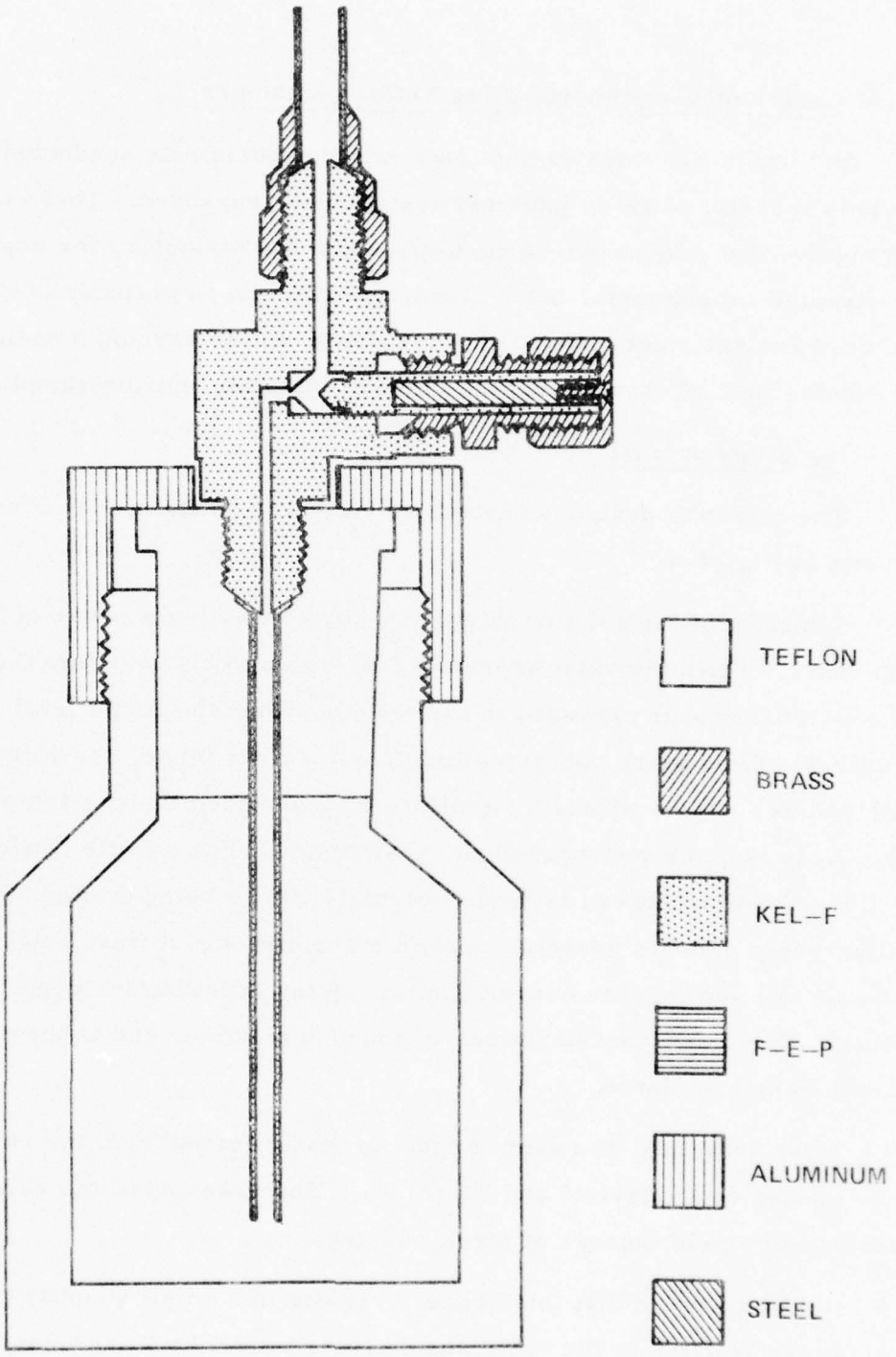


Figure 4-4. Vessel Used for Inhibited HDA Corrosion Work

before the actual sample is taken, or by inverting the container, allowing the trapped liquid to be 'blown' out by the internal vapour pressure. The latter technique, whilst being perhaps the most thorough method, can result in some loss of vapour.

Inhibited HDA was made up as described in Section 4.2(a). In all experiments carried out in the Teflon containers 120ml. of solution was used, this containing 0.6 wt% inhibitor in accordance with propellant specification. In each experiment two short rods of 321 stainless steel (each 14 mm. long and 18 mm. in diameter) were used; no pre-treatment of the steel samples was performed other than degreasing in Inhibisol. Accordingly, in all the experiments in this Section the surface area to volume ratio remains constant at $0.22 cm^{-1}$.

(b) Comparison of corrosion rates of 321 steel by uninhibited, modified and standard HDA at 34°

These experiments repeat those described under 4.2(b) above, but were carried out in the improved Teflon apparatus. They were carried out essentially to confirm that the important comparisons observed using the polypropylene apparatus were in fact true, and were not influenced by the nature of the container materials. The new Teflon apparatus also allowed work at a higher temperature without loss of vapour. These experiments were carried out at 34°C, which provided an opportunity to examine the effect of temperature in inhibited systems. Figures 4-5 and 4-6 show the observed corrosion rates for uninhibited, standard, and modified HDA. As in the experiments at 25° (Section 4.2 (b)), it is clear that while the use of HF as inhibitor very greatly reduces the rate of corrosion, PF_5 reduces the corrosion rate further still, so much so that in this experiment the rate was almost immeasurably small over 1000 hours.

The form of the corrosion profiles is also generally the same as in the 25° (polypropylene) results. The total weight loss per square metre for periods of 7, 14, and 28 days is given below; and the general picture closely resembles that already presented under 4.2(b).

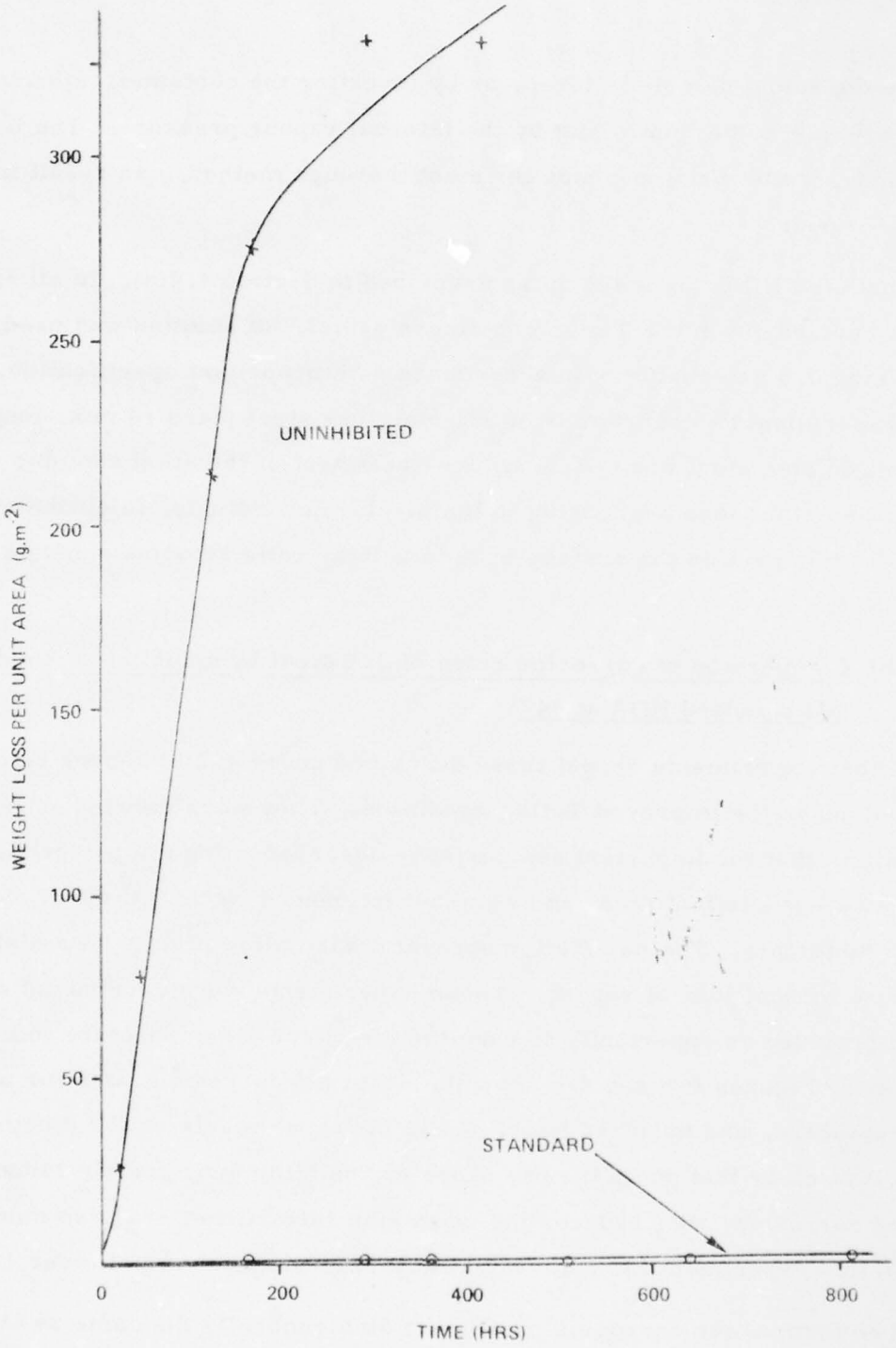


Figure 4-5. Corrosion of 321 Steel by Uninhibited and Standard HDA at 34°C (Teflon Vessels)

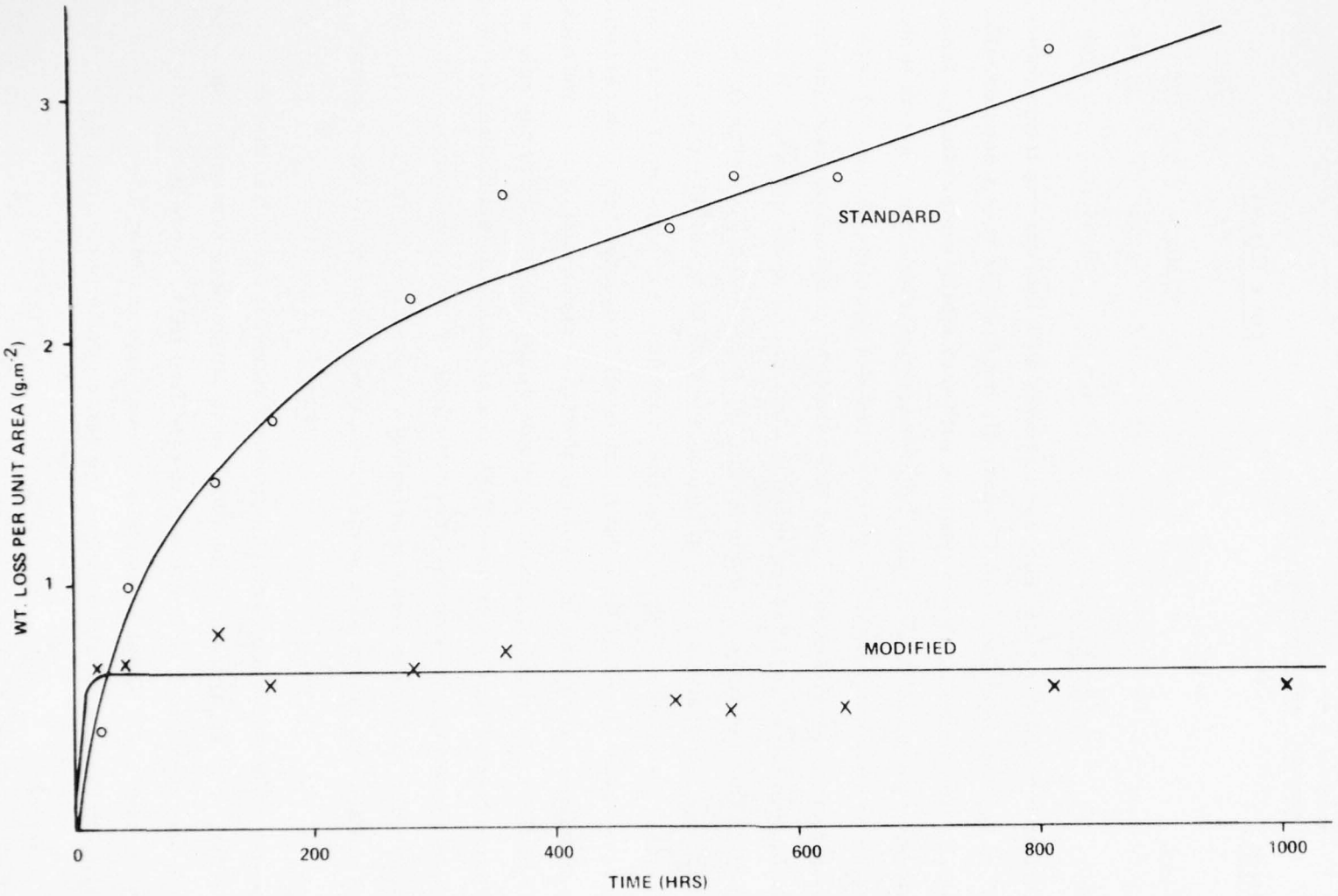


Figure 4-6. Corrosion of 321 Steel by Standard and Modified HDA at 34°C (Teflon Vessels)

Table 4-1. Comparison of weight loss per unit area ($g.m^{-2}$) in uninhibited, standard, and modified HDA

System	Time (Days)		
	7	14	28
Uninhibited	27.9	330	330
Standard	1.70	2.24	2.85
Modified	0.64	0.64	0.64

The uninhibited corrosion rate increases greatly with increase in temperature from 25° to 34° (as expected from Chapter 3), but there is now a considerable decrease in rate for the inhibited systems with increasing temperature. More work will be required to confirm this inverse temperature effect, but as there seems to be no reason to doubt it, we may consider possible causes. There is a possible clue in the report [1] that the solubility of chromium fluoride complexes in fuming nitric acid passes through a maximum at about 35°C. It seems quite possible that the position of the maximum in the solubility curve could change with the composition of the solution, and that in inhibited HDA, it could be appreciably lower than 35°C. If so, the solubility of chromium fluoride could even decrease over the range 25 - 34°C. It is also reported that such chromium fluoride complexes are much less soluble than the corresponding iron and nickel species, so that chromium corrosion products could play the same key role in the corrosion mechanism in inhibited HDA as does nickel in uninhibited liquids. It is also important to note that the concentrations of iron, chromium, and nickel in solution are in the same approximate proportions as in the steel. Thus, when one metal is no longer able to dissolve, the solution of all three metals stops.

An experiment has been carried out which supports the belief that the saturation effect is as significant in inhibited as in uninhibited systems. Figure 4-6 shows that when steel is immersed in modified HDA, there is an initial attack over a period of about 24 hours and metal appears in solution. Thereafter, the metal concentration remains the same over a period of 1000 hours.

In an attempt to determine whether the solution had become saturated at this low concentration level, the Teflon vessel was cooled to -10°C and opened against a slight counter-current of argon gas which prevented ingress of atmospheric moisture. Two more specimens of stainless steel, exactly similar to the original specimens, were added to the solution, the vessel was closed and the temperature was restored to 34°C. Analysis of samples of the HDA over the next 500 hours showed no significant increase in concentration of metals in solution. This result implies that in spite of the very low concentration of metals in modified HDA, this does indeed represent saturation of HDA by the type of corrosion product formed in the presence of PF_5.

(c) The effect of N_2O_4 concentration on the corrosion of 321 steel by HF-Inhibited, N_2O_4 - HNO_3 mixtures

The corrosion rates of four HF-inhibited solutions, containing 44, 30, 14 and 0 wt.% N_2O_4 in HNO_3, were measured. Each contained 0.6 wt.% HF and all were at a temperature of 34°C. The observed corrosion rates are shown in Fig. 4-7.

The most important result, which is immediately obvious, is the considerable increase in corrosivity of these solutions as the N_2O_4 concentration increases, particularly in the range of 20 to 44 wt.% N_2O_4, where the rate of corrosion increases by a factor of about 6. Fig. 4-8 shows weight loss curves for the four solutions for times of 200, 400 and 800 hours.

The curve for pure HNO_3 (Figure 4-7) is somewhat anomalous in showing a plateau during which no corrosion occurs, but for each of the HNO_3 - N_2O_4 mixtures (Fig. 4-7) the curves are of the same shape, and all show continuing corrosion at an almost constant rate, over periods up to 1000 hours. This may be due to slow solution of the corrosion product, but is more likely to reflect a slow change in the species present in the solution, with a slow change to a corrosion product having a higher solubility.

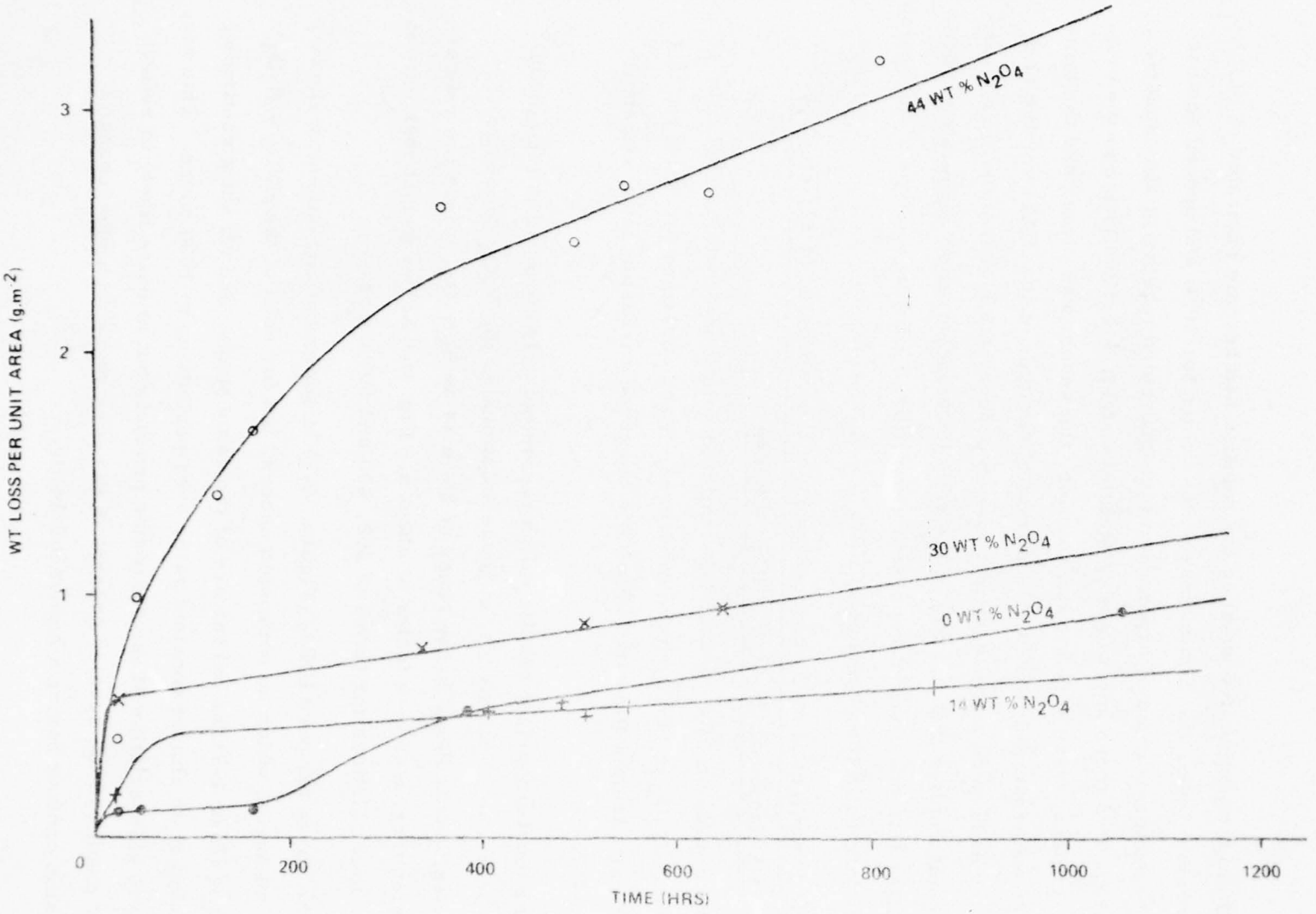


Figure 4-7. Corrosion Rates of 321 Steel by HF-Inhibited N_2O_4/HNO_3 Mixtures at 34°C

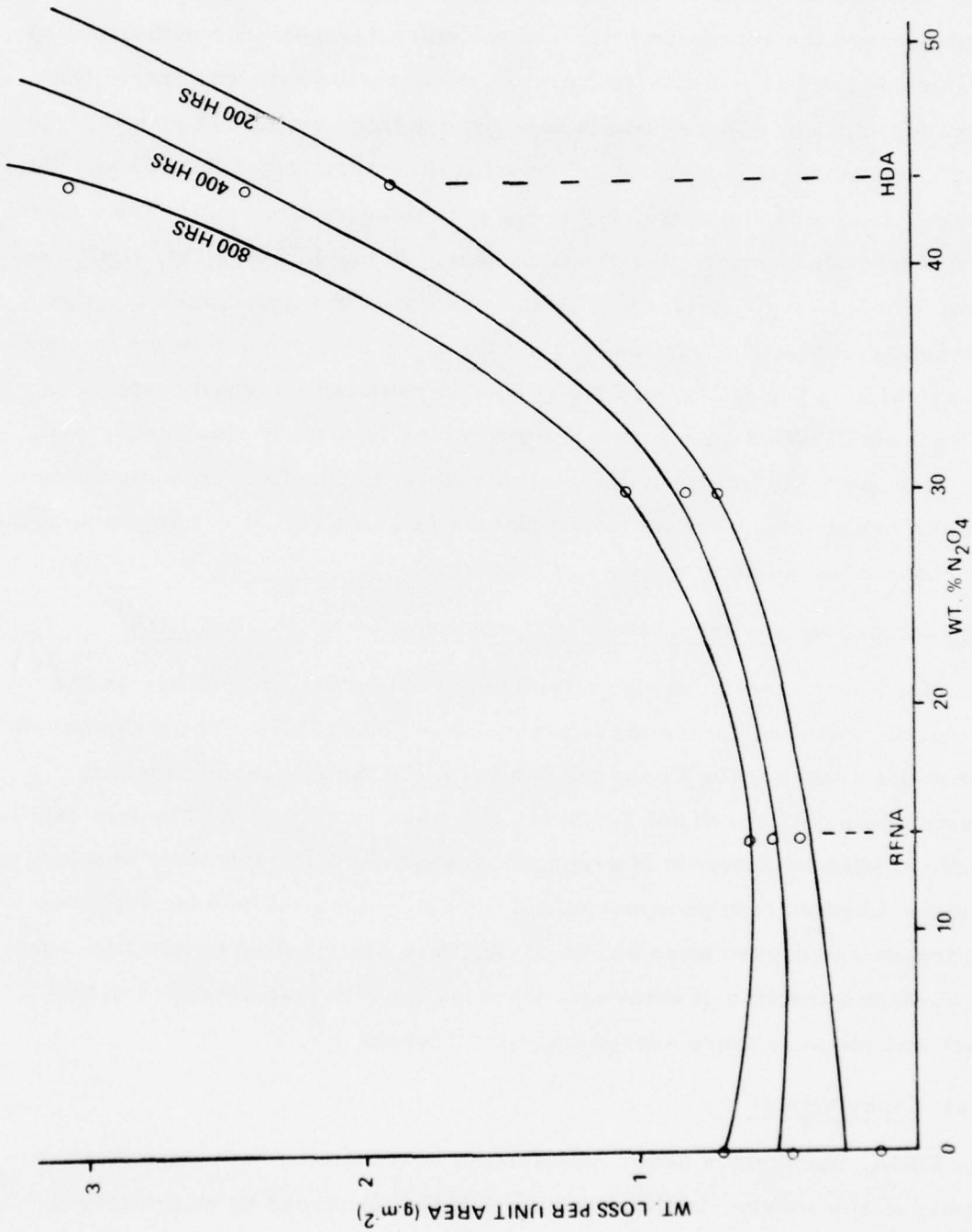


Figure 4-8. Effect of N_2O_4 Content on Corrosion of 321 Steel by HF-Inhibited Mixtures after 200, 400, and 800 Hours at 34°C

At the beginning of this Chapter, mention was made about the apparent conflict between our experimental results with uninhibited HDA, where additional N_2O_4 decreased the corrosion rate, and the storage experience with inhibited HDA which seemed to indicate an increase in corrosion rate with increasing N_2O_4 concentration. These results now remove this conflict because it is clear that N_2O_4 concentration operates in opposing directions with inhibited and uninhibited HDA. In comparing these, however, it is important to realise the different orders of magnitude involved in the two cases. In uninhibited HDA, N_2O_4 concentration has a very considerable effect on corrosion rates, which are themselves considerable. In relation to this, the rates of corrosion in the presence of HF are almost negligible, and N_2O_4 concentration in inhibited systems is exerting a small effect on a corrosion rate which is already relatively small. Theories on possible interpretations of this small N_2O_4 effect could be made, but this is better done when a clearer picture of exactly what is happening at the metal surface in inhibited systems is obtained.

4.4 Spectroscopic studies of steel surfaces exposed to inhibited HDA

In these experiments, it was attempted to obtain direct evidence on the nature of the metal surface after exposure to inhibited HDA. The technique of Electron Spectroscopy for Chemical Analysis (ESCA) was used to identify elements present on the metal surface. Previous examination of metals exposed to modified HDA by Electron Microprobe Analysis (EMP) and other spectrographic techniques detected both phosphorus and fluorine on the surface but indicated that nitrogen and oxygen were absent.[2] ESCA is more suited to thin film analysis, down to a fraction of coverage, whereas EMP is less sensitive in this respect and requires more substantial film thickness.

(a) Experimental

In ESCA, the surface under examination is irradiated with a strong monoenergetic X-ray source, in this case the $K\alpha$ line produced by an aluminum

anode. These high energy electrons penetrate atoms on the surface displacing other electrons from the core electron levels. The core electrons in a particular element are held by the nucleus with a binding energy characteristic to that system. This binding energy may be obtained by subtracting the kinetic energy of the displaced electrons from the energy of the incident radiation. Thus a spectrum is obtained consisting of monokinetic electron lines from which the core binding energies (E_B) may be calculated and the surface species identified. The core binding energies, though governed primarily by the atomic nucleus are also slightly dependent on the surrounding valence electrons involved in the chemical bonding of the atom. Thus the nature of the bonding and other factors associated with the environment of the atoms bring about small 'shifts' in the core binding energies. This form of ESCA is sometimes referred to as X-ray photoelectron spectroscopy (XPS). All the work described here is of the XPS form and all binding energies are core electron binding energies.

(b) Sample Preparation

Specimens of 321 steel were immersed in standard HDA, modified HDA and liquid anhydrous hydrogen fluoride respectively. The specimens, each 6mm square and 0.5mm thick, were immersed in 20ml. of the appropriate solution in a 15mm. diam. Kel-F tube fitted with a valve. They were not subjected to any prior surface treatment other than degreasing in Inhibisol. The three tubes were stored at room temperature for 20 days. At the end of this period the metal samples were recovered from the solutions, washed carefully in liquid N_2O_4 to remove all traces of inhibited solution, and dried in a current of argon gas.

(c) ESCA Examination

This was performed using an 'ESCA 3' instrument manufactured by Vacuum Generators, Surrey, England. The metal samples were mounted on the instrument probe in open air so that some absorbed atmospheric gases, predominantly CO_2, are to be expected.

Examination of each surface was carried out along the following lines:-

(1) A general 1000 eV scan, with the instrument scanning for a 20 minute period for electrons having a kinetic energy of 1500 to 500 eV. This preliminary scan reveals all the species present on the exposed surface.

(2) A narrow band scan of 10 or 20 eV over the region of the spectrum corresponding to a particular species, in this case fluorine (795 to 805 eV) and phosphorus (1345 to 1355 eV). This scan measures the precise position of the peaks, so that very small shifts in binding energy may be observed.

(3) The surface was then etched using a beam of high energy argon ions, thus removing material uppermost on the surface and revealing the material below.

(4) The general 1000 eV scan was repeated.

(5) The narrow band scan was repeated.

(6) This process could be repeated at will.

In this way a complete picture of all the elements present on the original surface, and below that surface could be obtained. A number of elements are revealed in the spectra which do not originate either in the steel or the solutions. Carbon has already been mentioned; this arises from adsorbed atmospheric CO_2, and the carbon peaks diminish considerably after initial etching of the surfaces. Gold and molybdenum peaks arise from the wire used to mount the steel samples on the ESCA probe.

Output from the ESCA spectrometer was recorded directly in graph form by pen recorder and also on punched paper tape. The resolution of ESCA spectrometers is such that peaks occurring very closely together in the spectrum (within 1 to 2 eV) cannot be separated. However, when an element is present in two different chemical species the E_B shifts are usually so small that only

a single broad peak is obtained, which often shows an assymetric shape due to differing intensities in the two component peaks. Such composite peaks may be resolved into their individual components by computer analysis, and for this reason it is necessary to store data, as in this case, on paper tape.

(d) Examination of the surface of 321 steel exposed to standard HDA

Fig. 4-9 shows the general spectrum before and after 90 seconds etching and the observed peaks are listed in Table 4-2. Before etching, both the fluorine and oxygen peaks are strong. After etching, the oxygen peak diminishes slightly, whilst the fluorine peak becomes more intense. The carbon peak diminishes considerably so that although some oxygen will arise from adsorbed CO_2, most of the oxygen is a true component of the surface.

A nitrogen peak would occur at an E_B of about 400 eV; there is no evidence of nitrogen, and this is a highly important observation from the point of view of the mechanism of corrosion. A general scan was also recorded after 15 seconds etching, but it shows only an intermediate situation between the two other scans and is not presented.

Narrow band scans over the E_B range 680 to 690 eV for the fluorine peak were carried out after etching for 0, 15, 30, and 90 seconds and the first two of these are shown in Figure 4-10. The scan of the original surface shows a reasonably symmetrical fluorine peak, centered at a binding energy of about 684.2 eV. After 15 seconds etching the peak changes in shape, intensity and position. The new peak is about twice as intense as the original, is assymetric, and occurs at 683.5 eV. The peaks recorded after 30 and 90 seconds etching are very much the same as that recorded after 15 seconds etching. It appears that the environment of the fluorine on the metal, the surface remains constant for an appreciable depth. The assymetric shape of the peak indicates however, that the fluorine atoms may be bonded in more than one way.

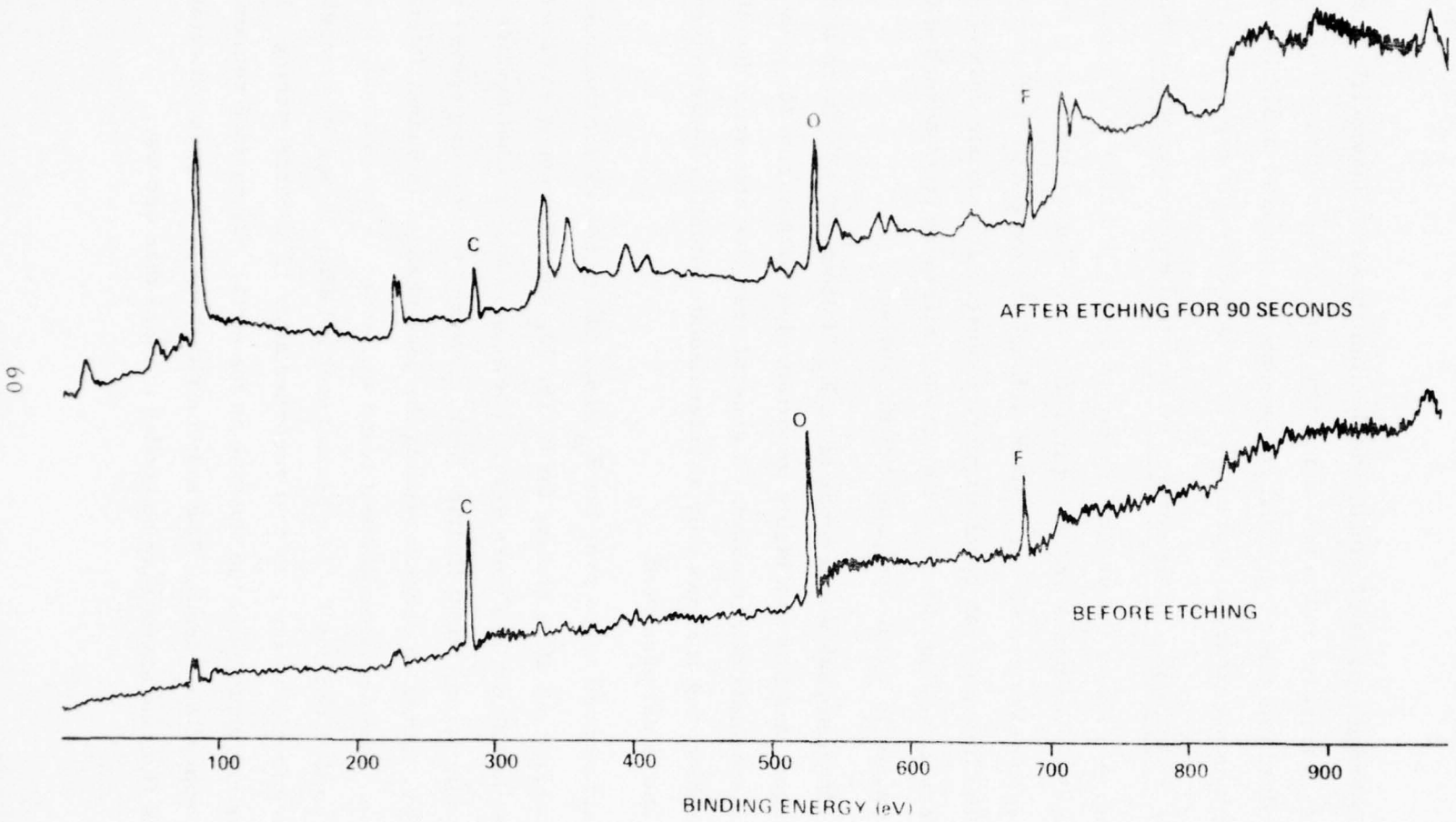


Figure 4-9. ESCA Spectra of Surface of 321 Steel after Exposure to Standard HDA

Table 4-2. General ESCA Spectrum of Surface of 321 stainless steel recovered from standard HDA

Binding energy, E_B (eV)		
As Received	After 90 sec. etch with argon gun	Assignment
80 w	80 vs	Au 4f
225 vw	225 m	Mo 3d
280 s	280 m	C 1s
	330), 350) m	Au 4d
525 vs	525 vs	O 1s
	575), 585) w	Cr 2p
	635 w	Au 4s
680 m	680 vs	F 1s
	710), 715) w	Fe 2p

(all bands above 750 eV are Auger emissions)

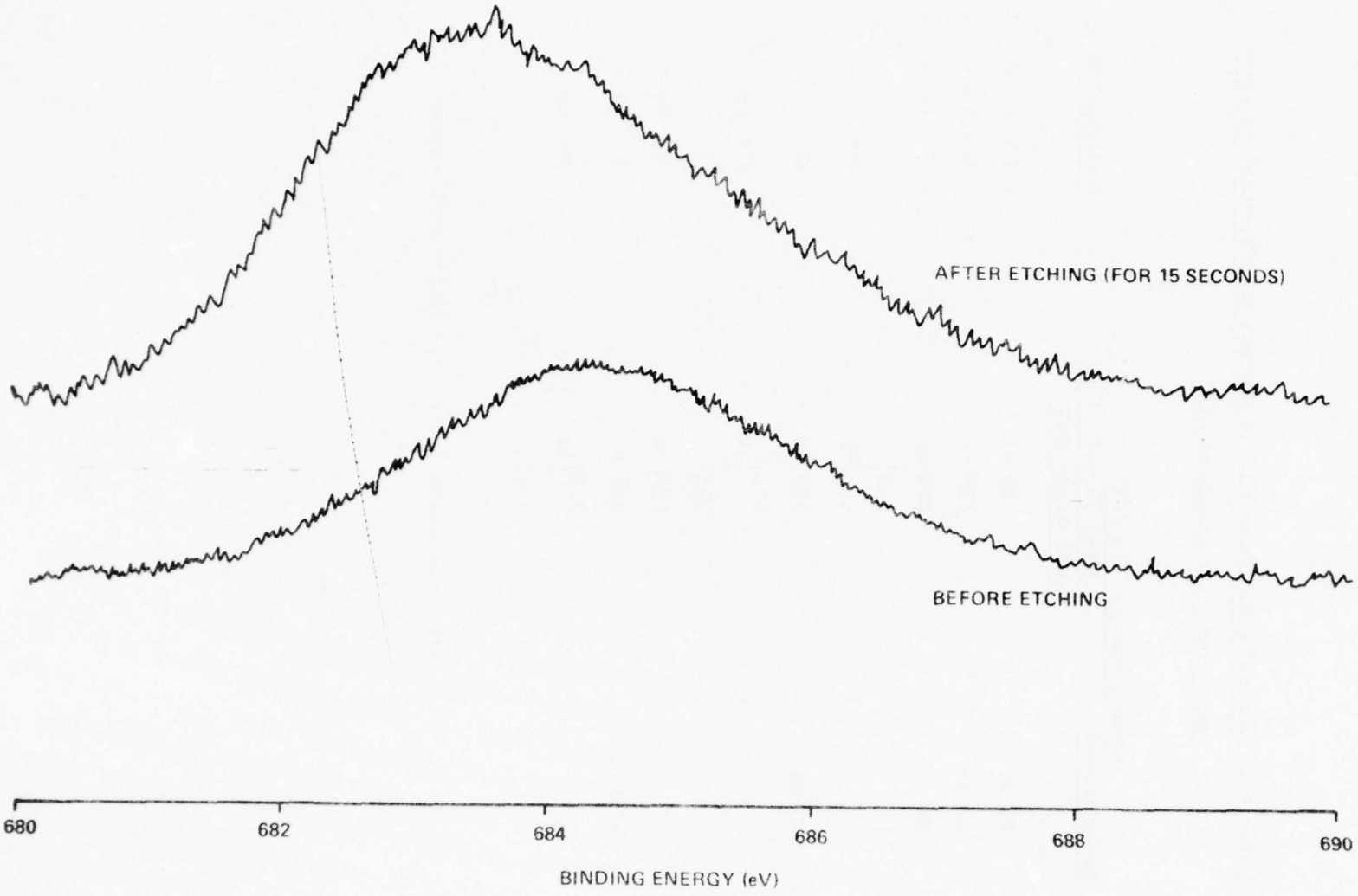


Figure 4-10. Detailed ESCA Spectra of Fluorine is Peak Observed on the Surface of 321 Steel Exposed to Standard HDA

(e) Examination of the surface of 321 steel exposed to modified HDA

Fig. 4-11 shows the general spectrum before and after 90 seconds etching and the observed peaks are listed in Table 4-3. Before etching, oxygen and fluorine peaks are quite strong while a weak peak attributable to phosphorus is discernable. After etching, the oxygen and fluorine peaks are still very strong. The oxygen peak has increased in intensity while the carbon peak has greatly diminished; this indicates that only a small amount of the oxygen on the surface is due to adsorbed atmospheric CO_2. The phosphorus peak is still weak after etching, and no nitrogen peaks are observed.

Narrow band scans for fluorine and phosphorus were carried out. These resemble Figure 4-10. As with standard HDA then, it appears that below the exposed surface a depth of reasonably homogenous fluoride-containing material exists, and again the asymmetric form of the peaks suggests the presence of more than one fluorine species.

The narrow band scans for the phosphorus reveal just how weak the peaks are compared to the fluorine peaks, but it must be remembered that ESCA is less sensitive to phosphorus than for fluorine or oxygen. The phosphorus peaks are quite symmetrical, and after initial etching remain at the same value of E_B.

(f) Examination of surface of 321 steel exposed to liquid anhydrous hydrogen fluoride

Figure 4-12 shows the general spectrum before and after 90 seconds etching. Before etching both oxygen and fluorine peaks are strong. After etching the oxygen peak is appreciably diminished, whilst the fluorine peak is considerably stronger. The decrease in the intensity of the carbon peak tends to suggest that in this case much of the oxygen may be associated with adsorbed CO_2, unlike the surfaces exposed to inhibited HDA. The narrow band scans for fluorine taken after 0, 15, and 90 seconds etching indicate quite a symmetrical peak, the position of which changes with etching from centering at about 685.2 eV to 686.6 eV after 90 seconds etching. The most noticeable aspect of

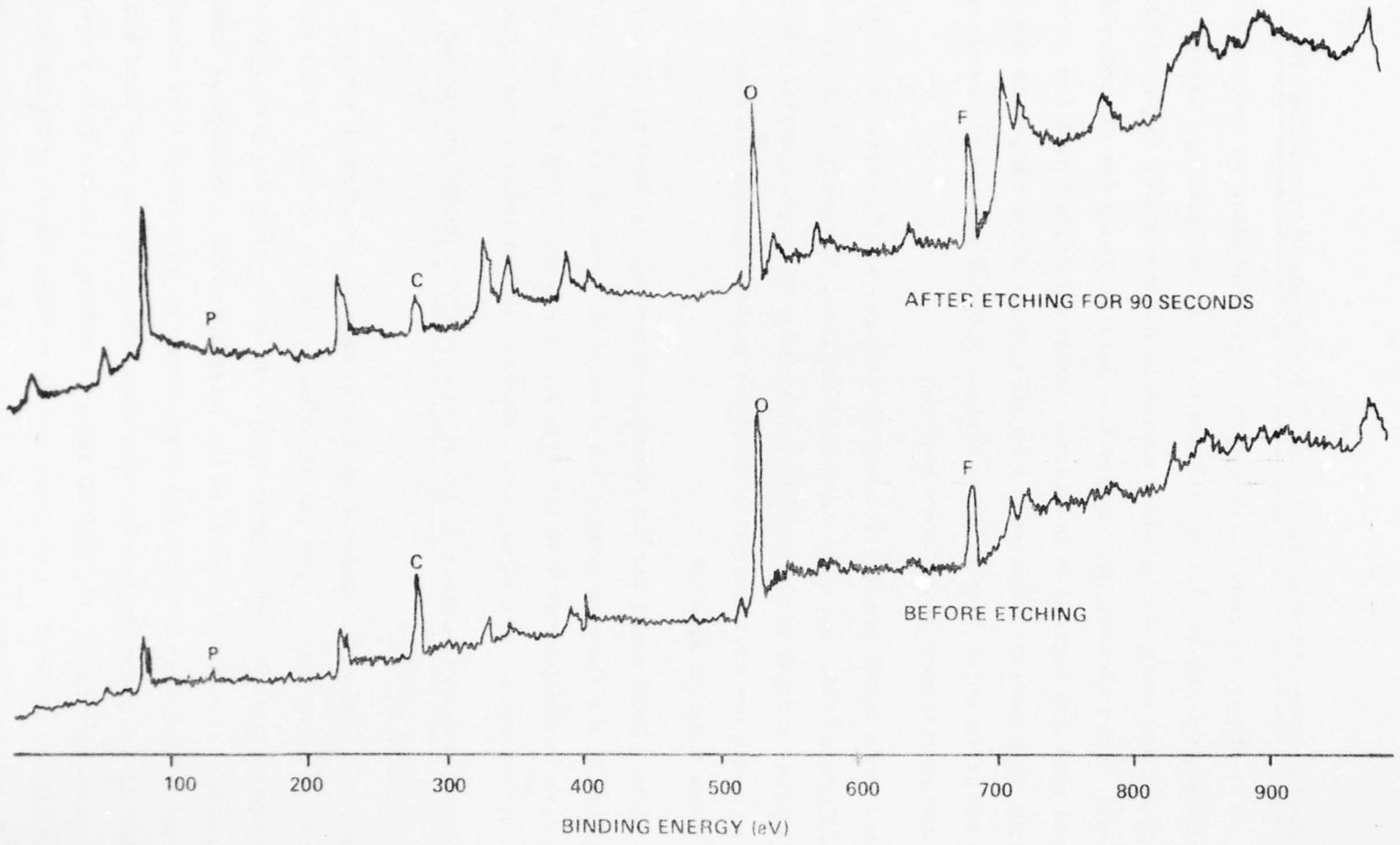


Figure 4-11. ESCA Spectra of Surface of 321 Steel After Exposure to Modified HDA

Table 4-3. General ESCA spectrum of surface of 321 stainless steel recovered from modified HDA

Binding energy, E_B (eV)		
As received	After 90 sec. etch with argon ions	Assignment
80 w	80 vs	Au 4f
125 vw	125 w	P 2p
225 w	225 m	Mo 3d
280 m	280 w	C 1s
330 vw	330) w	Au 4d
350 vw	350) w	
388 vw	388) w	Mo 3p
400 vw	400) w	
525 vs	525 vs	O 1s
	575) w	Cr 2p
	585) w	
	635 w	Au As
680 m	680 s	F 1s
710 vw	710) w	Fe 2p
715 vw	715) w	

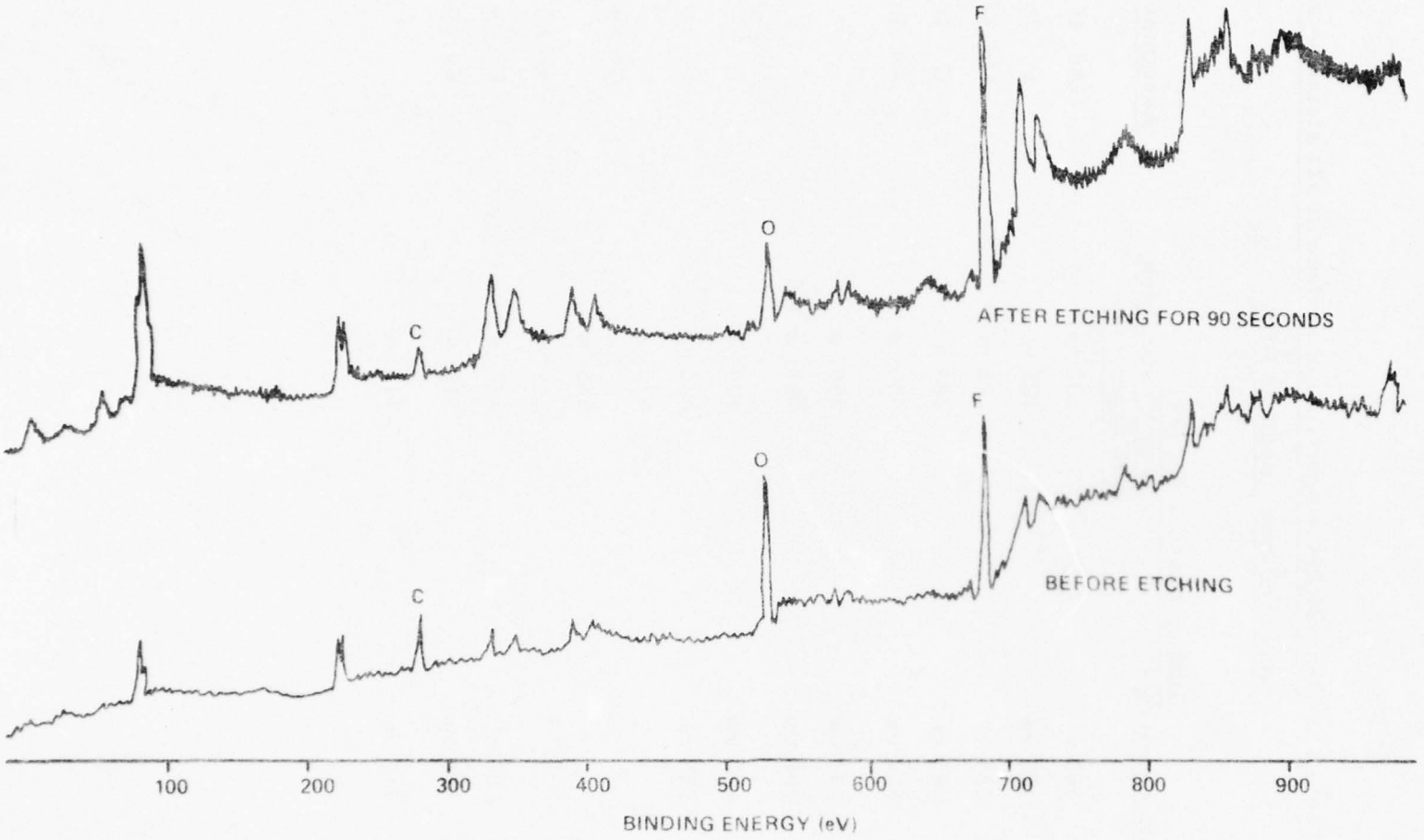


Figure 4-12. ESCA Spectra of Surface of 321 Steel After Exposure to Anhydrous HF

these spectra is the lower binding energy of the fluorine compared with that on surfaces exposed to inhibited HDA.

Table 4-4 lists the E_B values for the fluorine peaks of all the systems examined.

(g) Computer analysis of ESCA spectra

Some progress in the deconvolution of broad ESCA peaks has been achieved by computer assisted analysis, although satisfactory analysis of the recorded spectra proved to be difficult. Using a programme written[3] especially for ESCA spectra deconvolution on the University of Nottingham ICL 1906A computer, some of the fluorine spectra were successfully resolved into 2 individual peaks. Figures 4-13, 4-14, and 4-15 show the deconvoluted fluorine peaks from the steel surface exposed to modified HDA after etch times of 0, 15, and 90 seconds. In the case of the spectrum recorded before etching, the single asymmetric peak at E_B 684.5 eV resolves into an intense peak at 683.2 eV. After 90 seconds etching, the situation has changed to two peaks of nearly equal intensity centered at 684.5 and 683.2 eV. Similar results are also obtained for the surface exposed to standard HDA.

Complete computer analysis of all the spectra is now being carried out. In particular, attempts are being made to refine the analysis of some of the fluorine spectra as early results suggest that a third very weak peak may also be present. In general however, it can be concluded that there are at least two forms of fluorine species present on the surface of stainless steel exposed to either standard or modified HDA.

4.5 Discussion

As evidence accumulates, it is tending to prove that the major factor controlling corrosion is the solubility of the corrosion products. Major effects, like the big differences in extent of corrosion of 321 steel in uninhibited, standard and modified HDA can be related directly with the solubility of the metal nitrates, fluoro-compounds, and phosphorus-fluorine compounds formed as corrosion products in the different media. Other and relatively minor effects,

Table 4-4. Fluorine atom binding energies (eV)

System	Etchtime (seconds) 0	15	90
Standard HDA/321 steel	684.2	683.5	683.6
Modified HDA/321 steel	684.5	684.0	683.5
HDA/321 steel	685.2	686.0	686.6

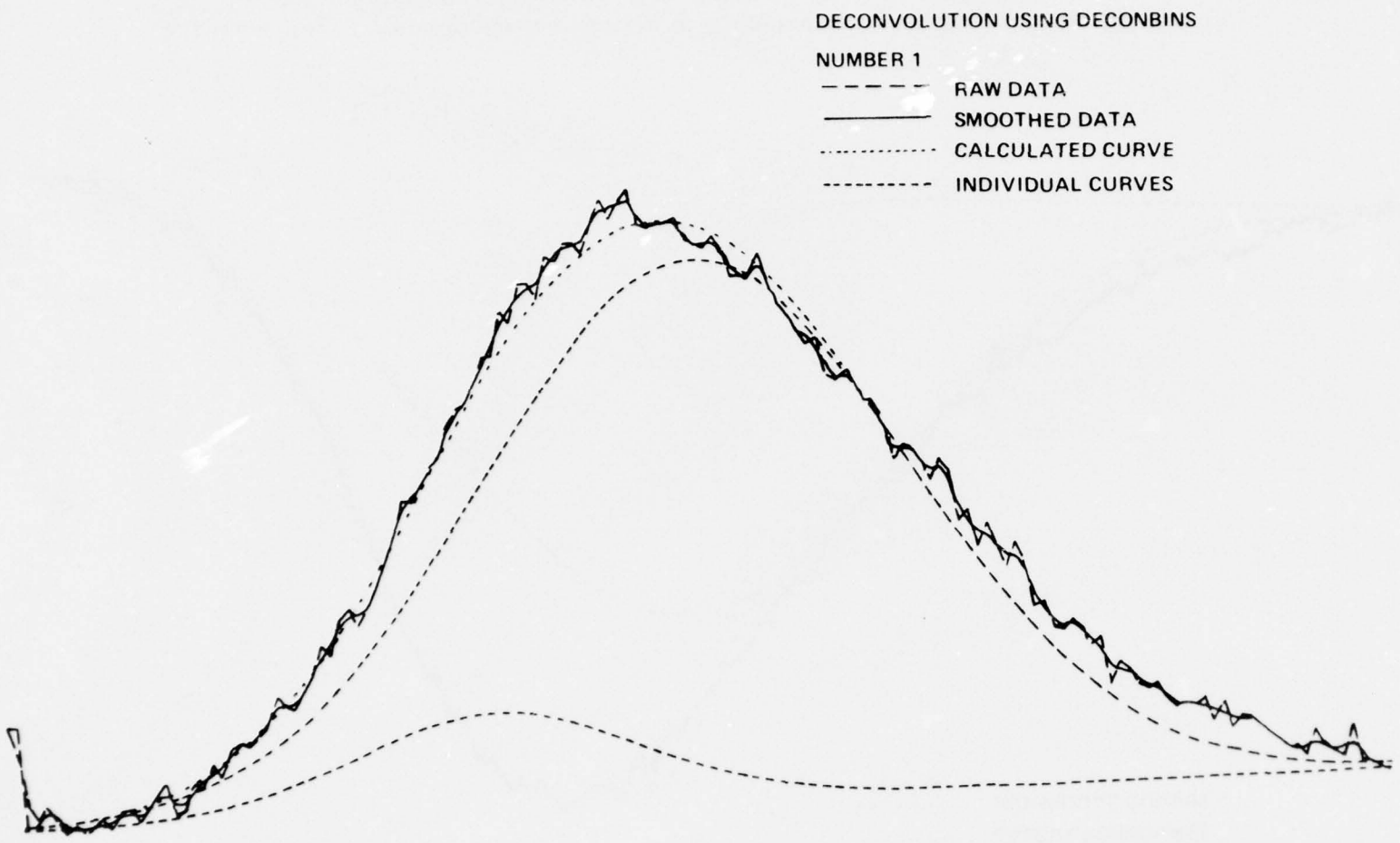


Figure 4-13. Computer Deconvolution of Fluorine is Peak Observed on 321 Steel Exposed to Modified HDA (Before Etching)

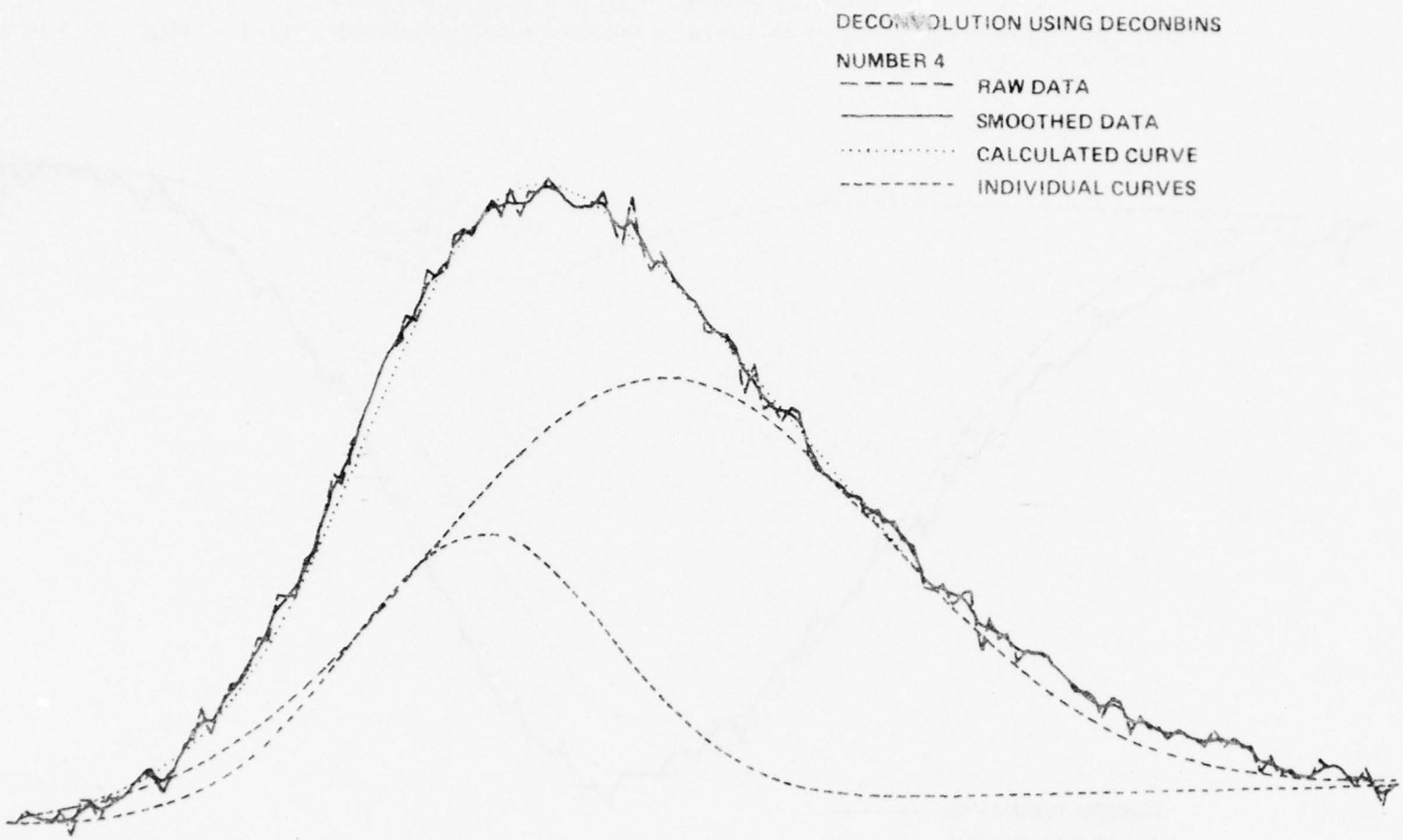


Figure 4-14. Computer Deconvolution of Fluorine is Peak Observed on 321 Steel Exposed to Modified HDA (After 15 Seconds Etching)

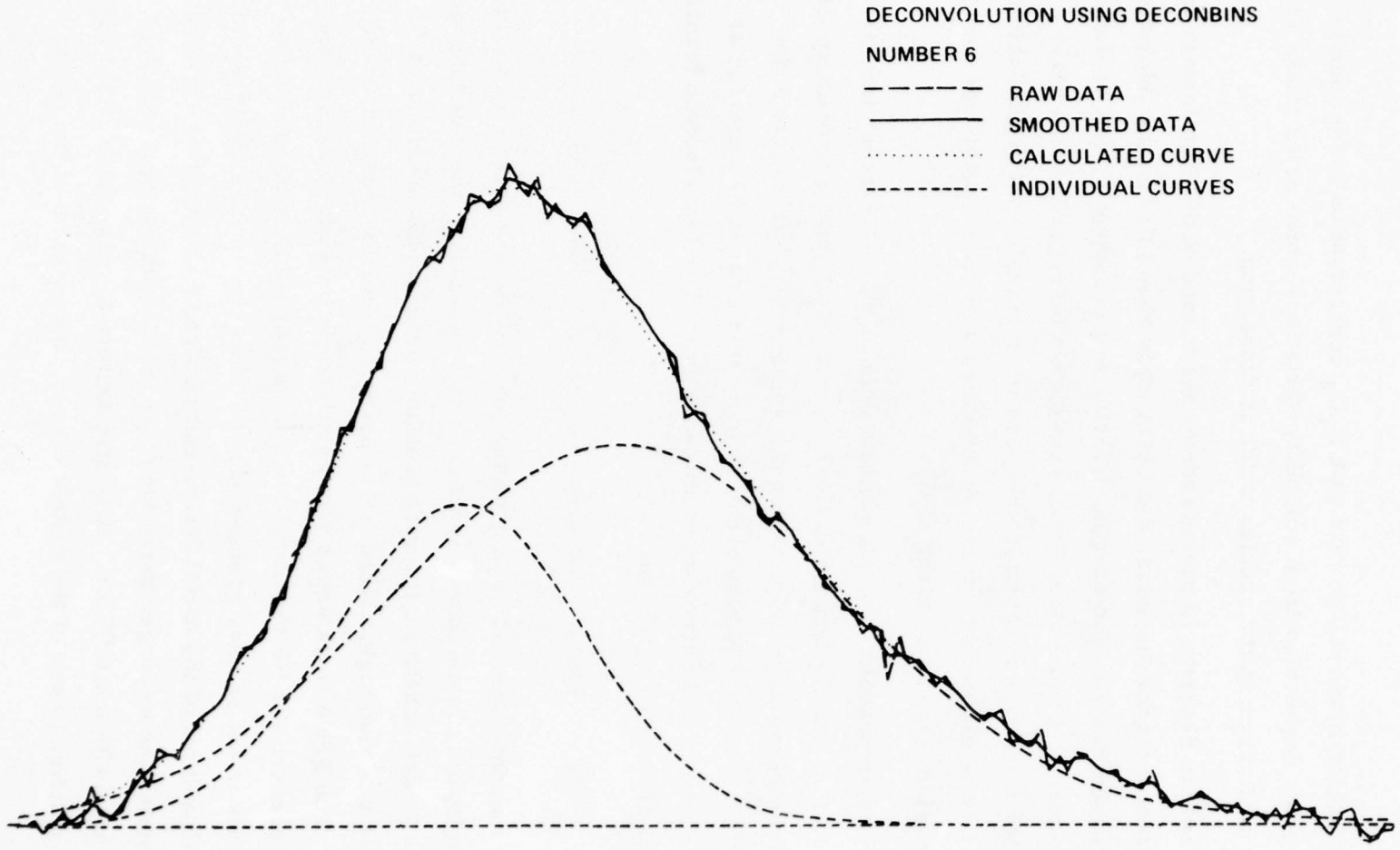


Figure 4-15. Computer Deconvolution of Fluorine is Peak Observed on 321 Steel Exposed to Modified HDA (After 90 Seconds Etching)

such as the variation in corrosion rate with N_2O_4 concentration in the inhibited systems, probably result also from solubility variations which arise either from change in the medium or in the species which is dissolving.

It is not easy to describe in precise terms the nature of the film formed at the metal surface. On the one hand, the ESCA work shows that in the inhibited systems oxygen and fluorine (or oxygen, fluorine and phosphorus) can be detected at the metal surface. On the other hand, this cannot be regarded as a rigid physical barrier to chemical reaction, because when transferred to uninhibited HDA the film has no protective effect. A "chemisorbed" film is perhaps the nearest description that can be given at this time.

The inhibitor is present in small quantity only (0.6%). Whatever interactions the HF or PF_5 may undergo with HNO_3 or with N_2O_4, the resultant species are present in small quantity only. Since the species NO_2^+ arises from the relatively large amount of HNO_3 present, it must in all cases be regarded as the attacking species, and corrosion in all cases is initiated by electron transfer from the metal surface to NO_2^+ i.e.

$$M + nNO_2^+ \longrightarrow M^{n+} + nNO_2$$

This transfer can only proceed so long as the ion M^{n+} is then able to move into solution in the liquid. In uninhibited systems, this is aided by the fact that the nitrate groups (which constitute the only available anions) can coordinate M^{n+} and solubilities are also high. When HF is present, fluoride provides a competing anion. The ESCA work shows that no nitrate is present at the surface, so that in the presence of HF the metal ion moves into solution as the fluoro-compound. This is not an easy process since F^- has poor coordinating powers, and the solubility limit of the metal fluoro-compounds is also quickly reached. Thereafter, metal can no longer move from the surface into a liquid which is already saturated with the M^{n+} ion. It is also believed, in the case of 321 steel, that when the solution of one of the metals ceases, the solution of the other

metals ceases simultaneously. This is supported by experiments described in Chapter 9.

Thoughout Chapters 3 and 4 frequent reference has been made to solubility factors, and it is now clear that a considerable amount of solubility data is required in these systems. This was not given the highest priority in this work because in the beginning there was no solid evidence to indicate that it was indeed the major factor, nor were the species which were formed in solution known. The rate studies (Chapters 3 and 4) have now provided evidence for the importance of solubility studies, and the subsequent Chapters in this report describe investigations on the nature of species dissolved in, and precipitated from, the various solutions. This will provide a firm basis for future work.

4.6 References

1. David M. Mason and John B. Rittenhouse, "Mechanism of Inhibiting Effect of Hydrofluoric Acid in Fuming Nitric Acid on Liquid-Phase Corrosion of Aluminium and Steel Alloys," Corrosion, 1958, 14, 345t.

2. H. Ph. Heubusch et al, Report AFRPL-TR-73-77, Bell Aerospace Company, 1973.

3. By courtesy of Dr. P. A. Brook. University of Nottingham.

5. CORROSION PRODUCTS OF STEELS WITH 100% HNO_3 and HDA.

5.1 Introduction

It was decided to investigate the reactions of steels with HNO_3/N_2O_4 mixtures (uninhibited or inhibited) in two stages, i.e. firstly to examine the reaction of a steel with a simple HNO_3/N_2O_4 mixture, containing approximately 55wt% HNO_3 and 45wt. % N_2O_4 (HDA) and then, secondly, to examine the reactions of the steel with HNO_3/N_2O_4 mixtures containing small quantities of HF (Standard HDA) or PF_5 (Modified HDA). In connection with this second stage it was also planned to investigate reactions of steel/HDA products with HF and PF_5 in HDA solution. This procedure should give a clearer picture of the background chemistry involved than simply a direct investigation of the very complex reactions of $HNO_3/HF/N_2O_4$ or $HNO_3/PF_5/N_2O_4$ systems with steels.

It seemed reasonable to assume that the predominent reactive species present in both standard and modified HDA would be the same as those present in simple HNO_3/N_2O_4 mixtures, as the amounts of HF or PF_5 present are relatively small. The species present in HNO_3/N_2O_4 mixtures are the products of equilibria such as the following:

$$N_2O_4 \rightleftharpoons NO^+ + NO_3^-$$

$$N_2O_4 \rightleftharpoons 2NO_2$$

$$2HNO_3 \rightleftharpoons NO_2^+ + NO_3^- + H_2O$$

$$HNO_3 + H_2O \rightleftharpoons H_3O^+ + NO_3^-$$

$$2HNO_3 \rightleftharpoons H_2NO_3^+ + NO_3^-$$

In the presence of metal cations, numerous reactions may occur to form a variety of possible metallo-species.

$M^{m+} + nNO_3^- \longrightarrow \left[M(NO_3)_n\right]^{(n-m)-}$	nitratometallate anion as NO^+ (N_2O_4 solvate) or NO_2^+ (N_2O_5 solvate) salt.
$M^{n+} + nNO_3^- \longrightarrow M(NO_3)_n$	anhydrous metal nitrate
$M(NO_3)_n + xH_2O \longrightarrow M(NO_3)_n \cdot xH_2O$	metal nitrate hydrate
$M^{m+} + nH_2O \longrightarrow \left[M(H_2O)_n\right]^{m+}$	n-aquometal cation as NO_3^- salt.

The stability of nitrosonium salts and anhydrous metal nitrates in HNO_3 and HNO_3/N_2O_4 mixtures has been demonstrated[1,2]; the formation of metal nitrate hydrates from 100% HNO_3 and anhydrous metal chlorides was reported some years ago[3] and the formation of nitrosonium nitrato-complexes from pure N_2O_4 or N_2O_4/organic solvent mixtures, via reactions with metals, or metal compounds, is particularly well established.[4] There is thus a possibility of any or all of these species being formed in the HNO_3/N_2O_4/steel reaction mixtures. The nature of the products formed, will, of course, depend on the mechanism of reaction between the metal and the corrosive agent, and the subsequent competition of ligands for the co-ordination sphere of the metal cation.

In order to gain an understanding of the mechanism of corrosion inhibition by HF or PF_5, and of product formation and properties in systems containing HF or PF_5, it seemed advisable firstly to establish the principal corrosion behaviour in, and the nature of the products arising from, uninhibited HDA.

The reaction of 321 stainless steel (80% Fe, 10% Ni, 10% Cr) with HNO_3 or HNO_3/N_2O_4 mixtures was expected to lead to a complex mixture containing iron, nickel, and chromium nitrato-species. It was therefore decided to examine the reactions of each of these metals in turn with HNO_3/N_2O_4 mixtures and to isolate and identify the products, on the expectation that the corrosion products of 321 stainless steel will be a mixture of the compounds formed in these individual reactions.

Properties of reaction products have been examined with particular reference to their solubility (and hence their tendency to precipitate and cause flow decay) or tendency to undergo changes in composition with corrosion mixture composition.

Following isolation and identification of solid reaction products, synthetic methods for their preparation in bulk was investigated, so that a more convenient and thorough investigation of their properties could be carried out.

5.2 The reaction of 321 stainless steel with 100% HNO_3 and HDA

Small pieces (ca $1cm^2$) of 321 stainless steel were immersed in about $20cm^3$ of 100% HNO_3. Identical specimens were also immersed in HDA. The resulting change in appearance of metal surface and solution with time were observed. Prior to immersion, the metal samples were abraded to remove surface oxide, washed with inhibisol to remove grease, and subsequently handled only with forceps. Small stoppered flasks were used as reaction vessels.

(a) 100% HNO_3

Two parallel sets of experiments were carried out, one at room temperature ($20^{\circ}C$), and one at $-20^{\circ}C$ to study the effect of any thermal decomposition of the acid. The results are presented in Table 5-1.

The green precipitate which formed in the reaction of 321 stainless steel with 100% HNO_3 at room temperature was isolated by decantation of the supernatant liquid, washing with 100% HNO_3, and drying in vacuum. Pieces of unreacted steel, at this stage matt-black in colour, were removed mechanically in a dry box.

The small quantity of green precipitate was examined by X-ray powder photography; insufficient being available for analysis. The powder photograph was found to be identical to that of $Ni(NO_3)_2 \cdot 2H_2O$, which has been well characterised by other workers, and has also been studied in considerable detail during the present investigations, as reported later (Section 5.4).

Table 5-1.

The reaction of 321 stainless steel with 100% HNO_3

Room temperature ($20^{o}C$)

Time after immersion	Appearance of metal	Appearance of Solution
Immediately	Bright shiny surface	Acid colourless; gas bubbles evolved.
5 minutes	" " "	Green solution.
16 hours	" " "	Darker green solution Gas evolution ceased.
30 hours	Metal darkening	" " "
19 days	Metal uniformly grey/black	Green precipitate forming. Atomic absorption showed Fe, Ni, Cr present.
4 weeks	Metal dark grey	Much green precipitate.

$-20^{o}C$

Time after immersion	Appearance of metal	Appearance of solution
Immediately	Shiny bright surface	Colourless
2 1/2 days	" " "	Acid very pale yellow
7 days	Dark patches on metal	Acid pale yellow
24 weeks	Metal uniformly dark grey	Green-brown solution; no precipitate.

(b) HDA

The reaction of 321 stainless steel with HDA was examined at room temperature ($20^{o}C$). The results are recorded in Table 5-2.

Table 5-2.

The reaction of 321 stainless steel with HDA at 20°C

Time after immersion	Appearance of metal	Appearance of Solution
Immediately	Bright shiny surface	Gas bubbles evolved
5 minutes	" " "	Green tinge
16 hours	" " "	Evolution of gas ceased; green solution. Atomic absorption indicated Fe, Cr, Ni present
2 days	Metal surface darkening	" " " "
36 weeks	Metal surface black	Green solution, no precipitate.

This preliminary investigation indicates that all three alloy components of 321 stainless steel enter solution, and may precipitate again given the right conditions.

5.3 The reaction of mild steel and iron with 100% HNO_3 and HDA

(a) Surface reactions

The well known phenomenon of surface passivation is an important feature of the corrosion of iron and mild steel (99% Fe, 1% C) by nitric acid of high concentration. In the present studies, reactions of the metal surface and phenomena associated with the microstructure of the metal were investigated. The reactions of mild steel with both 100% HNO_3 and HDA were studied, using samples of 20 gauge mild steel. The surface of samples were prepared in various ways.

(i) Mild steel/100% HNO_3

Small pieces of mild steel were cleaned by sand blasting and washed with inhibisol and acetone to remove surface grease. The samples were immersed in 100% HNO_3 at room temperature. After 4 days some darkening of the metal surface occurred. After 7 days the metal surface was a uniform grey, and a

grey precipitate had formed. This precipitate was isolated by decantation, and washed with dichloromethane. Traces of solvent were removed in a vacuum (10^{-3}mm, 20°C). The solid was found to be magnetic, and analysis indicated that it consisted of pure iron granules. Microscopic examination of the granules, and comparison with the appearance of the metal surface after polishing and etching with 2% HNO_3 in methanol to reveal the microstructure of the metal, indicated a close similarity between the grain size of the steel and the dimensions of the "precipitated" granules. In a separate experiment, the grain size of the metal was increased 1000-fold by slow annealing in a current of pure argon at 1000°C, and this steel was immersed in 100% HNO_3. At the end of 5 days the metal crumbled into small particles which again, on microscopic examination, were of similar grain size to the metal.

It is thus concluded that HNO_3 attack on mild steel leads to intergranular corrosion, i.e. corrosion occurs preferentially at the faces of the metal crystals where the increased internal stresses and accumulation of nodules of iron carbide (Fe_3C), and iron (III) sulphide and phosphide impurities, leads to an increased surface energy.

It was observed that when larger pieces of steel were immersed in 100% HNO_3, iridescent films were formed on the surface within a few seconds of immersion, presumably oxide films. As the metal surface was broken up, these films disappeared.

The effect of polishing and work hardening of mild steel was also investigated. 3" x 1/2" strips of 20 gauge mild steel were ground to a high surface shine using a diamond wheel. The surface was then degreased by washing with inhibisol and acetone. The polished metal was immersed in 100% HNO_3. After 2 days, the surface had "blistered", a film of polished metal lifting off the surface. Beneath this surface layer, granular metal was to be seen, presumably as a result of the intergranular corrosion. This film was ca. 0.05 mm in thickness. On strips of steel which had been prepared by guillotining of larger pieces, the edges were found to be less attacked by the acid, leaving a hollowed surface with raised

edges. These two observations would suggest that the work-hardening of the metal, caused by surface grinding etc., substantially reduces the rate of intergranular corrosion and subsequent disintegration of the metal.

The formation of a finely powdered metal precipitate, of high surface area compared with the original metal, suggests that intergranular corrosion is the dominant mode of corrosion in this system, chemical attack on the metal grains and bulk dissolution occurring at a very much slower rate. The presence of such metal crystallites could easily lead to serious blockage in flow systems.

(ii) Mild steel/HDA

Small pieces of mild steel were prepared as above and immersed in HDA. The metal surface darkened immediately. After 12 hours the surface was uniformly black. A sample was withdrawn and the surface examined. A thick black film, which could easily be scraped off using a spatula, covered the metal. Examination of the surface by X-ray diffractometry showed no diffraction lines other than those attributable to iron. X-ray powder photography indicated that the film also consisted of metallic iron.

After 2 1/2 days, the metal immersed in the HDA was no longer black, and a surface film could no longer be scraped off. A small amount of a black magnetic precipitate began to form at this stage.

In a separate experiment, a sample of mild steel which had been annealed at 1000°C was immersed in HDA, and the formation of a black film was again noted. Examination of the surface under an optical microscope showed that the surface consisted of the much larger grains, with deep clefts between them, indicative of intergranular corrosion. At some positions on the metal surface were 'holes' where metal grains appeared to have been removed. The metallic precipitate from this steel in HDA again consisted of particles identical in size to these grains. Both grains and particles appeared to be coated with a black film.

The disappearance of the loose black film after 2-3 days of immersion was unexpected. It possibly corresponds to the removal of the surface layer of metal

crystals: the blackness being a result of light absorption in the deep chasms formed between grains as intergranular material is removed. The black appearance of the actual metal grains appears to be due to a very thin layer of surface corrosion film, probably consisting of Fe_3O_4. This film, however, is formed in too minute a quantity to be conclusively detected by chemical analysis or X-ray powder photography.

The formation of this loose film seems to be related to the surface-to-volume ratio. Large strips of mild steel, 6" x 1/2", immersed in HDA did not form a loose black film, but merely developed a tenacious black colouration on the surface. When the surface layer was removed from these strips with abrasive, no black colouration was formed on reimmersion, suggesting that the build up of iron-containing species in the solution exerts a retarding effect on this phenomenon.

These experiments indicate that in both HNO_3 and HDA, intergranular attack is a dominant factor in the corrosion of mild steel. Stainless steel systems (see Section 5.2) also showed a blackening of the metal surface, although they were not examined in as much detail. The formation of metal crystallites from steels and HNO_3 -N_2O_4 mixtures could clearly lead to blockage of rocket engine jets and filters.

(b) Reaction products of mild steel and 100% HNO_3

In the course of the reactions between mild steel and 100% HNO_3, brown solutions were formed above the metal, due to the formation of iron-containing species in the solution. A steady increase in viscosity was noted, although at the iron concentrations experienced the liquid was still mobile enough to permit easy filtration through a porosity 3 sinter. The solution IR spectrum was recorded at this stage by the liquid film technique. The spectrum was found to be identical with that observed [1,2] in these laboratories for the solution products of the reaction between $FeCl_3$ and 100% HNO_3. (Fig. 5-1, Table 5-3).

The spectrum contains bands attributable to $[Fe(NO_3)_4]^-$ and nitric acid. Weak absorption in the region normally associated with the presence of NO^+

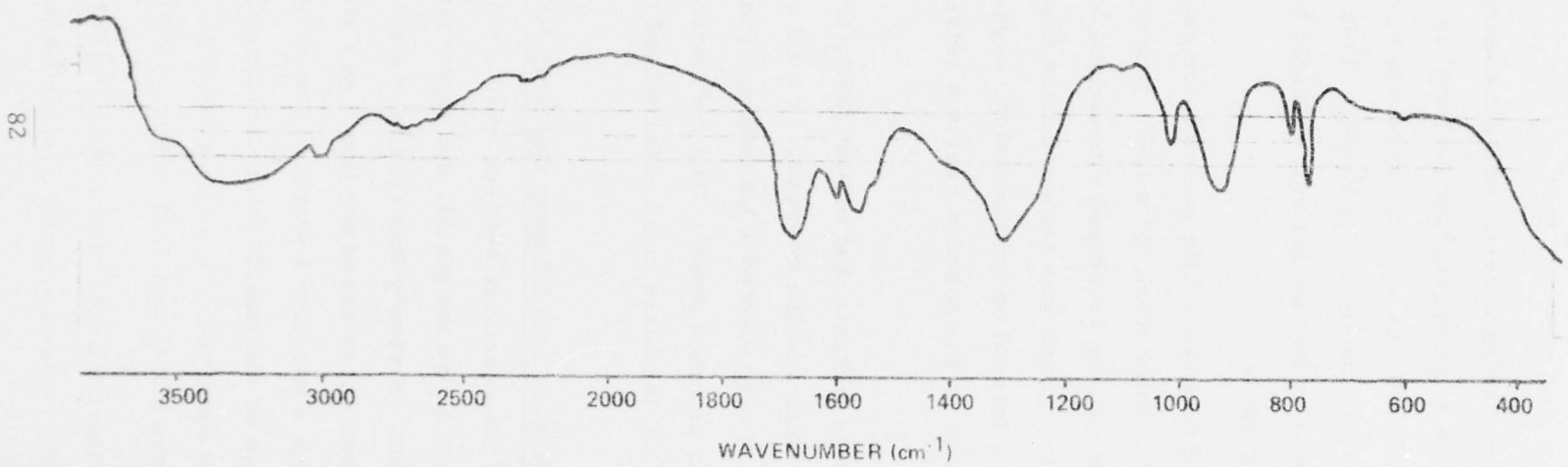


Figure 5-1. IR Spectrum of Mild Steel/HNO_3 Solution

Table 5-3. Infra red spectrum (cm^{-1}) of mild steel/HNO_3 solution and $FeCl_3$/HNO_3 solution

Absorption bands						Assignment
Mild Steel/HNO_3			$FeCl_3/HNO_3$			
3550	s	b				
3360	s	b	3400	m	vb	HNO_3
3000	m	sp	3000		sh	HNO_3
2700	m	vb				
2600	w	sh				
2280	w	b				NO^+
1675	s	sp	1680	m	sp	HNO_3
1600	m	sp	1600	m	sp	$Fe(NO_3)_4^-$
1560	m	b	1575	m	s	$Fe(NO_3)_4^-$
1310	s	sp	1300	s		HNO_3
1015	m	sp	110	m		HNO_3
925	s	b	925	s	b	HNO_3
800	m	sp	800	m		$Fe(NO_3)_4^-$
770	s	sp	770	m	s	HNO_3
605	w		605	w		HNO_3

(ca. 2300 cm^{-1}) was observed, this cation possibly arising by dissociation of N_2O_4 formed on reduction of nitrogen (V) (as HNO_3 or NO_2^+) by metallic iron.

The solution was filtered, and evacuated (10^{-3} mm, 20°C). After 24 hours, a viscous brown gum had formed, an infra-red spectrum of which showed very little difference to that of the solution. Attempts were made to leach out HNO_3 with dry CH_2Cl_2, which is miscible with 100% HNO_3. This was unsuccessful, a second immiscible layer being formed, and it was observed in other metal-HNO_3 - N_2O_4 systems (see Section 5.5 (b)) that increased metal ion concentration in HNO_3 or HNO_3 - N_2O_4 mixtures results in immiscibility with CH_2Cl_2. After about 7 days evacuation with occasional grinding, a light brown powder was obtained. This was found to be somewhat unstable, and over a period of weeks developed a slight vapour pressure of N_2O_4, even in a dry atmosphere. It was found to be extremely deliquescent, liquefying completely after about 10 minutes exposure to the atmosphere. On addition of water, it hydrolysed violently, evolving brown fumes.

The infra-red spectrum and X-ray powder photographs (FeK_α radiation) of the material were recorded (Fig. 5-2, Tables 5-4 and 5-5). Both were found to be identical to those of the material described as $Fe(NO_3)_3 \cdot 2H_2O$.[1,2] Analysis for iron and total nitrogen content was carried out. Found: Fe, 21.25; N, 14.86; $Fe(NO_3)_3 \cdot 2H_2O$ requires: Fe, 20.1; N, 15.15%. These results give an N:Fe ratio of 2.795:1. In the light of the X-ray powder pattern and the infra-red spectroscopic results, this ratio probably reflects partial decomposition of a trinitrate species.

Decomposition of $Fe(NO_3)_3 \cdot 2H_2O$ at 60°C is reported[1,2] to give $Fe_2O(NO_3)_4$, containing 29.9% Fe. Decomposition to other products such as $FeONO_3$ or Fe_2O_3, with loss of NO_2, would give even higher Fe contents.

Thermogravimetric analysis (T.G.A.) of the solid was therefore carried out to examine in more detail the decomposition reaction, which is said to yield $Fe_2O(NO_3)_4$ as an intermediate.[1,2] The apparatus used is illustrated in Fig. 6-5 and a full description of the method will be found in Section 6.2.

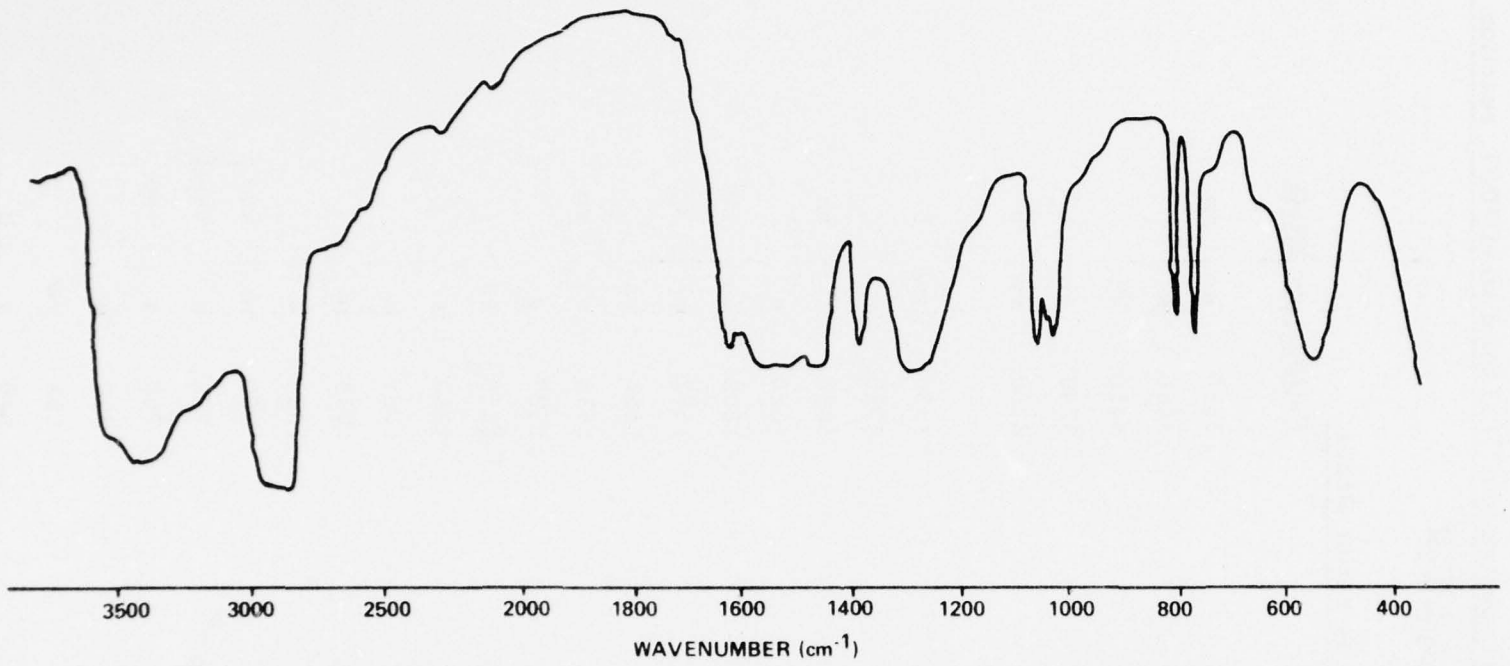


Figure 5-2. IR Spectrum of Mild Steel/HNO_3 Product

Table 5-4. Infrared spectra (cm^{-1}) of mild steel/HNO_3 reaction product, and $Fe(NO_3)_3 \cdot 2H_2O$

Absorption Bands						Assignment
Mild steel/HNO_3			$Fe(NO_3)_3 \cdot 2H_2O$			(c_{2v} bidentate nitrate model)
3530	s	sh	3560	s	sp	ν(OH)
			3460	s		ν(OH)
3400	s	b	3410	sh		
3220	w	sh	3240	vw	b	
2720	w	sh	2730	vw	b	
2560	m	sh				
2370	m	b	2330	vw	b	
2080	m	sp	2080	vw		
1620	s	sp	1630	s	sh	$\delta(H_2O)$
			1620	s		
1600	vw	sp	1603	vw	sp	
			1592	m	sp	
1550	vs	b	1556	vs		ν(NO*)
			1538	s	sp	
			1527	s		
1280	vs	sp	1285	vs		$\nu_{as}(NO_2)$
1260	s	sh	1260	s		
1052	s	sp	1051	s		
1037	m	sp	1034	m		$\nu_s(NO_2)$
1024	s	sp	1020	s		
805	s	sh	800	m	vsp	$\pi(NO_3)$
797	s	vsp	793	s	vsp	
765	s	sp	762	s	vsp	$\delta_s(NO_2)$
725	w	sh	720	w		$\delta_{as}(NO_2)$
650	w	sh	668	vw		
545	s	b	540	s	b	ν(Fe-O)

* uncoordinated oxygen atom

Table 5-5. X-ray powder patterns of mild steel/HNO_3 product and $Fe(NO_3)_3 \cdot 2H_2O$[1, 2]

Mild Steel/HNO_3		$Fe(NO_3)_3 \cdot 2H_2O$	
d(nm)	I	d(nm)	I
0.647	80	0.654	80
0.605	80	0.606	80
0.492	5	0.492	5
0.469	5		
0.406	50	0.407	40
0.375	5	0.374	2
0.367	15	0.368	20
0.355	20	0.359	20
0.343	10	0.344	5
0.383	100	0.335	100
0.318	15	0.320	15
0.312	18	0.315	15
0.296	15	0.299	10
0.279	10	0.281	15
0.273	5	0.273	5
0.265	5	0.267	5
0.259	5	0.259	10
0.249	10	0.248	10
0.246	10		
0.243	5	0.243	2
0.234	30	0.235	30
0.228	5	0.230	2
0.221	5	0.222	5
0.215	10		
0.211	5		
0.208	5	0.205	20
0.205	15		

(continued next page)

Table 5-5 (cont'd)

Mild Steel/HNO_3		$'Fe(NO_3)_3 \cdot 2H_2O'$	
d(nm)	I	d(nm)	I
0.195	10	0.196	20
0.192	5	0.190	10
0.189	7		

The T.G.A. shows a simple 1 step decomposition reaction (Figs. 5-3 and 5-4) reaching a maximum decomposition rate at about 142°C. It is interesting to note that at 60°C, the temperature said[1] to lead to complete dehydration of $Fe(NO_3)_3 \cdot 2H_2O$ and loss of NO_2 to form $Fe_2O(NO_3)_4$, reaction was almost negligible. There was no evidence of intermediates, the decomposition proceeding smoothly to a hydrated form of Fe_2O_3.

The reaction of $FeCl_3$ and 100% HNO_3

As part of the general area of corrosion product studies, the reaction of $FeCl_3$ and 100% HNO_3 was investigated as a preparative route to $Fe(NO_3)_3 \cdot 2H_2O$ and its derivatives. This reaction was initially studied by Hathaway and Underhill[3] and was subsequently repeated by Jones[1] and Addison[2].

The reaction of $FeCl_3$ with 100% HNO_3 gives a brown solution which was filtered to remove insoluble impurities. This solution requires several weeks of evacuation (10^{-2}mm) at room temperature to effect evaporation to dryness, becoming progressively more and more viscous before final solidification. The solid product is claimed by Jones[1], Addison[2], and Hathaway and Underhill[3] to be $Fe(NO_3)_3 \cdot 2H_2O$, but the composition is not reliably reproducible. However, both the infra-red spectrum and powder photograph of the product obtained in the present work are identical to those obtained by Jones[1] and Addison.[2] The inconsistency of the analytical results is therefore attributed to the tenacious nature of nitric acid as a solvent.

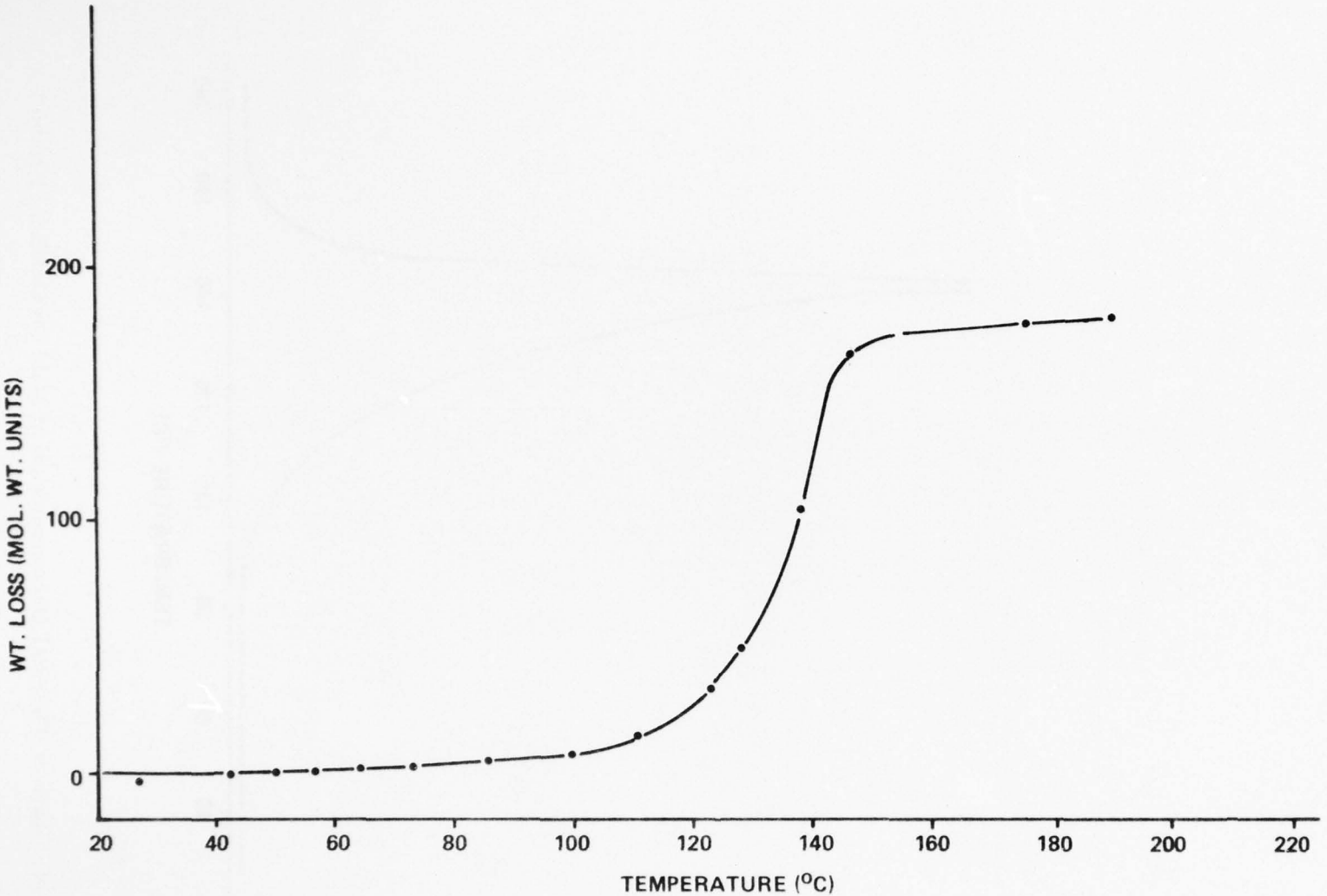


Figure 5-3. Thermogravimetric Analysis of Mild Steel/HNO_3 Product

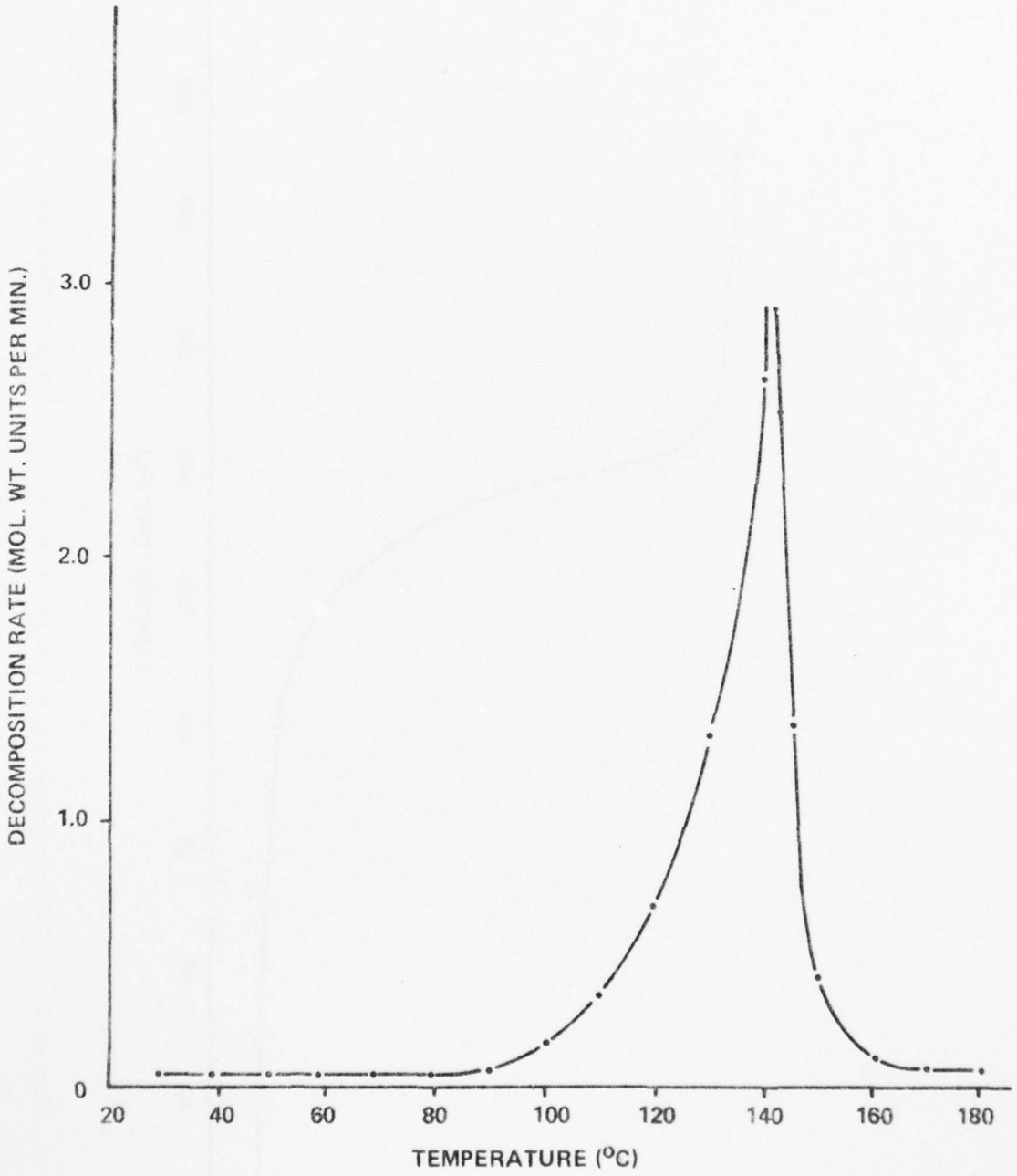


Figure 5-4. Rate of Thermal Decomposition of Mild Steel/HNO_3 Product

The product (taken to be $Fe(NO_3)_3 \cdot 2H_2O$), was then heated at 60°C for 3 days yielding a compound which analysed as $Fe_2O(NO_3)_4$. The infra-red spectrum and X-ray powder photograph for this compound again compared favourably with those quoted by Jones.[1]

The Mössbauer spectra of these two compounds were recorded and are shown in Figs. 5-5 and 5-6. Both spectra were run at room temperature and were found to be identical to spectra run at 77K, indicating that the compounds are polymeric. The spectrum of $Fe(NO_3)_3 \cdot 2H_2O$ shows three peaks but only the peak at 0.504mm. sec^{-1} is taken to be due to the compound $Fe(NO_3)_3 \cdot 2H_2O$. The shoulders are most probably due to impurities in the form of hydrolysis products. The fact that there is only one peak shows that there is only one type of iron site and that its electronic environment is spherically symmetrical.

Table 5-6

Peak Positions/mm. sec^{-1}		
$Fe(NO_3)_3 \cdot 2H_2O$	$Fe_2O(NO_3)_4$	
-0.165	-0.109	Centre 0.386
0.504	0.881	
0.960		

The Mössbauer spectrum of $Fe_2O(NO_3)_4$ can be interpreted as a clearly split doublet with a splitting of 0.990mm. sec^{-1}. This shows that the compound is pure and that there is only one type of iron site. The fact that the spectrum exhibits quadrupole splitting shows that the electronic environment of iron is unsymmetrical in some way. In previous work at the University of Nottingham[1] on the thermal decomposition of the compound $Fe(NO_3)_3 \cdot 1.5N_2O_4$, the spectrum recorded of a decomposition product, assumed to be $Fe_2O(NO_3)_4$, was similar to that quoted above, having a symmetrical doublet centered at 0.309 mm. sec^{-1} with a quadrupole splitting value of 0.928 mm. sec^{-1}.

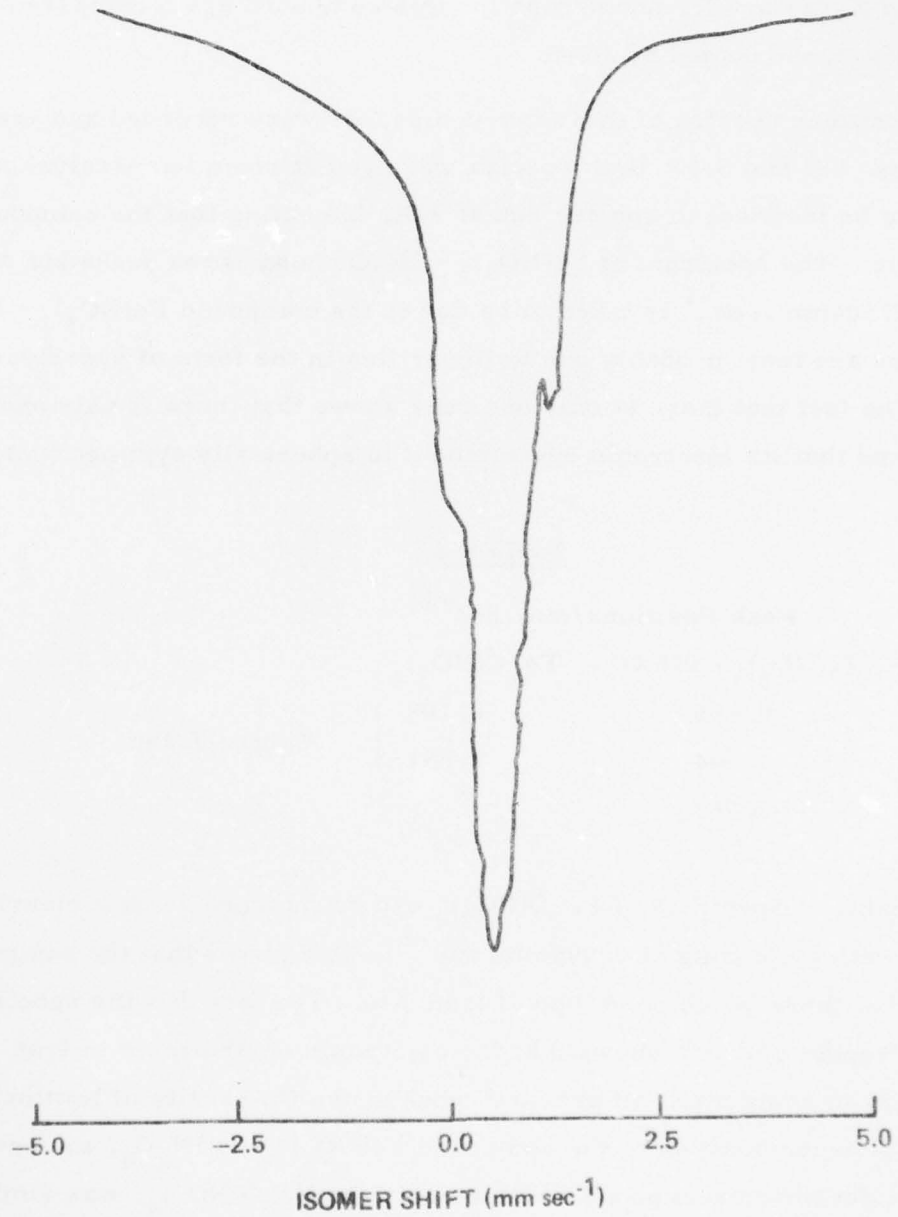
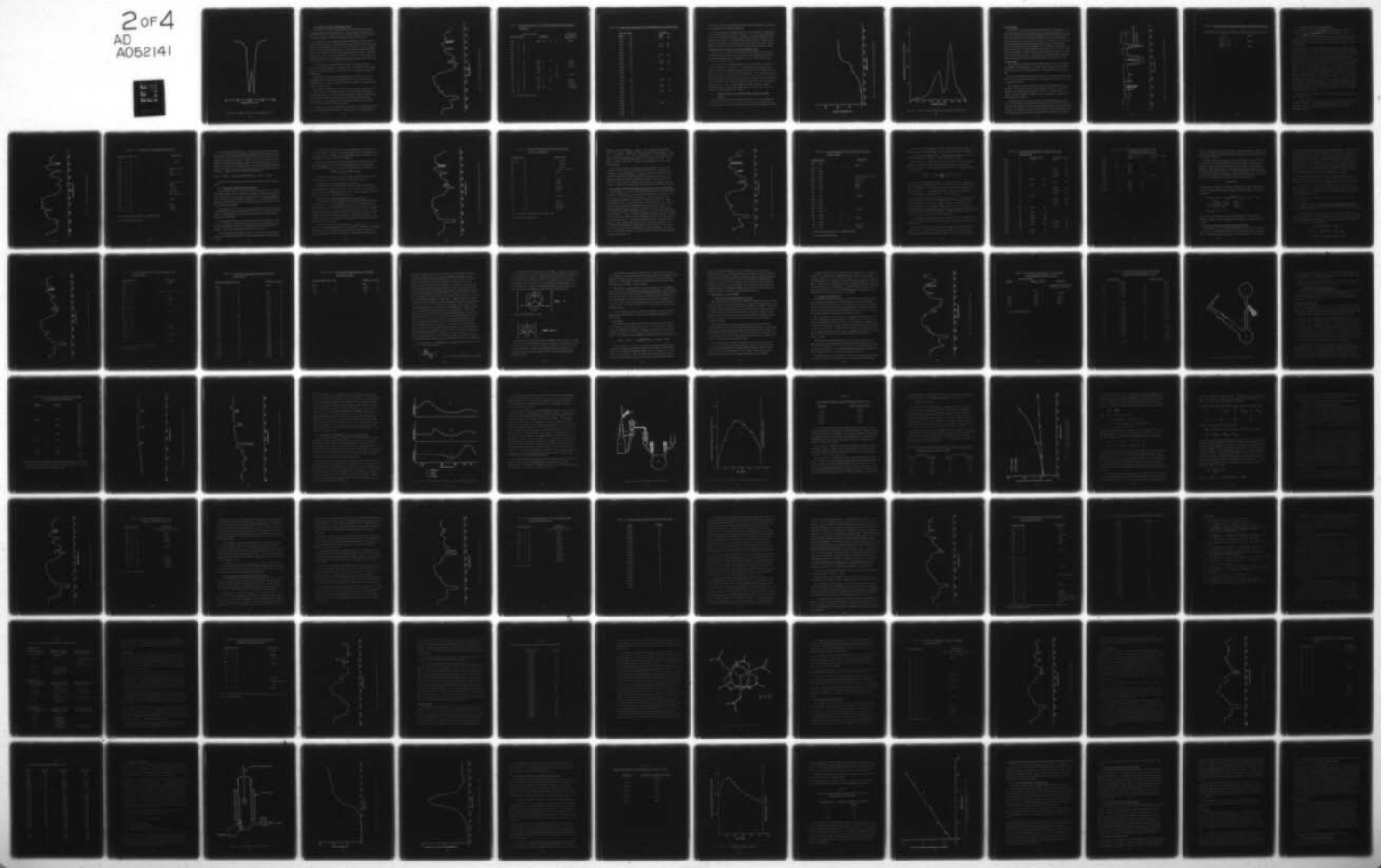
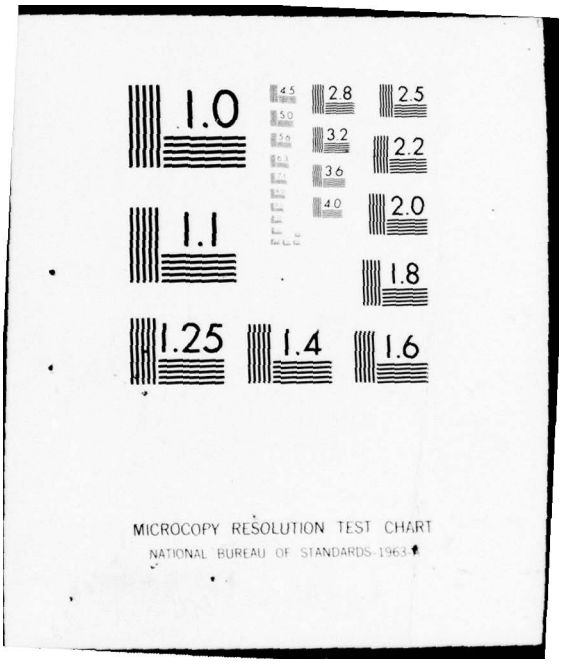


Figure 5-5. Mössbauer Spectrum of $Fe(NO_3)_3 \cdot 2H_2O$ at 77K

AD-A052 141 NOTTINGHAM UNIV (ENGLAND) DEPT OF INORGANIC CHEMISTRY F/G 7/2
HDA CORROSION CHEMISTRY.(U)
DEC 77 C C ADDISON, N LOGAN AFOSR-74-2709
UNCLASSIFIED AFRPL-TR-77-65 NL

2 OF 4
AD
A052141




1.0
1.1
1.25
1.4
1.6
1.8
2.0
2.2
2.5
2.8
3.2
3.6
4.0
4.5
5.0
5.6
MICROCOPY RESOLUTION TEST CHART
NATIONAL BUREAU OF STANDARDS-1963-A

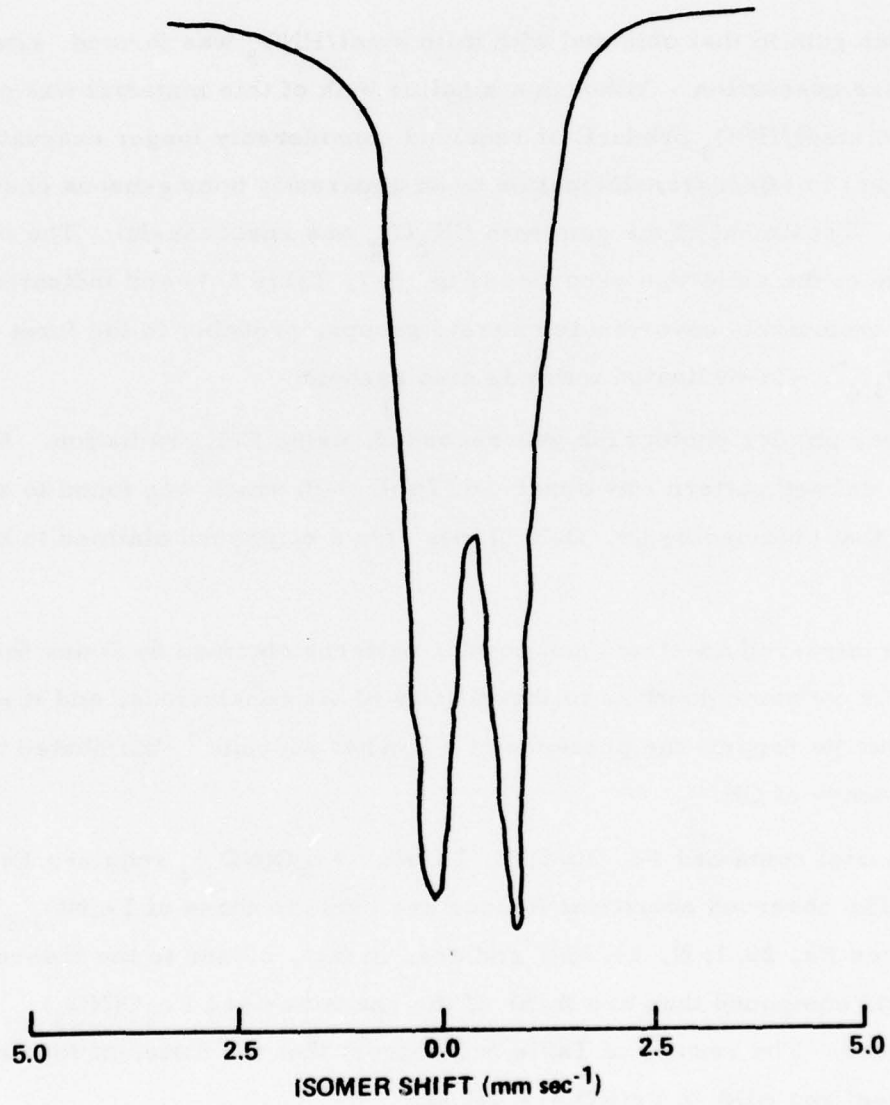


Figure 5-6. Mössbauer Spectrum of $Fe_2O(NO_3)_4$ at 77K

(c) Reaction Products of Mild Steel and HDA

Small pieces of mild steel were prepared as described above, and were immersed in HDA, at room temperature. Little change in appearance of the solution was observed, due to the red brown colour of HDA. After 7 days the solution was filtered, and the liquid evaporated down (10^{-3}mm, 20°C).

A similar gum to that obtained with mild steel/HNO_3 was formed, after about 24 hours evacuation. Although a smaller bulk of this material was present than the mild steel/HNO_3 product, it required considerably longer evacuation (about 2 weeks) to effect transformation to an apparently homogeneous chestnut brown solid. Treatment of the gum with CH_2Cl_2 was unsuccessful. The infra-red spectrum of the solid was recorded (Fig. 5-7, Table 5-7) and indicates the presence of exclusively co-ordinated nitrate groups, probably in the form of the anion $Fe(NO_3)_4^-$. Co-ordinated water is also present.

The X-ray powder photograph was recorded, using FeK_δ radiation. A strong, well defined pattern was observed (Table 5-8) which was found to agree closely with that obtained by Dr. D.H. Jones[1] for a compound claimed to be $Fe_2O(NO_3)_4$.

Both the infra-red spectrum and powder patterns obtained by Jones for $Fe_2O(NO_3)_4$ leave some doubt as to the validity of his conclusions, and it is significant that he reports the presence of a band at 3400cm^{-1} "attributed to the residual presence of OH."

The material contained Fe, 20.5; N, 15.4%. $Fe_2O(NO_3)_4$ requires Fe, 29.7; N, 14.9%. The observed analytical figures are close to those of $Fe(NO_3)_3 \cdot 2H_2O$ (requires Fe, 20.1; N, 15.2%), and are, in fact, closer to the theoretical values for this compound than are those of the characterised $Fe_2O(NO_3)_4$ discussed above. The results of Table 5-8 suggest that the material formed from mild steel and HDA is $Fe(NO_3)_3 \cdot 2H_2O$.

It is believed that the correspondence between the X-ray powder photographs of the mild steel/HDA product and the compound identified as $Fe_2O(NO_3)_4$ by

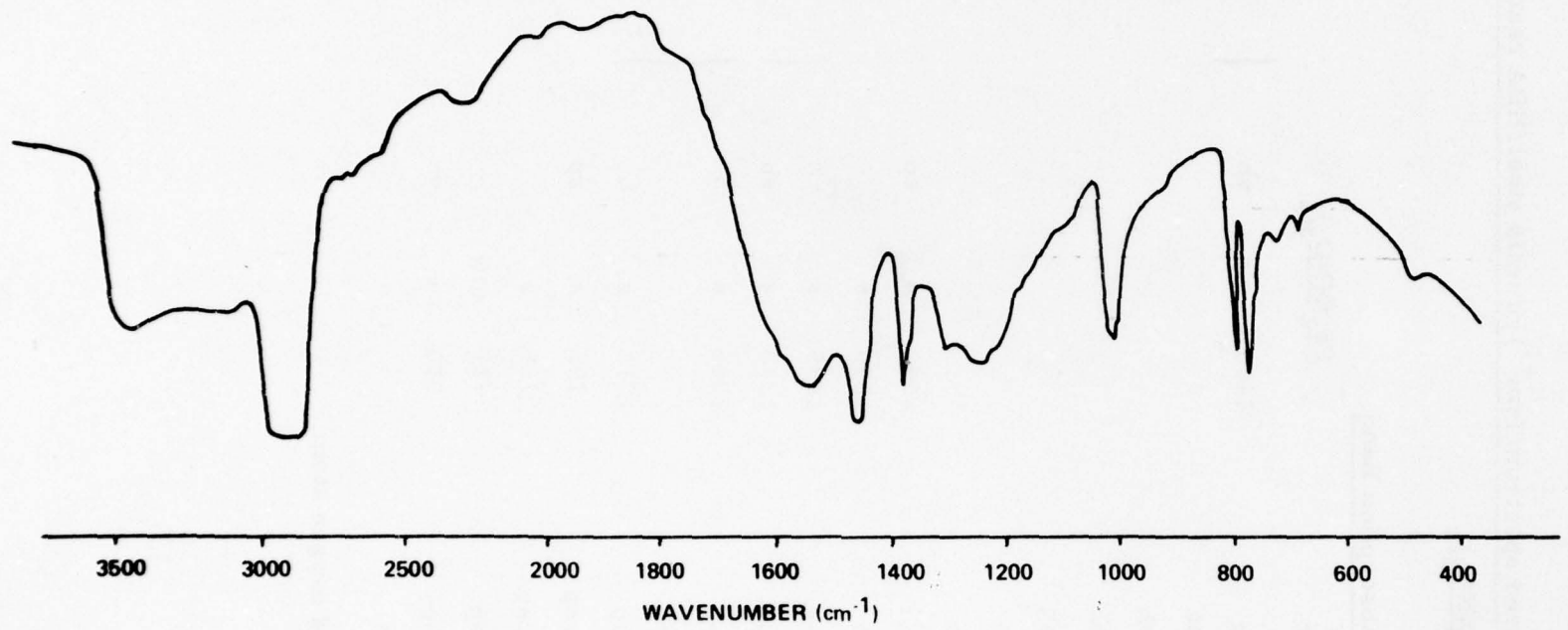


Figure 5-7. IR Spectrum of Mild Steel/HDA Product

Table 5-7. Infrared spectrum (cm^{-1}) of mild steel/HDA reaction product and $Fe_2O(NO_3)_4$

Absorption Band						Assignment
mild steel/HDA			$Fe_2O(NO_3)_4$			(C_{2v} bidentate nitrate model)
3500	m	b	3400	ms	vb	ν(OH)
3100	m	sh				
2725	w	sh				
2670	w	sh				
2560	m	sh				
2300	w	b				
2030	w	b				
1580	m	sh	1590	s	sp	$\delta(H_2O)$
1550	s	b	1550	s		ν(NO*)
1300	s	sp	1275	s		$\nu_{as}(NO_2)$
1250	s	b	1250	s	sh	
1030	s	sh	1045	s	b	
1020	s	sh				$\nu_s(NO_2)$
1012	s	sp	1015	s	b	
802	s	vsp	793	s	sp	$\pi(NO_3)$
774	s	vsp	765	s		$\delta_s(NO_2)$
725	w	sp	722	mw		$\delta_{as}(NO_2)$
690	w	sp	550	w	vb	ν(Fe-O)
490	w	b				

* unco-ordinated oxygen atom

Table 5-8. X-Ray Powder Photographs of Mild Steel/HDA product and $Fe_2O(NO_3)_4$

Mild steel/HDA		$Fe_2O(NO_3)_4$	
d(nm)	I	d(nm)	I
0.783	70	0.786	60
0.722	10		
0.615	100	0.617	100
0.536	20	0.523	40
0.517	70		
0.505	5		
0.466	40	0.466	40
0.445	20		
0.429	80	0.430	80
0.395	70	0.395	60
0.383	10		
0.358	60	0.359	60
0.345	5		
0.388	5		
0.326	5		
0.320	40	0.320	20
0.313	5		
0.307	30	0.309	20
0.294	15		
0.279	10	0.282	10
0.271	5		
0.261	5		
0.257	5		
0.248	10	0.248	5
0.246	5		
0.239	5		
0.234	10		
0.229	10		

D. H. Jones is due to hydrolysis of the latter in the X-ray capillary, and that the two compounds are therefore not identical.

The I. R. spectra of the two products show close similarities, implying that there is little difference in nitrate co-ordination. It is thus considered that both solids are of composition $Fe(NO_3)_3 \cdot 2H_2O$, but are different structural modifications of this compound. The work described later on the reactions of nickel (Section 5.4) and aluminum (Section 6) also indicate that there is little chemical difference between the reaction products of these metals with HNO_3, or HDA.

Thermogravimetric analysis of the mild steel/HDA product

The T. G. A. was carried out to compare as many properties of the mild steel/HDA corrosion product as possible with the corresponding properties of the mild steel/HNO_3 product. The apparatus of Fig. 6-5 was used, and the technique is described in Section 6.2.

The T. G. A. shows substantial differences to that of $Fe(NO_3)_3 \cdot 2H_2O$, (see Section 5.3b and Figs. 5-8 and 5-9). The decomposition takes place in two stages, reaching their maxima at about 103°C and 136°C, the second decomposition step occurring at about twice the rate of the first. The intermediate is fairly stable, and its decomposition is slow. The intermediate plateau occurs after the loss of approximately 80 molecular weight units, assuming a formula of $Fe(NO_3)_3 \cdot 2H_2O$ for the starting solid, with a molecular weight of 278. This corresponds to a loss of $H_2O + NO_3$ (=80) and suggests formation of a basic species $FeOH(NO_3)_2$ rather than the iron(II) intermediate, $Fe(NO_3)_2 \cdot H_2O$. This suggestion is merely hypothesis at this stage.

(d) Gaseous Products of the mild steel/HNO_3 and mild steel/HDA reactions

The gaseous products were investigated using the gas collection apparatus described in Section 5.4 (b). 5mm squares of mild steel sheet (ca. 1mm thick) were used and the surface was cleaned by sand blasting and washing with inhibisol.

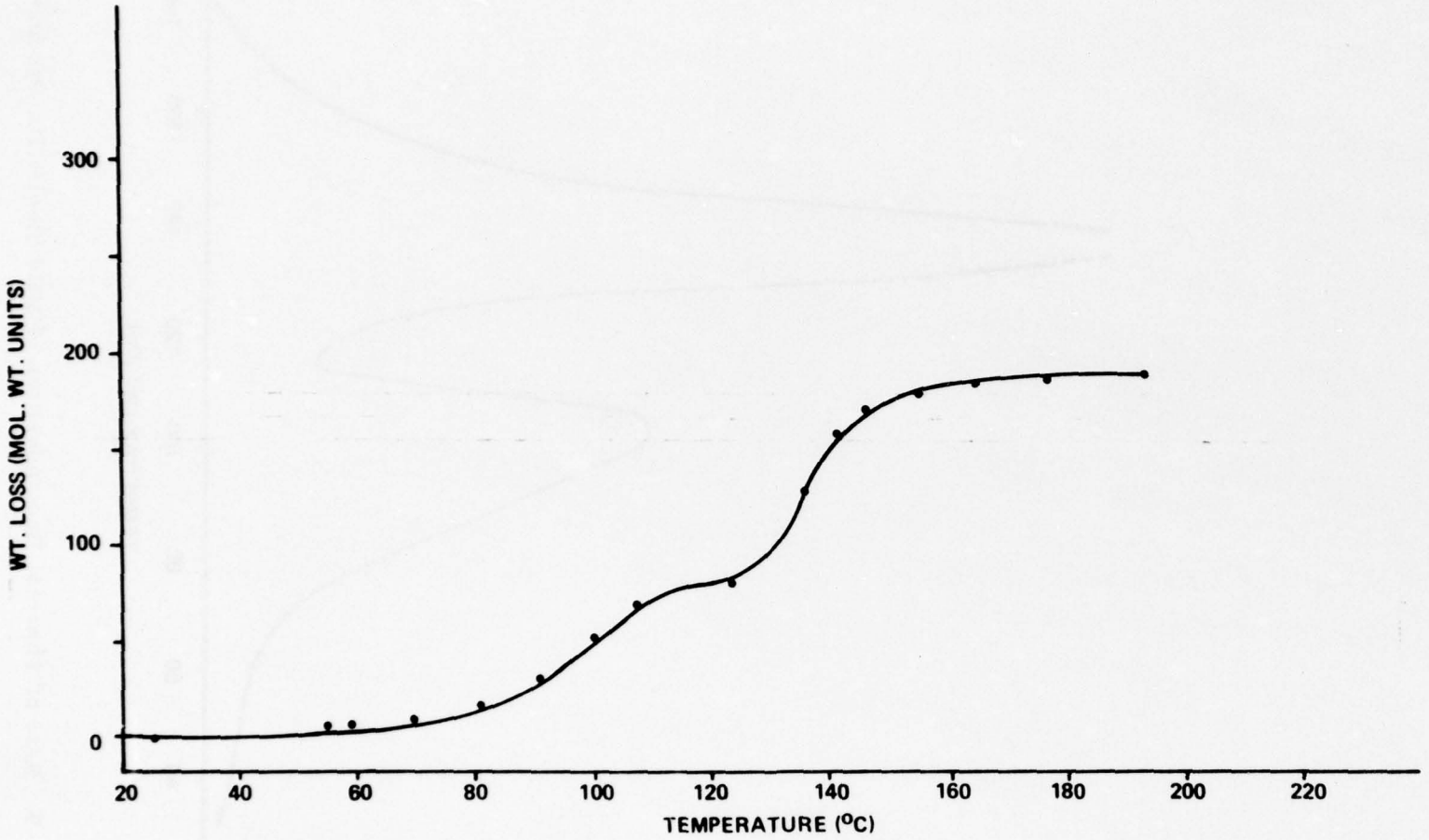


Figure 5-8. Thermogravimetric Analysis of Mild Steel/HDA Product

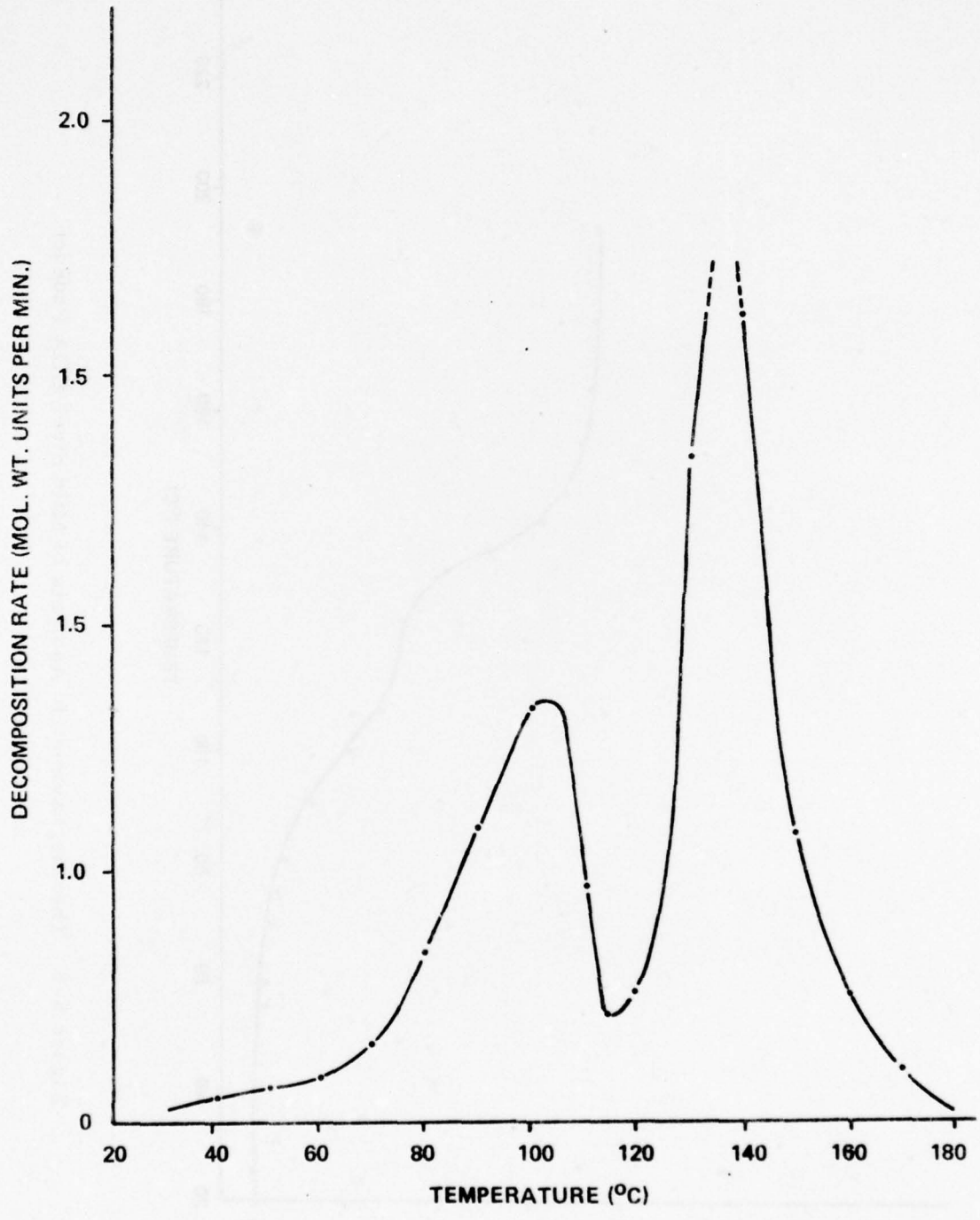


Figure 5-9. Rate of Thermal Decomposition of Mild Steel/HDA Product

Mild steel/HNO_3

About 50ml of a colourless gas was collected at 20°C in about 4 days. An increase in rate of gas collection with time was experienced initially, but this is believed to be due to the considerable solubility of N_2O in 100% HNO_3, little gas being evolved until the solution became saturated. The gas was examined by mass spectroscopy, which showed a strong peak at $^m/_e$ 44 (M. W. of N_2O = 44). The mass spectrum also showed a large number of peaks corresponding to various nitrogen and oxygen containing species, the situation being further confused by the presence of background peaks from traces of air. This method was therefore abandoned, and further investigation of gaseous products was carried out by infra-red spectroscopy. Comparison with the nickel/HNO_3 system (see Section 5.4(b) below) assisted confirmation that the colourless gas was N_2O.

Mild Steel/HDA

The gaseous products of the mild steel/HDA reaction were collected in the same manner as described above. The rate of gas evolution was slower than that observed in the mild steel/HNO_3 reaction, the bulb being filled in about 7 days.

The gas was transferred to an infra-red gas cell, fitted with silverchloride windows to prevent attack by HNO_3 etc. The spectrum is shown in Fig 5-10 and is tabulated in Table 5-9.

The spectrum is largely obscured by the very intense bands due to N_2O_4 and HNO_3. The ν_3 band of N_2O is clearly visible at 2230cm^{-1}, and the ν_1 absorption is discernable as a shoulder at 1280cm^{-1}. A band at 2330cm^{-1} is conspicuous and is probably assignable to CO_2, resulting from oxidation of the carbon present in the steel.

Further studies on the gaseous products of metal/HNO_3/N_2O_4 reactions were carried out on the nickel system (see Section 5.4(b)), where this reaction occurred more rapidly, and gave more easily characterisable solution and solid products. It is considered however that N_2O has been definitely identified in the steel/HNO_3/N_2O_4 reaction products, and that the two systems are analogous.

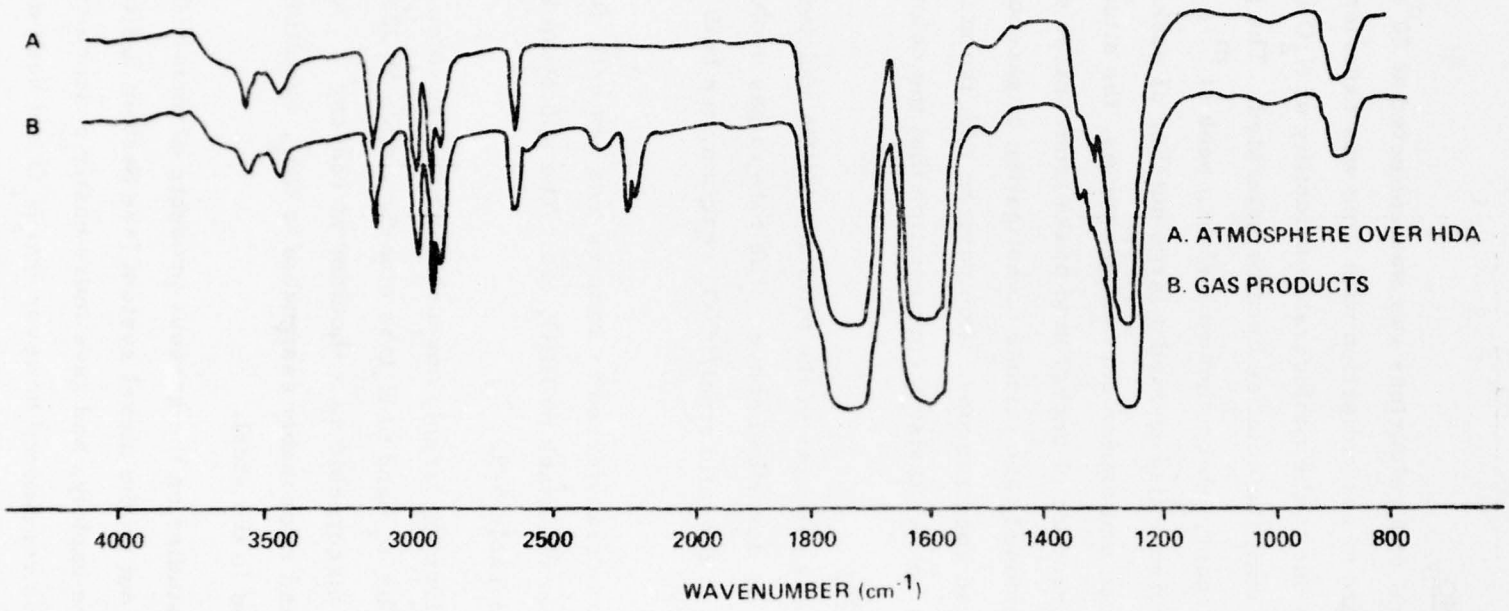


Figure 5-10. IR Spectrum of Gaseous Products of Mild Steel/HDA Reaction

Table 5-9. Infra-red spectrum of Gaseous Products of Mild Steel/HDA reaction

(Only peaks not occurring in the HNO_3/N_2O_4 vapour phase mixture are shown.)

cm^{-1}				$N_2O cm^{-1}$	
2330	w	b			
2235	m	sp	)	2224	ν_3
2200	m	sp	)		
1285	w	sh		1285	ν_1

(e) Synthetic routes to corrosion products

The reaction of $FeCl_3$ with 100% HNO_3 to yield $Fe(NO_3)_2 \cdot 2H_2O$ has been discussed in detail [1,2], and subsequently reexamined (Section 5.3(b)).

The reaction between $FeCl_3$ and HDA has not been previously reported and hence was investigated as a possible means of preparing the interesting mild steel/HDA product in greater bulk, and more rapidly than by the direct reaction of metal and acid.

$FeCl_3$(3g) was weighed into a Schlenck tube in a dry box, cooled in liquid nitrogen to moderate any violent reaction and cooled HDA (ca $25cm^3$) was added. A vigorous reaction occurred even at low temperature, much NOCl was evolved, and the mixture was allowed to warm slowly to room temperature. After 24 hours, the mixture was filtered to remove any Fe_2O_3 etc. present as a decomposition product of $FeCl_3$. A clear brown solution was obtained. Solution spectra of this showed bands attributable to $Fe(NO_3)_4^-$. The solution was evacuated (20^oC, 10^{-3}mm), and passed through a gummy stage. After about 1 week, the product consisted of an apparently homogenous, pale brown solid. The infra-red spectrum of the material was recorded (Fig. 5-11, Table 5-10). A very intense peak is present at $2295cm^{-1}$, with a shoulder at $2240cm^{-1}$, which are characteristic of the NO^+ and $N_4O_6^{2+}$ species[5] present in the compounds $Fe(NO_3)_3 \cdot N_2O_4$ and $Fe(NO_3)_3 \cdot 1.5N_2O_4$, respectively. A broad band, signifying the presence of co-ordinated water, occurs at 3500-$3000cm^{-1}$ (ν(OH)). The corresponding $\delta(H_2O)$ band is seen at $1675cm^{-1}$. Weak, broad bands at $960cm^{-1}$ and $1100cm^{-1}$ could not be definitely assigned.

The X-ray powder photograph of the material was found to be the same as that of $Fe(NO_3)_3 \cdot 2H_2O$.

These results appear to indicate that the reaction of HDA with $FeCl_3$ yields a mixture of $Fe(NO_3)_3 \cdot 1.5N_2O_4$ and $Fe(NO_3)_3 \cdot 2H_2O$. The stability of $Fe(NO_3)_3 \cdot 1.5N_2O_4$ in HDA has been demonstrated by the University of Nottingham laboratories.

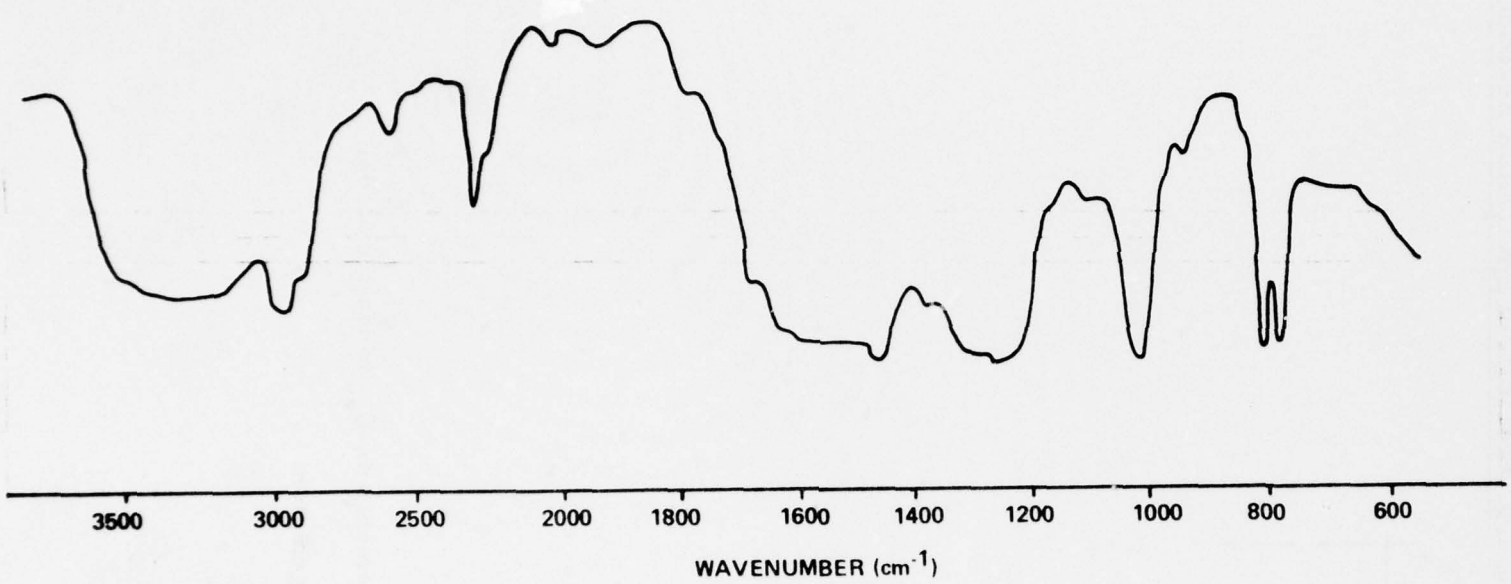


Figure 5-11. IR Spectrum of $FeCl_3$/HDA Product

Table 5-10. I.R. Spectrum of $FeCl_3$/HDA Reaction Product

Absorption band (cm^{-1})			Assignment+
3500	s	sh	)
			)
3200	s	b	) ν(OH)
			)
3170	s	b	)
2570	m	sp	N_2O_4 (molecular)
2295	s	sp	NO^+
2240	m	sh	$N_4O_6^{2+}$ (ref. 5)
2030	w	sp	
1940	w	b	
1770	m	sh	N_2O_4 (molecular)
1675	m	sh	$\delta(H_2O)$
1550	vs	vb	ν_s(N-O*)
1265	vs	b	$\nu_{as}(NO_2)$
1265	w	sp	N_2O_4 (molecular)
1100	w	b	
1020	s	sp	$\nu_s(NO_2)$
930	m	sp	
800	s	vsp	$\pi(NO_3)$
770	s	sp	$\nu_s(NO_2)$
570	w	sh	ν(Fe. OH_2)

+Nitrate group assignments on C_{2v} bidentate Model

*Unco-ordinated oxygen atom

The formation of $NO^{+}[Fe(NO_3)_4]^{-}$ in the reaction between $FeCl_3$ and HDA, whereas the reaction between the metal and HDA yields a hydrated nitrate only, is interesting. It is possible that the presence of excessive amounts of water, produced by reactions involving the reduction of nitric acid in HDA by the steel, enhances the formation of $Fe(NO_3)_3 \cdot xH_2O$. On the other hand, the much more anhydrous conditions of the $FeCl_3$ reaction, where no decomposition of the nitric acid to give water occurs in the course of the reaction, favour the formation of $Fe(NO_3)_3 \cdot 1.5N_2O_4$, possibly by affecting the equilibrium:

$$2H_2O + Fe(NO_3)_3 \cdot 1.5N_2O_4 \rightleftharpoons Fe(NO_3)_3 \cdot 2H_2O + 1.5N_2O_4$$

The exact composition of the mixed reaction product was not investigated further.

(f) The reaction of HDA with Fe_2O_3 and Fe_3O_4

The formation of black coatings on the surface of mild steel left in contact with HDA and HNO_3, and the possibility of formation of oxide passivation films on the metal led to the investigation of these reactions of Fe_2O_3 and Fe_3O_4 with HDA. The experiment described above (Section 5.3.(e).) shows that different products can be obtained from the reactions between (i) a metal itself or (ii) one of its compounds, with HDA.

Small samples of each oxide were immersed in HDA in sealed boiling tubes. No immediate reactions were observed and the tubes were set aside for several weeks. At the end of this time the solutions were filtered and evaporated to dryness ($20^{\circ}C$, 10^{-3}mm).

The Fe_2O_3/HDA reaction was found to yield only a small quantity of solid material. The infra-red spectrum of this was weak and poorly resolved. The powder photograph was found to be identical with that of the Fe_2O_3 starting material, and it was assumed that no reaction had occurred.

The Fe_3O_4/HDA solution pumped down to a viscous gum, and ultimately gave a dry, chestnut brown solid, of similar appearance to the mild steel HDA product.

The infra-red spectrum and X-ray powder photographs of this solid were found to be identical to those of the mild steel/HDA product described above. It was found to contain 20.98%Fe (cf. mild steel/HDA product, 20.52% Fe.) It is thus assumed that the two products are identical.

This implies that the same iron products would be obtained from solution whether the reaction between mild steel and HDA took place via the direct route, metal $\xrightarrow{HDA}$ products or via an intermediate Fe_3O_4 passivation film, i.e.

$$Fe \xrightarrow{HDA} \text{Surface } Fe_3O_4 \xrightarrow{HDA} \text{Products}$$

The apparent inertness of Fe_2O_3 toward HDA suggests that Fe_2O_3 films do not participate in the mechanism of the mild steel/HDA reaction.

(g) Reactions of corrosion products with liquid N_2O_4

The reactions of the various corrosion products of mild steel/HNO_3 and mild steel/HDA with N_2O_4 were studied in order to obtain a more complete picture of the mild steel/HNO_3/N_2O_4 system, and to examine changes in corrosion products with N_2O_4 concentration in more detail.

(i) Treatment of the mild steel/HNO_3 solution with liquid N_2O_4

A solution of the mild steel/HNO_3 reaction products was prepared by allowing mild steel to react with 100% HNO_3 for one week. The solution was then filtered to remove metal crystallites and sufficient N_2O_4 to make the mixture up to HDA composition was added. No reaction was observed on mixing, and the mixture was allowed to stand for one month. At the end of this time no visible change had occurred in the mixture, and it was evaporated to dryness. The mixture passed through a gummy phase and ultimately a light brown apparently homogeneous solid was formed.

The infra-red spectrum of the material was recorded, (Fig. 5-12, Table 5-11) and suggests the presence of at least three components. Broad bands characteristic of co-ordinated H_2O are observed at 3300cm^{-1} and 1680cm^{-1}, together with bands at 2298cm^{-1} and 2220cm^{-1} which suggest the presence of

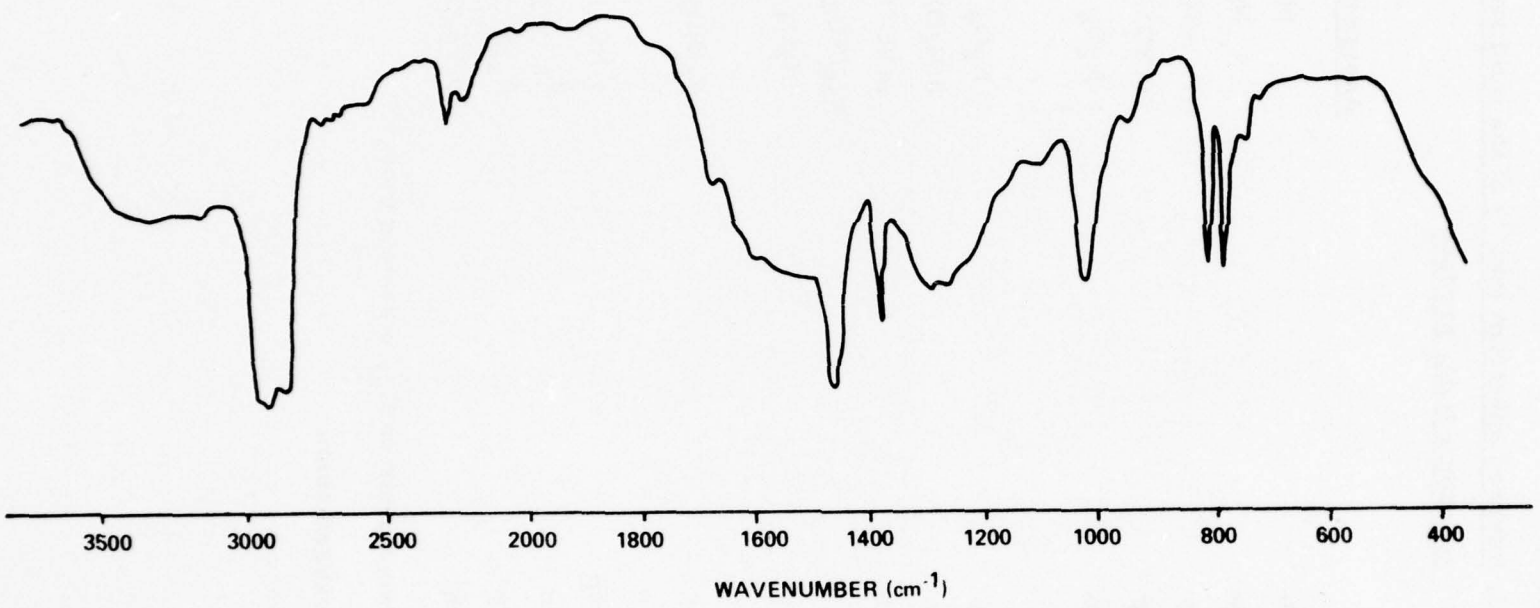


Figure 5-12. IR Spectrum of (Mild Steel/HNO_3) Solution + N_2O_4 Product

Table 5-11. Infrared spectrum (cm^{-1}) of the mild steel/HNO_3 solution + N_2O_4 product

Absorption band		Assignment +
3700-3300	vs vb	ν(O-H)
2570	m sp	N_2O_4
2292	s sp	$\nu(NO^+)$
2240	s sp	$\nu(NO^+)$ in $N_4O_6^{2+}$ (ref 5)
2040	m sp	) N_2O_4
1930	m b	)
1760	m sp	N_2O_4
1670	m sh	$\delta(H_2O)$
1530	vs vb	$\nu(NO^*)$
1300	vs b	$\nu_{as}(NO_2)$
1265	s sp	N_2O_4
1100	m b	
1020	s sp	$\nu_s(NO_2)$
930	m sp	
795	s vsp	$\pi(NO_3)$
770	s sp	$\delta_s(NO_2)$
720	w sp	$\delta_{as}(NO_2)$
570	w sh	ν(Fe-O)

+ Nitrate group assignments on C_{2v} bidentate model

* Unco-ordinated oxygen atom.

$Fe(NO_3)_3 \cdot N_2O_4$ and $Fe(NO_3)_3 \cdot 1.5N_2O_4$. The co-ordinated nitrate band at $1035cm^{-1}$ is a singlet, characteristic of compounds of the type $Fe(NO_3)_3 \cdot xN_2O_4$. The co-ordinated nitrate band of the compound $Fe(NO_3)_3 \cdot 2H_2O$ at $1051cm^{-1}$ is absent, unless the slight splitting at 1045 cm^{-1} is caused by this band. Bands appear at $1100cm^{-1}$ and $930cm^{-1}$, similar to those present in the $FeCl_3$/HDA reaction product.

In view of the obviously mixed nature of this compound, no analysis was carried out, as this would be confused by the variable iron content of mixtures of $Fe(NO_3)_3 \cdot N_2O_4$ and $Fe(NO_3)_3 \cdot 1.5.N_2O_4$. The infra-red spectrum is very similar to that of the $FeCl_3$/HDA solid reaction product (Fig. 5-11), and it is likely that a mixture of similar constitution is formed. Here, however, the presence of N_2O_4 solvates of $Fe(NO_3)_3$ in this mixture is unexpected, since the presence of water as a decomposition product of the nitric acid would be expected.

(ii) The reaction of the mild steel/HNO_3 solid reaction product with liquid N_2O_4

Approximately 0.5g. of the mild steel/HNO_3 solid product was immersed in about 10ml. of pure dry N_2O_4. Immediately on addition, the solid became sticky. The mixture was left for 6 weeks to equilibrate. At the end of this time the excess N_2O_4 was decanted off, and the solid residue was pumped dry. After evacuation for 15 hours, the initially gummy solid was quite dry. The infra-red spectrum and X-ray powder photograph of this material were recorded. The infra-red spectrum (Fig. 5-13, Table 5-12) shows very clearly the presence of co-ordinated water, and NO^+ probably as $N_4O_6^{2+}$, i.e. the ion cluster $(NO^+)_3NO_3^-$ (peak at $2235cm^{-1}$).[5] The co-ordinated nitrate band $\nu_s(NO_2)$ in the $1060\text{-}1000cm^{-1}$ region shows the characteristic triplet of $Fe(NO_3)_2 \cdot 2H_2O$ with the lower member of the triplet at $1025cm^{-1}$ of increased intensity relative to its usual intensity in $Fe(NO_3)_3 \cdot 2H_2O$, suggesting the presence of an underlying intense band. The co-ordinated nitrate $\pi(NO_3)$ and $\delta_s(NO_2)$ bands in the $810\text{-}730cm^{-1}$ region show fine structure characteristic of both $Fe(NO_3)_3 \cdot 2H_2O$ and $Fe(NO_3)_3 \cdot 1.5N_2O_4$. There is a weak band at $1100cm^{-1}$ similar to that in the mild steel/HNO_3 solution + N_2O_4 product (Table 5-11.)

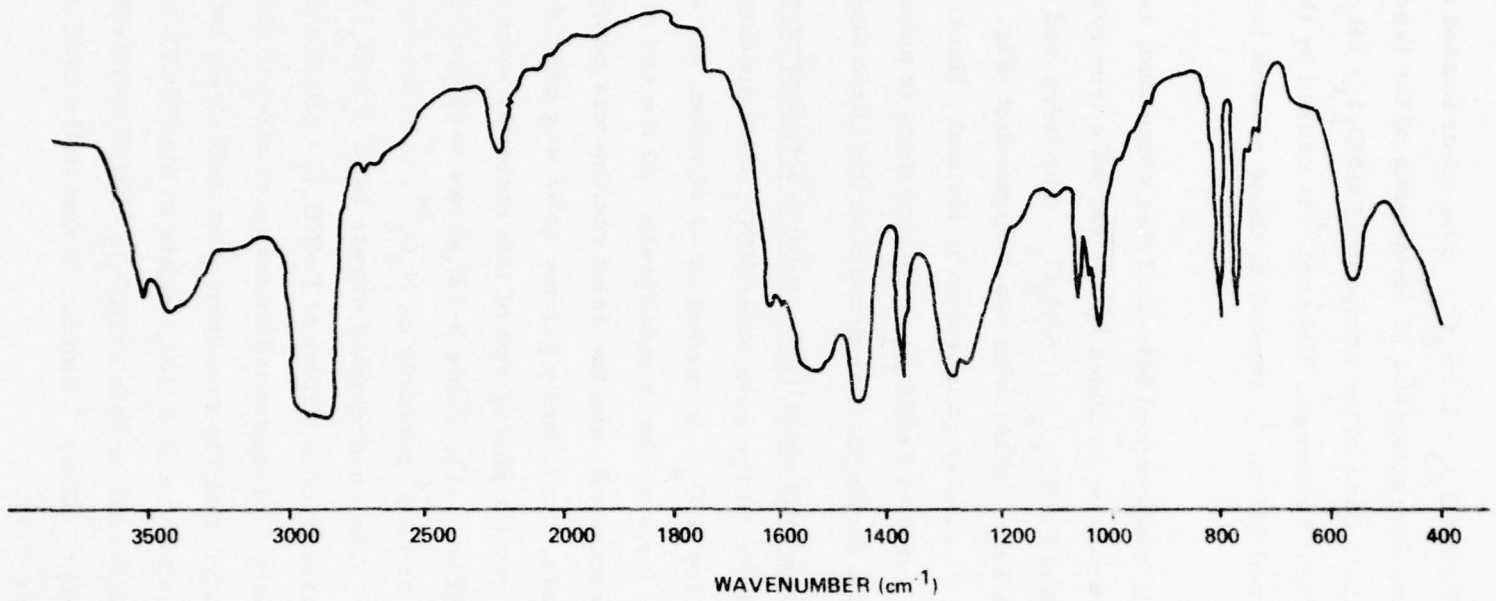


Figure 5-13. IR Spectrum of Mild Steel/HNO_3 Product + N_2O_4

Table 5-12. Infrared spectrum (cm^{-1}) of mild steel/HNO_3 solid product + N_2O_4

Absorption band		Assignment+
3540	s sp	ν(OH)
3440	s b	
2730	w sp	
2560	w sh	
2235	s sp	$\nu(NO^+)$ in $N_4O_6^{2+}$ (ref. 5)
2090	w sh	$2x\nu_s$ (NO_2)
1740	w sh	N_2O_4
1620	w sp	δH_2O
1592	w sp	ν(NO*)
1550	vs b	
1285	vs sb	$\nu_{as}(NO_2)$
1260	s sp	
1150	m sh	
1100	w b	
1055	s sp	$\nu_s(NO_2)$
1037	m sp	
1025	vs sp	
803	vs sh	$\pi(NO_3)$
795	vs sp	
790	vs sp	δ_s (NO_2)
550	vs b	ν(FeO)

+ Nitrate group assignments on C_{2v} bidentate model.

* Unco-ordinated oxygen atom.

The X-ray powder photograph shows lines attributable to the presence of both $Fe(NO_2)_3 \cdot 2H_2O$ and $Fe(NO_3)_3 \cdot 1.5N_2O_4$, and very little else. (Table 5-13).

It is thus concluded that $Fe(NO_3)_3 \cdot 2H_2O$ reacts with liquid N_2O_4 to give an equilibrium mixture of $Fe(NO_3)_3 \cdot 1.5N_2O_4$ and $Fe(NO_3)_3 \cdot 2H_2O$.

Previous University of Nottingham work[2] examined the interaction between $Fe(NO_3)_3 \cdot 1.5N_2O_4$ and liquid N_2O_4 containing a small amount of water by ^{1}Hn. m. r. and, taken in conjunction with the above results, suggests the existence of the equilibrium

$$Fe(NO_3)_3 \cdot 1.5N_2O_4 \underset{N_2O_4}{\overset{H_2O}{\rightleftharpoons}} Fe(NO_3)_3 \cdot 2H_2O$$

The previous work indicated that $Fe(NO_3)_3 \cdot 1.5N_2O_4$ was stable in liquid N_2O_4 containing up to 0.22wt% water, but was converted to $Fe(NO_3)_3 \cdot 2H_2O$ at higher water concentrations. It was therefore decided to examine the equilibrium from the other extreme, i.e. to measure the uptake of water by dry liquid N_2O_4 in contact with $Fe(NO_3)_3 \cdot 2H_2O$, by ^{1}Hn. m. r. of the liquid N_2O_4.

A weighed amount of mild steel/HNO_3 reaction product was transferred to a small Schlenck tube. To this was added sufficient liquid N_2O_4 to ensure that if complete conversion to $Fe(NO_3)_3 \cdot 1.5N_2O_4$ occurred, the solubility limit of "water" (or more correctly, HNO_3) in N_2O_4 would not be exceeded, and no second phase would be formed (assuming no drastic modification of the HNO_3/N_2O_4 phase diagram by the presence of $Fe(NO_3)_3 \cdot 1.5N_2O_4$ or $Fe(NO_3)_3 \cdot 2H_2O$, as indicated by conductivity studies reported in Section 2.)

The mixture was allowed to equilibrate for 4 months at 20°C. At the end of this time a pronounced green colour had developed in the N_2O_4, and the solid had become sticky.

Samples of the N_2O_4 were withdrawn with a pipette and transferred to 4mm diameter n. m. r. tubes, which were then flame sealed. A set of calibration standards was also prepared spanning the range 0.2 to 1.0wt% "H_2O" in N_2O_4.

Table 5-13. X-ray powder photograph of mild steel/HNO_3 solid product + N_2O_4

d(nm)	I	$Fe(NO_3)_3 \cdot 2H_2O$ d (nm)	I	$Fe(NO_3)_3 \cdot 1.5N_2O_4$ d (nm)	I
1.019	3				
0.934	5				
0.817	5			0.82	10
0.752	5			0.76	60
0.722	10			0.720	70
0.683	5			0.681	30
0.655	90	0.654	80		
0.629	5			0.631	80
0.609	90	0.606	80		
0.566	5			0.565	30
0.547	3			0.545	5
0.519	5			0.520	15
0.492	5	0.492	5		
0.462	10			0.461	100
0.455	5			0.442	30
0.427	3			0.427	30
0.408	80	0.407	40		
0.400	3				
0.376	20	0.374	2		
0.368	20	0.368	20		
0.358	20	0.359	20		
0.342	10	0.344	5	0.344	60
0.335	100	0.336	100	0.336	5
0.327	5			0.328	40
0.319	5	0.320	15		
0.314	5	0.313	15		

Table 5-13. (Cont'd) X-ray powder photograph of mild steel/HNO_3 solid product + N_2O_4

d (nm)	I	$Fe(NO_3)_3 \cdot 2H_2O$ d (nm)	I		$Fe(NO_3)_3 \cdot 1.5N_2O_4$ d (nm)	I
0.307	3				0.308	20
0.299	20	0.299	10			
0.282	25	0.282	15			
0.273	5	0.274	5			
0.267	5	0.267	5			
0.260	3			)	0.260	20
				)		
0.258	3			)		
0.250	3	0.251	10			
0.247	3	0.248	10			
0.243	5	0.243	2			
0.238	3	0.235	30			

A linear relationship of peak area to "H_2O" content was established, and the "H_2O" content of the N_2O_4 which had been equilibrated with the mild steel/HNO_3 product was found by comparison.

The water content of the N_2O_4 from this equilibration reaction was found to be 0.382 wt.%. The Schlenk vessel had contained 13.438g. N_2O_4 and 1.648g. $Fe(NO_3)_2 \cdot 2H_2O$. From these figures the amount of water removed from the $Fe(NO_3)_3 \cdot 2H_2O$ was calculated, and this indicated that approximately 24% conversation of this solid to $Fe(NO_3)_3 \cdot 1.5N_2O_4$ had taken place. It is acknowledged that from these figures the equilibrium constant should theoretically be derivable, however, the equilibrium is complicated by the parallel equilibrium

$$N_2O_4 \rightleftharpoons 2NO_2$$

at the temperature employed. At 20°C the equilibrium mixture contains about 0.1% NO_2, so the mixture can be treated as virtually pure N_2O_4. Hence for the equilibrium:

$$Fe(NO_3)_3 \cdot 2H_2O + 1.5N_2O_4 \overset{K_{eq}}{\rightleftharpoons} Fe(NO_3)_3 \cdot 1.5N_2O_4 + 2H_2O$$

$$K_{eq} = \frac{Fe(NO_3)_3 \quad 1.5N_2O_4}{Fe(NO_3) \quad 2H_2O} \cdot \frac{[H_2O]^2}{[N_2O_4]^{3/2}}$$

$$\text{hence } K_{eq} = 4.7 \times 10^{-6}$$

This low value for the equilibrium constant indicates the greater stability of $Fe(NO_3)_2 \cdot 2H_2O$ with respect to N_2O_4 than of $Fe(NO_3)_3 \cdot 1.5N_2O_4$ with respect to H_2O.

(iii) Reaction of the mild steel/HDA solid product with N_2O_4

Approximately 0.5g. of the mild steel/HDA product was immersed in about 10ml. of N_2O_4. Immediately on addition, the solid became gummy, and after 1 hour, the solid had been completely converted to a brown oil. After 24 hours

the oil had solidified, and the N_2O_4 over the solid was replaced. This mixture was allowed to stand for 3 weeks, at the end of which time the solid material appeared to be no longer gummy. Excess N_2O_4 was decanted off and the solid evacuated. After 20 hours the solid was completely dry and resembled the chestnut colour of the original compound. The infra-red spectrum was recorded (Fig. 5-14, Table 5-14). This showed the presence of co-ordinated water and $N_4O_6^{2+}$ ($2230cm^{-1}$). The $1015cm^{-1}$ band of co-ordinated nitrate was a singlet, and the nitrato-bands in the $700-810cm^{-1}$ region show fine structure characteristic of both the mild steel/HDA product and $Fe(NO_3)_3 \cdot 1.5N_2O_4$.

The X-ray powder photograph (Table 5-15) corresponds almost exactly with the powder photograph of $Fe(NO_3)_3 \cdot 1.5N_2O_4$, few other lines being observed. The X-ray powder lines of the mild steel/HDA product do not appear on the film.

It thus seems likely that the mild steel/HDA product reacts with N_2O_4 in a manner analogous to the reaction of the mild steel/HNO_3 product. The presence of co-ordinated water as indicated by the infra-red spectrum (Table 5-14) suggests an equilibrium process.

No n. m. r. studies were carried out on the mild steel/HDA solid product - liquid N_2O_4 system.

(h) Possible structures of mild steel/HNO_3 and mild steel/HDA products

Considerable attention was given to the question of the molecular formulae and structure of these compounds.

Formulation of these products as e. g. $Fe(NO_3)_3 \cdot 2H_2O$ and $Fe(NO_3)_3 \cdot H_2O$ carries no implication as to their structures. One possibility for $Fe(NO_3)_3 \cdot 2H_2O$ would be $[Fe(H_2O)_4(NO_3)_2]^+[Fe(NO_3)_4]^-$ involving two structrually distinct iron species. However, formulations such as

$$(H_3O^+)_2[Fe_3O(NO_3)_9]^{2-} \cdot 3H_2O,$$

$$[Fe_3O(NO_3)_6 \cdot (H_2O)_3]^+NO_3^- \cdot 2HNO_3 \cdot 2H_2O$$

or $[Fe_3O(NO_3)_6 \cdot (H_2O)_2(OH)] \cdot 3HNO_3 \cdot 2H_2O$

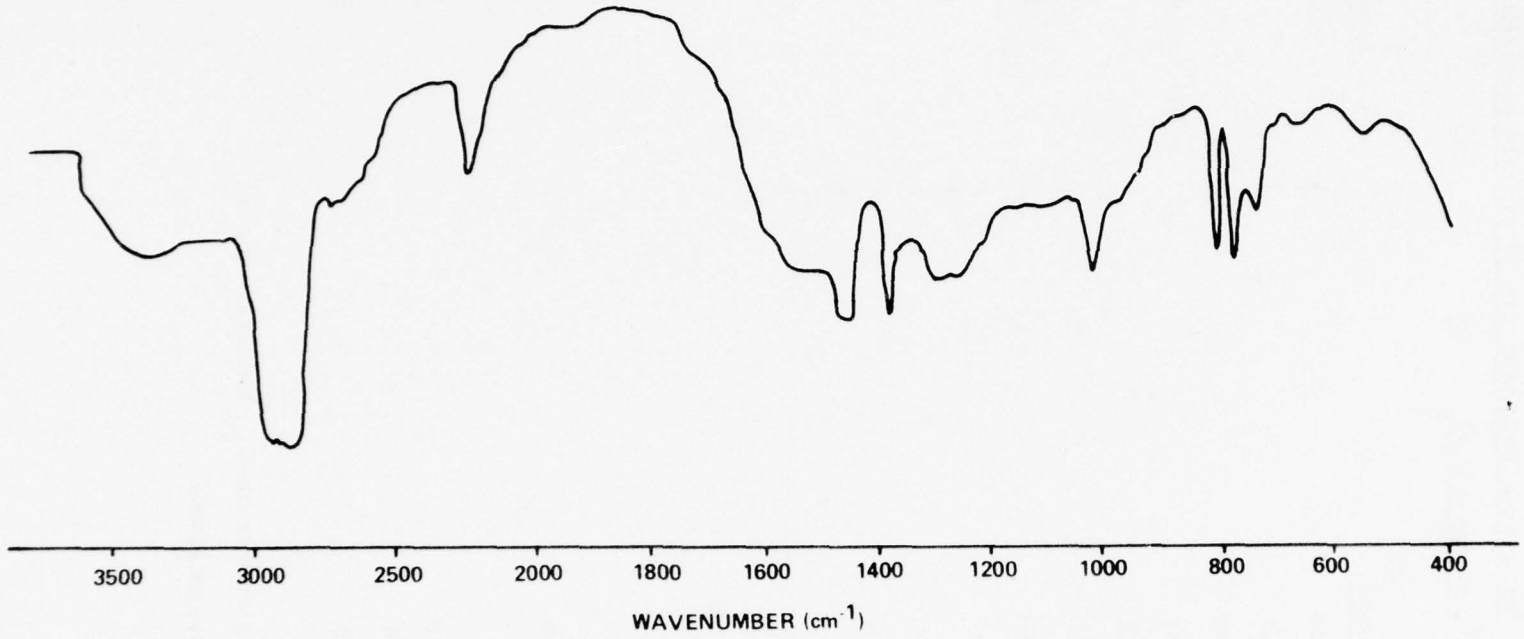


Figure 5-14. IR Spectrum of Mild Steel/HDA Product + N_2O_4

Table 5-14. Infra-red spectrum (cm^{-1}) of mild steel/HDA solid product + N_2O_4

Absorption band				Assignment[+]
3540	m	sh	)	ν(OH)
3370	s	b	)	
2720	w	sp		
2230	s	sp		$\nu(NO^+)$ in $N_4O_6^{2+}$ (ref. 5)
1930	w	b		
1740	m	sh		N_2O_4
1620	w	sh		$\delta(H_2O)$
1595	m	sh	)	
			)	ν(NO*)
1545	vs	vb	)	
1280	vs	b	)	
			)	$\nu_{as}(NO_2)$
1260	s	sh	)	
1100	vw	b		
1015	m	sp		$\nu_s(NO_2)$
920	w	sh		
800	s	vsp		$\pi(NO_3)$
768	s	sp	)	$\delta_s(NO_2)$
			)	
740	w			
725	w	sp		$\delta_{as}(NO_2)$
650	w	b		
540	w	b		ν(FeO)

+ Nitrate group assignments on C_{2v} bidentate model.

* Unco-ordinated oxygen atom.

Table 5-15. X-ray powder photograph of mild steel/HDA solid product + N_2O_4

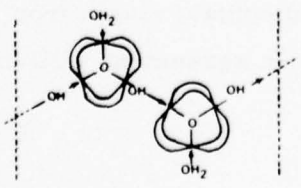
Mild Steel/HDA solid + N_2O_4		$Fe(NO_3)_3 \cdot 1.5N_2O_4$	
d(nm)	I	d(nm)	I
1.014	5		
0.926	10	0.93	20
0.817	5	0.82	10
0.762	30	0.76	60
0.718	50	0.720	70
0.636	50	0.631	80
0.566	40	0.565	30
0.549	5	0.545	5
0.517	10	0.520	15
0.492	10	0.486	2
0.462	100	0.461	100
0.445	5	0.442	30
0.429	10	0.427	30
0.410	60	0.410	30
0.376	50	0.377	70
0.359	40	0.360	60
0.344	50	0.344	60
0.337	60	0.366	5
0.327	50	0.328	40
0.317	20	0.318	25
0.308	10	0.308	20
0.299	10	0.300	20
0.282	50	0.281	50
0.270	5	0.268	10
0.260	15	0.260	20

Table 5-15. (cont.) X-ray powder photograph of mild steel/HDA solid product + N_2O_4

Mild Steel/HDA solid + N_2O_4		$Fe(NO_3)_3 \cdot 1.5N_2O_4$	
d(nm)	I	d(nm)	I
0.251	5	0.245	50
0.245	15	0.240	15
0.239	5	0.234	15

containing the M_3O triangular units described in connection with the product $Al_3O(NO_3)_7 \cdot 8H_2O$ (section 6.1(b)) are also empirically $Fe(NO_3)_3 \cdot 2H_2O$. It is therefore possible that these hydrated nitrato-iron compounds contain Fe_3O units, with the same kind of triangular oxygen-centered structures. The Mössbauer spectra imply that the iron atoms are in identical, spherically symmetrical environments, and that the complexity of the infrared spectra in the covalent nitrate stretching and deformation regions is consistent with a complex arrangement of bridging and terminal nitrates. As mentioned earlier, however, the infrared spectrum does not indicate the presence of ionic nitrate, as required by the formulation $[Fe_3O(NO_3)_6 \cdot (H_2O_3)]^{+} NO_3^{-} \cdot 2HNO_3 \cdot 2H_2O$. Nevertheless, a variety of possible structures containing Fe_3O nitrato-species can be proposed, all of which are, of course, speculative at this stage. The two-stage thermal decomposition (Section 5.3(c)) of the mild steel/HDA product, $Fe(NO_3)_3 \cdot 2H_2O$, to give a compound formulated empirically as $Fe(OH)(NO_3)_2$ at 103°C, which subsequently decomposes at 136°C, suggests that $Fe(OH)(NO_3)_2$ contains a more stable unit than its precursor, possibly of the form $[Fe_3O(NO_3)_6(OH) \cdot (H_2O)]$ (empirically). The similarity of the single decomposition temperature of the mild steel/HNO_3 product (142°C) to that of the 2nd decomposition step of the mild steel/HDA product (136°C) (Section 5-3(b) and (c)), could indicate that the mild steel/HNO_3 compound contains the same trinuclear unit as the intermediate $Fe(OH)(NO_3)_2$, and the temperature 136°C - 142°C represents the temperature at which this unit decomposes. On this basis the lower temperature of 103°C may represent the temperature at which the trinuclear unit present in the mild steel/HDA product decomposes to form a different trinuclear unit in $Fe(OH)(NO_3)_2$.

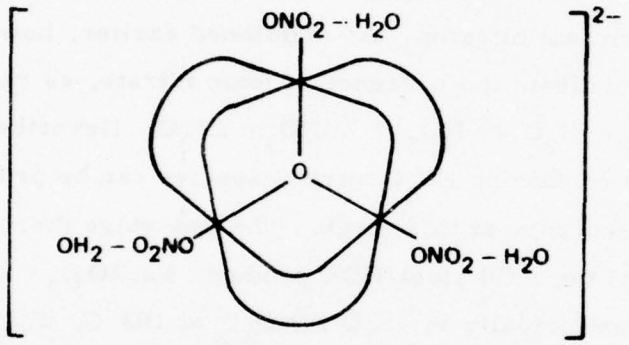
A possible structure of $Fe(OH)(NO_3)_2$, incorporating trinuclear units, is the polymeric, OH bridged system(I):



(I)

(N. B. Fe-O-Fe angle expected to be ca 109°)

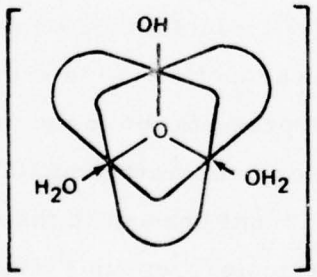
A vast variety of possible structures for $Fe(NO_3)_3 \cdot 2H_2O$ can be suggested, some involving discrete molecular units, some involving polymeric bridged oligomers and infinite chain species. Bridging in these structures could be via bridging NO_3^- groups, HNO_3 molecules (cf. bridging acetic acid molecules in the analogous "manganic acetate" 18 or by water and hydrogen bonding. Two possible structures of empirical composition $Fe(NO_3)_3 \cdot 2H_2O$, which could break down to give $Fe(OH)(NO_3)_2$ in the form above, are (II) and (III).



$(H_3O)_2^+$ (II)

i. e. $(H_3O^+)_2\,[Fe_3O(NO_3)_9]^{2-} \cdot 3H_2O$

and



$3HNO_3 \cdot 2H_2O$ (III)

Structure (III), involving 3 molecules of HNO_3 per unit in the lattice, bonded simply by hydrogen bonding to the nitrates or the waters, could allow for considerable variations in stoichiometry as HNO_3 is lost by evacuation or decomposition during preparation. Both these structures would contain single iron environments approximating to spherical symmetry, in agreement with the Mössbauer results.

The possibility of alternative structures (e. g. II and III) for species of the same empirical composition could account for the isolation of two compounds, both ostensibly $Fe(NO_3)_3 \cdot 2H_2O$, from mild steel/HNO_3 and mild steel/HDA, as a result of a critical balance between the concentrations of H_2O from the HNO_3 self-dissocation, and NO_3^-, in these systems.

Structure (III), containing water molecules coordinated to the $M_3O(NO_3)_6$ unit, is similar in coordination to the suggested intermediate I, and this might be expected to undergo thermal breakdown of its $[Fe_3O(NO_3)_6(OH) \cdot (H_2O)_2]$ units at a temperature similar to the decomposition temperature of the intermediate I. The decomposition of structure (II) to structure (I) at a lower temperature, by loss of three water molecules and displacement of the three terminal nitrate ligands as nitric acid would be expected to occur readily and is consistent with the TGA results.

It is less simple to propose structures for $Fe(NO_3)_3 \cdot H_2O$ which satisfy inter alia the requirements of a single iron environment and the absence of ionic nitrate.

(i) Discussion

The above-described experiments indicate a complex interrelationship of compounds across the $Fe/HNO_3N_2O_4$ system. High concentrations of N_2O_4 favour the formation of $Fe(NO_3)_3 \cdot 1.5\text{-}N_2O_4$ as a precipitate, as shown in the flow decay experiments involving propellant grade N_2O_4 containing traces of water[2]. The formation of this compound is doubtless related to the equilibrium:

$$Fe(NO_3)_3 \cdot 2H_2O + 1.5N_2O_4 \rightleftharpoons Fe(NO_3)_3 \cdot 1.5N_2O_4 + 2H_2O.$$

No data is available on the interrelationship between the products of the reactions of mild steel and HNO_3, and mild steel and HDA. The formation of two distinct compounds is apparently unique to the iron system, i. e. in comparison to the chromium, nickel, and aluminium systems (see Sections 5. 4, 5. 5 and 6), and no simple interconversion appears to be possible by adding

N_2O_4 to the mild steel/HNO_3 solution. This would seem to imply that the formation of the mild steel/HDA product is due to a different reaction mechanism by which iron is brought into solution, and not to a simple 'dehydration' process in solution. The results of the corrosion rate determination experiments of Section 3 would seem to indicate that N_2O_4 acts simply as an inert diluent and that there is no difference in mechanism. This conclusion is supported by the formation of N_2O in both HNO_3 and HDA/metal reactions. The formation of two products would seem therefore to be an idiosyncrasy of iron.

5.4 The reaction of nickel with HDA

(a) Solid reaction products and solution species

Small pieces of pure nickel foil were cleaned with inhibisol to remove surface grease, and were introduced into about 20 ml. of HDA at room temperature ($20^{\circ}C$), against a counter-current of Argon to exclude atmospheric moisture. Immediately on addition of the metal, bubbles of gas were evolved, and the region of liquid around the metal developed a green colouration. The rate of reaction was rapid and sufficient heat was evolved to raise the temperature of the mixture by about $10^{\circ}C$. The mixture was subsequently cooled to about $0^{\circ}C$ to prevent rapid evaporation of N_2O_4.

After about 2 hours, the reaction appeared to have ceased, with some unreacted nickel present. A green solution had been formed, and a large quantity of blue-green crystals had been deposited on and around the metal. Agitation of the mixture to clear the metal surface of any surface layer of crystals which may have prevented access of acid to the metal and caused premature cessation of the reaction, failed to promote any further reaction.

The reaction mixture was filtered through a sintered glass disc under dry nitrogen, and the mixture of unreacted metal and crystals was washed several times with dry dichloromethane to remove HNO_3 and N_2O_4. Finally, excess CH_2Cl_2 was removed under vacuum (10^{-3}mm, $20^{\circ}C$), unreacted metal was removed with forceps, and a blue-green free-flowing powder remained.

The infra-red spectrum of this powder was recorded (Fig. 5-15, Table 5-16) and found to be identical to the published spectrum of nickel nitrate dihydrate $Ni(NO_3)_2 \cdot 2H_2O$.[6] The X-ray powder-photograph was also recorded (Table 5-17), and similarly found to be identical to the published powder photograph of $Ni(NO_3)_2 \cdot 2H_2O$.[7] Analysis of the compound for nickel content (Appendix B.4(c)) confirmed its identity (Found: Ni, 25.8%, $Ni(NO_3)_2 \cdot 2H_2O$ requires Ni, 26.8%). On evacuation of the filtrate (10^{-3}mm, 20°C), a further quantity of this product, again identified by X-ray powder photograph, was deposited.

(b) Gaseous reaction products

Identification of the gaseous products, evolved during the Ni/HDA reaction, was an essential prerequisite to an understanding of the reaction mechanism. The equilibria referred to in Section (5.1) indicate that a number of electrophilic species are present in solution, any of which appear to be potentially capable of reduction by the metal (as judged from standard E^o values which are, of course, strictly applicable only to aqueous solutions of unit activity.)

Gaseous products were collected in a glass and teflon apparatus (Fig. 5-16). The entire apparatus was filled with HDA, or 100% HNO_3, from which any low-boiling dissolved gases had been removed by repeated freezing in liquid nitrogen, evacuation (10^{-3}mm) and re-melting. Filling with liquid was carried out against a counter current of Argon. Cleaned nickel foil was then introduced down the side arm B, against a counter-current of Argon. A magnetic stirring bar in the lower bulb 'A' kept the metal surface free from any adhering coating of solid $Ni(NO_3)_2 \cdot 2H_2O$.

When sufficient gas for examination had collected above the liquid in the upper bulb D, any remaining liquid was displaced by Argon bubbled down a capillary tube passed down B, into A. The tap was then closed and the apparatus was cut using a glass knife at C. A suitable standard taper adaptor was glass-blown onto the upper bulb D at C, to allow connection to a vacuum line.

The gaseous products of the reaction of nickel with both 100% HNO_3 and HDA were examined by infra-red spectroscopy in a 10cm gas cell fitted with AgCl

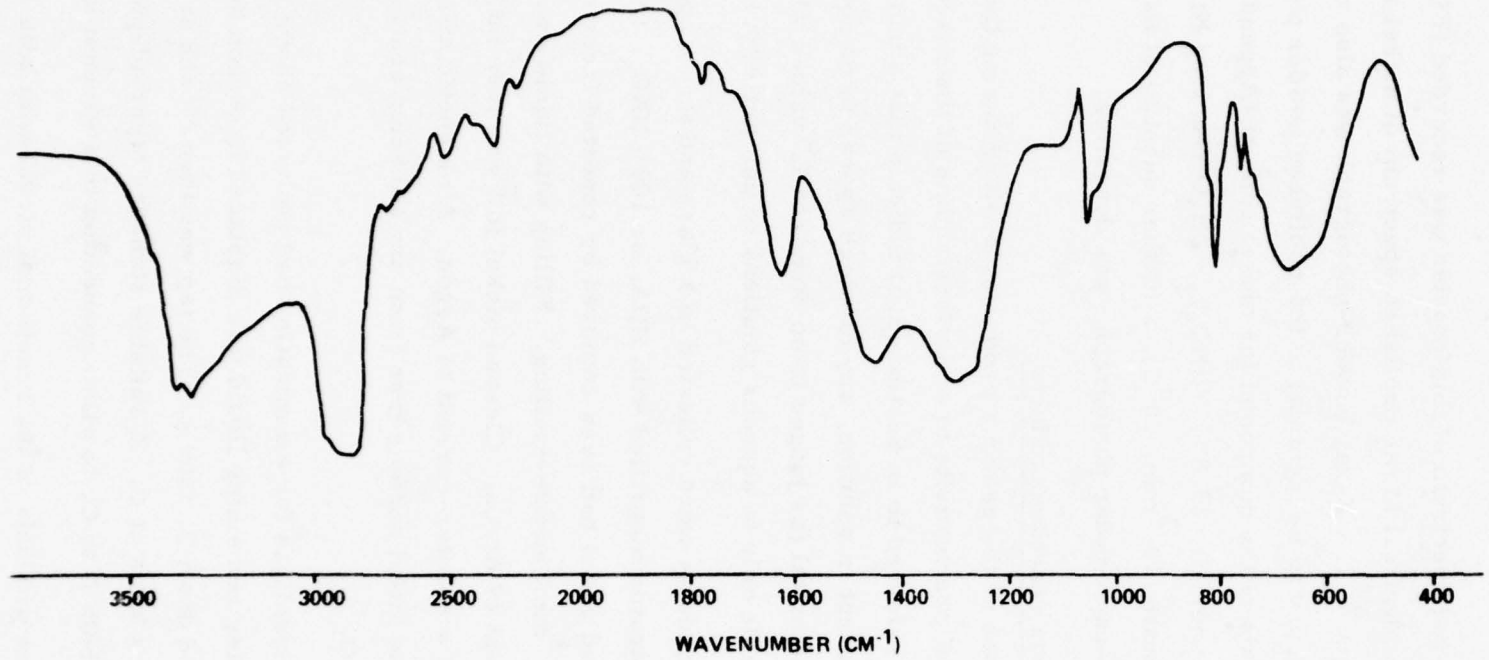


Figure 5-15. IR Spectrum of Nickel/HDA Product

Table 5-16. The infra-red spectrum (cm^{-1}) of the Ni/HDA reaction product and $Ni(NO_3)_2 \cdot 2H_2O$[6]

Absorption Bands		
Ni/HDA	$Ni(NO_3)_2 \cdot 2H_2O$	Assignment
		(Assignments appropriate to unidentate co-ordination)
	1560)	
	)	$\nu_{as}(NO_2^*)$
	1540)	
1308	1310	$\nu_s(NO_2^*)$
1050	1060	$\nu_s(NO)$
809	810	$\pi(NO_3)$
762	760	

* = unco-ordinated oxygens.

Table 5-17. The X-ray powder photograph of the Ni/HDA reaction product, and of $Ni(NO_3)_2 \cdot 2H_2O$

Ni/HDA product		$Ni(NO_3)_2 \cdot 2H_2O$	
I	d(nm)	I	d(nm)
60	0.5749	43	0.575
100	0.4840	100	0.483
50	0.4180	21	0.413
90	0.3720	88	0.3715
60	0.3420	26	0.343
		34	0.338
70	0.2970	27	0.296
		21	0.2938
70	0.2790	40	0.278
5	0.2640	9	0.262
30	0.2547	18	0.254
30	0.2473	12	0.248
5	0.2421	20	0.2465
5	0.2378		
30	0.2319	26	0.2316
40	0.2236	31	0.2240
10	0.2190	22	0.2197
50	0.2116	9	0.2110
70	0.2056	39	0.2060
		20	0.2040
5	0.2000		

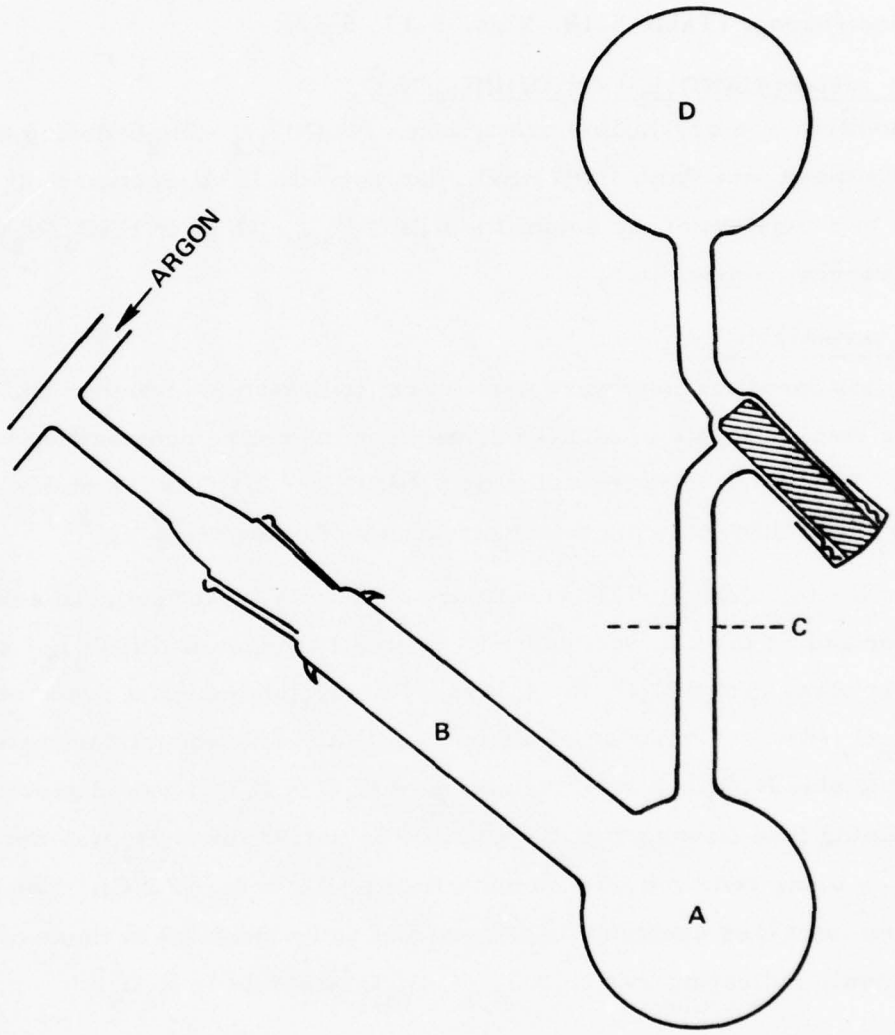


Figure 5-16. Gaseous Products Collection Apparatus

windows. N_2O_4 and HNO_3 were removed by cooling the bulb D to -78°C, both these components being solid at this temperature. The residual contents of D were then allowed to expand into the gas cell.

N_2O has been conclusively identified in the gaseous reaction products by infra-red spectroscopy (Table 5-18, Figs. 5-17, 5-18).

(c) The system $Ni(NO_3)_2 \cdot 2H_2O/HNO_3/N_2O_4$

The deposition of a crystalline precipitate of $Ni(NO_3)_2 \cdot 2H_2O$ during the reaction of 321 stainless steel with 100% HNO_3, but not with HDA (Section 5.2), prompted an investigation of the solubility of $Ni(NO_3)_2 \cdot 2H_2O$ in HNO_3/N_2O_4 mixtures of varying composition.

Preliminary investigations

Preliminary investigations were carried out to determine whether $Ni(NO_3)_2 \cdot 2H_2O$ was the stable hydrate of nickel nitrate over the entire composition range HNO_3-N_2O_4. The above work indicates that $Ni(NO_3)_2 \cdot 2H_2O$ is the stable species in 100% HNO_3, and this confirms the observations of other workers.[3,9]

The reaction of $Ni(NO_3)_2 \cdot 2H_2O$ with dry N_2O_4 was investigated to see if any dehydration or adduct formation occurred. A small amount of $Ni(NO_3)_2 \cdot 2H_2O$ was allowed to stand in dry N_2O_4 for 4 days. No development of a green colouration by the N_2O_4 (due to formation of nitrous acid, and subsequent decomposition to NO, forming blue N_2O_3 - a sure indication of H_2O in N_2O_4) was observed, the powder remaining free flowing. At the end of this period the N_2O_4 was decanted off, last traces being removed on a vacuum frame (10^{-3}mm, -20°C). The powder photograph and infra-red spectrum of the product were identical to those of the starting material, indicating that $Ni(NO_3)_2 \cdot 2H_2O$ is stable in N_2O_4.

Electronic spectra of solutions of $Ni(NO_3)_2 \cdot 2H_2O$ in 100% HNO_3 and in N_2O_4/HNO_3 mixtures were recorded to examine the nature of coordination of the Ni^{2+} cation in solution. These studies were hindered by the low solubility of $Ni(NO_3)_2 \cdot 2H_2O$ in HNO_3 and HNO_3/N_2O_4 mixtures, and by the intense U.V. absorptions of both HNO_3 and N_2O_4 at wavelengths below 450nm. These spectra

Table 5-18. The infra-red spectra of Ni/HNO_3 and Ni/HDA gaseous products, and N_2O[8] (cm^{-1})

Ni/HNO_3	Ni/HDA	N_2O	
		4736	
		4420	
		3837	
		3751	
3545	3490	3483	
		3366	
	2920	2800	
		2789	
		2777	
	2550	2565	
		2463	
2235	2235	2224	ν_3
		1885	
		1879	
		1873	
1710*	1655*		
1320	1300	1285	ν_1
		1167	

Peaks marked * in the Ni/HNO_3 and Ni/HDA spectra are believed to be due to organic impurities resulting from reaction of traces of acetone etc., used to clean the teflon tap assembly, with HNO_3 or N_2O_4.

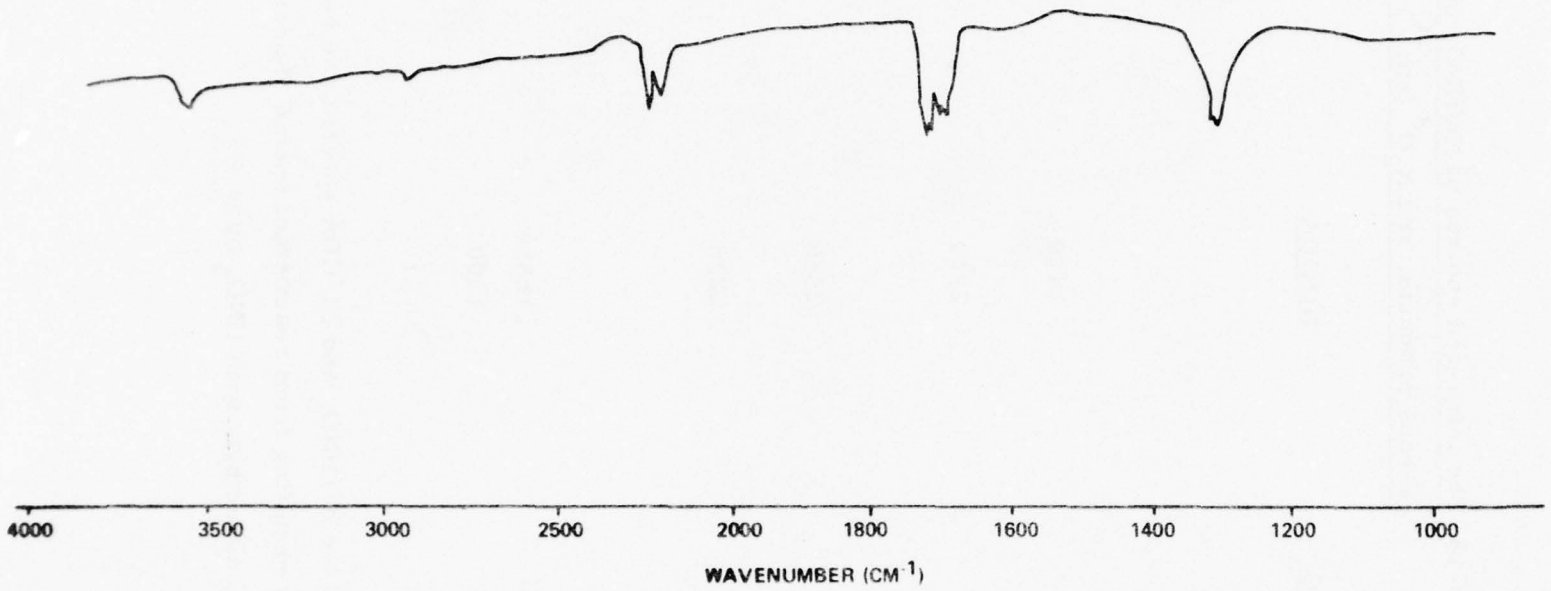


Figure 5-17. IR Spectrum of Gaseous Products of Ni/HNO_3 Reaction

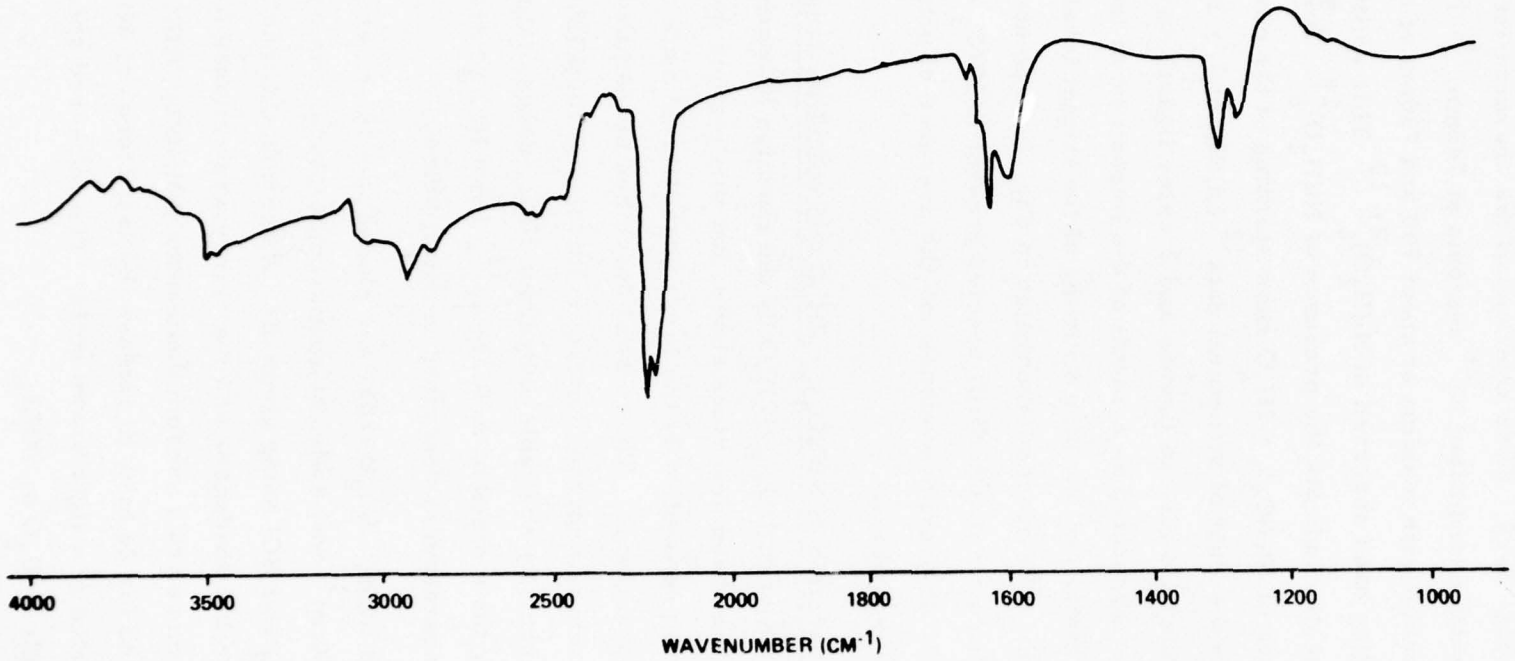


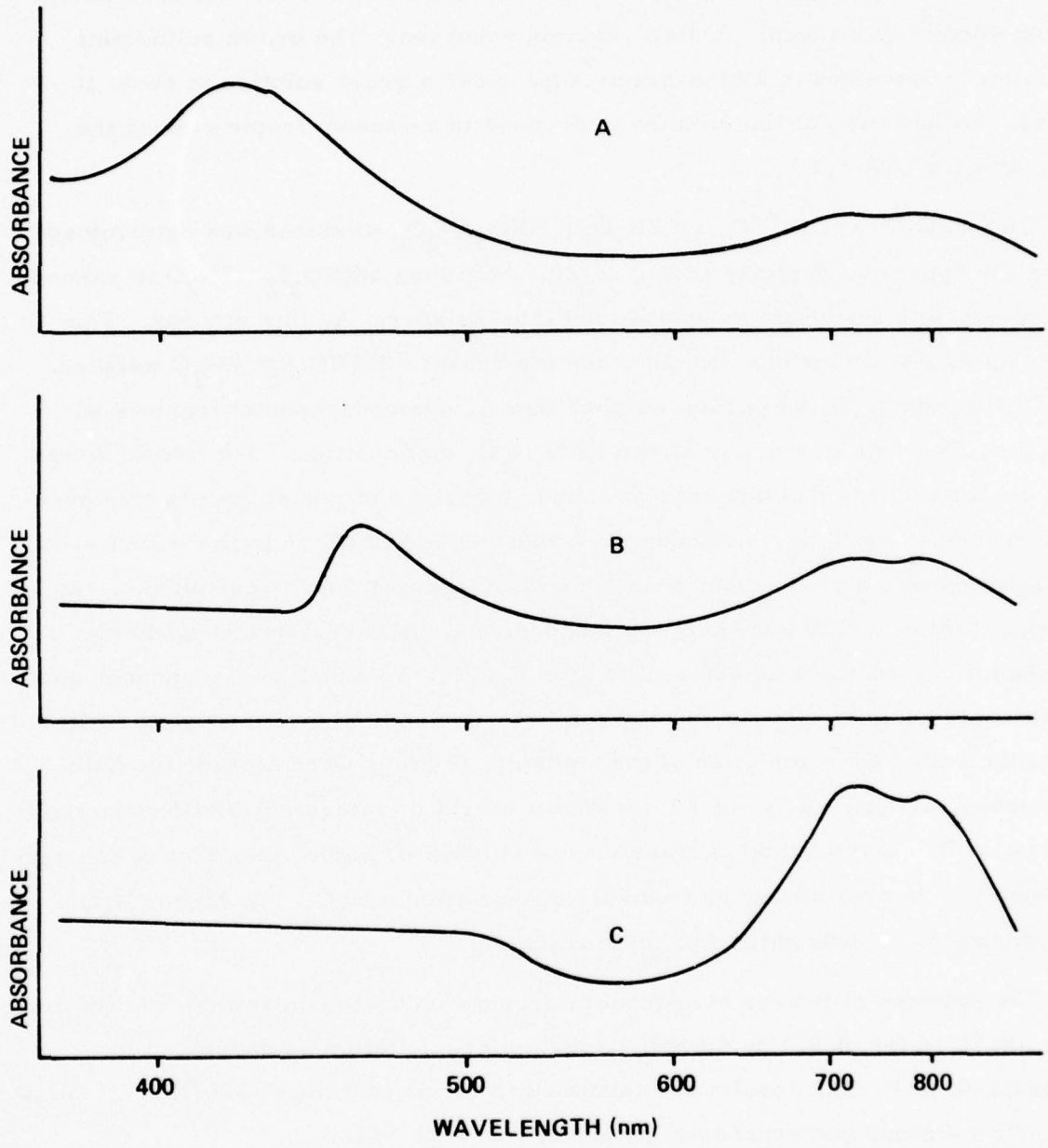
Figure 5-18. IR Spectrum of Gaseous Products of Ni/HDA Reaction

are presented in Fig. 5-19. They show one of the characteristic absorption bands of octahedrally coordinated Ni^{2+} systems at 745nm.[10] This band showed splitting into a doublet with maxima at about 790 and 730nm of similar appearance to the corresponding band observed in $Ni(H_2O)_6^{2+}$.[10] This splitting, however, does not unequivocably indicate the presence of $Ni(H_2O)_6^{2+}$. Solid state diffuse reflectance spectra of $Ni(NO_3)_2 \cdot 2H_2O$ show splitting of the peaks, into two or three peaks.[11] In the light of structural data[12] on $Ni(NO_3)_2 \cdot 2H_2O$, which shows co-ordination by 4 nitrate ligands and 2 water ligands in the crystal, this splitting has been interpreted as a result of the imposition of tetragonal D_{4h} symmetry on the metal ion, causing splitting of the triplet level into a singlet and a doublet level. The spectra illustrated in Fig. 5-19 do not therefore provide unequivocal identification of the Ni(II) species present in HNO_3 and the HNO_3/N_2O_4 solutions, but do provide evidence for the presence of octahedrally coordinated nickel in these species.

(d) Bulk preparation of $Ni(NO_3)_2 \cdot 2H_2O$ and solubility studies

The preparation of $Ni(NO_3)_2 \cdot 2H_2O$ by the reaction between metallic nickel and HNO_3 or HDA has been described above, but this method was found to be inconvenient for the preparation of the large quantities of material needed for the solubility measurements. The method described by Hathaway and Underhill[3], involving the reaction of anhydrous nickel chloride and 100% HNO_3, was employed. The lack of commercially available anhydrous $NiCl_2$ necessitates the preparation of this material by the method of A. R. Pray[13], from $NiCl_2 \cdot 6H_2O$ and thionyl chloride. The preparation is described in detail below.

Finely divided $NiCl_2 \cdot 6H_2O$ (20g) was placed in a flask, and freshly distilled thionyl chloride ($50cm^3$) was added at room temperature. An endothermic reaction occurred, SO_2 and HCl being given off. After bubbling had ceased, the flask was fitted with a reflux condenser and the slurry was refluxed for 2 hrs. Excess $SOCl_2$ was then removed to a vaccum desiccator containing KOH, and the flask was allowed to stand for 24 hrs. to remove the last traces of $SOCl_2$. The product at this point consisted of a light brown solid. The infra-red spectrum showed no bands attributable to H_2O or $SOCl_2$.



A. 100% HNO_3

B. 1% N_2O_4

C. 45% N_2O_4

Figure 5-19. Absorption Spectra of $Ni(NO_3)_2 \cdot 2H_2O$ in HNO_3/N_2O_4 Mixtures

10g of this product was transferred to a dry Schlenck tube, and 100% HNO_3 (about $40cm^3$) was added. A slow reaction occurred. The brown solid being completely converted to a blue-green solid under a green solution in about 16 hours. Evaporation of the mixture to dryness in a vacuum frame yielded the pure dihydrate $Ni(NO_3)_2 \cdot 2H_2O$.

The solubility of $Ni(NO_3)_2 \cdot 2H_2O$ in HNO_3/N_2O_4 mixtures was determined using the apparatus depicted in Fig. 5-20. Sufficient $Ni(NO_3)_2 \cdot 2H_2O$ to ensure an excess, was finely ground and loaded into the vessel A, in a dry box. The neck, a, was sealed with a stopper, and the vessel + $Ni(NO_3)_2 \cdot 2H_2O$ weighed. 100% HNO_3 and N_2O_4 were then weighed into A, against a counter-current of nitrogen, to give a mixture of known $HNO_3N_2O_4$ composition. The vessel A was then sealed with the B14 adaptor, attached by springs to resist the positive pressure developed by N_2O_4, suspended in a thermostated bath up to the level b---b, and agitated with a mechanical shaker for 24 hours to achieve equilibrium. At the end of this time, the shaker was stopped, and the bulb B was weighed and attached to A, via the side arm. The taps T_1, T_2, T_3 and T_4 were opened, and the saturated solution forced by nitrogen pressure applied at c through the filter d into the bulb. On completion of the transfer, the taps were closed, the bulb B detached, cleaned and weighed. A known weight of saturated solution was thus present in B. This method of transfer was employed, rather than that of applying suction at e, to prevent any appreciable evaporation of N_2O_4. At higher N_2O_4 concentrations, B was chilled prior to transfer.

The contents of B were evacuated to dryness on a vacuum frame, and the contents analysed for nickel by dimethylglyoxime precipitation as described in Appendix B.4(c). The results are tabulated in terms of grams of $Ni(NO_3)_2 \cdot 2H_2O$ per 100g solution, and expressed graphically in Fig. 5-21.

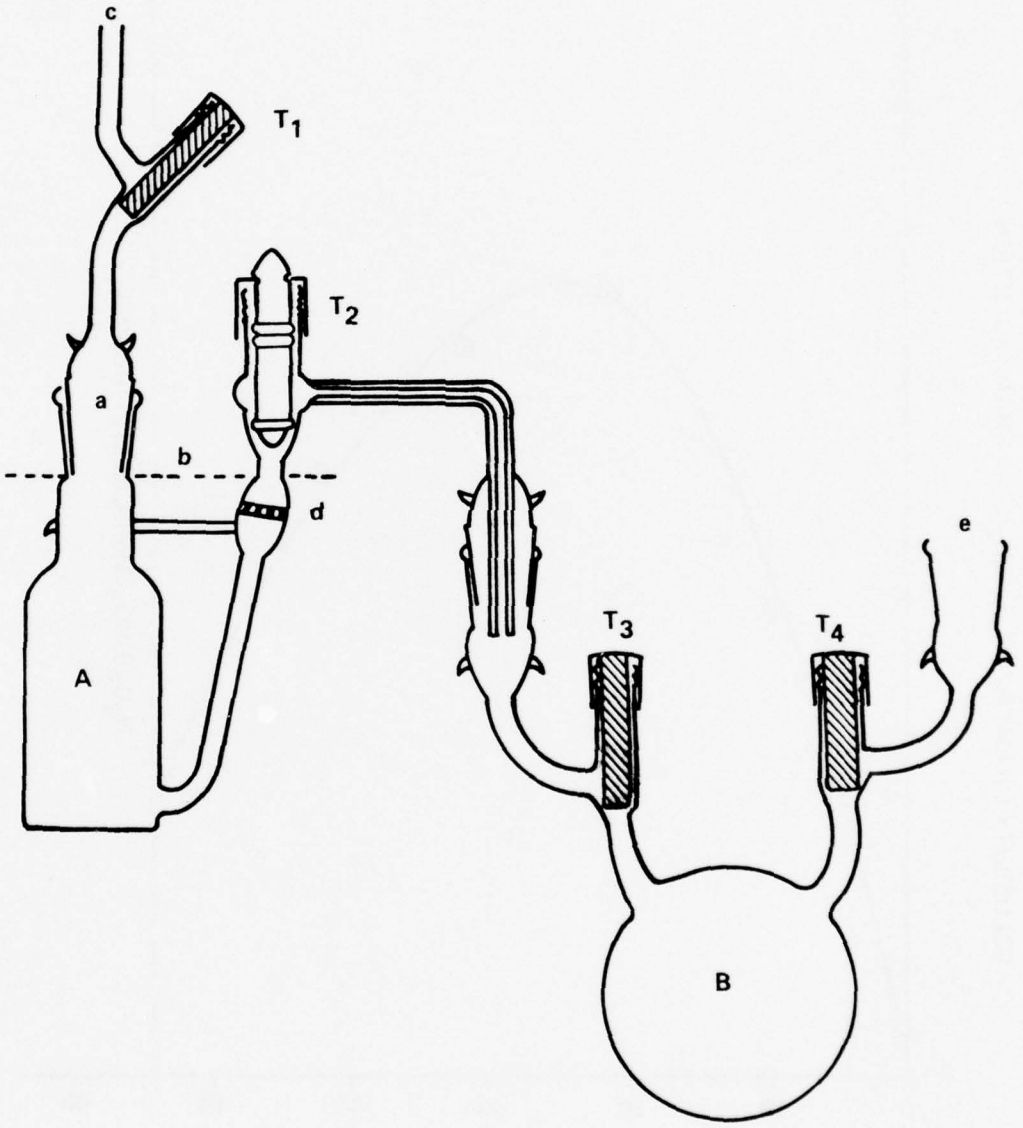


Figure 5-20. Solubility Determination Apparatus

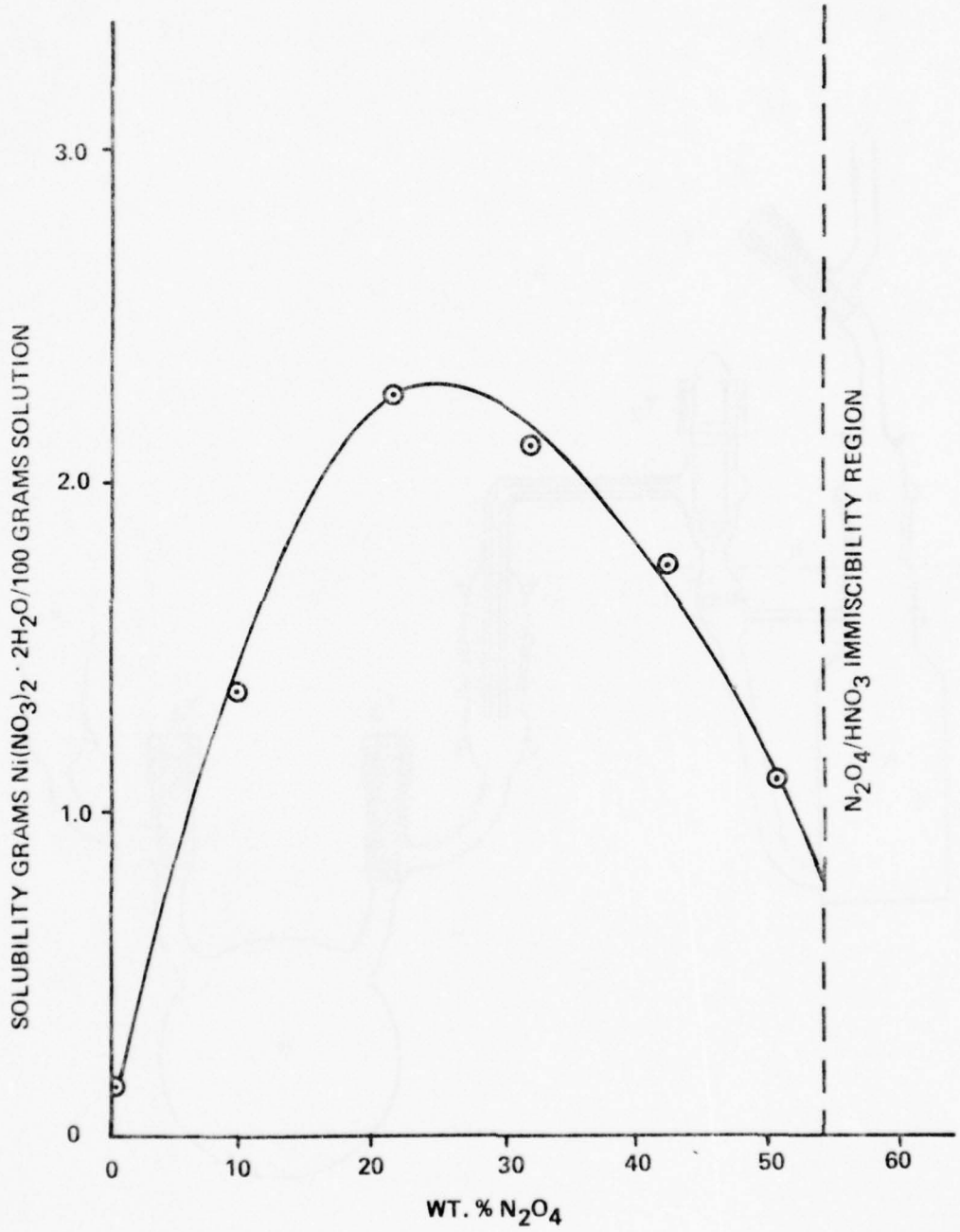


Figure 5-21. Solubility of $Ni(NO_3)_2 \cdot 2H_2O$ in HNO_3/N_2O_4 Mixtures at 0°C

Table 5-19.

The solubility of $Ni(NO_3)_2 \cdot 2H_2O$ in HNO_3/N_2O_4 mixtures at $0^{\circ}C$

Wt% N_2O_4	Solubility g/100g solution
0	0.1532
9.49	1.354
21.06	2.279
31.59	2.110
41.78	1.750
50.37	1.093

As can be seen from Fig 5-21 the solubility passes through a well-defined maximum at about 23.5 wt% N_2O_4, the maximum solubility of $Ni(NO_3)_2 \cdot 2H_2O$ being about 2.3g per 100g of solution. The solubility of $Ni(NO_3)_2 \cdot 2H_2O$ in 44% N_2O_4/HNO_3 mixture is about 1.52g per 100g approximately ten times its value in 100% HNO_3 (0.1532g/100g) which explains the lack of precipitation in the HDA/321 stainless steel system.

The presence of a solubility maximum in N_2O_4/HNO_3 mixtures, is unusual as $Ni(NO_3)_2 \cdot 2H_2O$ is soluble to only a minute extent in liquid N_2O_4, and the anticipated result of a solubility study of this type would be a linear decrease in solubility with increasing N_2O_4 content.

Early work by C. C. Addison[14] on reaction rates in N_2O_4/organic solvent mixtures, gave curves which passed through similar maxima with changing composition, and it is likely that a related phenomenon is taking place here. The conductivity of HNO_3/N_2O_4 mixtures[15] shows a maximum at approximately the same composition as the position of the solubility maximum of $Ni(NO_3)_2 \cdot 2H_2O$, and it seems possible that the increase in solubility of $Ni(NO_3)_2 \cdot 2H_2O$ over the

composition range 0-23.5% N_2O_4 is due to the increase in dielectric constant of the medium caused by the ionisation of the N_2O_4 in the nitric acid, i.e.

$$N_2O_4 \rightleftharpoons NO^+ + NO_3^-$$

The decrease in solubility of $Ni(NO_3)_2 \cdot 2H_2O$ at N_2O_4 concentrations of 23.5 - 58.0% is probably related to the fall in conductivity of the N_2O_4/HNO_3 mixture previously mentioned, in that additional N_2O_4 added to the HNO_3 no longer ionises to a great extent, the dielectric constant no longer increases, and the solubility of $Ni(NO_3)_2 \cdot 2H_2O$ decreases with increasing N_2O_4 concentration as a direct result of its very low solubility in pure N_2O_4. The above ionisation equilibrium may also enhance solubility by virtue of further complexing of nickel by nitrate ligands yielding species of the type $(NO^+)_2[Ni(H_2O)_2(NO_3)_4]^{2-}$.

The effect of temperature on the solubility of $Ni(NO_3)_2 \cdot 2H_2O$ in HNO_3/N_2O_4 was studied by preparing two solutions of HNO_3/N_2O_4 of known composition, adding a portion of this to the $Ni(NO_3)_2 \cdot 2H_2O$ in the vessel, and proceeding as before at each of the selected temperatures. The results are given in Table 5-20 and illustrated graphically in Fig. 5-22.

Table 5-20. Effect of temperature on the solubility of $Ni(NO_3)_2 \cdot 2H_2O$ in HNO_3/N_2O_4 mixtures (g. solute/100g solution)

15.7 wt. % N_2O_4		32.5 wt. % N_2O_4	
Temp. °C	Solubility	Temp. °C	Solubility
-8.2	1.967	-18.0	1.82
0	1.960	0	2.15
10.6	2.002	1.0	2.24
11.0	2.001	10.2	2.37
18.0	2.057	21.0	3.37
31.0	2.103		

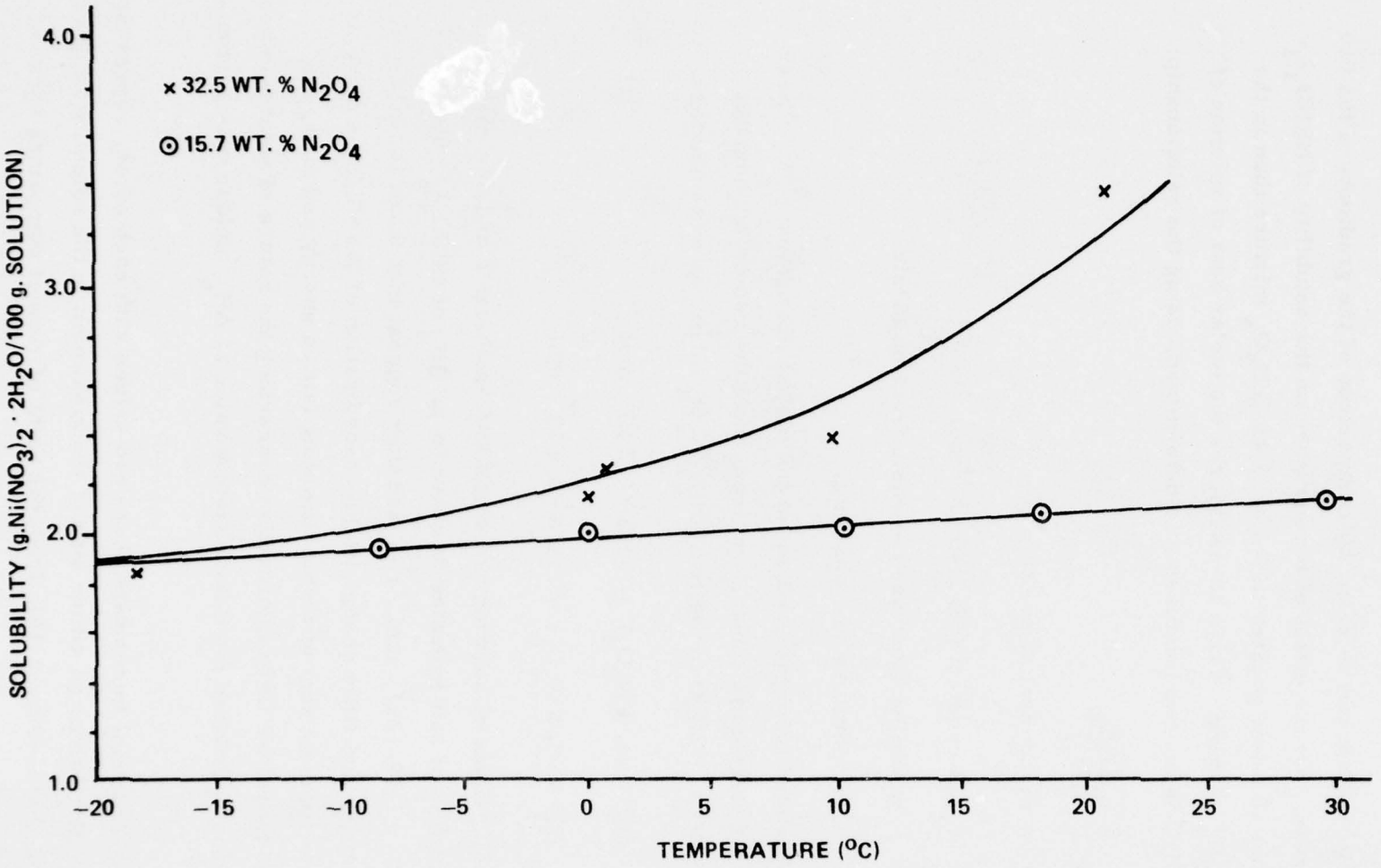


Figure 5-22. Effect of Temperature on Solubility of $Ni(NO_3)_2 \cdot 2H_2O$ in HNO_3/N_2O_4

From Fig. 5-22 it can be seen, by comparison of the gradients of the two solubility curves, that the effect of temperature on the solubility of $Ni(NO_3)_2 \cdot 2H_2O$ is almost 10 times greater in the 32.5 wt. % N_2O_4 mixture than in the 15.7 wt. % N_2O_4 mixture. From these figures the molar heat of solution of $Ni(NO_3)_2 \cdot 2H_2O$ in the two mixtures was determined, using the relationship:

$$\Delta H_s = R\left(\frac{\partial \ln x}{\partial 1/T}\right)$$

where: ΔH_s = molar heat of solution

R = gas constant (=8.3143 $JK^{-1}mol^{-1}$)

x = solubility expressed as mole fraction solute.

T = temperature in ^{o} absolute.

ΔH_s being calculated from the gradient of the plot of ln$x$ against $^{1}/_{T}$. These plots were found to be quite linear, and from them the two molar heats of solution of $Ni(NO_3)_2 \cdot 2H_2O$ in the two HNO_3/N_2O_4 mixtures were obtained.

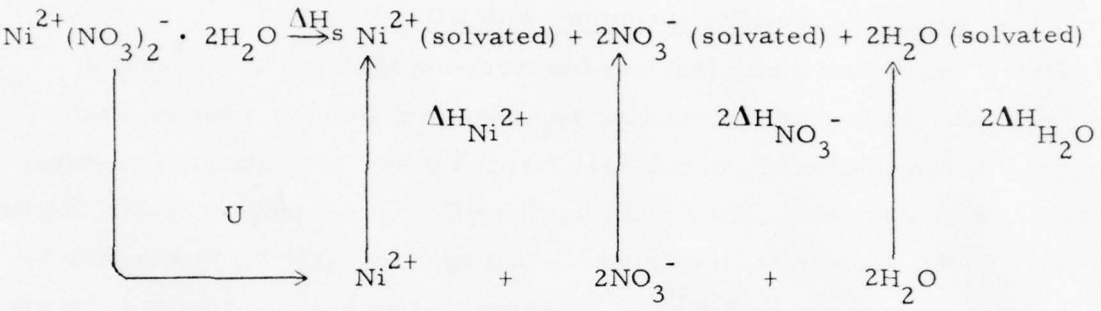
$$\Delta H_s \ (15.7 \text{ wt. \% } N_2O_4) = -1.2 \pm 0.3 \text{ kJ mol}^{-1}$$

$$\Delta H_s \ (32.5 \text{ wt. \% } N_2O_4) = -5.8 \pm 0.4 \text{ kJ mol}^{-1}$$

These molar heats of solution are small and exothermic and of a magnitude comparable to ΔH_s of salt hydrates in water (e.g. ΔH_s of $Ni(SO_4)_2 \cdot 6H_2O$ in water at 25^{o}C = -10.12kJ mol^{-1})[19], and they suggest that there is little overall energy change, and little change in the co-ordination of the Ni(II) on dissolution. ΔH_s is a complex sum of terms involving lattice energy and energy of solvation, and therefore little information concerning the nature of solute-solvent interactions can be deduced from the absolute value of ΔH_s, unless it is particularly large.

It is however useful to compare these two values with each other, representing as they do ΔH_s values on either side of the maximum in the solubility/solvent composition isotherm (Fig. 5-19), from the point of view of comparing solution

processes on either side of this maximum. The ΔH_s of $Ni(NO_3)_2 \cdot 2H_2O$ on the N_2O_4 - rich side of the isotherm is more exothermic than the ΔH_s value on the HNO_3 - rich side. From the Born-Haber cycle below,



where U = lattice energy of $Ni(NO_3)_2 \cdot 2H_2O$

ΔH_x = enthalpy of solvation of species x in the HNO_3/N_2O_4 mixture

$$\Delta H_s = U - \Delta H_{Ni^{2+}} - 2\Delta H_{NO_3^-} - 2\Delta H_{H_2O}$$

The value of U being constant, the difference in ΔH_s values must be a result of different solvation enthalpies of Ni^{2+}, NO_3^- and H_2O in the two mixtures. The reduced dielectric constant of the medium on the N_2O_4-rich half of the solubility/solvent composition isotherm would tend to decrease the solvation energy on this side of the isotherm. All other things being equal, it seems likely then that the chemistry involved in solvation of the Ni^{2+}, NO_3^-, and H_2O is different on the two sides of the curve, and that complex octahedrally co-ordinated Nickel (II) species may be present in solution on the N_2O_4-rich side of the curve. The free energy change of solvation, ΔG, for a spherical ion in solution in a liquid of dielectric constant E is given by:

$$\Delta G = \frac{-N_A z^2 e^2}{2R} \left(1 - \frac{1}{E}\right)$$

where z = valency, e = electronic charge, R = radius.

and clearly the energetics of solvation are dependent on the parameters of the solvated ion as well as on dielectric constant of the solvent.

5.5 The reaction of chromium and hexacarbonylchromium (O) with HDA

(a) The reaction of metallic chromium with HDA

Powdered chromium metal (4g) was immersed in HDA (ca 50 cm^3.) in a stoppered flask. No immediate reaction was observed although after several days some slight evolution of gas bubbles, trapped in the solid until the mixture was shaken, was observed. After this time the HDA had assumed a darker colour, presumably due to the formation of green Cr(III) species. (Cr(VI) is known to be unstable in the presence of N_2O_4.[16, 17]) Determination of the chromium content of the mixture by atomic absorption spectroscopy indicated the presence of about 40ppm Cr(III).

After 1 month, the mixture was filtered to remove excess metal, and the now dark green solution was evaporated on a vacuum line (10^{-3}mm, 20°C.) After 18 hours a dark green gummy residue remained, quite small in bulk compared to the analogous iron (Section 5.3), nickel (Section 5.4) and aluminium (Section 6.1) systems. After 3 days evacuation, the gum was dry enough to permit grinding to a free-flowing dark green powder. The infra-red spectrum of this material was recorded (Fig. 5-23, Table 5-21). The spectrum is indicative of the presence of exclusively co-ordinated nitrate groups. Broad bands characteristic of the presence of co-ordinated water were also observed. A small peak at 2270cm^{-1}, typical of the N-O^+ stretching frequency is characteristic of compounds of the type $(NO^+)_n[M(NO_3)_x]^{n-}$ containing "N_2O_4 of solvation." The X-ray powder photographs (CuK_α and FeK_α radiation) indicated that the material was amorphous. The solid was found to be extremely deliquescent and all manipulations were carried out in a dry box.

Analysis of the product was carried out for chromium, total nitrogen, and nitrite (following hydrolysis) to determine whether any N_2O_4 was present in either the molecular form or as NO^+ and coordinated nitrate. The product was found

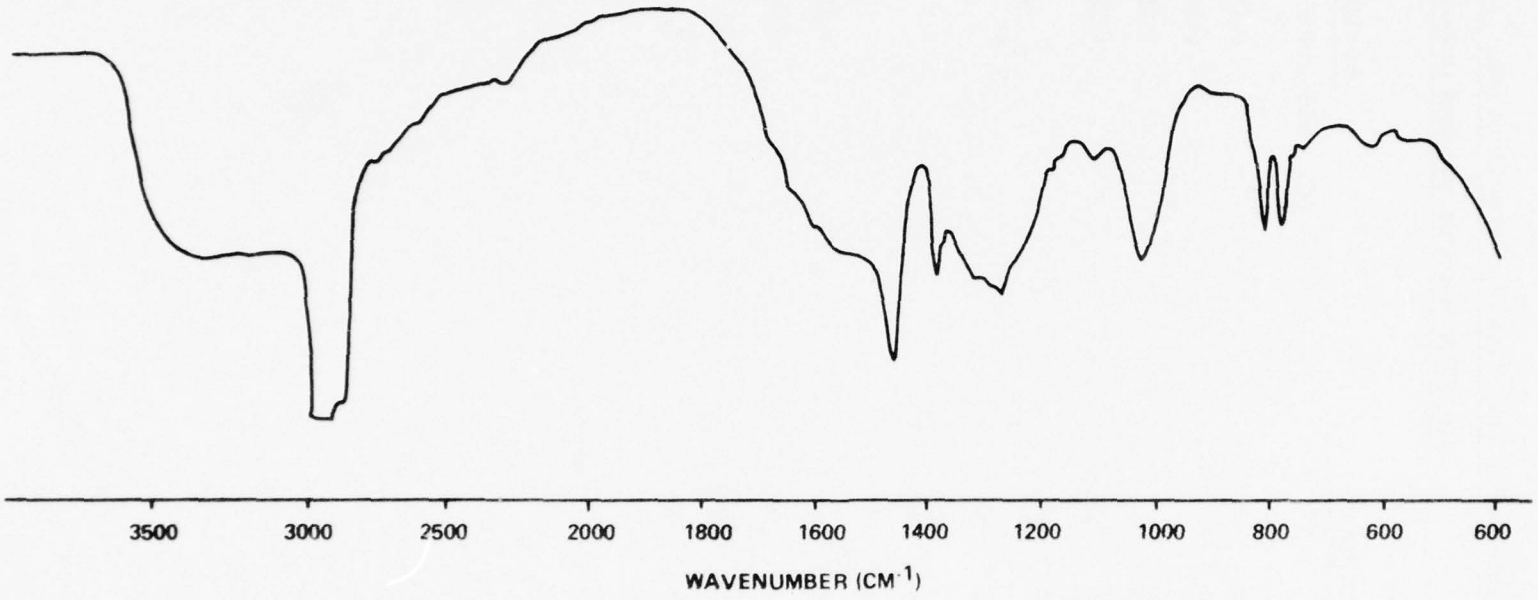


Figure 5-23. IR Spectrum of Cr/HDA Product

Table 5-21. The infra-red spectrum (cm^{-1}) of the Cr/HDA reaction product (nujol mull)

Absorption Band			Assignment (C_{2v} bidentate nitrate model)
3300	vs	vb	ν(OH)
2285	w		$\nu(NO^+)$
1680	w		$\delta(H_2O)$
1600	w	sh	ν(NO*)
1310	m	sh	$\nu_{as}(NO_2)$
1290	m	sh	
1263	m	sp	
1100	m	b	
1020	s	sp	$\nu_s(NO_2)$
800	s	vsp	$\pi(O_2NO^*)$
770	s	vsp	$\delta_s(NO_2)$
730	vw	sp	$\delta_{as}(NO_2)$

* Unco-ordinated oxygen atom.

to contain Cr, 11.5%; N, 16.2%; N_2O_4 (as nitrite) 2.0%. The solid contains only a small quantity of combined N_2O_4 ($Cr(NO_3)_3 \cdot 2N_2O_4$ requires 43.6%N_2O_4.) The figure for chromium is low, and suggests that the material is a solvate of $Cr(NO_3)_3$ possibly containing water and/or nitric acid. The Cr:N ratio is 1:5.2, and gives evidence for the presence of nitric acid, although this could not be clearly discerned from the infra-red spectrum. The material showed no tendency to decompose however, giving identical analytical results even after a further period of evacuation.

The formulation giving closest agreement with the above analytical figures is $Cr(NO_3)_3 \cdot 2HNO_3 \cdot 4H_2O$. It is interesting to note that recent work by Greenwood[17] has shown $Cr(NO_3)_5^{2-}$ to be the predominant nitrato-anion of Cr(III). For example, the compound $Cs_2Cr(NO_3)_5$ has been obtained from the reaction of $Cr(CO)_6$ with 100% HNO_3 in the presence of $CsNO_3$. It is therefore tempting to speculate that the product $Cr(NO_3)_3 \cdot 2HNO_3 \cdot 4H_2O$ might have the constitution $(H_3O^+)_2[Cr(NO_3)_5]^{2-} \cdot 2H_2O$.

As mentioned above, the reaction of metallic chromium with HDA was very slow, and only small quantities of product could be obtained at a time. A possible alternative, synthetic route to the same material was therefore investigated in an attempt to prepare bulk quantities for examination.

(b) The reaction of hexacarbonylchromium (O) with HDA

$Cr(CO)_6$ was chosen as a possible starting compound, since, in common with the metal, it contains chromium in the zero oxidation state and should therefore undergo a similar oxidation reaction to metallic chromium. Replacement of carbonyl by nitrato-ligands was expected to proceed via evolution of inert CO, and no possibly interfering products, such as NOCl, should be formed.

$Cr(CO)_6$ (ca 1g.) was added to HDA (ca 30 cm^3), cooled to -78°C.) No reaction occurred at this temperature, the $Cr(CO)_6$ remaining unchanged in appearance in the acid mixture. On warming, a reaction commenced, with evolution of gas and formation of a green solution. The reaction was quite smooth at room temperature (20°C) and on completion a dark green solution remained. This

was set aside in a refrigerator at -20°C for several days in an attempt to promote crystallization, but without success. The solution was therefore evaporated on a vacuum line (10^{-3}mm, 20°C.) After evacuation for 2 days, a dark green gum remained in the flask. After 7 days the material was dry enough to allow preparation of mulls for infrared spectroscopy and powders for X-ray powder photography.

The infra-red spectrum is shown in Fig. 5-24 and tabulated in Table 5-22. The spectrum is again consistent with the presence of entirely co-ordinated NO_3^-, and co-ordinated H_2O, and is very similar to the spectrum obtained for the product of the metallic chromium/HDA reaction. A small peak at 2290cm^{-1}, assigned to NO^+ was observed.

The X-ray powder pattern is listed in Table 5-23. This material was not amorphous. None of the lines in this powder pattern coincide exactly with lines in the powder photograph of the compound $Cr(NO_3)_3 \cdot 2N_2O_4$, as calculated from Crystallographic Program NRC-21 using unit cell parameters determined by Greenwood.[17]

The material was analysed for chromium (15.9%), total nitrogen (13.6%), and nitrite (equivalent to 3.9% N_2O_4.) These figures differ from those for the chromium/metal HDA product. The Cr:N ratio was 1:3.19, indicating the presence of only a small quantity of nitric acid or "N_2O_4 of solvation." The analytical results correspond most closely to the formulation $Cr(NO_3)_3 \cdot 5H_2O$ (requires Cr, 15.9%; N, 12.8%) and the crystallinity of the product, as indicated by the powder photograph, suggests a well-defined stoichiometric compound.

In view of the formation of viscous gums during the later stages of evacuation of the reaction mixtures described in this section, it is clear that the chromium nitrate species formed have exceedingly high solubility in the HNO_3/N_2O_4 mixture. In such cases, a gradual increase in viscosity occurs as the solution becomes more and more concentrated and solidification only occurs after prolonged evacuation.

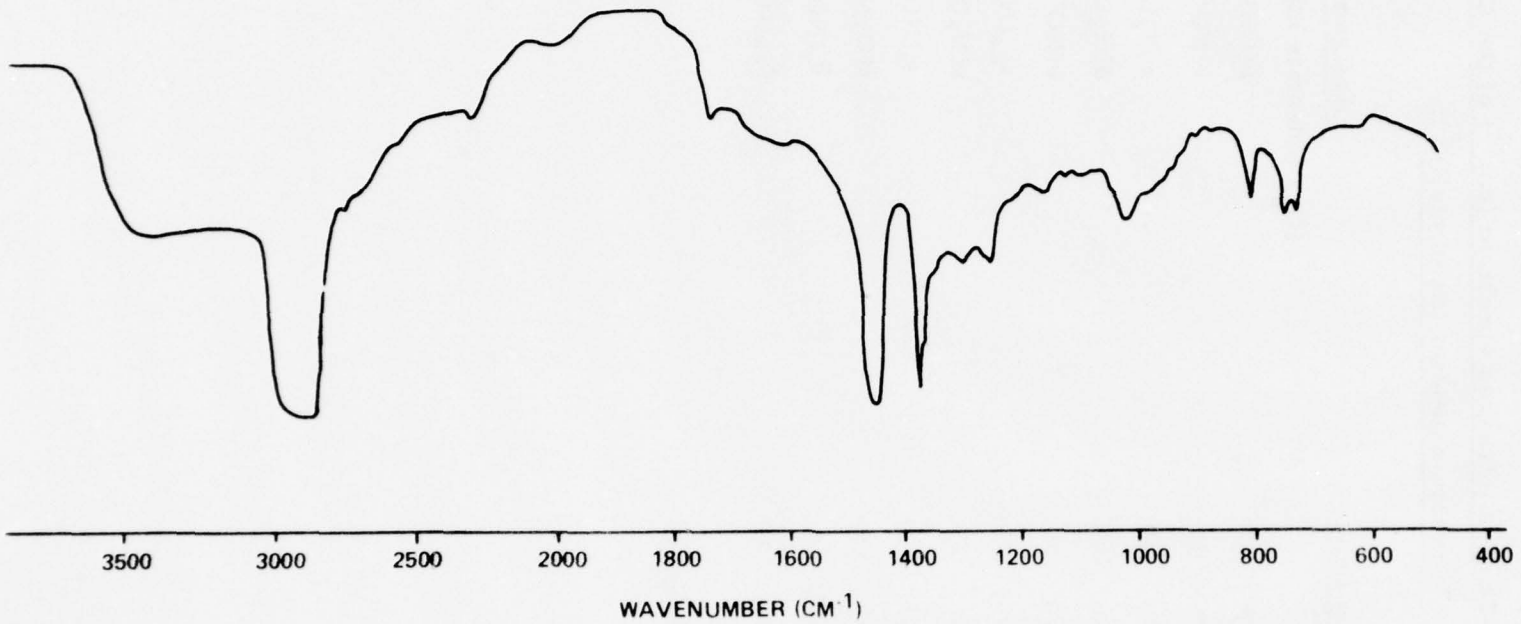


Figure 5-24. IR Spectrum of $Cr(CO)_6$/HDA Product

Table 5-22. The infra-red spectrum (cm^{-1}) of the $Cr(CO)_6$/HDA reaction product (nujol mull)

Absorption Band			Assignment (C_{2v} bidentate nitrate model)
3400	vs	vb	$\nu(OH)$
2290	m	sp	$\nu(NO^+)$
1730	m.	sp	$\nu(N_2O_4)$
1680	m.	sh.	$\delta(H_2O)$
1620	m.	sh.	$\nu(NO^*)$
1300	m.	sp.	$\nu_{as}(NO_2)$
1255	m.	sp.	$\nu(N_2O_4)$
1020	s.	sp.	$\nu_s(NO_2)$
800	m.	vsp	$\pi(O_2NO^*)$
740	m.	sp.	$\delta_s(NO_2)$
725	m.	sp.	$\delta_{as}(NO_2)$

* Unco-ordinated oxygen.

Table 5-23. The X-ray powder pattern of the $Cr(CO)_6$/HDA product

d(nm)	Intensity
0.6320	30
0.5824	95
0.4792	20
0.4595	20
0.4308	10
0.4168	15
0.3424	10
0.3295	100
0.3151	30
0.3015	30
0.2778	5
0.2513	20
0.2354	30
0.2174	10
0.2135	10
0.2030	5
0.1975	5
0.1909	10
0.1879	10
0.1840	5
0.1671	3
0.1641	3

It was thus decided to attempt to prepare a solution containing a very large proportion of chromium nitrato-species in the hope of saturating the solution and obtaining a crystalline reaction product. To this end, just sufficient HDA (ca $3cm^3$) was added to dissolve ca lg. of hexacarbonyl chromium (O) at 0^oC. On completion of the reaction a dark green viscous solution was formed which deposited no crystals, even on strong cooling. A large excess of dry dichloromethane was then added in an attempt to "salt out" a solid chromium-containing product. Although dichloromethane is miscible in all proportions with mixtures of 100% HNO_3 and N_2O_4, it was found to be immiscible with the chromium-containing solution, forming a separate upper liquid layer and no solid was salted out. This immiscibility of CH_2Cl_2 with HNO_3/N_2O_4 mixture containing metal ions was found to be a general phenomenon; even after several weeks, no further change was observed in the system, the liquids remaining immiscible.

A sample of a $Cr(CO)_6$/HDA gum, formed by 2 days evacuation of the $Cr(CO)_6$ and HDA reaction product, containing ca. 0.7g. of $Cr(CO)_6$ in ca. $3cm^3$ of HDA was continuously extracted with dry dichloromethane in a sealed Soxhlet extractor at 40^oC in a dry argon atmosphere. After 14 days, the extraction was stopped, and excess dichloromethane was removed under vacuum (10^{-3}mm. 20^oC). A dark green solid remained, the infrared spectrum and powder photograph of which were identical to those of the solid isolated by evacuation of the $Cr(CO)_6$/HDA solution to dryness, i.e. the solid identified as $Cr(NO_3)_3 \cdot 5H_2O$.

On leaving a sample of a $Cr(CO)_6$/HDA gum, obtained by evacuation, containing approximately lg $Cr(CO)_6$ in ca. $3cm^3$ HDA, in a refrigerator at -20^oC for 5 months in a sealed vessel, it was found that the gum had separated into a mass of dark green crystals, and a small bulk of a very mobile upper layer. The mixture was filtered by gentle suction through a porosity 3 glass sinter, cooled to -20^oC by a methcol-filled cooling jacket. The crystals were washed well with a small amount of HDA, cooled almost to its freezing point, and were freed from excess HDA by evacuation (10^{-3}mm, 20^oC) for 15 hours. The infrared spectrum and powder photograph of the dry crystals were found to be identical to those of the product characterised as $Cr(NO_3)_3 \cdot 5H_2O$ and were isolated by evaporation

of a more dilute $Cr(CO)_6$/HDA solution. Weak absorptions at 2295cm^{-1}, and at 1740cm^{-1} in the infrared spectrum again suggested the presence of a trace of $Cr(NO_3)_3 \cdot 2N_2O_4$. It therefore appears that the ultimate product of the $Cr(CO)_6$/HDA reaction, whether solid is obtained by evacuation of a solution to dryness, by extraction with CH_2Cl_2 or by allowing slow crystallization from a concentrated solution (i.e. a gum), is the pentahydrate, $Cr(NO_3)_3 \cdot 5H_2O$. The filtrate remaining after the green crystals had been isolated was evacuated (20°C 10^{-3}mm). The liquid was found to evaporate to dryness in about 15 hours depositing a minute amount of a deep purple, completely dry solid. This solid was found to be extremely deliquescent, becoming green as it absorbed water. The infrared spectrum and powder photograph of this material were recorded (Fig. 5-25, Tables 5-24, 5-25), and found to be completely different from those of any of the previously isolated solids. The infrared spectrum (Fig. 5-25) was consistent with the presence of solely co-ordinated nitrate. The NO_2 symmetric stretching mode occurs at the slightly higher frequency of 1055cm^{-1}, compared to 1020cm^{-1} in the chromium/HDA product and the $Cr(CO)_6$/HDA products. The weak bands at 2360, 900, 890, 660, and 610cm^{-1} may be assignable to molecular nitric acid vibrations. No peaks were present in the 2298cm^{-1} region indicating the absence of NO^+.

The powder photograph was well defined, and contained no lines attributable to $Cr(NO_3)_3 \cdot 5H_2O$ or $Cr(NO_3)_3 \cdot 2N_2O_4$.

Analysis of the compound (Found: Cr, 14.31; N, 20.5%) was found to agree closely with the composition $Cr(NO_3)_3 \cdot 2HNO_3$ (requires: Cr; 14.3; N, 19.3%.)

The association of '$Cr(NO_3)_3$' with two molecules of HNO_3 in this material could indicate a preference of chromium to form a complex ion of the $Cr(NO_3)_5^{2-}$ 'type' in this species, octahedral co-ordination being maintained by co-ordination of the two molecules of nitric acid instead of two nitrate groups as in $Cr(NO_3)_5^{2-}$. This complex has been shown to be the dominant nitrato-anion of Cr(III).[17]

In view therefore of the great solubility of chromium-containing nitrato-species in HDA, it seems unlikely that their presence would contribute to flow decay or blockage of any kind, even if their concentration in the mixture became high. The slowness of the reaction between Cr metal and HDA seems to preclude this possibility.

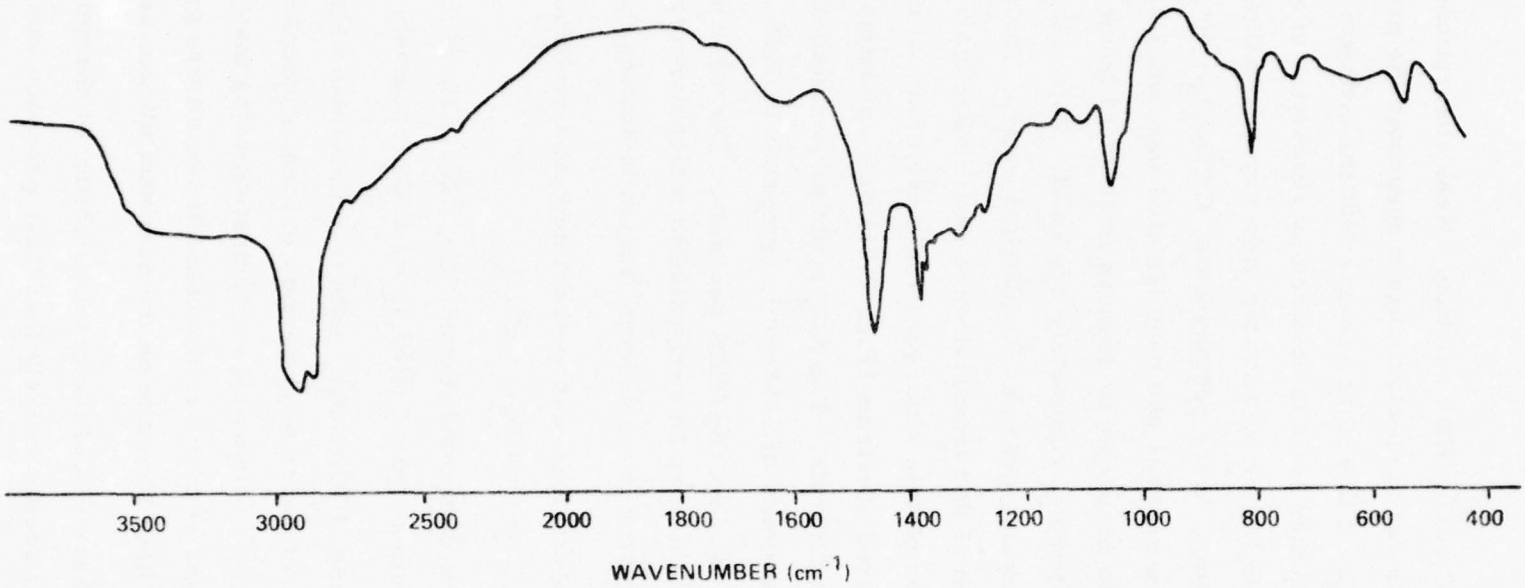


Figure 5-25. IR Spectrum of the Purple $Cr(CO)_6$/HDA Product

Table 5-24. The infrared spectrum (cm^{-1}) of the purple $Cr(CO)_6$/ HDA product (Nujol mull)

Absorption Band			Assignment[+]
3300	vs	vb	ν(OH)
2720	w	sp	
2360	w	sp	$\nu_{as}(NO_2^+)$
1760	w	sh	N_2O_4
1600	m	b	$\delta(H_2O)$
1540	w	sh	$\nu(NO^*)$
1365	m	sp	
1320	s	sp	$\nu_{as}(NO_2)$
1285	m	sh	
1270	m	sp	
1220	m	sh	
1100	m	b	
1055	s	vsp	$\nu_s(NO_2)$
1020	s	sh	
975	w	sh	
900	w	sh	$\delta(NO_2)$ (in HNO_3)
890	w	sh	
860	w	sh	
815	m	sh	$\pi(NO_3)$
805	s	vsp	
780	w	sh	$\delta_s(NO_2)$
730	m	sp	$\delta_{as}(NO_2)$
660	w	sh	ν(N-OH) (in HNO_3)
610	m	b	δ(O-N-OH) (in HNO_3)
540	w	sp	νCr-O

+ Nitrate group vibrational assignments on the basis of C_{2v} bidentate nitrate.

* Unco-ordinated oxygen atom.

Table 5-25. The X-ray powder pattern of the purple $Cr(CO)_6$/HDA product

d(nm)	Intensity
0.6804	10
0.6411	8
0.6021	75
0.5712	15
0.5304	20
0.5092	2
0.4691	5
0.4392	100
0.3814	90
0.3450	80
0.3348	70
0.3162	60
0.2938	50
0.2803	60
0.2736	5
0.2665	10
0.2562	50
0.2459	5
0.2402	10
0.2319	20
0.2199	20
0.2130	10
0.2079	5
0.2034	10
0.2000	5
0.1898	5
0.1939	5

5.6 References

1. D. H. Jones, Ph. D. thesis, Nottingham, 1972.
2. C. C. Addison, "Flow Decay," AFRPL-TR-72-84.
3. B. J. Hathaway and A. E. Underhill, J. Chem. Soc., 1960, 648.
4. C. C. Addison, "Chemistry in Liquid Dinitrogen Tetroxide" in Chemistry in Non-aqueous Ionising Solvents (C. C. Addison, W. Karcher and H. Hecht, Eds.), Vieweg-Pergamon, 1967, p. 1.
5. C. C. Addison, L. J. Blackwell, B. Harrison, D. H. Jones, N. Logan, E. K. Nunn and S. C. Wallwork, Chem. Comm., 1973, 347.
6. C. C. Addison and D. J. Chapman, J. Chem. Soc., 1965, 819.
7. D. Weigel, B. Imelik and P. Laffite, Bull. Soc. Chim. (France), 1962, 544.
8. G. M. Begun and W. H. Fletcher, J. Chem. Phys., 1958, 28, 414.
9. A. Sieverts and L. Schreiner, Z. Anorg. Chem., 1934, 219, 105.
10. F. A. Cotton and G. Wilkinson, Advanced Inorganic Chemistry, 3rd Ed., Interscience, 1972, pp. 893-894.
11. B. J. Hathaway, D. G. Holah and M. Hudson, J. Chem. Soc., 1963, 4586.
12. L. Berger and S. A. Friedberg, Phys. Rev., 1964, 136A, 158.
13. A. R. Pray, Inorg. Synth., 1957, 5, 153.
14. C. C. Addison, J. C. Sheldon and N. Hodge, J. Chem. Soc., 1956, 3900.
15. G. D. Robertson, D. M. Mason and B. H. Sage, Ind. Eng. Chem., 1952, 44, 2928.
16. A. H. Norbury, Ph. D. thesis, Nottingham, 1962.
17. A. J. Greenwood, Ph. D. thesis, Nottingham, 1975.
18. W. Hessel and C. Romers, Rec. Trav. Chim., 1969, 88, 545.
19. J. W. Mellor, Comp. Treat. Inorg. Theor. Chem., 1936, 15, 459.

6. CORROSION PRODUCTS OF ALUMINIUM WITH 100% HNO_3 AND HDA

The corrosion of aluminium by HDA was investigated in a manner parallel to that employed for steels (Section 5) i.e. a preliminary examination of the reaction between aluminium and HDA was carried out, followed by a study of the reaction products, with special reference to any properties likely to affect the storage or flow of HDA.

6.1 The Reaction of metallic aluminium with 100% HNO_3 and HDA

(a) Preliminary study

Small pieces (ca 0.5cm^2) of 6021 aluminium (99% Al, 1% Mg) were abraded on a grinding wheel, degreased with inhibisol, and dried. A number of these pieces were immersed in 100% HNO_3, (ca 20cm^3) at room temperature (20°C) and at -20°C, and identical specimens were also immersed in HDA at room temperature. The appearance of the solution and metal surface was observed in each case over a period of time, and the results are recorded in Table 6-1.

These observations showed that the reaction of aluminium with 100% HNO_3 and HDA was slow, the rate being of an order of magnitude comparable with that of the much less electropositive chromium. The ultimate deposition of a crystalline product occurred in the HDA/aluminium mixture. Mellor[1] has shown that the hydrate $Al(NO_3)_3 \cdot 6H_2O$ is the stable species in $Al/HNO_3/H_2O$ solutions containing greater than 81wt% HNO_3, and no further investigation of the products of the Al/HNO_3 reactions was performed, attention being focussed on the more relevant Al/HDA system.

(b) Further investigation of the Al/HDA reaction

In view of the slowness of formation of reaction products in the Al/HDA system, the reaction was repeated using a large quantity of pure aluminium turnings in HDA, in order to expose a much larger surface area to reaction. On immersion of the aluminium turnings, bubbles of gas were evolved, their observation in this case probably being a result of the much larger amounts of starting materials employed. After 3 months, a thick crust of pale yellow solid

Table 6-1.

The reaction of metallic aluminium with 100% HNO_3 and HDA

Al/HNO_3 -20°C

Time after immersion	Appearance of Metal	Appearance of solution
Immediately	Shiny scratched surface	Acid colourless
12 hours	"	No obvious reaction acid possibly becoming yellow
7 days	"	Acid slightly yellow
5 weeks	some slight darkening of metal	" " "
18 months	Dark patches on metal	" " "

Al/HNO_3, 20°C

Time after immersion	Appearance of Metal	Appearance of Solution
Immediately	Shiny scratched surface	Acid colourless
2 1/2 days	Metal darkening	Acid pale yellow
4 1/2 days	Black patches on metal	Acid pale yellow
7 days	Metal quite black	Acid yellow green
5 weeks	Metal dissolving away	Acid yellow

Al/HDA, 20°C

Time after immersion	Appearance of Metal	Appearance of Solution
Immediately	Shiny scratched surface	No apparent reaction
20 hours	" "	" " "
3 days	Possibly some darkening	" " "
9 days	Metal darkening in places and corroding	" " "
3 months	Black patches; metal dissolving	Small crystals being deposited.

had been formed around the walls of the flask. The flask was transferred to a dry box, the mother liquor decanted off, and the unreacted metal removed with forceps. Both the solid product and solution were then subjected to further examination.

Solid Product

The solid product was washed several times with dry dichloromethane to remove excess HDA, and excess CH_2Cl_2 was then removed in vacuum (20°C, 10^{-3} mm). After about 2 hours evacuation the product had become a free-flowing, pale yellow powder, having apparently lost its crystallinity during washing and evacuation. The solid was found to be somewhat unstable, developing, after a few days, an atmosphere of N_2O_4.

Analysis of the compound for aluminium (Appendix B.4(d)) and nitrogen (Appendix B.4(f)) gave Al, 9.37%; N, 13.7%. These figures are close to the calculated values for the composition $Al(NO_3)_3 \cdot 4H_2O$ required (Al, 9.48%; N, 14.7%), which is a hitherto unreported hydrate. It is also possible that the compound is some form of basic or oxide nitrate. The existence of such basic species is an important feature of the nitrate chemistry of aluminium[2], and it would not be surprising to encounter such a species here.

An analysis of the material for nitrate via U.V. - visible spectrophotometric observation of the nitrate group $n \rightarrow \pi^*$ transition at 302.5nm, and comparison with KNO_3 standard solutions, indicated that it contained 63.9% NO_3^-, corresponding to 14.4%N, and therefore confirmed that all the nitrogen is present in the form of nitrate.

The infrared spectrum of the material was recorded and is tabulated below (Table 6-2) and illustrated in Fig. 6-1. The material was found to give a good quality nujol mull, but gave a poorly resolved spectrum, which appears to be a characteristic of hydrated aluminium nitrate species, also being experienced with the compound $Al(NO_3)_3 \cdot 6H_2O$, described in Section 6.2.

Although difficult to interpret, the spectrum possesses features indicative of both ionic and unidentate covalent nitrate groups (see Table 6-2). The

Table 6-2. The infra-red spectrum (cm^{-1}) of the Al/HDA Solid Reaction product (Nujol Mull)

Absorption Band				Assignment[+]
3100	vs	vb		ν(OH)
1650	s	b		$\delta(H_2O)$
1380	s	vb		$\nu_d(NO_2)$ ion
1071	s	sp	)	
			)	ν(NO) uni
1051	s	sp	)	
			)	
1020	m	sp	)	
862	m	b		
809	s	sp		$\pi(NO_3)$ uni
730	m	sp		$\delta_{as}(NO_2^*)$ uni or δ_d (NO_2) ion
570	m	sp		ν(AlO)

+ nitrate assignments based on C_s unidentate model (uni) and D_{3h} ionic model (ion)

* Unco-ordinated oxygen atom

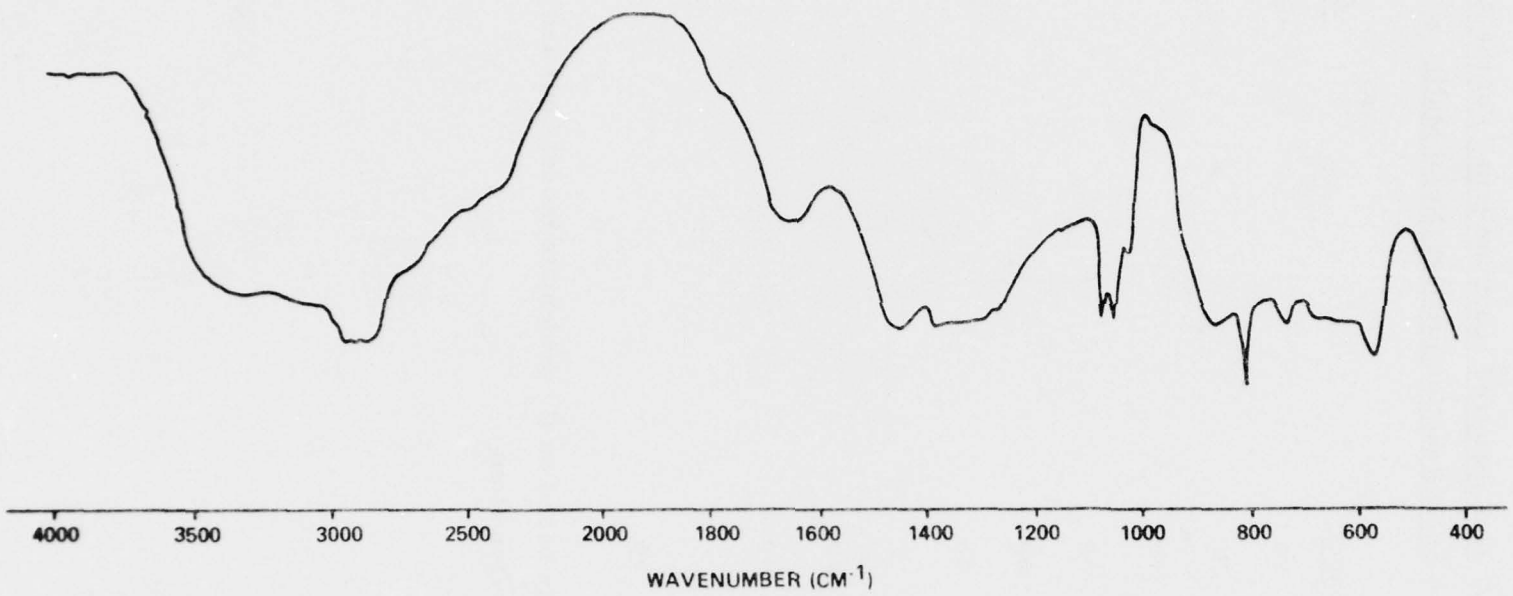


Figure 6-1. IR Spectrum of Al/HDA Solid Reaction Product

broadening, and shifting of the H_2O bending mode to a higher frequency ($1650cm^{-1}$) than the usual $1620\text{-}1630cm^{-1}$, as observed in such metal nitrate hydrate as $Fe(NO_3)_3 \cdot 2H_2O$[3] suggests that there is some hydrogen bonding in the solid. Hydrogen bonding has been reported[4] in $Al(NO_3)_3 \cdot 9H_2O$. The band at the low frequency of $570cm^{-1}$ is assigned to the $Al\text{-}OH_2$ stretch of an aquo-co-ordinated aluminium cation.

The powder photograph of the material was recorded using CuK_α radiation. The pattern was well defined and is listed below, (Table 6-3).

This solid product was obtained from the Al/HDA system by washing and evacuation of the crystalline precipitate. It appears to be a well-defined hydrated nitrate of aluminium of formula $Al(NO_3)_3 \cdot 4H_2O$. The loss of crystallinity on washing and evacuation suggested that decomposition of the initially formed solid material might be taking place under these conditions. The formation of small crystals in the reaction mixture, described in the preliminary studies, using small pieces of aluminium metal, suggested that an X-ray structure determination on one of these crystals, immersed in the mother liquor and sealed in a capillary tube, might be possible. This procedure was in fact successful; the crystals were conclusively identified as the compound $Al(NO_3)_3 \cdot 6H_2O$ and the structure determination is proceeding. The detailed results of this investigation are described in Section 6.6. The work described above leads to the conclusion that on washing $Al(NO_3)_3 \cdot 6H_2O$ with CH_2Cl_2, followed by fairly prolonged evacuation, it is converted to the lower hydrate $Al(NO_3)_3 \cdot 4H_2O$.

Solution Products

The supernatant liquid above the crystals was evaporated on a vacuum line (20^oC, 10^{-3}mm). After a short period of evacuation, a floculent pale yellow precipitate was seen to form where drops of liquid had evaporated on the sides of the flask. After 24 hours, all the liquid had been removed, leaving a large bulk of pale yellow frothy solid. This froth was found to be quite dry and readily crumbled to a pale yellow powder (referred to hereafter as "the evaporate.") The speed of drying was comparable with that of the nickel/HDA system, no

Table 6-3.

X-ray powder photograph of the Al/HDA solid reaction product

d-spacing (nm)	Intensity
0.6752	5
0.6276	5
0.5901	60
0.5712	10
0.5669	20
0.5007	5
0.4667	5
0.4371	100
0.4227	40
0.3914	20
0.3767	95
0.3587	5
0.3504	5
0.3398	90
0.3276	90
0.3129	90
0.3035	5
0.2938	85
0.2846	10
0.2777	50
0.2720	10
0.2642	5
0.2605	5
0.2486	60
0.2378	20
0.2319	60
0.2189	30
0.2106	40
0.2017	30
0.1955	20
0.1920	20
0.1879	20
0.1847	25
0.1806	25
0.1773	10

"gummy" phase occurring. This is probably related to the mode of association of water with the aluminium nitrate system, implying that the degree of intermolecular hydrogen bonding is low, and that the structure consists of discretely hydrated units.

The evaporate was analysed for aluminium and total nitrogen content. The values obtained were Al, 12.21%; N, 14.79%. These results differ from those for the crystalline precipitate and lead to the low N:Al ratio of 2.34:1. The analytical figures agree most closely with those for the composition $Al_2O(NO_3)_4 \cdot Al(NO_3)_3 \cdot 8H_2O$ (requires: Al, 12.00%; N, 14.81%.). "Al_2O" moieties are found in other nitrato-compounds of aluminium, largely dominating the chemistry. The compound $Al_2O(NO_3)_4 \cdot 2AlONO_3$ is postulated as a possible decomposition product of aluminium nitrato-species, and the compound $Al_2O(NO_3)_4$ and $Al_2O(NO_3)_4 \cdot 2.4N_2O_4$ are well characterised[2]. It should however be noted that the evaporate can equally well be formulated as $Al_3O(NO_3)_7 \cdot 8H_2O$. Such "$M_3O$" systems are a well known feature of the acetate chemistry of tripositive transition metals, e.g. the compound $[Cr_3O(OAc)_6 \cdot (H_2O)_3]^+Cl^- \cdot 6H_2O$ has been shown[5] by x-ray crystallography to involve a triangular arrangement of the three chromium atoms, linked by the central "basic" oxygen atom situated in the same plane, octahedral coordination of each chromium atom being completed by the six bridging acetate ligands and three water molecules in terminal positions. The similar geometry of acetate and nitrate confers very similar coordination properties on these ligands. The compound $[Ir_3O(NO_3)_9]^+NO_3^-$ has been characterised by Harrison and Logan[6] and the cation almost certainly shows a similar structure to the above chromium (III) oxo-acetate, but with unidentate nitrate groups now occupying the terminal coordination positions of the three linked octahedra (Fig. 6-2). On the basis therefore, of these considerations, it is tentatively suggested that a likely constitution of the evaporate consistent with its composition, is $[Al_3O(NO_3)_6 \cdot (H_2O)_3]^+NO_3^- \cdot 5H_2O$.

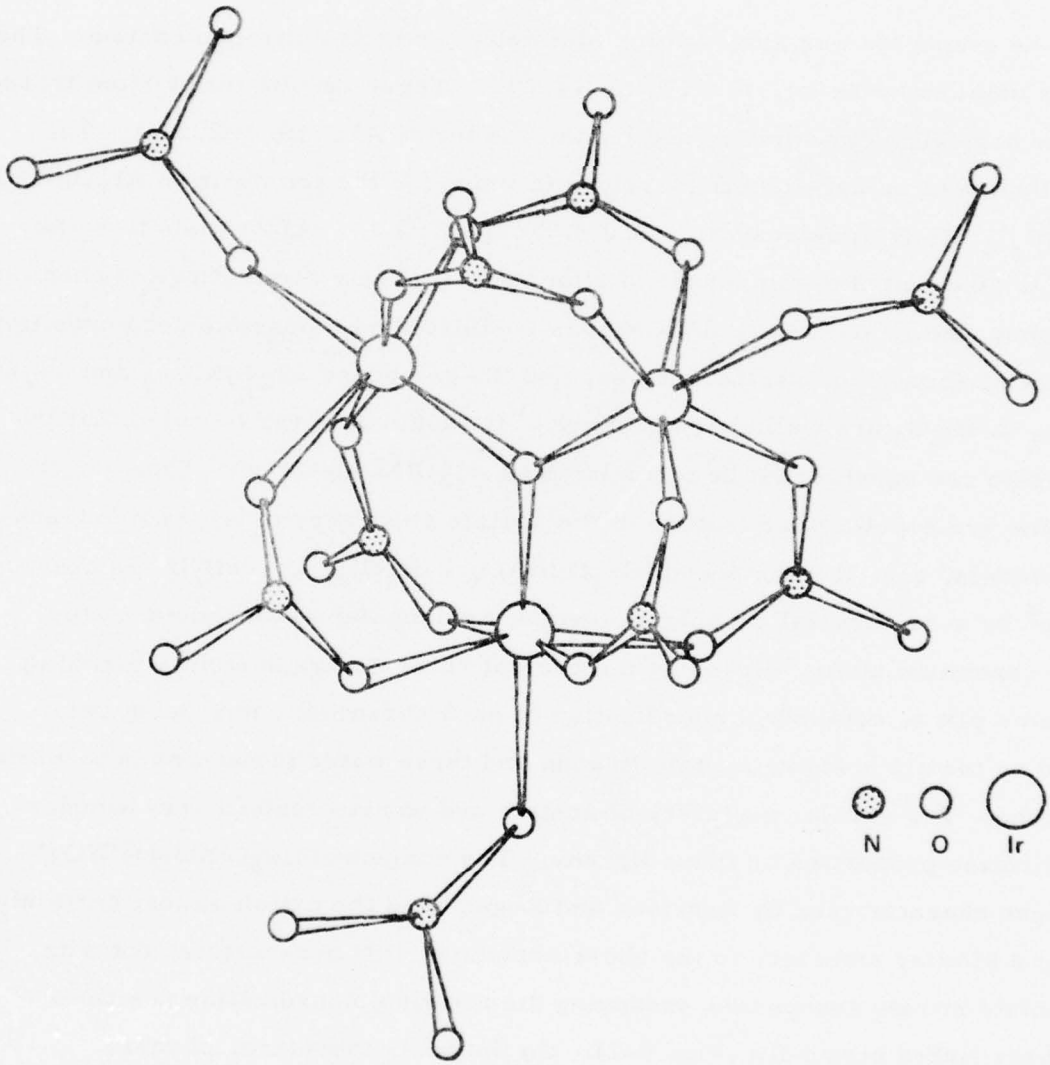


Figure 6-2. Proposed Structure of $Ir_3O(NO_3)_9^+$

The evaporate gave a good quality mull, but a poorly resolved infrared spectrum. The spectrum (Table 6-4, Fig. 6-3) is again difficult to interpret but does not exclude the possibility of the presence of both coordinated and ionic nitrate. The H_2O bending frequency at $1670cm^{-1}$, again suggests some degree of hydrogen bonding in the evaporate.

It is relevant to mention that the evaporate was found to react vigorously with water, with the evolution of much heat and brown fumes, whereas the solid precipitate did not react in this way, hydrolysis occurring quite smoothly. These observations may reflect a difference in the mode of bonding of the nitrate groups in the two compounds.

The powder photograph of the evaporate was recorded using CuK_α radiation. The solid was found to be amorphous, no lines being seen on the film.

There is still therefore some doubt about the exact nature of this compound. It is apparently a stable hydrated aluminium oxide nitrate, no decomposition (as signified for example by the evolution of N_2O_4) occurring even over a period of several months in a dry atmosphere. In the absence of X-ray crystallographic data, little further progress towards structural characterisation of the evaporate can be made. However the technique of ^{23}Al nuclear magnetic resonance spectroscopy might throw some light on the nature of Al species in HDA solution.

6.2 Some Properties of $Al(NO_3)_3 \cdot 6H_2O$

The verification that the initial product of the reaction between aluminium metal and HDA, i.e. the precipitate of small crystals, was $Al(NO_3)_3 \cdot 6H_2O$ (see Section 6.6) led to a more extensive examination of the properties of this evidently key compound, in the Al/HDA system, with the intention of comparing these properties with those of the compounds $Al(NO_3)_3 \cdot 4H_2O$ and $Al_3O(NO_3)_7 \cdot 8H_2O$ discussed above. The decomposition of $Al(NO_3)_3 \cdot 6H_2O$ appeared to be of special relevance, as this may occur where solid deposits are formed in fuel flow systems. These investigations necessitated the

Table 6-4. The infra-red spectrum (cm^{-1}) of the Al/HDA evaporate (nujol mull)

Absorption Band			Assignment (C_{2v} bidentate nitrate and D_{3h} ionic nitrate model)
3300	vs	vb	ν(OH)
2350	w	sh	
2250	w	sh	
1720	m	sh	
1670	m	b	$\nu(H_2O)$
1620	w	sh	$\delta(NO^*)$
1370	s	sh	$\nu_d(NO_2)$ ion
1310	w	b	
1265	m	sp	$\nu_{as}(NO_2)$
1100	m	b	
1050	m	sh	ν_s(NO)
1020	s	sp	
870	w	sh	
820	w	sh	$\pi(NO_3^-)$ ion
800	s	sp	$\delta_s(NO_2)$
670	w	b	ν(AlO)

* Unco-ordinated oxygen atom.

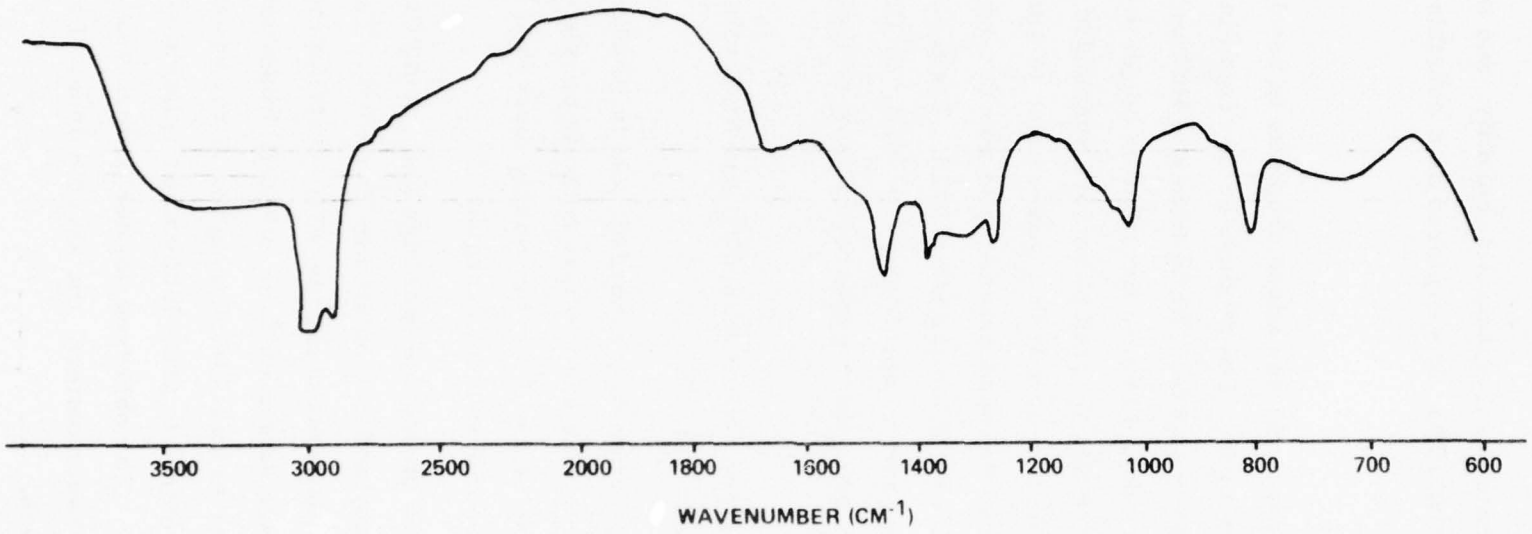


Figure 6-3. IR Spectrum of $Al_3O(NO_3)_7 \cdot 8H_2O$

preparation of this material in substantial quantity, and the reaction of anhydrous $AlCl_3$ with fuming (95%) HNO_3 was explored as a possible synthetic route for this purpose.

(a) Preparation

Fuming nitric acid (95%) was added dropwise to powdered $AlCl_3$ against a counter current of nitrogen. The mixture being cooled in solid CO_2 to moderate the extremely vigorous reaction. White fumes of HCl and brown fumes of NOCl were evolved. After about 4 hours, the solution began to deposit colourless crystals. The mixture was filtered to remove suspended impurities and was allowed to stand, protected by a P_4O_{10} guard tube, to allow volatilisation of NOCl. After 24 hours, the supernatant liquid was decanted off, and the crystals washed with a little ice-cold fuming nitric acid. Excess nitric acid was removed by careful evacuation on a vacuum frame (10^{-3}mm, 20°C.) A colourless crystalline residue was obtained, which appeared to show no tendancy to lose its crystallinity on evacuation.

Analysis was carried out for Al(8.30%) and N(12.6%), $Al(NO_3)_3 \cdot 6H_2O$ requires: Al, 8.41%; N, 13.1%.

The infra-red spectrum was recorded, and is illustrated in Fig. 6-4 and tabulated in Table 6-5. The spectrum is entirely consistent with the presence of solely ionic nitrate. As with the previously discussed solids, the spectrum is poorly resolved in the 1300-600cm^{-1} region.

The X-ray powder photograph was obtained, using CuK_α radiation. The pattern is well defined, and is tabulated in Table 6-6. The powder pattern was compared with that calculated using the NRC crystallographic program No. NRC-21, having at this stage determined the unit cell dimensions to be a=b=c=13.711A°, and the cell symmetry to be cubic, during the X-ray crystal structure determination. This was considered to provide the most reliable check on the purity and nature of the product. The observed powder pattern was found to compare closely with the calculated powder pattern, the small number of absent reflections allowing a close comparison.

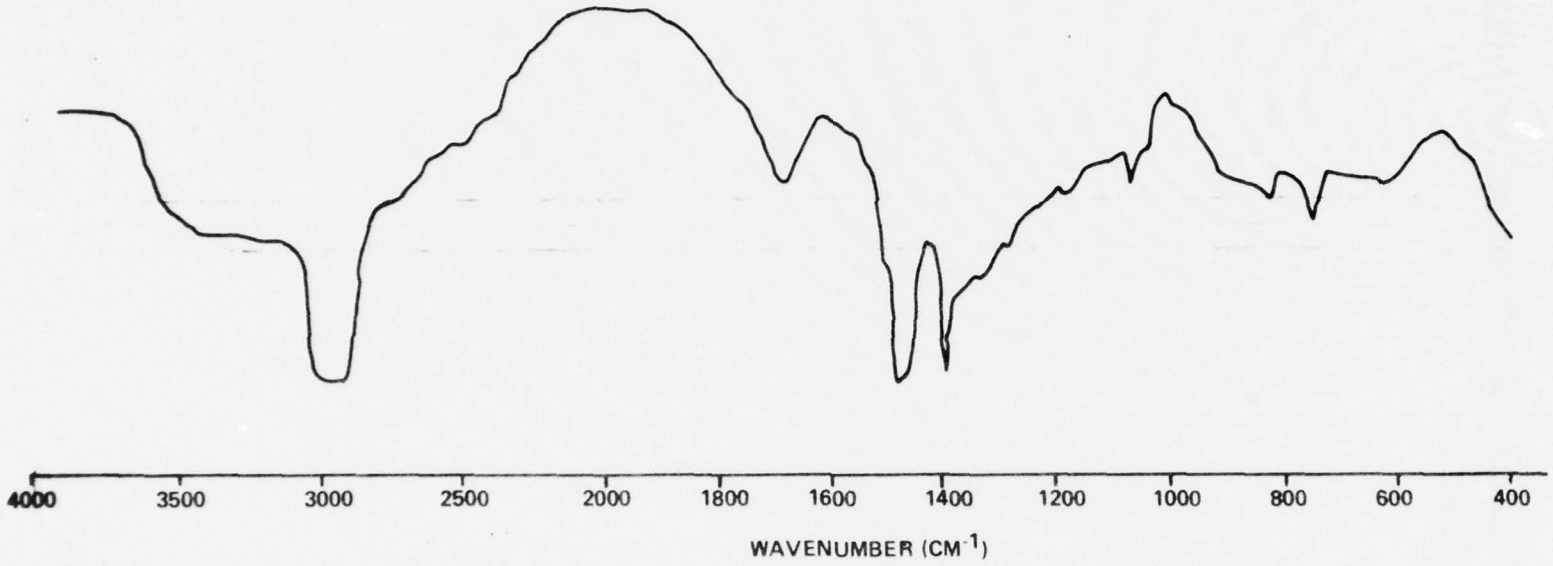


Figure 6-4. IR Spectrum of $Al(NO_3)_3 \cdot 6H_2O$

Table 6-5. The Infra-red spectrum (cm^{-1}) of $Al(NO_3)_3 \cdot 6H_2O$ (nujol mull)

Absorption Band			Assignment (D_{3h} Ionic Model)
3200	vs	vb	ν(O-H)
2490	m	sh	
2380	m	sh	
1680	s	sp	$\delta(H_2O)$
1380	vs	b	$\nu_d(NO_2)$
1325	m	sp	
1275	m	sp	
1175	w	sp	
1065	w	sp	
825	w	sp	$\pi(NO_3)$
740	m	sp	$\delta_d(NO_2)$
610	w	sp	ν(Al-O)

Table 6-6.

The X-ray powder photograph of $Al(NO_3)_3 \cdot 6H_2O$

d(nm)	Intensity	d(calc.)(nm)	Indexing (hkl)
0.691	90	0.685	(020)
0.623	30	0.613	(210)
0.586	80	0.560	(211)
0.521	5		
0.495	30	0.485	(202)
0.437	5	0.434	(300)
0.425	30	0.413	(131)
0.400	80	0.396	(222)
0.389	20	0.380	(023)
0.374	50	0.366	(132)
0.357	30		
0.344	60	0.343	(400)
0.327	30	0.323	(330)
0.309	20	0.307	(420)
0.292	70	0.292	(332)
0.281	20	0.279	(242)
0.270	20	0.269	(431)
0.262	30	0.264	(115)
0.251	70	0.250	(521)
0.245	40	0.242	(440)
0.237	40	0.238	(522)
0.228	40	0.228	(244)
0.222	50	0.222	(523)
0.217	30	0.217	(620)
0.212	30	0.212	(451)
0.207	40	0.207	(262)
0.202	40	0.202	(361)
0.198	10	0.198	(444)
0.194	10	0.194	(534)
0.191	20	0.192	(155)
		0.190	(640)
0.187	20	0.188	(641)
0.184	40	0.183	(642)
0.179	10	0.179	(535)
0.177	5	0.176	(634)

(b) Thermal decomposition

The thermal decomposition of $Al(NO_3)_3 \cdot 6H_2O$ was studied by thermogravimetric analysis, i. e. the observation of weight loss of the sample against temperature, at a constant heating rate. It was hoped to detect the presence of any intermediate hydrates (e. g. $Al(NO_3)_3 \cdot 4H_2O$), or oxide nitrates (e. g. $Al_2O(NO_3)_4$ or $AlONO_3$) en route to the ultimate decomposition product Al_2O_3.

The apparatus is illustrated in Fig. 6-5. The sample was loaded into the weighed glass bucket in a dry box, and a stream of dry argon was passed through the apparatus via the tap when the apparatus was removed from the box, to prevent ingress of atmospheric moisture. The bucket was suspended from the pan of an accurate balance, and the apparatus was heated electrically by the heating coil. The temperature inside the vessel was measured by means of a thermocouple mounted inside, close to the bucket. The bucket was maintained for 10 minutes at each temperature to allow equilibration, and the weight recorded at the end of this time. The results are presented graphically in Figs. 6-6 and 6-7; the former showing the weight loss with temperature, and the latter the rate at which decomposition occurs with temperature.

Conversion of weight readings obtained into a function expressing the molecular weight loss was achieved by using the equation

$$\text{Weight loss} = \frac{w}{W} . M \text{ molecular weight units}$$

where w = weight loss in grams

W = weight of sample in grams

M = molecular weight (= 320.98 for $Al(NO_3)_3 \cdot 6H_2O$)

The results show a simple one-step decomposition of the nitrate, reaching a maximum rate at about 140°C, followed by a slow decomposition at temperatures above about 195°C, probably corresponding to dehydration of hydrate aluminium oxide. At the temperature at which the experiment was discontinued the composition appeared to be close to that of Al_2O_3.

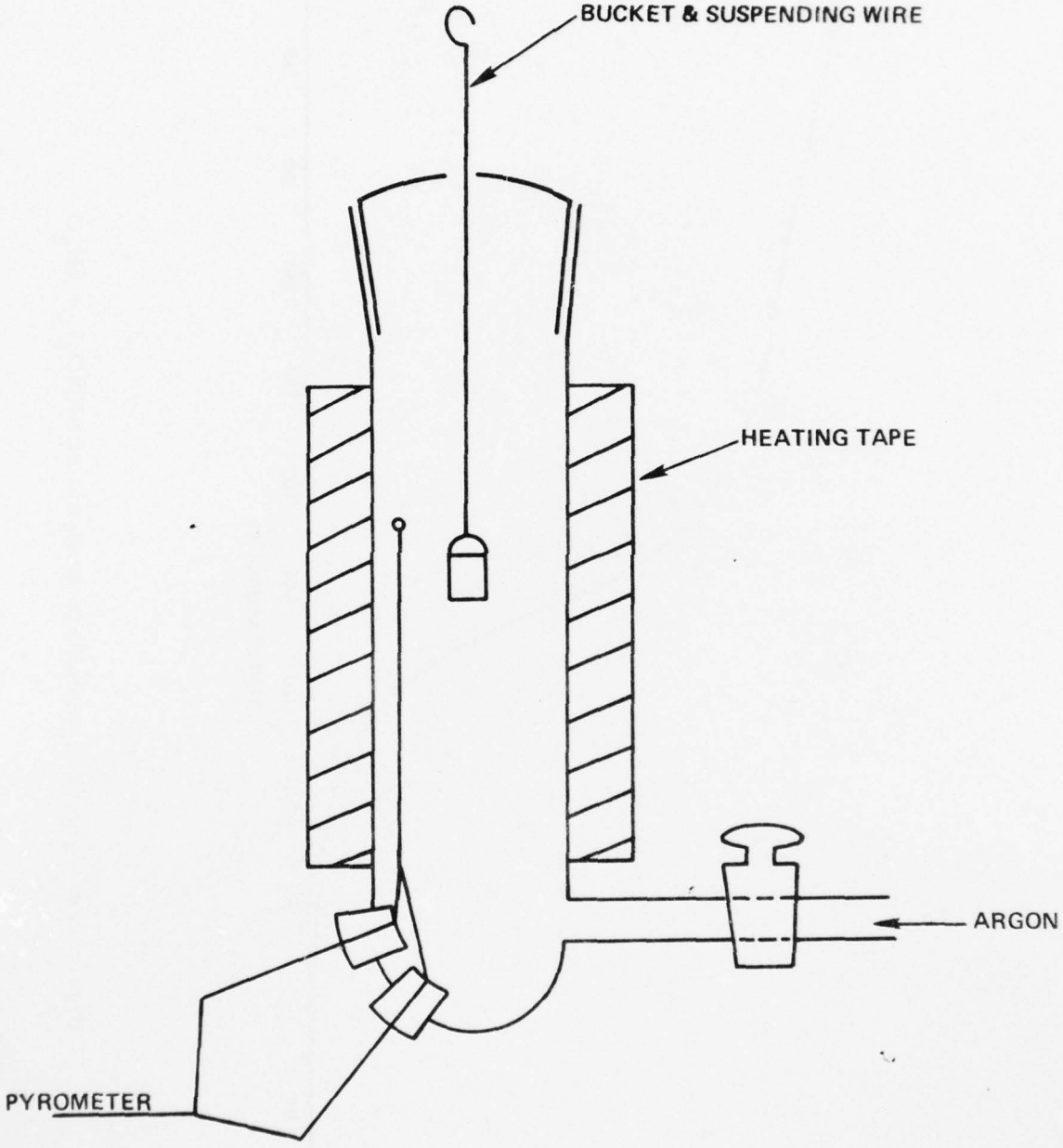


Figure 6-5. Furnace for T. G. A. Measurement

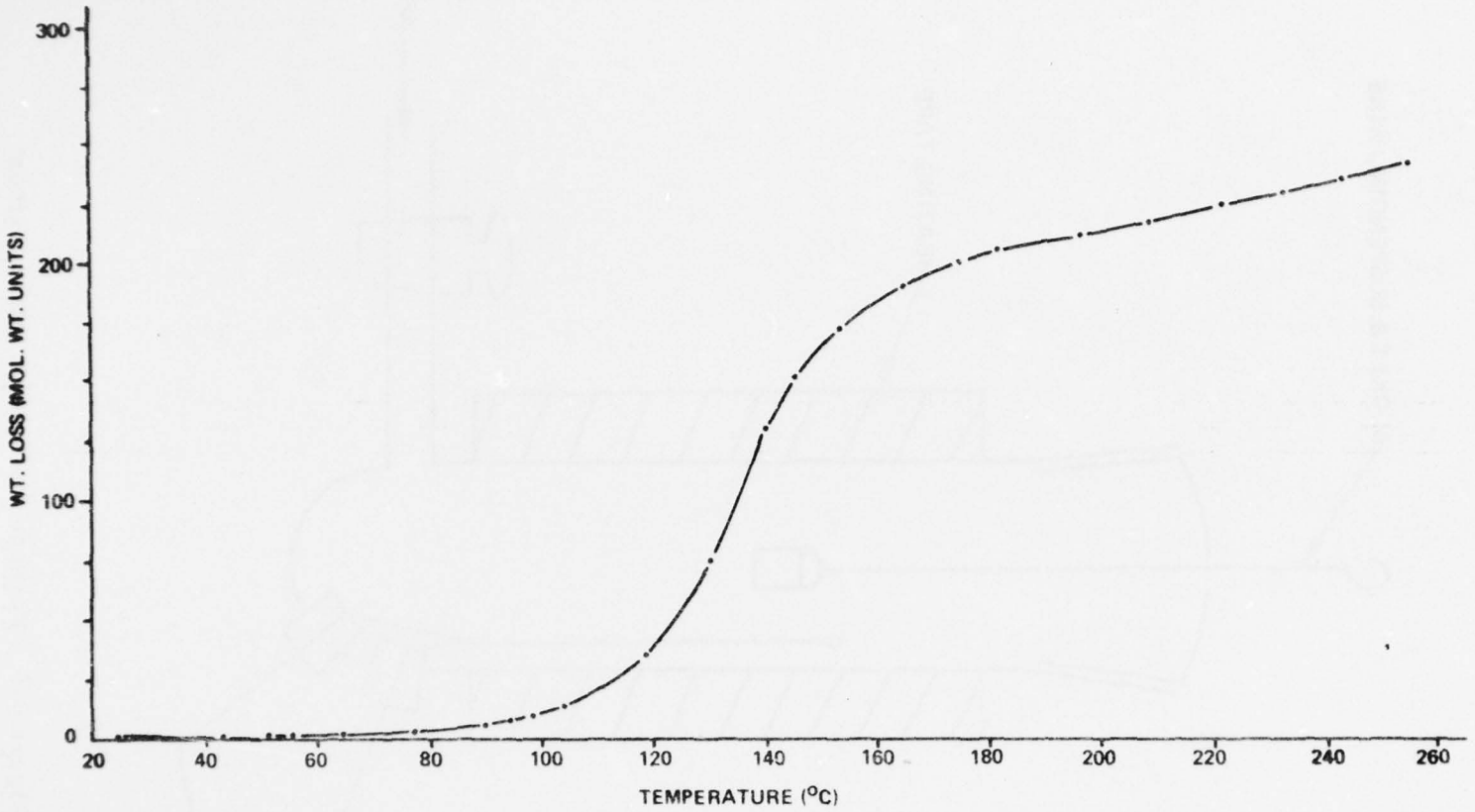


Figure 6-6. Thermogravimetric Analysis of $Al(NO_3)_3 \cdot 6H_2O$

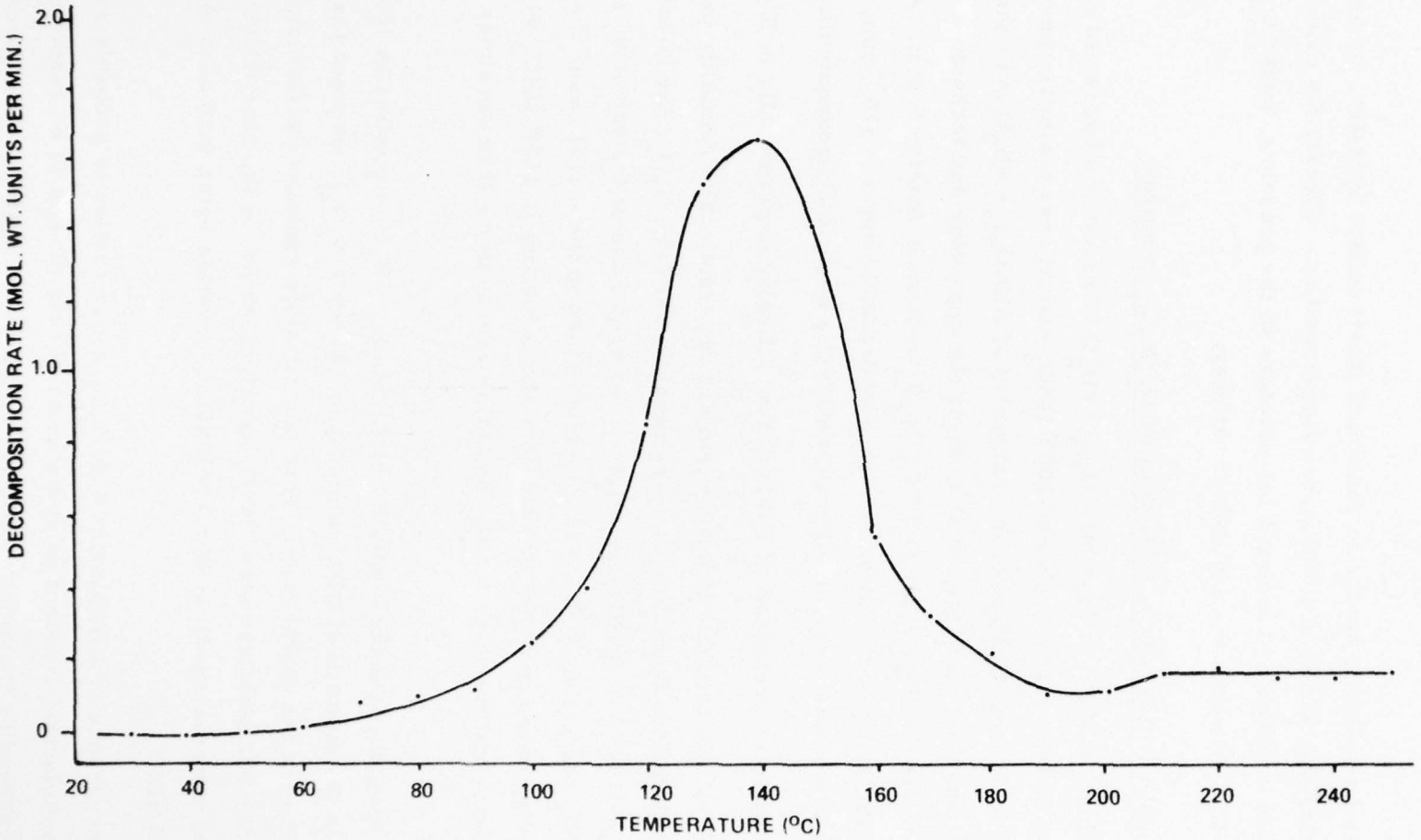


Figure 6-7. Rate of Thermal Decomposition of $Al(NO_3)_3 \cdot 6H_2O$

There is no evidence for the formation of intermediate hydrates, or oxide nitrates during the course of the thermal decomposition. Clearly the mode of decomposition in vacuum at ambient temperature in the presence, possibly of N_2O_4 or HNO_3, proceeds via a different pathway.

6.3 The solubility of $Al(NO_3)_3 \cdot 6H_2O$ in HNO_3/N_2O_4 mixtures

The formation of crystals of $Al(NO_3)_3 \cdot 6H_2O$ in reaction mixtures of Al with HDA, but not in the reaction between 100% HNO_3 and Al over a similar period of time prompted an investigation of the solubility of $Al(NO_3)_3 \cdot 6H_2O$ over the HNO_3-N_2O_4 composition range, at 0^oC using the apparatus and techniques described for the $Ni(NO_3)_3 \cdot 2H_2O/HNO_3/N_2O_4$ system in Section 5.4(c). After filtration of the saturated solution, it was evaporated to dryness (10^{-3} mm, 20^oC), and the aluminium was determined gravimetrically using 8-hydroxyquinoline.

The results are presented in Table 6-7 and displayed graphically in Fig. 6-8.

Close parallels with the nickel system are apparent. The solubility passes through a well defined maximum at approximately 10.7wt% N_2O_4, the solution containing ca 1.4wt% of $Al(NO_3)_3 \cdot 6H_2O$. The magnitude of the enhanced solubility in HNO_3 containing N_2O_4 is however less than in the nickel case, the maximum being only some 50% greater than the solubility in 100% HNO_3 whereas the maximum solubility value for the nickel system is more than ten times that in 100% HNO_3.

It is noteworthy that the solubility of $Al(NO_3)_3 \cdot 6H_2O$ is greater in 100% HNO_3 than in the mixture of HDA composition (44 wt % N_2O_4), whereas the reverse is true in the nickel case. This fact possibly explains the formation of crystals in the 321 stainless steel/HNO_3 reaction but not in the steel/HDA reaction, and the reverse situation with aluminium, crystals being formed in Al/HDA but not in Al/HNO_3.

This occurrence of a maximum with N_2O_4 concentration is probably related to the same dielectric constant or complexing effects thought to be responsible for the corresponding maximum exhibited by the nickel system. The lower N_2O_4

Table 6-7.

The solubility of $Al(NO_3)_3 \cdot 6H_2O$ in HNO_3/N_2O_4 mixtures at $0^{\circ}C$

Wt % N_2O_4	Solubility (g. solute/100g. solution)
0	0.9022
4.89	1.187
10.71	1.403
14.65	1.324
19.22	1.246
26.59	1.089
44.66	0.864

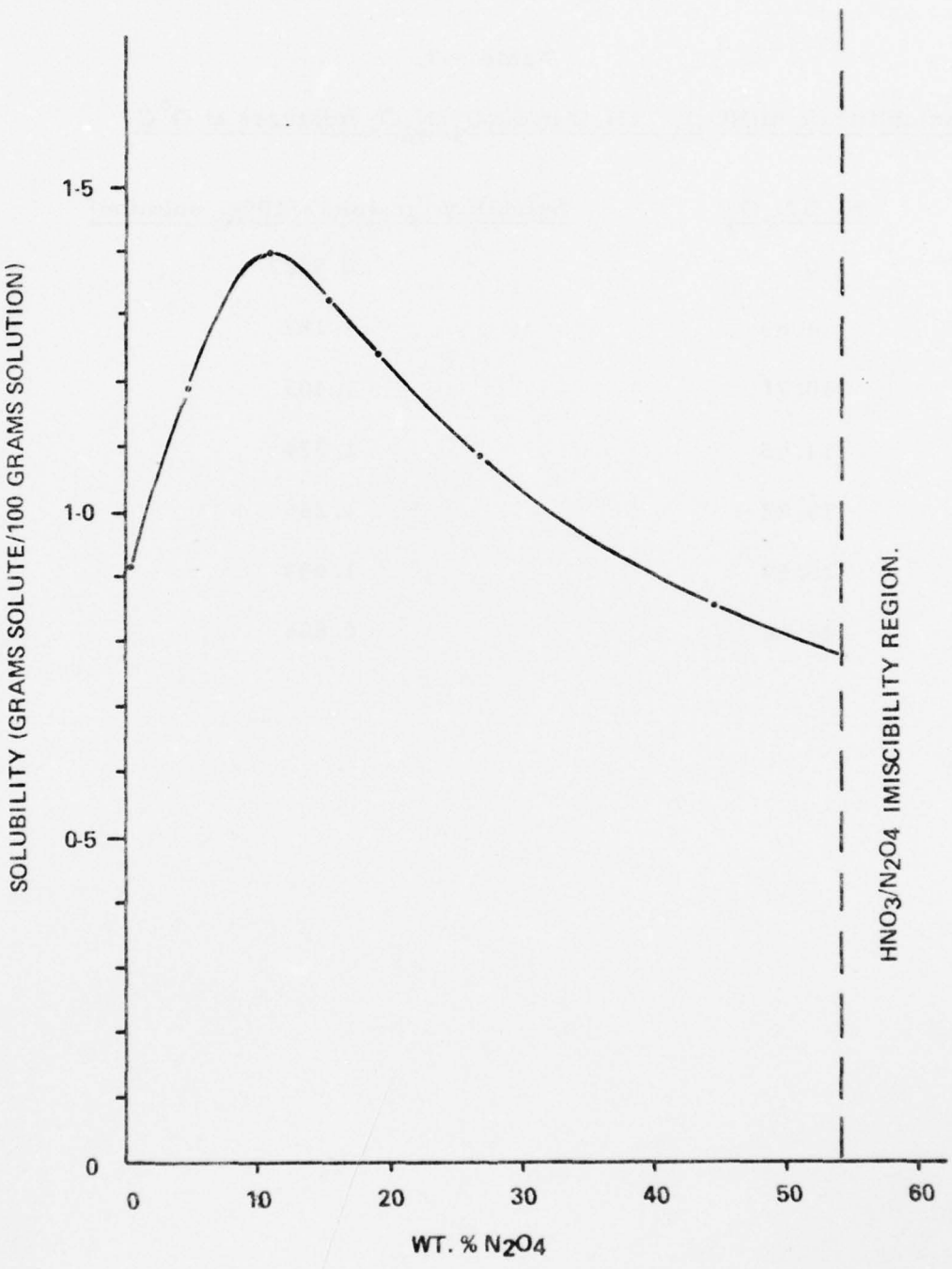


Figure 6-8. Solubility of $Al(NO_3)_3 \cdot 6H_2O$ in HNO_3/N_2O_4 Mixtures at 0^oC

concentration at which solubility maximum is obtained in the aluminium case may be related to the amount of "water" introduced into the system by the nitrate hydrate i. e. $Ni(NO_3)_2 \cdot 2H_2O$ introduces only two molecules of water per Ni(II) into the system, whereas $Al(NO_3)_3 \cdot 6H_2O$ introduces 6 molecules per Al(III).

The effect of temperature on the solubility of $Al(NO_3)_3 \cdot 6H_2O$ was measured using a 15.64wt% solution of N_2O_4 in HNO_3.

The method used was the same method used in the above determinations. The results are presented in Table 6-8 below, and graphically in Fig. 6-9.

Table 6-8.

Effect of temperature on the solubility of $Al(NO_3)_3 \cdot 6H_2O$ in HNO_3/N_2O_4 (15.64 wt. % N_2O_4)

Temperature ^{o}C	Solubility (g. $Al(NO_3)_3 \cdot 6H_2O$/100g. solution)
-16.05	0.952
-9.1	1.175
0.0	1.309
10.20	1.490
22.00	1.937

Over the ca. $40^{o}C$ temperature range studied, the effect of temperature was to cause an essentially linear increase in solubility. Using these results the molar heat of solution was calculated from the plot of Inx against $^{1}/_{T}$ in the same manner as for the nickel system (see Section 5.2). A linear plot was again obtained from which the molar heat of solution was calculated to be -8.3 ± 0.3 kJ mol^{-1}. This molar heat of solution is again comparable to the heat of solution of salt hydrates in water, and suggests that there is little change in co-ordination around the aluminium on dissolution.

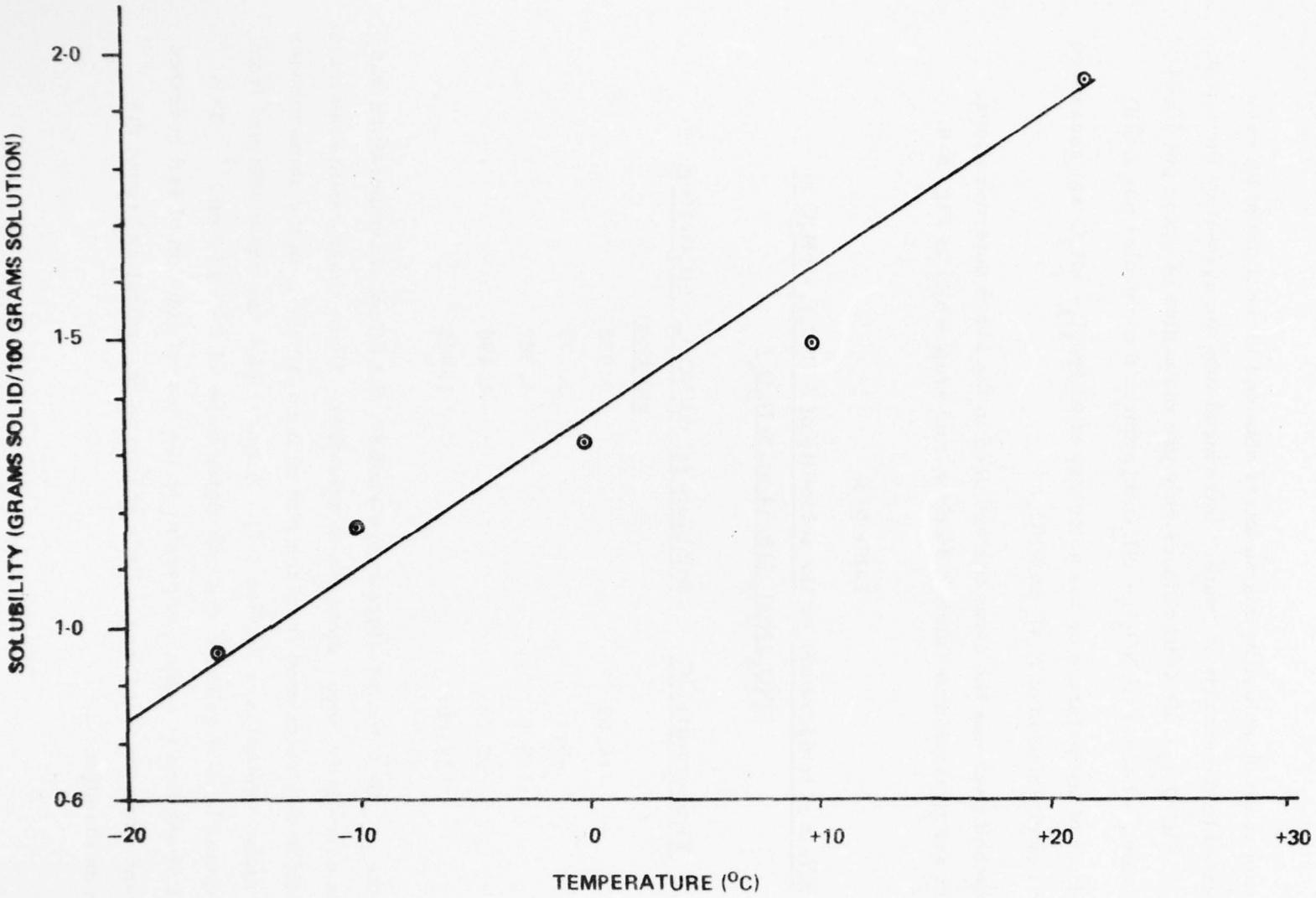


Figure 6-9. Variation of Solubility of $Al(NO_3)_3 \cdot 6H_2O$ in 15.64wt% N_2O_4/HNO_3 Mixture with Temperature

6.4 Reactions of aluminium nitrate tetra- and hexa-hydrates with N_2O_4 and HDA

In the light of the unexpected range of products obtained from solutions of aluminium in HDA, and the apparently ready decomposition of $Al(NO_3)_3 \cdot 6H_2O$ when separated from its mother liquor, a thorough investigation of the reactions of $Al(NO_3)_3 \cdot 6H_2O$ and $Al(NO_3)_3 \cdot 4H_2O$ with N_2O_4 and HDA was carried out to determine if any effects of N_2O_4 composition etc., on the products in the $Al/HNO_3/N_2O_4$ system could be detected.

(a) The reaction of $Al(NO_3)_3 \cdot 4H_2O$ and N_2O_4

The reaction between $Al(NO_3)_3 \cdot 4H_2O$ (prepared as described in Section 6.1(c)) and N_2O_4 was examined by leaving a small sample of the hydrate in contact with dry N_2O_4 in a sealed vessel. On addition of N_2O_4 to the solid, no green colour (typical of the reaction of H_2O with N_2O_4) was observed. After 24 hours the material appeared to have become slightly gummy and the N_2O_4 was replaced by a fresh sample. The N_2O_4 was subsequently changed 4 times at intervals of 48 hours to drive any equilibrium reaction to completion. The solid was then allowed to remain in contact with N_2O_4 for a further two months.

At the end of this time, the N_2O_4 was decanted off, the solid was washed with fresh N_2O_4, and finally dried in a gentle stream of dry nitrogen with occasional shaking and grinding. The product was a fine, free-flowing pale yellow powder.

The X-ray powder photograph was found to be identical to that of the $Al(NO_3)_3 \cdot 4H_2O$ starting material. The infra-red spectrum was also found to be similar, but strong peaks attributed to molecular N_2O_4 were observed at $1730cm^{-1}$, $1250cm^{-1}$ and $745cm^{-1}$. Analysis of the solid indicated low aluminium and high total nitrogen content (Found Al, 8.45%; N, 16.6%.) It is considered that these figures reflect the presence of N_2O_4 trapped in particles of the solid (i.e. occluded). This phenomenom parallels the observations of Section 6.5, where dichloromethane was similarly trapped in a solid matrix when solvent was removed by a gentle stream of nitrogen.

It is therefore concluded that no reaction occurs between $Al(NO_3)_3 \cdot 4H_2O$ and N_2O_4.

(b) The reaction of $Al(NO_3)_3 \cdot 6H_2O$ and N_2O_4

A parallel study was carried out on this reaction. This experiment showed that no transformation of the solid to a gum occurs and that no green colour is developed in the N_2O_4. It is relevant to note that earlier work by Addison and Chapman[7] showed that the reaction between N_2O_4 and potassium aluminium sulphate dodecahydrate, $KAl(SO_4)_2 \cdot 12H_2O$, results in the removal of 6 molecules of water to give $KAl(SO_4)_2 \cdot 6H_2O$. $KAl(SO_4)_2 \cdot 12H_2O$ consists of $[K(H_2O)_6]^+$, $[Al(H_2O)_6]^{3+}$ and SO_4^{2-} units, and it is likely that the water molecules are removed from the hexa-aquopotassium cation by N_2O_4, in which the cation $[Al(H_2O)_6]^{3+}$ persists as a stable unit. The presence of this unit in $Al(NO_3)_3 \cdot 6H_2O$ (and possibly in $Al(NO_3)_3 \cdot 4H_2O$), explains the stability of these hydrates with respect to N_2O_4.

(c) The reaction of $Al(NO_3)_3 \cdot 6H_2O$ and HDA

In connection with one of the solubility determination experiments described in Section 6.3, $Al(NO_3)_3 \cdot 6H_2O$ was left in contact with HDA in the solubility apparatus. At the end of the experiment, the HDA was decanted off, and the remaining solid dried in vacua (10^{-3}mm. $20^{\circ}C$). The resulting pale yellow solid was examined by X-ray powder photography, and was found to have undergone complete converstion to $Al(NO_3)_3 \cdot 4H_2O$. It is possible that $Al(NO_3)_3 \cdot 6H_2O$ is only stable in contact with its solution in HDA, and that removal of HDA leads to subsequent dehydration. Further studies with a variety of HNO_3/N_2O_4 mixtures also produced dehydration of the 6-hydrate to the 4-hydrate on evacuation of the solid to remove excess liquid. This tends to indicate that the 6-hydrate may convert to the 4-hydrate merely on prolonged evacuation.

6.5 The reaction of $AlCl_3$ with HDA

This reaction was examined for possible suitability as a route to the preparation of Al/HDA corrosion products in substantial quantity. $AlCl_3$ was measured out in a dry box into a dry flask. The flask was cooled in solid CO_2/methcol to

moderate the reaction, and a counter-current of nitrogen passed. HDA was added carefully, whereupon a vigorous reaction occurred, brown fumes of NOCl being evolved. The mixture was set aside for 16 hours at $0^{o}C$, and was then filtered to remove insoluble impurities. On cooling of the mixture to encourage crystallisation, separation of an upper immiscible layer occurred - a phenomenon not experienced with HDA itself. It is thus possible that the presence of aluminium in solution would modify the N_2O_4/HNO_3 phase diagram to a greater extent than does iron.

Over a period of about five days, a thick crust of crystals formed on the walls of the flask. This delayed crystallisation may be related to the rate of evaporation of NOCl through the guard tube, since it is conceivable that retention of NOCl will enhance the solubility of dissolved metal species by increasing the dielectric constant of the medium and promoting the formation of nitrosonium chloro-complexes.

The supernatant liquid was decanted from the crystalline precipitate in a dry box, and the solid product and solution were subjected individually to investigation.

Solid Products

The solid precipitate was treated in two ways. A first sample was washed with dichloromethane several times to remove HDA and was then evacuated overnight. Analysis of the material showed that it contained Al, 9.23%; and N, 14.79%. These figures are close to those for the hydrate $Al(NO_3)_3 \cdot 4H_2O$ described above (Section 6.1(c), Al, 9.37%; N, 13.7%.) The infra-red spectrum and X-ray powder photograph were identical in all respects to those of $Al(NO_3)_3 \cdot 4H_2O$.

A second sample was similarly washed with dry dichloromethane, but in this case, the solvent was not removed by evacuation, but by directing a powerful stream of dry nitrogen onto the solid, with occasional shaking and grinding, until an apparently dry free-flowing fine powder was formed. It was hoped that these more moderate conditions would lessen the likelyhood of decomposition of the

solid. The infra-red spectrum and X-ray powder pattern of this material were again found to be identical to those of $Al(NO_3)_3 \cdot 4H_2O$.

The analytical figures for the material are close to those of $Al(NO_3)_3 \cdot 6H_2O$ (Found: Al, 8.54%; N, 13.44%, $Al(NO_3)_3 \cdot 6H_2O$ requires Al, 8.42%; N, 13.1%). In the light of the evidence provided by infra-red spectroscopy and X-ray powder photography, it is considered that this agreement is fortuitous and perhaps indicates that all the CH_2Cl_2 was not removed from larger particles of solid in the stream of nitrogen. The X-ray powder photographs and infra-red spectra were recorded before the analysis was carried out, indicating that if $Al(NO_3)_3 \cdot 6H_2O$ is formed initially, decomposition to the tetrahydrate had occurred by the time these were recorded. There is no evidence for a decomposition in the reverse sense i.e. $Al(NO_3)_3 \cdot 4H_2O \longrightarrow Al(NO_3)_3 \cdot 6H_2O$, which would probably have occurred in the X-ray capillary if sealing had been incomplete allowing ingress of atmospheric moisture.

Solution Products

The clear solution which had been decanted off from the crystals was evaporated to dryness on a vacuum frame ($20^{\circ}C$, 10^{-3}mm). After evacuation overnight, a pale yellow froth was formed, which on grinding gave a pale yellow, free-flowing powder. The infra-red spectrum and X-ray powder photograph were identical to those of the residue from the evaporated Al/HDA solution, (Section 6.1(d)), an amorphous material being formed in both cases. The analytical figures, too were similar to those of the Al/HDA evaporation residue (Found Al, 12.21%; N, 14.44%, cf Al/HDA evaporation residue: Al, 12.21%; N, 14.8%.) This indicates that the Al/HDA reactions and $AlCl_3$/HDA reactions both lead to the same oxide nitrate hydrate species on evaporation of the solution, namely $Al_3O(NO_3)_7 \cdot 8H_2O$.

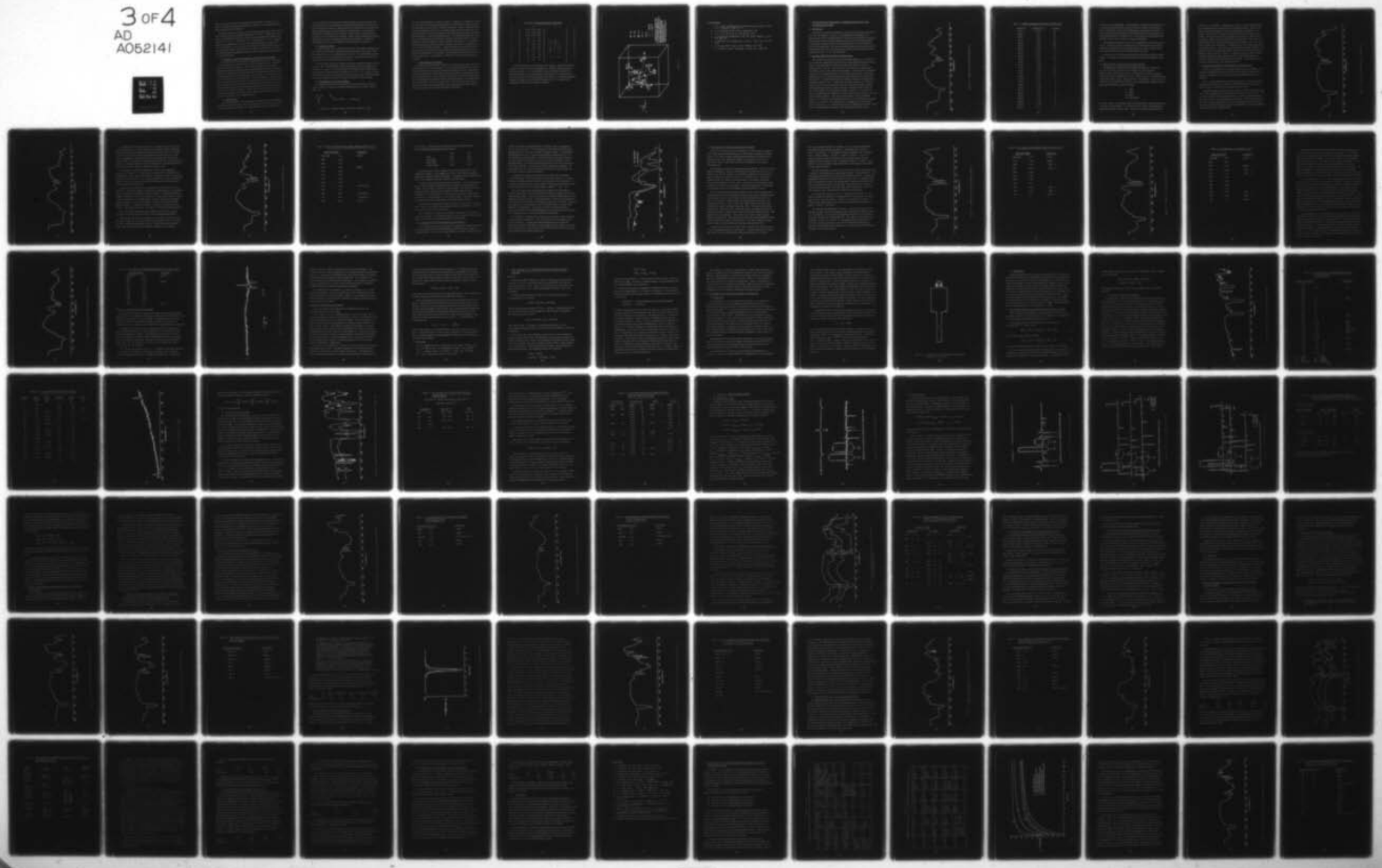
6.6 Single crystal X-ray investigation of the Al/HDA solid product

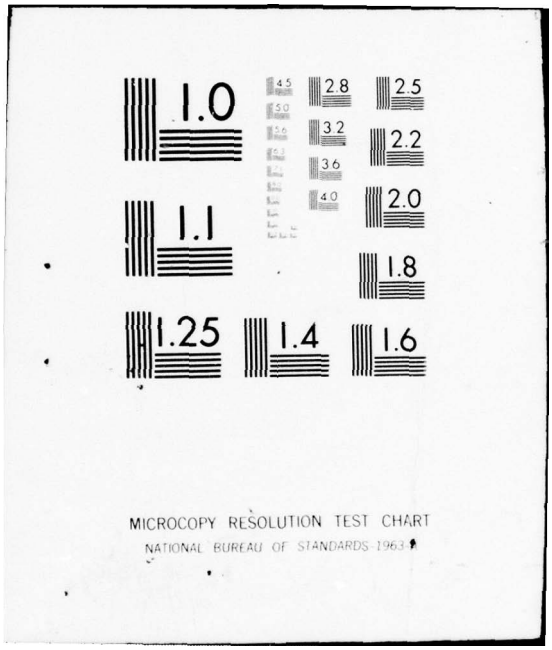
(a) Crystal mounting and X-ray photography

A small crystal of the product which separates from solution when aluminium metal reacts with HDA was sealed with a thin-walled, Lindemann glass capillary

AD-A052 141 NOTTINGHAM UNIV (ENGLAND) DEPT OF INORGANIC CHEMISTRY F/G 7/2
HDA CORROSION CHEMISTRY.(U)
DEC 77 C C ADDISON, N LOGAN AFOSR-74-2709
UNCLASSIFIED AFRPL-TR-77-65 NL

3 OF 4
AD
A052141




1.0
1.1
1.25
1.4
1.6
1.8
2.0
2.2
2.5
2.8
3.2
3.6
4.0
4.5
5.0
5.6
MICROCOPY RESOLUTION TEST CHART
NATIONAL BUREAU OF STANDARDS-1963-A

tube (0.3mm diam.) under an atmosphere of dry nitrogen in a glove box. In order to prevent decomposition during data collection, a small quantity of HDA was also sealed into the capillary.

Oscillation, and zero and first layer Weissenberg photographs were recorded with a Nonius camera using CuK_α radiation ($\lambda = 1.5418A^o$). Photographic symmetry revealed that the crystals are cubic and the systematically absent reflections ($h + k + l = 2n + 1$, Okl when $k = 2n + 1$ and Okl when $l = 2n + 1$) index the space group, unequivocally, as Ia3, with a unit cell dimension of ca $13.7A^o$. The crystal density, 1.747, measured by flotation of N-heptane/bromoform mixtures therefore indicates that the unit cell contains 8 formula units. The unit cell dimension was subsequently refined by a least-squares procedure based on 12 intense reflections.

(b) Structural restrictions imposed by cell symmetry and contents

In the space group Ia3, the number of general positions is 48. Since there are 8 molecules in the unit cell, there will be 8 aluminium atoms, 24 nitrate groups, and 48 water molecules. Thus, only the water molecules will be expected to occupy the general positions and the aluminium atoms and nitrate groups will occupy the 8-fold and 24-fold special positions respectively. Each 8-fold position has 3-fold symmetry and is also a centre of inversion while the 24-fold positions have 2-fold symmetry. The first condition is readily acceptable to a single atom (Al), but the 2-fold symmetry of the nitrate group position requires that it be positioned with the 2-fold axis passing through the nitrogen and the oxygen atom such that this axis forms the O-N-O angle bisector with respect to the two other O atoms. These restrictions clearly prove helpful in evaluating a solution to the structure since these symmetry features must be apparent in the atomic co-ordinates produced.

(c) Data collection

The 3-fold symmetry of the cubic space group Ia3 gives rise to symmetry equivalences of the type hkl = klh = lhk for any set of h, k, and l, and so only one third of the data is unique. For computational reasons (see later) each

reflection was collected separately so that the structure could be solved using the orthorhombic crystal subgroup Ibca where these equivalences do not occur. Approximately 1230 intensity measurements were collected in the range $20 \leq 50^{o}$ using pyrolysed graphite monochromatised CuK_{α} radiation. Few reflections beyond 50^{o} in 2θ appeared to be observed. Three standard reflections were measured every 100 reflections to monitor crystal setting and quality but showed insignificant variation in intensity throughout data collection. Lorentz and polarization corrections were applied, but any absorption was ignored.

(d) Structure solution

In order to confer exact 3-fold symmetry in the orthorhombic subgroup Ibca, each of the cubic symmetry equivalent sets was averaged, and the mean value was assigned to each formally equivalent reflection. It was noted that, as would be expected, each formally equivalent reflection, when measured, agreed well with the other two reflection intensities in the set.

The MULTAN multisolution program was used to generate a solution with the 170 E's >1.40. Although Σ2 was unable to determine any 'known phases', the reflections 2 1 5 and 1 5 2 were used from a convergence test as origin fixing reflections and, together with the reflections 5 2 1, 4 1 7, 7 4 1, and 2 2 2 which were each assigned arbitrary phases, formed the starting set. The best solution was used to calculate an E map, the features of which are now discussed.

(e) Interpretation of the E map solution

The labelling sequence used to describe the atoms in $Al(NO_3)_3 \cdot 6H_2O$ is shown in Figure 6-10 and the information obtained from the E map is listed in Table 6-8.

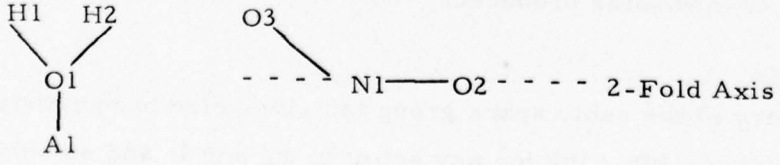


Figure 6-10. Labelling scheme for atoms in $Al(NO_3)_3 \cdot 6H_2O$

The twelve largest peaks are listed in column 'a' and their co-ordinates in column 'b'. Since the E map has been calculated for the orthorhombic crystal subgroup, several peaks in the list will be related by symmetry. The first two peaks show three fold rotational symmetry of co-ordinates and represent a single atom in a general position. This can be assigned to the oxygen atom of the water molecule. The fourth peak is clearly the aluminium atom. The remaining peaks are, therefore, due to atoms in the nitrate group. Atoms in the nitrate group, in special positions, on the two fold axis, have coordinates in the form x, o, 1/4 and the coordinates from the E map have been converted to this form by subtracting 1/2, 1/2, 1/2 and are listed in column 'c'. Sufficient peaks can be found to obtain at least one set of coordinates for each nitrate group atom although the full set of symmetry related peaks is not present. The hydrogen atoms H1 and H2 were not visible in the E map. The solution is, therefore, consistent with space group symmetry.

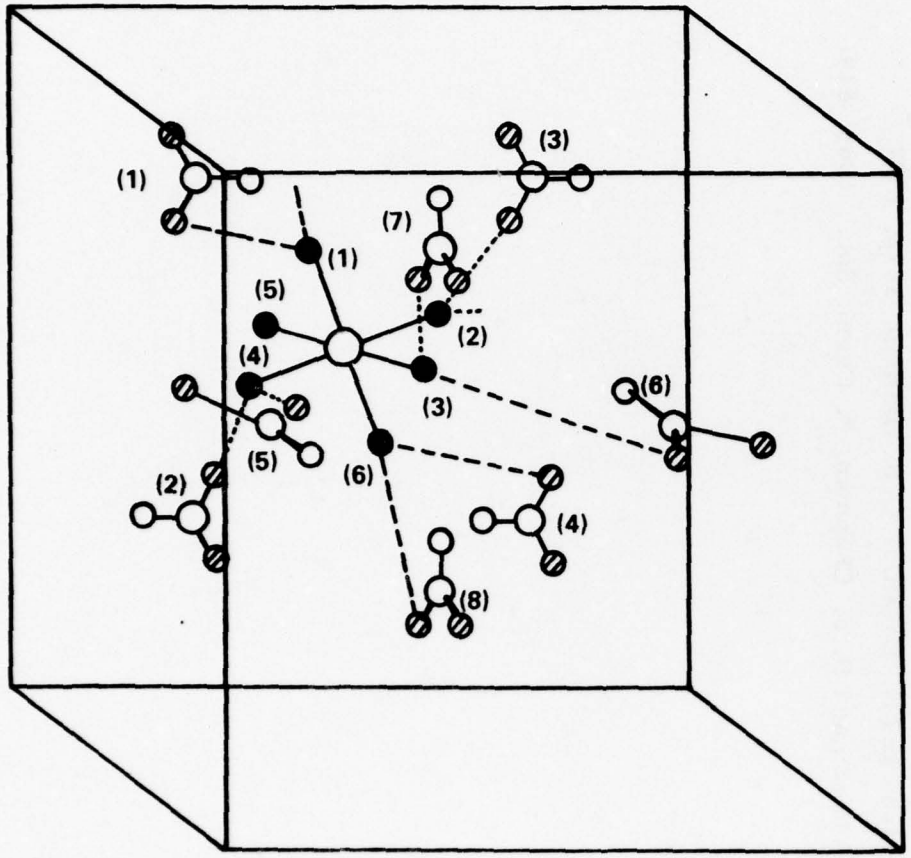
(f) *Refinement of the structure*

Using the co-ordinates listed in Table 6-8, refinement was performed in the space group Ia3 using a cubic data set. This data was obtained from the orthorhombic data set by averaging the symmetry equivalent reflections. Refinement converged isotropically, and a difference Fourier synthesis suggested positions for the hydrogen atoms. With isotropic variation for the hydrogen and aluminium atoms and anisotropic variation for other non-hydrogen atoms, refinement again converged and the residual is currently 10%. The temperature factors for the nitrate group atoms are unusually large in this compound and suggest that there is some movement of the nitrate group atoms in the lattice.

Table 6-8 E map peaks and their assignment

a	b			c			d
1	0.38	0.44	0.53				01
2	0.52	0.39	0.44				01
3	0.44	0.56	0.37				01
4	1/2	0	1/2				Al
5	3/4	.78	1/2	1/4	.28	0	Nl
6	.67	3/4	1/2	.17	1/4	0	03
7	0	.83	1/4	0	.17	1/4	03
8	.79	1/2	3/4	.29	0	1/4	Nl
9	3/4	1/2	.67	1/4	0	.17	03
10	0	3/4	.21				?
11	.86	1/2	3/4	.36	0	114	02
12	0	3/4	.13				?

A rigid body analysis of the structure for $Al(NO_3)_3 \cdot 6H_2O$ showed that the structure consists of discrete $Al(OH_2)_6^{3+}$ units, and ionic nitrate groups, as illustrated in Fig. 6-11. The hydrogen atoms of the water molecules are hydrogen-bonded to nitrate oxygen atoms, generating a 3-dimensional array. Full details of this X-ray investigation and its results (e. g. detailed interatomic distances and angles) are presented in the thesis of R. F. Walker (Ph. D., Nottingham, 1976) and are available on request.



O(3)

O(2)

O(1)

N

Al

2.763 Å

2.732 Å

PROJECTION OF THE UNIT CELL OF $Al(NO_3)_3.6H_2O$ FROM (0, 0, 0) TO (1.0, 0.5, 1.0) ALONG THE B AXIS SHOWING ATOMS INVOLVED IN HYDROGEN BONDING SCHEME AROUND Al(0.5, 0.5, 0.5). (N.B. NOT DRAWN TO SCALE)

Figure 6-11.

6.7 References

1. J. W. Mellor, Comprehensive Treatise on Inorg, and Theor. Chem., Vol. 5, Longmans, 1924, p. 360.
2. P. M. Boorman, Ph. D. Thesis, Nottingham, 1964.
3. D. H. Jones, Ph. D. Thesis, Nottingham, 1972.
4. P. Herpin and K. Sundarsanen, Bull. Soc. Franc. Mineral. Crist., 1960, 88, 595.
5. A. Earnshaw, B. N. Figgis and J. Lewis, J. Chem. Soc. (A), 1966, 1956.
6. B. Harrison and N. Logan, J. C. S. (Dalton), 1972, 1587.
7. C. C. Addison and D. J. Chapman, J. Chem. Soc., 1965, 819.

7. REACTIONS OF HF WITH METAL CORROSION PRODUCTS IN HDA AND RELATED STUDIES

7.1 Introduction

The work on the effect of inhibitors on the corrosion of metals by HDA falls under several headings. However, having gained some knowledge of the chemical nature of the dissolved species, it was obviously important to examine how far and in what ways these dissolved species were influenced by addition of the inhibitor, especially since reactions which occur in bulk solution may occur at the surface also. The work described in this section is concerned with the identification of new products formed by reaction of the original corrosion products (from Fe, Cr, Ni, and Al) with HF.

7.2 Reaction of HF with Fe/HDA corrosion products

The reaction was carried out in all-Teflon/FEP apparatus. A solution of iron in HDA was prepared by immersion of a spectroscopically pure iron rod in HDA at room temperature for about six weeks, after which the solution contained about 1.5% iron. About 20 mls. of the solution were pipetted into the reaction vessel, then frozen in liquid nitrogen. An amount of HF (sufficient to convert all Fe present into FeF_3) was distilled onto the solid. As this was allowed to warm, a yellow colouration gradually penetrated as the HF mixed with the HDA. A mobile liquid was first produced, which gelled suddenly after standing for about an hour. The gel was sufficiently rigid as to be unchanged when the reaction tube was inverted. The gel then slowly liquified, giving a mobile phase and a smaller amount of the gel. Attempts to filter off the gel were unsuccessful, due to blocking of the filters by the gel. Liquid film IR spectra of both layers were obtained, and the mobile layer was put onto a vacuum frame to pump overnight. This gave a small amount of green crystalline material, for which the infra-red spectrum (Figure 7-1) and powder photograph (Table 7-1) are shown. The liquid film infra-red spectra were sufficiently similar to Figure 7-1 as to indicate that the same compound was involved. None of the crystals obtained have been of high enough quality to allow single

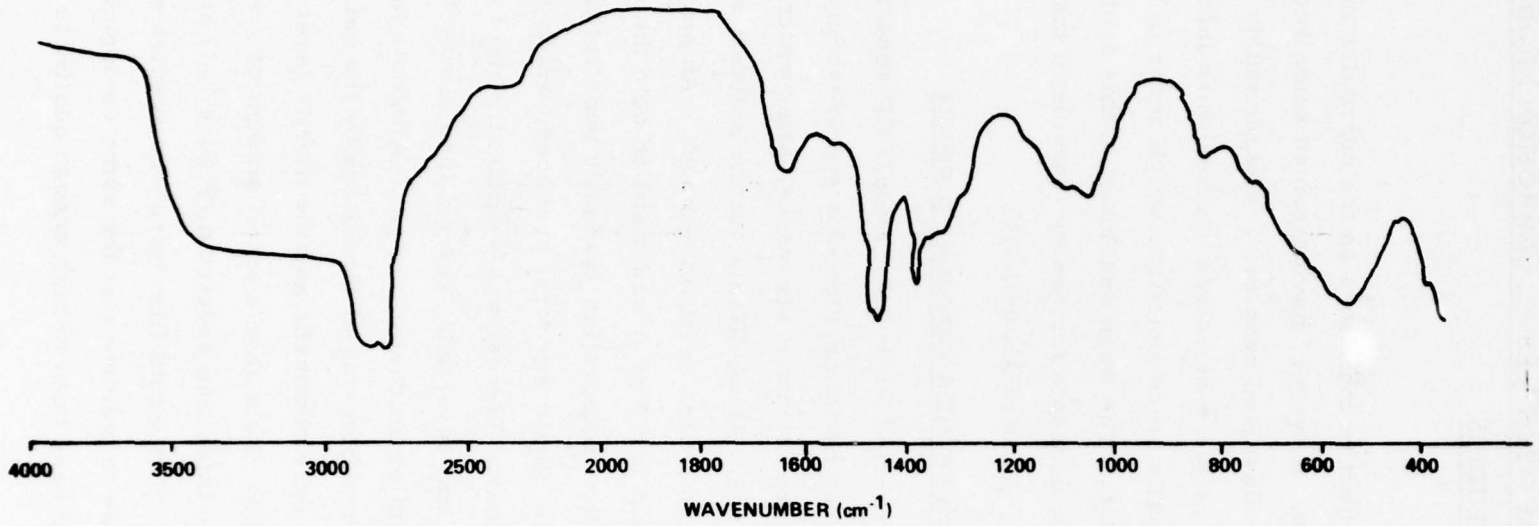


Figure 7-1. IR Spectrum of Product ex Fe/HDA + HF

Table 7-1. Powder Photograph of Product ex Fe/HDA + HF

2θ Values	d-Spacing (Å)	Intensity
17.00	6.54	50
20.00	5.57	40
28.50	3.93	20
29.50	3.80	40
32.50	3.46	20
35.00	3.22	100
40.50	2.80	10
42.50	2.67	2
43.50	2.61	2
46.00	2.48	10
55.00	2.10	10
59.00	1.97	5
60.50	1.92	2
61.50	1.89	30
63.00	1.85	25
67.00	1.75	15
69.00	1.71	2
71.00	1.67	2
73.00	1.63	5
74.00	1.61	5
75.00	1.59	2
82.50	1.47	5
84.00	1.45	5
90.50	1.36	2
94.00	1.32	2
102.50	1.24	2
105.00	1.22	5
112.50	1.16	2

crystal X-ray crystallography. The formation of the gel does not always occur. In several experiments using a similar procedure, addition of HF produced only a mobile liquid, which after pumping gave a green glass-like product. Its infra-red spectrum showed that it was essentially the same compound as was sometimes produced in crystalline form. Small portions of this product were analysed for iron, NO^+ (as nitrite), nitrate, and fluorine.

The compound contained 43.0% Fe, but insignificant amounts of nitrite and nitrate. Fluorine analysis was difficult due to interference by iron; however, assuming the compound to be a fluoride hydrate of iron (III), the iron content lies close to that required for the monohydrate $FeF_3 \cdot H_2O$.

A solution of Fe in HDA was also produced by dissolving anhydrous $FeCl_3$ in HDA. The products of reaction with HF were the same as those described above.

7.3 Reaction of $FeF_3 \cdot 2H_2O$ with HNO_3/N_2O_4 mixtures

The experiments described above suggest that when HF is added to a solution of corrosion products of iron in HDA, the transformation $Fe(NO_3)_3 \cdot 2H_2O \rightarrow FeF_3 \cdot H_2O$ occurs. It was therefore relevant to examine whether the reverse reaction could occur, wholly or in part, if the fluoride was immersed in various N_2O_4 - HNO_3 mixtures. The dihydrate, $FeF_3 \cdot 2H_2O$, was used since it is available in pure form. This compound was treated on a small scale with excess of four different liquids;

i) HNO_3
ii) N_2O_4
iii) HDA
iv) N_2O_4/EtOAc

In all four cases, the compound, which was initially pink, changed to green, and was shown to be amorphous. In view of the colour change, the dihydrate was treated with HDA on a larger scale. About 5g. of the starting material was

ground up to a fine powder, transferred to a 50cm.^{3} round bottomed flask fitted with a magnetic stirrer, and about 30cm.^{3} of HDA was added. Again a colour change, this time from pink to brown, occurred almost immediately. The mixture was stirred for two days, during which time a thick suspension was formed. This was converted to a precipitate by the addition of about 10mls. of dry CH_2Cl_2, which is miscible with HDA in all proportions. The product was separated on a filter stick; its infra-red spectrum is shown in Fig. 7-2, and it was also shown to be amorphous. Chemical analysis of the product showed that it contained 39.9% Fe. The evidence suggests that the original compound is not changed in nature by immersion in HDA, and that it is still an iron (III) fluoride hydrate (compare Figures 7-2 and 7-3). Possibly the H_2O content is reduced somewhat below $FeF_3 \cdot 2H_2O$ towards the $FeF_3 \cdot H_2O$ produced when the corrosion product reacts with HF (Section 7.2 above). $FeF_3 \cdot 2H_2O$ requires 37.3%Fe, whereas $FeF_3 \cdot H_2O$ requires 42.7%Fe.

7.4 The Reaction of HF with Chromium/HDA corrosion products

In view of the slowness of the reaction between chromium and HDA, it was decided to investigate the reaction of HF with a chromium-containing HDA mixture by preparing the chromium solution from hexacarbonylchromium (O) and HDA.

10 ml. of a one weight percent solution of chromium in HDA was prepared by dissolving about 0.6 g. of $Cr(CO)_6$ in 10cm.^{3} of HDA containing 45 weight percent N_2O_4. This reaction is described in Section 5.5(b).

This solution was contained in a Kel-F tube (3/4" diam) fitted with suitable Kel-F valves and adaptors to allow connection to a Kel-F vacuum frame. The solution was frozen in liquid nitrogen; 0.27g. of HF were then distilled onto the frozen mixture, from a weighed Kel-F container. The chromium present in the mixture would require about 0.2g. HF for complete conversion to CrF_3, this weight of HF also bringing the solution composition up to the approximately one weight percent of propellant HDA.

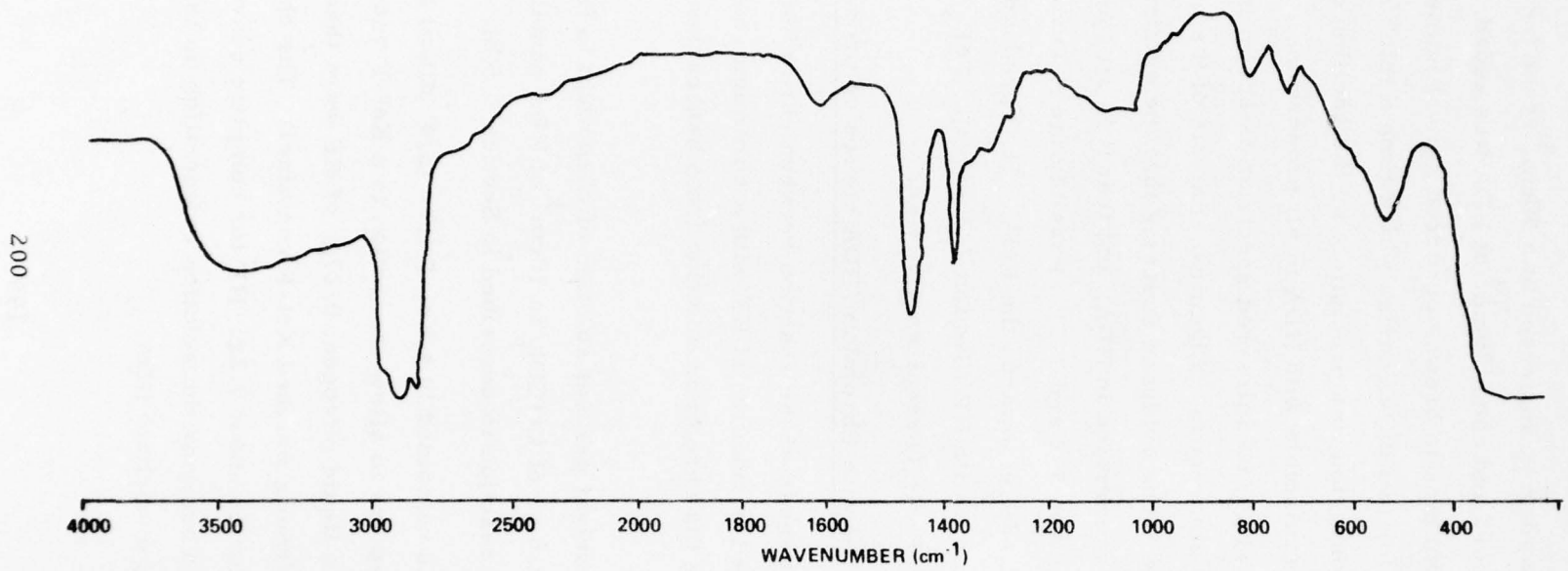


Figure 7-2. IR Spectrum of Product ex $FeF_3 \cdot 2H_2O$ + HDA

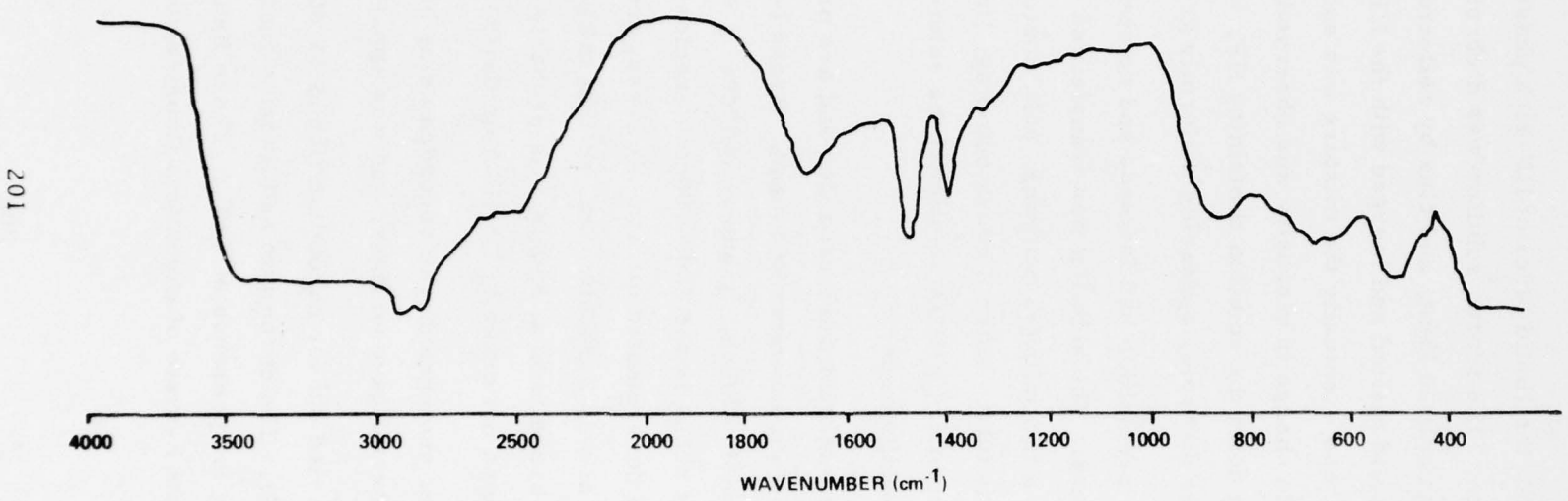


Figure 7-3. IR Spectrum of $FeF_3 \cdot 2H_2O$

On addition of HF, the liquid layer of HF-rich phase on top of the frozen solution became green. The frozen solution was dichroic before HF addition, being deep red by transmitted light, and blue by reflected light. As the upper levels of the frozen solid melted and merged with the HF rich layer, these colours disappeared, and eventually the mixture was entirely converted to a green solution. Little change in viscosity was observed, and no precipitate was formed. On freezing down the solution containing HF, it was observed that the mixture was no longer dichroic, appearing uniformly green.

After 7 days, no precipitate had formed, and no visible change had occurred in the mixture. The solution was transferred to a Schlenk tube and pumped down. After a few minutes pumping, solid matter began to be deposited around the walls of the tube. After 2 hours pumping, (in contrast to the period of days required by normal Cr/HDA solutions) the solution had evaporated to a dark green free flowing powder.

IR spectra of the material were recorded and are presented in Fig. 7-4, Table 7.2. The spectrum shows no NO^+ band. Broad bands due to co-ordinated water are visible at 3750-2500cm^{-1}, and at 1650cm^{-1}, suggestive of hydrogen bonding. Weak bands occur in the 1200-700cm^{-1} region of the spectrum, which could be attributed to co-ordinated nitrate. However, total nitrogen analysis showed the presence of only 2-3% nitrogen, so that the assignment of these bands is dubious. A broad band at 550cm^{-1} is probably a chromium-fluorine stretch. This band does not occur in Cr/HDA or $Cr(CO)_6$/HDA product spectra.

The X-ray powder photograph was recorded using both CuK_α and FeK_α radiation, but the material gave no lines, and was apparently amorphous.

Analysis was carried out for chromium (found 33.80%), fluorine (38.22%), and total nitrogen (3%). The chromium and fluorine figures give a F:Cr ratio of 3.09:1, confirming the presence of CrF_3. These figures do not coincide exactly with any simple hydrate of chromium fluoride, but lie closest to

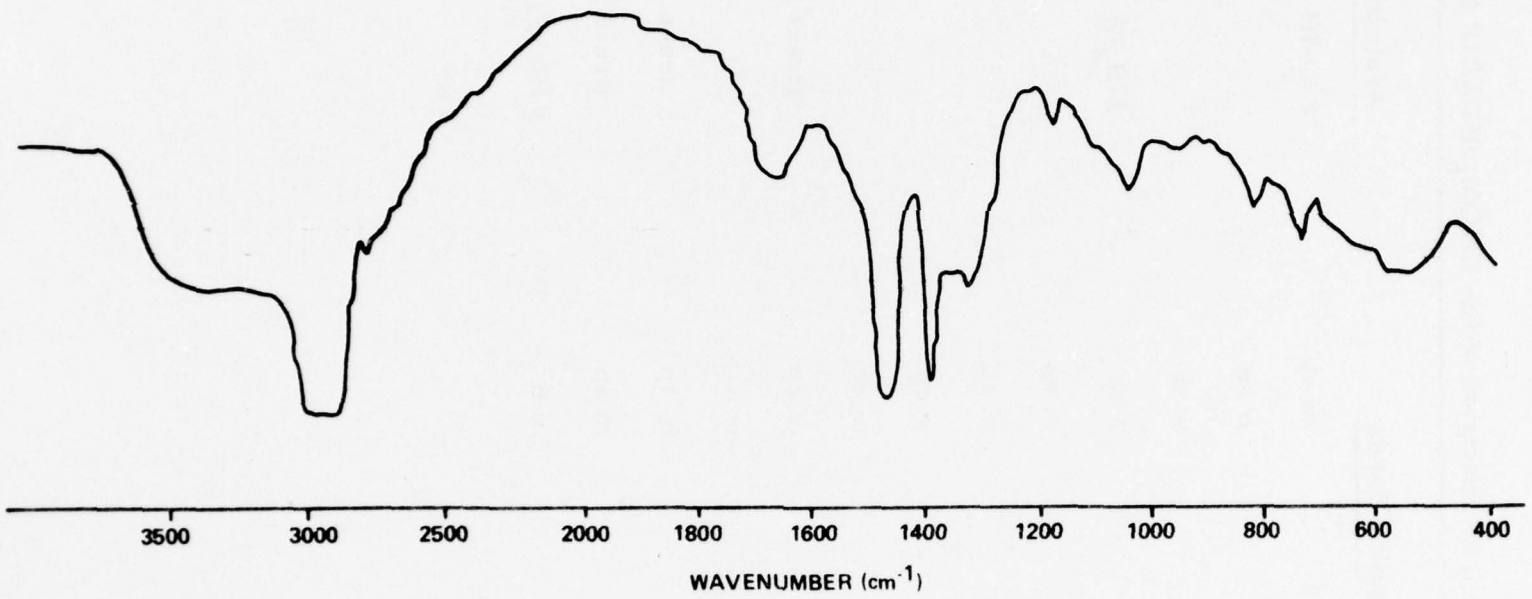


Figure 7-4. IR Spectrum of $Cr(CO)_6$/HDA/HF Product

Table 7-2. The I. R. Spectrum of the $Cr(CO)_6$/HDA/HF Product (cm^{-1})

Absorption Bands		Assignment
3700-2500	vs vb	ν (O-H)
2780	w sp	
2350	w sh	
1650	s sp	$\delta(H_2O)$
1310	m sp	
1265	m sh	
1155	w sp	
1100	m sh	
1025	m sp	•(trace NO_3^-)?
950	w b	
810	m sp	(trace NO_3^-)?
725	m sp	(trace NO_3^-)?
550	m b	ν (Cr-F)

$CrF_3 \cdot 2.5H_2O$. The chromium and fluorine analytical figures for some chromium (III) fluoride hydrates are given below.

	%Cr	%F
CrF_3	47.7	52.2
$CrF_3 \cdot 2H_2O$	35.9	39.3
$CrF_3 \cdot 3H_2O$	31.9	35.0
$CrF_3 \cdot 2.5H_2O$	33.75	37.0

The precise nature of this compound is still to be determined. It may contain lattice water, but the rapidity with which it separated from solution would seem to suggest a definite compound. It probably contains $Cr(H_2O)_6^{3+}$ and CrF_6^{3-} units by analogy with other chromium fluoride species.

A variety of chromium-fluorine species are known. CrF_3 is unattacked by HNO_3, and $CrF_3 \cdot 3H_2O$ is insoluble in water, and hence probably insoluble in HDA. $CrF_3 \cdot 3.5H_2O$ is known in two modifications, one dark green and the other pale green. The pale green compound is isomorphous with the tetrahydrate, $[CrF_3(H_2O)_3] \cdot H_2O$. Various species of unusual stoichiometry are known e.g. $Cr_3F_8 \cdot 11H_2O$, i.e. $CrF_2 \cdot Cr_2F_6 \cdot 11H_2O$. Chromium chemistry is characterised by a marked tendency to form polynuclear species.

An attempt to investigate the product by diffuse reflectance U.V./visible spectroscopy, in the hope of seeing absorption bands corresponding to two Cr^{III} environments, gave inconclusive results.

As no precipitate of solid matter is formed, no gelation, and no obvious change in viscosity, it is considered unlikely that this compound "$CrF_3 \cdot 2.5H_2O$" plays a major role in flow decay phenomena in inhibited HDA.

7.5 The Reaction of HF with Nickel/HDA corrosion products

A saturated solution of $Ni(NO_3)_2 \cdot 2H_2O$ was prepared by shaking an excess of $Ni(NO_3)_2 \cdot 2H_2O$ with HDA containing 45% N_2O_4 and centrifuging to remove suspended matter. This solution contained about 1.5wt % Ni. (Section 5.4(C)).

$10cm.^3$ of this solution was pipetted into a 3/4" diam. Kel-F tube against a counter current of Argon. The nickel present in this solution would require approximately 0.06 g. HF for complete conversion to NiF_2. It was decided to add approximately 0.2g. in order to bring the HF concentration up to 1-2%, corresponding to propellant HDA. The solution was frozen down in liquid N_2 as before to give a green solid, and 0.216g. of HF were distilled in from a weighed receiver. The liquid formed a yellow layer on top of the green glass. (N.B. NiF_2 is yellow). On melting, the mixture became homogeneous. No precipitate, gum, or increase in viscosity was observed, and no change was seen to occur over a period of three days.

A sample of the gas above the mixture was removed for examination by IR spectroscopy, to detect the presence of any NOF, NO_2F, etc., formed, but there was little evidence of either of these species in the IR spectrum. It is noteworthy that there was a vapour pressure of HF above the solution, the HF fundamental being visible in the vapour phase at $3880cm^{-1}$. (Fig. 7-5).

The green solution was decanted off into a Schlenk tube and pumped to dryness. A pale blue-green solid was formed, identical in appearance with the initial $Ni(NO_3)_2 \cdot 2H_2O$. The infrared spectrum and powder photograph were also identical with $Ni(NO_3)_2 \cdot 2H_2O$. The small quantity of solid left was analysed for nickel and found to contain 23.3% Ni ($Ni(NO_3)_2 \cdot 2H_2O$ requires 26.8%). Agreement is not ideal, but it is acceptable in view of the small amount of sample used (0.0378 g.) in the analysis. This figure is more in accordance with the evidence of IR and X-ray powder photography that no reaction has occurred, and it is certainly too low for any simple nickel fluoride hydrate.

It is therefore concluded that no reaction occurs between nickel-containing species in HDA, and added HF. This is in sharp contrast to the behaviour of iron and chromium. It seems likely that flow decay does not involve the separation of nickel fluoride species, though added HF may influence corrosion at the metal surface. The presence of HF in HDA would have little effect on the nickel solubilities described in Section 5.4.

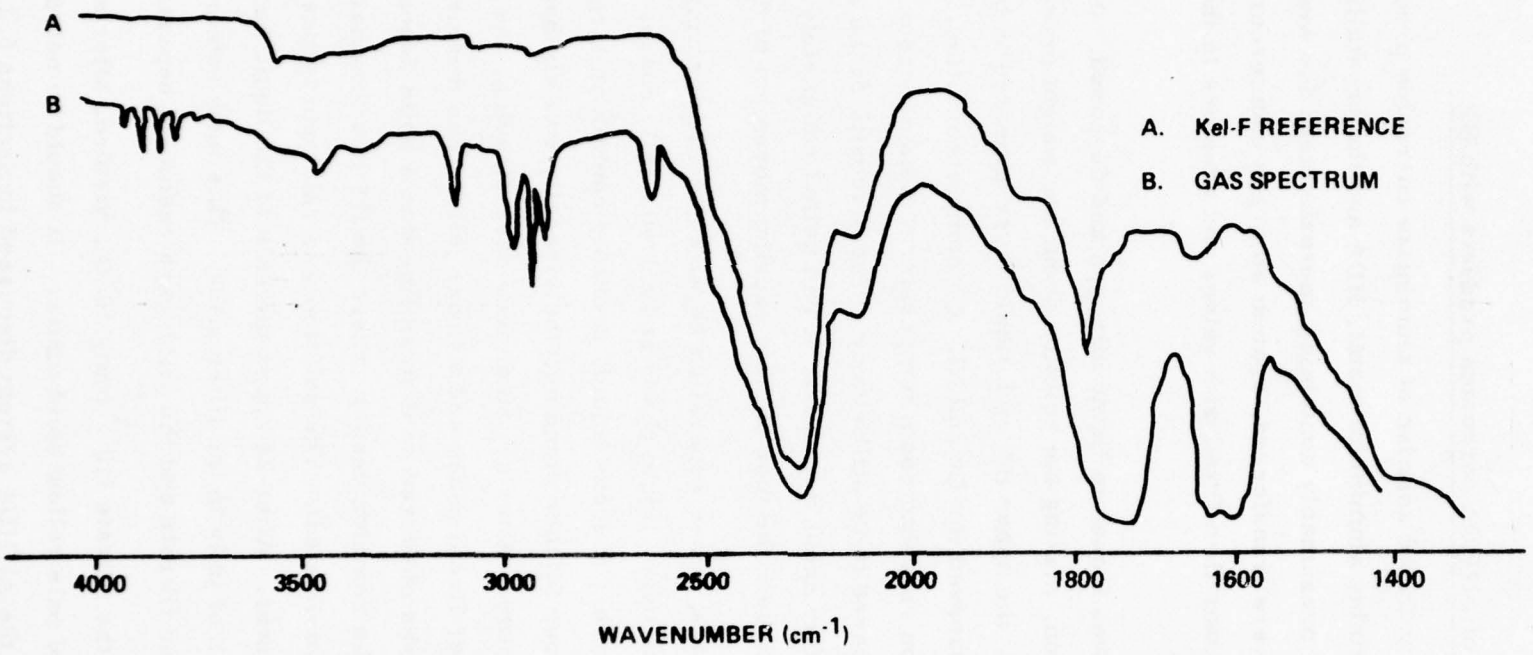


Figure 7-5. IR Spectrum of Vapour Above $Ni(NO_3)_2 \cdot {}^2H_2O$/HDA/HF Mixture

7.6 The reaction of Al/HDA corrosion products with HF

20 $cm.^3$ of a saturated solution of aluminium corrosion products, pipetted from a flask containing aluminium metal, HDA and the crystalline precipitate (Section 6.1), and presumably containing approximately one weight percent of $Al(NO_3)_3 \cdot 6H_2O$, were transferred, against an argon countercurrent, to a Kel-F tube. This was then fitted with valves and adaptors in the manner described above.

The solution was frozen in liquid nitrogen and degassed. 0.25 g. of HF were added by distillation, making the solution about one weight percent in HF. On addition of the HF, the upper HF rich liquid layer appeared to be more viscous than previously observed for Cr and Ni. On complete melting, the solution appeared cloudy; on reaching room temperature, a homogenous liquid was formed which appeared to be still cloudy. The viscosity of the mixture steadily increased until, after about 5 minutes, it had gelled completely. At this stage, it was possible to invert the tube without causing movement of the gel.

After 10 minutes, phase separation began to occur, forming approximately equal volumes of an upper liquid phase and a lower jelly phase. Shaking formed a homogeneous but very viscous liquid, probably containing large pieces of jelly. After one hour further standing, the viscosity was almost back to the normal liquid mobility. After a further four days standing, the system had settled into an upper liquid phase and a lower jelly. The mixture was filtered at this stage. (It was observed on dismantling that a solid deposit had formed around the top of the reaction vessel, where the HF had originally entered. This deposit was not investigated). The solution was reluctant to pass through a porosity 3 glass sinter. After 24 hours the bulk of the liquid had passed through, leaving a large bulk of jelly in the filter stick. This jelly retained the orange colour of HDA. The filtrate and the jelly were examined separately.

Evacuation of the filtrate (10^{-3} mm, 20°C), yielded, after about four hours, a minute quantity of pale yellow solid matter. It should be noted that no "froth" was formed, as in the Al/HDA system discussed in Sections 6.1 and 6.4.

There was insufficient product for analysis. The X-ray powder photograph showed that the material was amorphous. The IR spectrum is given in Figure 7-6 and Table 7-3. The spectrum shows the presence of co-ordinated water. Peaks at 1320cm^{-1}, 1265cm^{-1}, 1020cm^{-1}, 810cm^{-1}, and 725cm^{-1} could conceivably indicate the presence of co-ordinated nitrate, but this assignment is by no means certain. The peaks at 1150cm^{-1}, 1100cm^{-1}, and 1020cm^{-1} occur in the products described below, which contain no more than trace quantities of nitrate.

The jelly remaining in the filter stick was found to be quite firm and resistant to stirring. On immersion of a small sample in water, it dissolved slowly. The remaining jelly was split into two halves and treated in two ways. One half was pumped down directly on a vacuum frame (10^{-3}mm, 20°C). It rapidly pumped down to a small bulk of white, free flowing solid. No froth was observed, and from the appearance of the bulk of the solid, it was clear that the majority of the aluminium was present in the jelly rather than in the filtrate. The X-ray film showed no lines, indicating that the material was amorphous.

The IR spectrum is shown in Fig. 7-7, and tabulated in Table 7-4. The spectrum shows the presence of co-ordinated water, and the same grouping of peaks at 1150, 1100, and 1025cm^{-1} present in the pumped down filtrate. A broad, poorly resolved band at the low end of the spectrum shows features at 800cm^{-1}, 725cm^{-1}, and 650cm^{-1}.

The material was analysed for aluminium. Fluorine interfered with the analysis, and was removed by evaporating the solid to dryness with aqua regia (3:1vv HCl/HNO_3). The material was analysed for fluorine using the specific electrode, as described in Appendix B.4(e). The results of the analyses were as follows: Aℓ, 22.1; F, 32.8; N, 3.3. ($Al(OH)F_2 \cdot 2H_2O$ requires Aℓ, 22.9, F 32.2%). Although this basic species may have formed by hydrolysis of aluminium (III) fluoride during evacuation, it is consistent with the tendency of aluminium to form basic species.

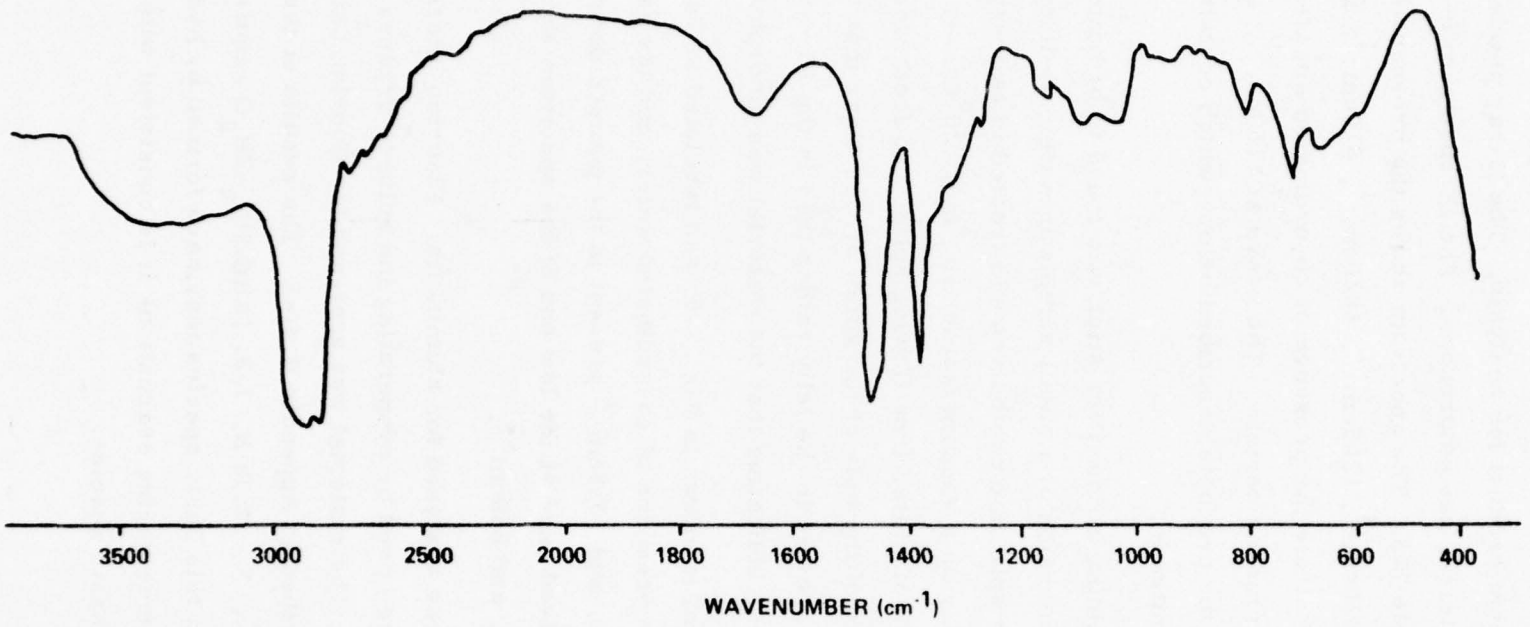


Figure 7-6. IR Spectrum of Evacuated Al/HDA/HF Filtrate

Table 7-3. I.R. Spectrum of Al/HDA/HF Solution Product (cm^{-1})

Absorption Bands		Assignment
3700-2520	vs vb	ν(O-H)
1670	s sp	$\delta(H_2O)$
1320	m sh	(NO_3^- ?)
1265	m sh	(NO_3^- ?)
1150	m sp	
1100	m sp	
1050	m sp	
950	w b	
810	m sp	(NO_3^- ?)
725	m sp	(NO_3^- ?)
670	m b	ν(Al-F)

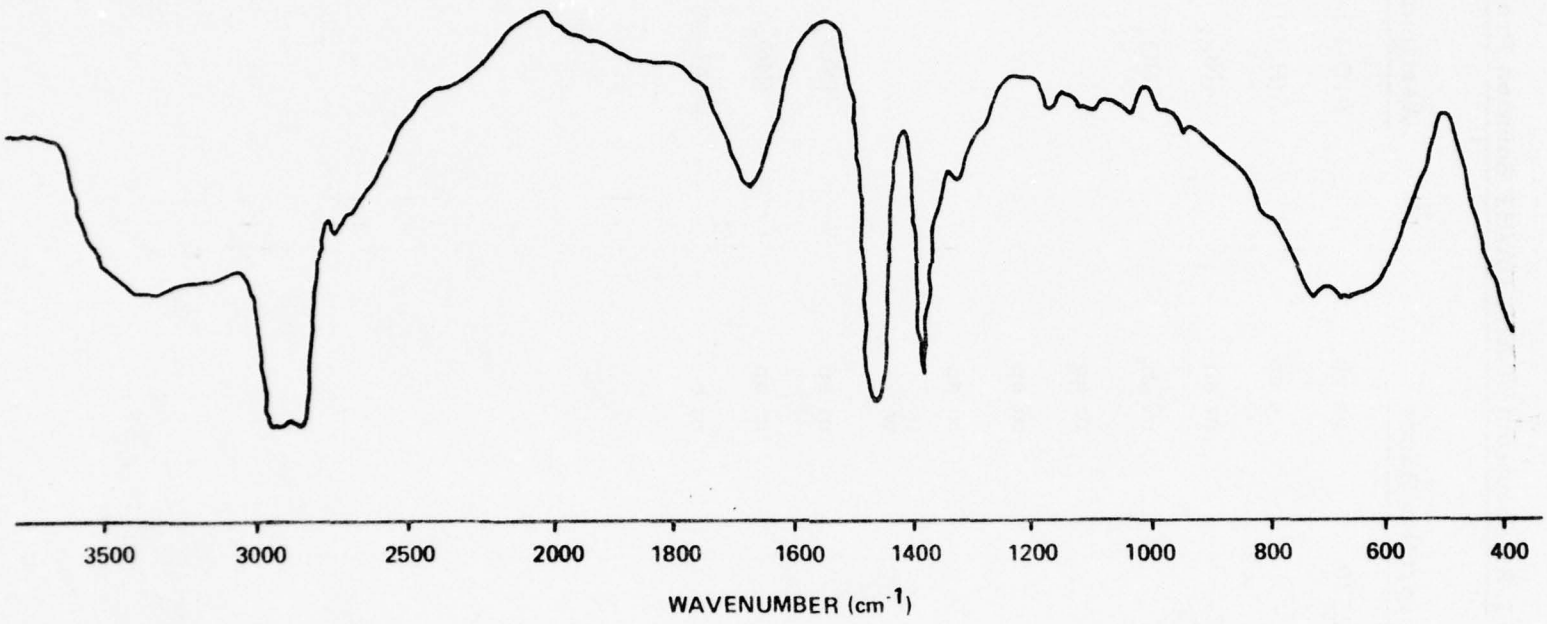


Figure 7-7. IR Spectrum of Evacuated Al/HDA/HF Gel

Table 7-4. I.R. Spectrum of Al/HDA/HF Gel cm^{-1}

Absorption Bands		Assignment
3710-2800	vs vb	ν(O-H)
2720	w sp	
1670	s sp	$\delta(H_2O)$
1310	m sp	(NO_3^- ?)
1265	m sh	(NO_3^- ?)
1150	m sp	
1100	m sp	
1025	m sp	
935	w sh	
800	w sh	(NO_3^- ?)
725	w sp	(NO_3^- ?)
650	s b	ν(Al-F)

The second half of the jelly was left to stand in dry dichloromethane in the hope of leaching out HDA and precipitating any solid matter. After standing overnight, no change had occurred in the jelly, so excess $CH_2C\ell_2$ was decanted off and the gel pumped to dryness. After a short while, a dry, free flowing white powder was formed. The material was found to be amorphous. The IR spectrum was identical with that of the pumped-down jelly. Aluminium analysis was carried out, with the same precaution of removing fluorine. The material contained 21.7% Al, and on the basis of this, it is assumed that dichloromethane had no effect on the jelly. It is perhaps relevant to record that both solids hydrolysed violently with water and were completely soluble in water.

In a second experiment, 0.51 g. of HF were distilled into 25cm^3 of Al/HDA solution, giving a solution containing about 1.3wt % HF. In this case no gelling was observed. The material was allowed to stand for seven days at 0°C, during which time no change in the material was observed. The solution was then filtered through a porosity 3 sintered glass filter, through which it passed rapidly. A minute amount of jelly was observed to collect on the filter. Both solution and jelly were evacuated to dryness on a vacuum frame (10^{-3} mm, 20°C). The liquid was rapidly pumped down to give a small bulk of white, free-flowing powder, which was shown by X-ray powder photography to be amorphous. The jelly was pumped down to a very small bulk of the same white powder, so that it appears that, in this experiment, the majority of the aluminium was present in the solution rather than in the jelly.

The infrared spectrum of the pumped-down solution (Figure 7-8, Table 7-5) was found to be similar to that of the product already described. It contained the group of three peaks at 1150, 1100, and 1025 cm^{-1}, and the broad, poorly resolved band around 800-600cm^{-1}. Aluminium analysis showed that the solid contained 21.72% Al, in good agreement with the previously obtained values for Al/HDA/HF products. A Kjeldahl analysis for total nitrogen indicated the presence of ca. 2% nitrogen, and this is regarded as an impurity. On the basis of these results, the identity of the material is considered to be the same as the products previously described.

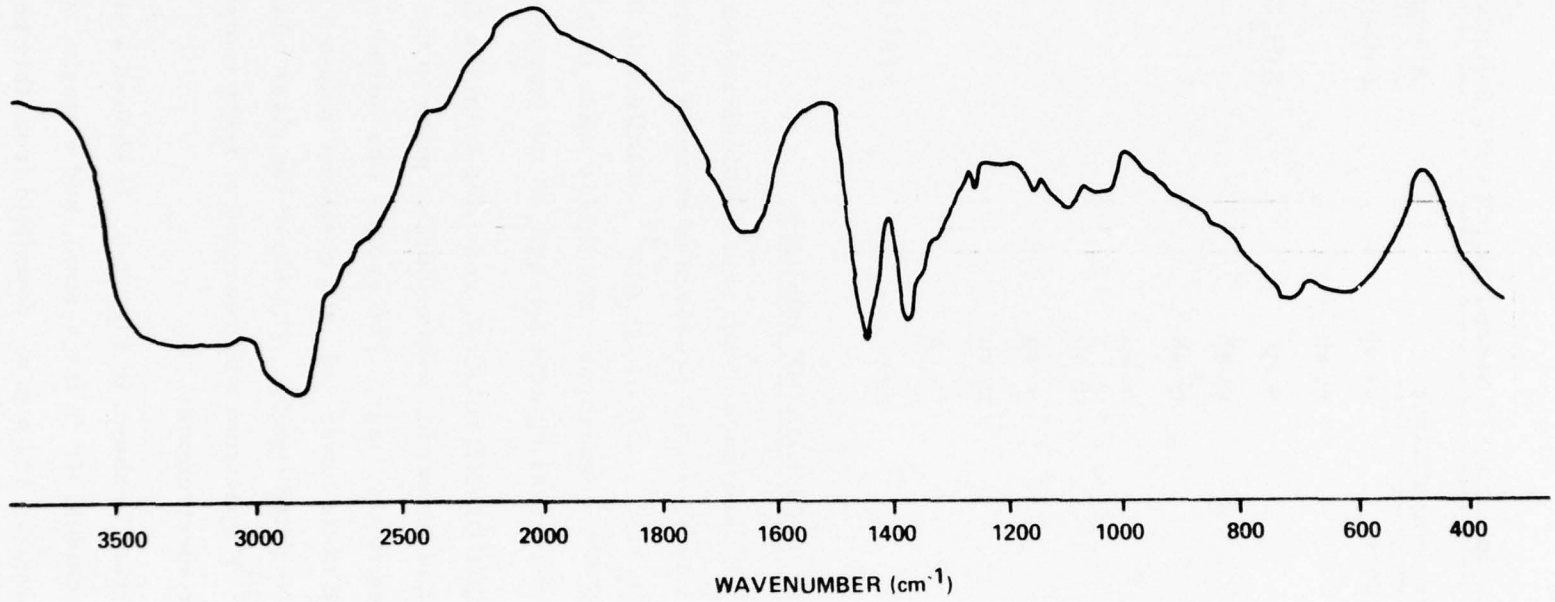


Figure 7-8. IR Spectrum of Evacuated Al/HDA/HF Solution II

Table 7-5. I.R. Spectrum of Second Al/HDA/HF Solution Products (cm^{-1})

Absorption Bands		Assignment
3700-2550	vs vb	ν (O-H)
2330	m sh	
1650	s sp	$\delta(H_2O)$
1310	m sh	
1265	m sh	
1150	m sp	
1100	m sp	
1020	m sp	
800	m sp	
720	m sp	
600	s b	ν (Al-F)

^{19}F n.m.r. studies on Al/HDA/HF solutions

Work on the ^{19}F resonance of aqueous solutions containing $Al(NO_3)_3 \cdot 9H_2O$ and $AlF_3 \cdot 9H_2O$[1], has shown the presence of complex species such as AlF_4^- (aq.), $(H_2O)_3AlF_3$, $(H_2O)_4AlF_2^+$, and $(H_2O)_5AlF^{2+}$, manifesting themselves in the form of a series of ^{19}F resonances. Mention is made in this work of the broadening effect of increasing acid strength on the complexed fluorine resonances.

A sample of Al/HDA/HF solution, resulting from the 2nd experiment in which no gelation had occurred, was withdrawn prior to the filtration, using a Kel-F tube attached to a syringe. The sample was introduced into a narrow Kel-F tube, sealed at its lower end, and contained within a normal 4mm glass nmr tube in which it fitted tightly. The top of the glass tube was closed with a plastic cap. The ^{19}F spectrum was recorded at room temperature using a Varian HA100 nmr spectrometer.

The ^{19}F spectrum is shown in Fig. 7-9. It showed a single sharp resonance corresponding to residual HF in the system, and a single, very broad line centred at approximately 330 p.p.m. downfield from this peak. The absolute

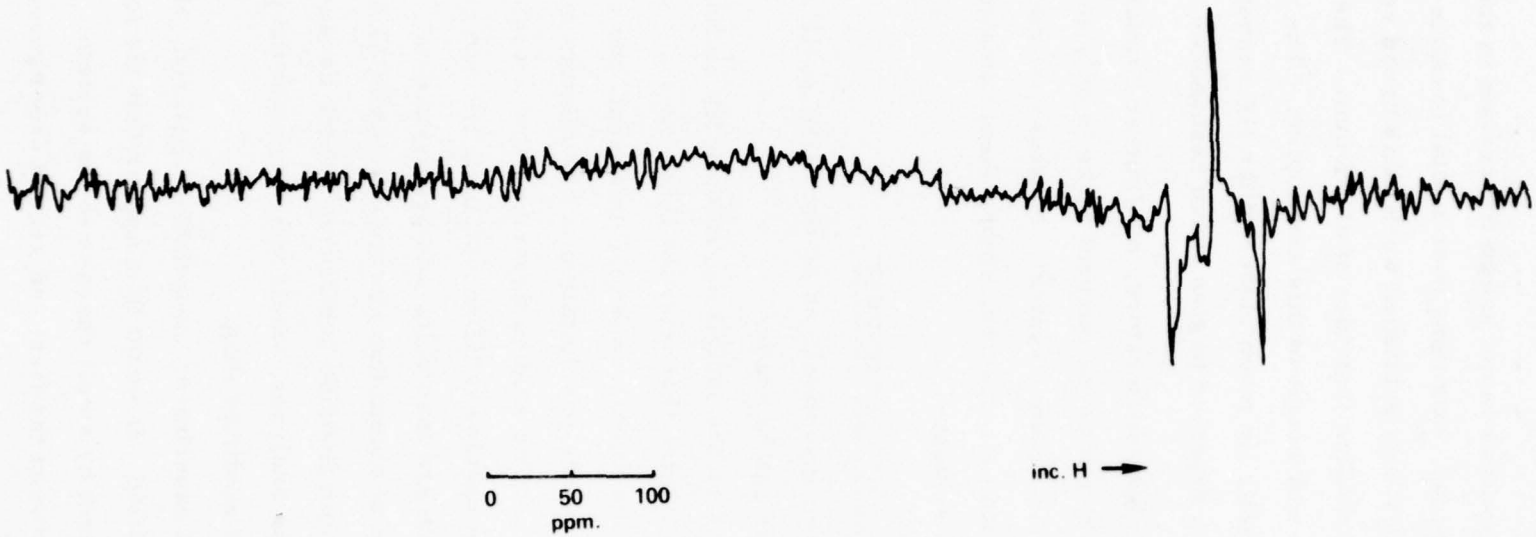


Figure 7-9. ^{19}F nmr Spectrum of Al/HDA/HF Solution

position of the HF resonance is not known for certain in this medium. The resonance was very broad, extending over a total baseline width of approximately 250 p.p.m. By analogy with published work, this broad resonance is consistent with the presence of complex fluorides of aluminium. The broadness of the resonance would also add weight to this assumption. The resonances of NOF/HF solvates, and NOF itself, lie much closer to the HF resonance (in liquid HF at least)[4] and would be expected to give sharp resonances.

It is possible that low temperature, or Fourier Transform n.m.r. would resolve the broad peak, but at the moment there is only sufficient data to draw rough analogies with the aqueous system. However, it would appear from this that other fluorine containing species, among them complex aluminium fluorides, may be present in the system.

Commentary on the aluminium reactions

From the results of investigations on the Al/HDA/HF system, two important observations can be made:

(a) Previous work on the inhibiting effect of HF on fuming nitric acid corrosion of aluminium[2], states that whereas large crystals of a hydrated aluminium nitrate are formed in the mixture when HF is absent, the effect of addition of HF to the system causes the precipitation of "aluminium nitrate hydrate" in the form of small crystals. The studies described above would seem to indicate that aluminium nitrate species in HDA containing HF are rapidly converted to fluoride species, which are insoluble, and precipitate out. There is no evidence at all for the presence of aluminium nitrate species in Al/HDA/HF, and indeed the tenacity of aluminium fluoride complexes, which cause so much hindrance in conventional fluorine analyses, would weigh against the presence of such species in standard or modified HDA.

(b) In the second experiment, no gelation occurred, although the formation of Al/F species was verified. It would thus appear that the formation of gels is affected to a great extent by small changes in the system. The difference in HF concentrations between the first and second experiments is small, and it is

unlikely that the rate of addition was much different. The possibility has been suggested that the HF used in the second experiment was slightly wet, and that this is the relevant factor, though it is difficult to see how the minute amount of water transferred would cause such a drastic change in the system, since it has been shown[3], that the effect of metal cations in "anhydrous" HNO_3 is to force the equilibrium:

$$2HNO_3 \rightleftharpoons H_2O + NO_2^+ + NO_3^-$$

to the right, by removal of water to form $M(H_2O)_n^{m+}$ species. The crystallisation of stable $Al(NO_3)_3 \cdot 6H_2O$ from Al/HDA supports this argument.

The principal difference between the two experiments would seem to be the degree of (presumably) hydrogen bonding between the precipitate nuclei of the gel cage structure. The nature and physical quantity of the precipitates formed in either case would appear to be the same, and it is only possible to explain the observations by considering the interactions between these particles. It is likely that HF bridges are formed between the AlF_3 nuclei and $Al(H_2O)_6^{3+}$ units, probably involving complex species such as AlF_4^- etc. A possible mode of bonding might be:

$$\text{Al-F. . . .H-F. . . . .H-}\overset{\overset{\text{H}}{|}}{\text{O}}\text{-Al}$$

Other bonding modes are of course possible. If this were the case, then the rate of gelation and stability of the gel may be dependent on the concentration of HF in a manner analogous to the pH dependence of the kinetics of formation, etc., of gelatine-water systems.

7.7 References

(1) N. A. Matwiyoff and W. E. Wageman, Inorg. Chem., 1970, 9, 1031.

(2) D. M. Mason, and J. B. Rittenhouse, Corrosion, 1958, 14, 345.

(3) B. J. Hathaway and A. E. Underhill, J. Chem. Soc. 1963, 4586.

(4) F. Seel, 'Angewandte Chemie,' 1965, 4, 635.

8. SOME CHEMISTRY OF PHOSPHORUS PENTAFLUORIDE IN HNO_3 AND HDA

Summary

1. When PF_5 is added to HNO_3 or its mixtures with N_2O_4, it will react with the medium, and some experiments have been carried out to determine the nature of the species formed. These are the species which will combine with metal ions during corrosion, and will then dissolve as soluble salts or will precipitate.

Published results indicate that when PF_5 reacts with pure HNO_3, the following species are produced:

$$NO_2PF_6,\ HF,\ POF_3,\ \text{and}\ H_3PO_4$$

and this has been confirmed using ^{19}F n.m.r. spectra. Additionally hydrolysis of POF_3 may introduce the fluorophosphoric acids $H(PO_2F_2)$ and $H_2(PO_3F)$. With N_2O_4, PF_5 reacts to give:

$$NOPF_6,\ NO_2POF_4,\ NO_2F,\ \text{and}\ POF_3.$$

When added to HDA, PF_5 appears to produce species which are more characteristic of N_2O_4 than HNO_3. No HF is formed, and $NOPF_6$ and HPO_2F_2 predominate.

2. In the case of 321 steel, phosphoric acid has some corrosion inhibiting properties when added to HDA. Since H_3PO_4 is also a possible (though minor) product of the PF_5-HDA reaction, the precipitates formed when H_3PO_4 is added to solutions of the relevant metals in HDA have been studied. These solutions were formed either by reaction of HDA with the metals, or by dissolving the metal nitrates in HDA. The following products were identified:

$$FePO_4 \cdot 3H_3PO_4$$

$$Ni_3(PO_4)_2 \cdot 2\text{-}4\ H_3PO_4 \cdot 16H_2O$$

$$CrPO_4 \cdot 4H_2O$$

$$AlPO_4 \cdot H_3PO_4 \cdot O\text{-}9\ H_2O$$

All products are phosphates. In some cases the metal phosphates separate as adducts with H_3PO_4, and there is variable hydration. All the phosphates have low solubility in HDA, and are gelatinous.

3. A series of experiments was designed to examine the influence of PF_5 on dissolved corrosion products. In the absence of inhibitor, corrosion leads to solutions of metal nitrate hydrates in HDA. The equilibrium we are interested in is therefore:

metal nitrate in solution + species formed from PF_5 $\rightleftharpoons$ metal fluoride-phosphates

To obtain sufficient quantities of product for analysis, concentrations of PF_5, somewhat greater than the specification value have been used, and there are pronounced variations in the behaviour of the different metals. A solution of iron nitrate in HDA was treated with PF_5; a precipitate formed, having a composition near $FeF_3 \cdot H_3PO_4$. All such precipitates are complex and are associated with some H_3PO_4 and coordinated water, and may contain the $PO_2F_2^-$ ion. A similar precipitate is obtained when mild steel dissolves in modified HDA, so that in the solution the equilibrium in the case of iron lies well to the right hand side. Aluminium would appear to behave similarly, the precipitate having the approximate composition $AlF_3 \cdot 2AlPO_4$. In the case of chromium, a solution of the nitrate was obtained by adding chromium carbonyl to HDA; subsequent addition of PF_5 gave a gelatinous precipitate which was difficult to separate; the product obtained on evaporation to dryness is less meaningful, but had the approximate composition $CrF_3 \cdot 0.15\ CrPO_4$. Again, it would appear that chromium resembles iron and aluminium in that the above equilibrium lies far to the right hand side.

The behaviour of nickel is in sharp contrast. Nickel metal was allowed to dissolve in modified HDA until precipitation took place, when the pure compound $Ni(NO_3)_2 \cdot 2H_2O$ separated. Since this is the product obtained in uninhibited HDA, the above equilibrium now lies to the left, and the corrosion products in the case of nickel are not influenced by added PF_5. These reservations are clearly relevant to the mechanism of inhibition. When the solution is evaporated to dryness, a fluoride-phosphate mixture is obtained, but these are forcing conditions and are not relevant to the equilibria operating in HDA.

8.1 Preparation and manipulation of phosphorus pentafluoride

(a) Preparation

The availability of an ICI 60 Amp fluorine generator in the Department of Chemistry at the University of Nottingham prompted the preparation of phosphorus pentafluoride by the direct combination of elemental red phosphorus and gaseous fluorine[1,2,3]. Fluorine is prepared in this generator by electrolysis of a mixture of hydrogen fluoride and potassium fluoride, of approximate composition $KF \cdot 2HF$, at 80°C. The maximum rate of preparation of gaseous fluorine was $40g.hr^{-1}$ at 60A, and the rate of evolution was readily controllable by adjusting the electrolytic current. The fluorine prepared in this way was purified by passage first through a Kel-F trap cooled to -85°C in a stream of cold gaseous nitrogen, to condense out any HF vapour, followed by a Kel-F 'U' tube containing pellets of dried NaF to remove final traces of HF as $NaF \cdot 2HF$. The purified gas was then conveyed through a fluoroplastic vacuum system to the reaction vessel.

Red phosphorus was purified by boiling with water to remove P_4O_{10} (which would have resulted in formation of POF_3), followed by washing with acetone to remove organic impurities (which would have formed fluorocarbons), and finally by drying in a vacuum (10^{-3}mm, 65°C) for 48 hr.

An accurately known weight (ca. 10g) of purified red phosphorus was transferred, using a small funnel fitted with an extension tube, onto the ledge (a)

of the reaction vessel, Fig. 8-1, care being taken to avoid spillage into the central well (b). This reaction vessel consisted of a cylindrical silver soldered nickel canister of about 500cm^3 capacity, fitted with an adaptor (c) enabling connection via a monel metal valve with Teflon compression seats, to the Kel-F vacuum system. This vessel had previously been conditioned by filling with fluorine, and heating to 200°C, to remove any contaminants likely to form volatile species. The vessel containing red phosphorus was connected to the vacuum system via c, and evacuated to 10^{-5}mm. The central well (b) was cooled to -196°C in liquid nitrogen, and fluorine was carefully admitted to the system. A vigorous and strongly exothermic reaction ensued, the temperature of the vessel around the ledge (a) rising to about 60°C. The rate of addition of fluorine was controlled so as to maintain a steady reaction, with a pressure of about 5-10mm in the vacuum system, as monitored by a pressure gauge, PF_5 condensing as a solid in the central well.

The addition of fluorine was discontinued when the pressure in the vessel rose to above about 50mm, indicating that no more fluorine was reacting. This point was found to coincide closely with the addition of the theoretical amount of fluorine, 30.65g, required by the stoichiometry

$$2P + 5F_2 \longrightarrow 2PF_5$$

as calculated from the amount of electricity passed. The solid in the well was then evacuated to 10^{-5}mm, while cooled in a liquid nitrogen/2-chloropropane slush bath (-117°C), thus removing any residual fluorine (b.p., -188°C) and leaving PF_5 (m.p.t, ca. -92.5°C[4,5]), plus a trace of POF_3 impurity (m.p., -68°C[6]) as solids. Finally, the PF_5 was transferred from the reaction vessel, with the central well cooled to -78°C in a methcol/CO_2 bath to retain POF_3 as a solid, into a steel cylinder, cooled to -196°C and fitted with a valve and vacuum line connection, in which it was stored under several atmospheres pressure.

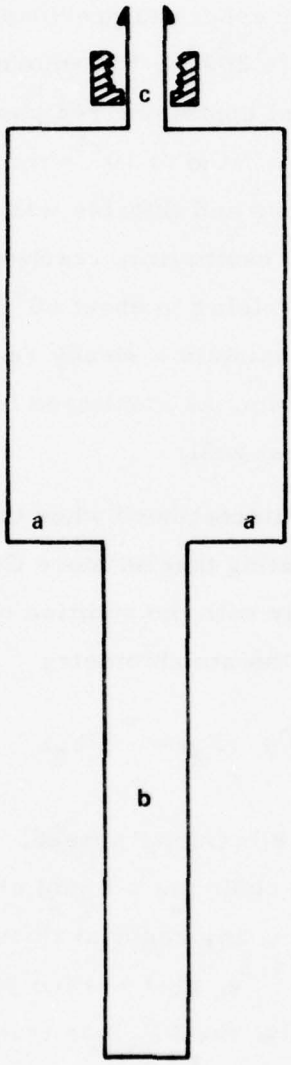


Figure 8-1. Reaction Vessel for Phosphorus Pentafluoride Preparation. 1/2 Scale

(b) Manipulation

Phosphorus pentafluoride was transferred through the Kel-F vacuum line previously described for the manipulation of hydrogen fluoride (Appendix B. 1.). Reactions were carried out in the 0. 75 inch diameter Kel-F tubes fitted with needle valve adaptors, also previously described. Amounts of PF_5 of known weight could be added to other reactants after determining the volume of a permanent section of the vacuum line. By measuring the pressure of PF_5 in this system, a simple pressure/weight relationship could be established. The purity of the PF_5 was checked by gas phase infrared spectroscopy[7], and no more than small amounts of POF_3 were found to be present. As an added precaution however, the PF_5 cylinder was cooled to -78°C before usage, to ensure that any POF_3 was, as far as possible, retained. Samples handled in this way contained about 4% non-condensibles at -196°C.

8. 2 The reaction of phosphorus pentafluoride with 100% HNO_3 and HDA

Some preliminary investigations of these reactions were carried out to establish the nature of the solution products, as a prelude to the examination of the metal nitrate hydrate/HNO_3/N_2O_4/PF_5 systems.

The products of reaction of PF_5 and HNO_3, had already been characterised[8, 9, 10]. The reaction

$$4HNO_3 + 5PF_5 \longrightarrow 4NO_2PF_6 + HF + H_3PO_4 \qquad (I)$$

occurs under pressure and the reaction

$$HNO_3 + 2PF_5 \longrightarrow NO_2PF_6 + POF_3 + HF, \qquad (II)$$

occurring at ordinary pressures, requires a trace of HF for its initiation.

Similarly, the reactions between PF_5 and N_2O_4 have been examined[11], and although by no means fully characterised, suggest that $NOPF_6$ is formed as a solid product, with POF_3 as a gaseous by-product. The likelihood of more

complex species being present in the product is suggested, and the reactions below are proposed:

$$2NO_2 + 2PF_5 \longrightarrow NOPF_6 + NO_2POF_4$$

$$NO_2POF_4 \longrightarrow NO_2F + POF_3$$

Both NO_2PF_6 and $NOPF_6$ have been characterised by their X-ray powder patterns[11].

(a) The reaction of PF_5 with 100% HNO_3

A small sample of 100% HNO_3 was cooled to liquid nitrogen temperature under vacuum in a 15mm. internal diameter Kel-F tube, connected to the PF_5 vacuum frame through a Kel-F valve. Five weight percent PF_5 was then admitted, and the mixture was allowed to attain room temperature. A white crystalline solid formed on the liquid surface, sinking to the bottom of the tube on agitation. An infrared spectrum of the gas above the liquid at this stage was recorded (Fig. 8-2, Table 8-1) and showed the presence of HF and POF_3 as well as HNO_3 and a little PF_5. The white crystals could be partly dissolved by gentle warming of the tube, and more crystals were precipitated by cooling the tube in ice. A larger scale reaction was carried out using 16g. of 100% HNO_3 and 25wt. % PF_5 and the white crystals were filtered off using a sinter, and dried under vacuum. The product was then handled under strictly anhydrous conditions. It was identified by powder photography as NO_2PF_6 (Table 8-2) and its Raman spectrum confirmed this (Fig. 8-3), showing peaks only at 756cm^{-1} for PF_6^- and 1412cm^{-1} for NO_2^+. Analysis of the product showed: N, 9.1%; P, 15.8%: NO_2PF_6 requires: N, 7.3%; P, 16.2%. It was assumed that the product was still contaminated with a trace of HNO_3. These observations are consistent with reactions (I) and (II) above, however as the ^{19}F nmr work

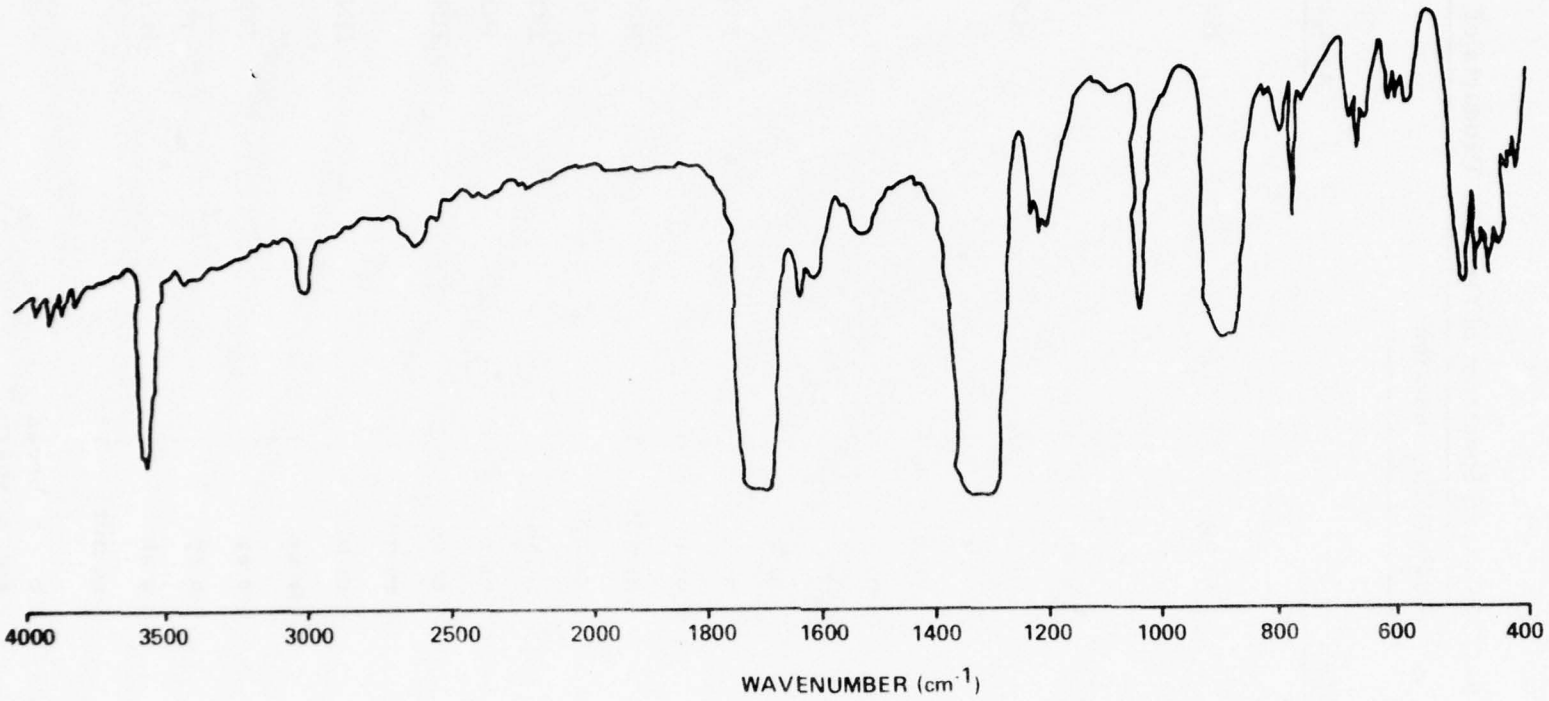


Figure 8-2. IR Spectrum of Gas Products of HNO_3/PF_5 Reaction

Table 8-1. Infrared Spectrum of Gaseous Products of PF_5/ 100% HNO_3 reaction

Absorption band (cm^{-1})		Assignment
3930)		
3890)	m sp	HF
3850)		
3800)		
3550	s sp)	
3000	m)	HNO_3
2600	m b)	
1700	vs b)	
1630	m	
1600	m	
1520	m b	
1420	w	POF_3
1320	vs b)	
1200	m mlt)	HNO_3
1030	vs sp	PF_5
990	m sh	POF_3
880	vs b	POF_3/HNO_3
765	m sp	HNO_3
650	m mlt	
590	m mlt	HNO_3
485	s sp)	
465	s sp)	POF_3
445	s sp)	
430	s sh)	HNO_3
410	m mlt)	

m = medium
s = strong
w = weak
vs = very strong
b = broad
sp = sharp
sh = shoulder
mlt = multiple

Table 8-2. X-ray Powder Diffraction Data for NO_2PF_6

Intensity	d(obs.) (Å)	d(lit.) (Å)	Intensity	d(obs.) (Å)	d(lit.) (Å)
2	6.55		10	1.87	
5	5.21		30	1.80	1.79 w
100	4.72	4.67 s	30	1.77	1.77 w
50	4.31	4.31 w	10	1.72	
100	3.75	3.74 s	50	1.63	1.63 w
80	3.06	3.06 m	5	1.57	
40	2.82		10	1.53	
30	2.73	2.72 w	20	1.52	
30	2.59	2.58 w	20	1.50	
10	2.53		5	1.46	
10	2.38	2.38 w	10	1.44	
90	2.31	2.30 m	10	1.41	
10	2.21		10	1.39	
80	2.16	2.15 m	10	1.37	
80	1.96	1.96 m	5	1.35	
			10	1.31	

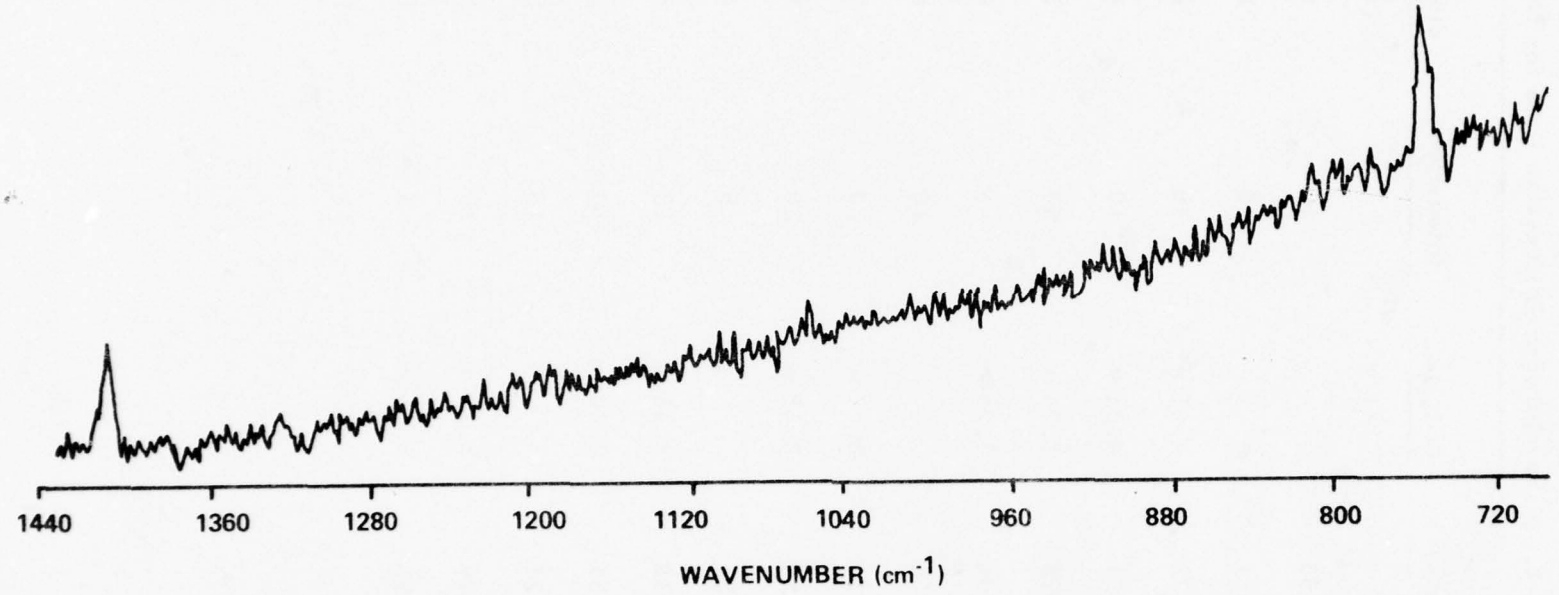


Figure 8-3. Raman Spectrum of NO_2PF_6

described below indicates, it also seems conceivable that POF_3 in HNO_3 may itself be partially hydrolysed forming fluorophosphoric acids i.e.

$$POF_3 + H_2O \underset{-HF}{\overset{+H_2O}{\rightleftharpoons}} H(OPOF_2) \underset{HF}{\overset{H_2O}{\rightleftharpoons}} H_2(OPO_2F) \underset{HF}{\overset{H_2O}{\rightleftharpoons}} H_3(PO_4)$$

this will be discussed later.

(b) The reaction of PF_5 with HDA

The reaction of PF_5 with HDA was carried out in a 150 x 3mm Kel-F nmr tube flared at its upper end and attached by a brass compression fitting nut to a Kel-F valve assembly. To 1.05g of HDA contained in this tube a small amount of PF_5 was added. An immediate deposition of a white crust around the upper part of the tube and around the liquid surface occurred. This crust subsequently broke off and precipitated through the liquid. The solubility of the material was found to be extremely susceptible to N_2O_4 concentration: removal of a little N_2O_4 by evacuation caused immediate precipitation of fine crystals, and addition of a little more N_2O_4 caused dissolution. The solubility was also found to be affected by small temperature changes.

The gas phase infrared spectrum of the vapour above the mixture at this early stage (Fig. 8-4, Table 8-3) showed the presence of POF_3, and a complete absence of PF_5 or HF. After 18 hours, the absorption bands due to POF_3 had diminished significantly in intensity. No HF was detectable by infrared spectroscopy even at this stage.

The solid precipitate was isolated by heat sealing the n.m.r. tube above the liquid surface, centrifuging to compress the solid as a pellet into one end of the tube, flicking the liquid to the other end, and finally cutting the tube in half in a dry box. The solid in the end of the tube was then dried under vacuum ($20^{o}C$, 10^{-3}mm). The resulting small bulk of dry white solid was examined by Raman spectroscopy and X-ray powder photography. The Raman spectrum showed only two peaks, a strong peak at $736cm^{-1}$, and a weak peak at $2348cm^{-1}$.

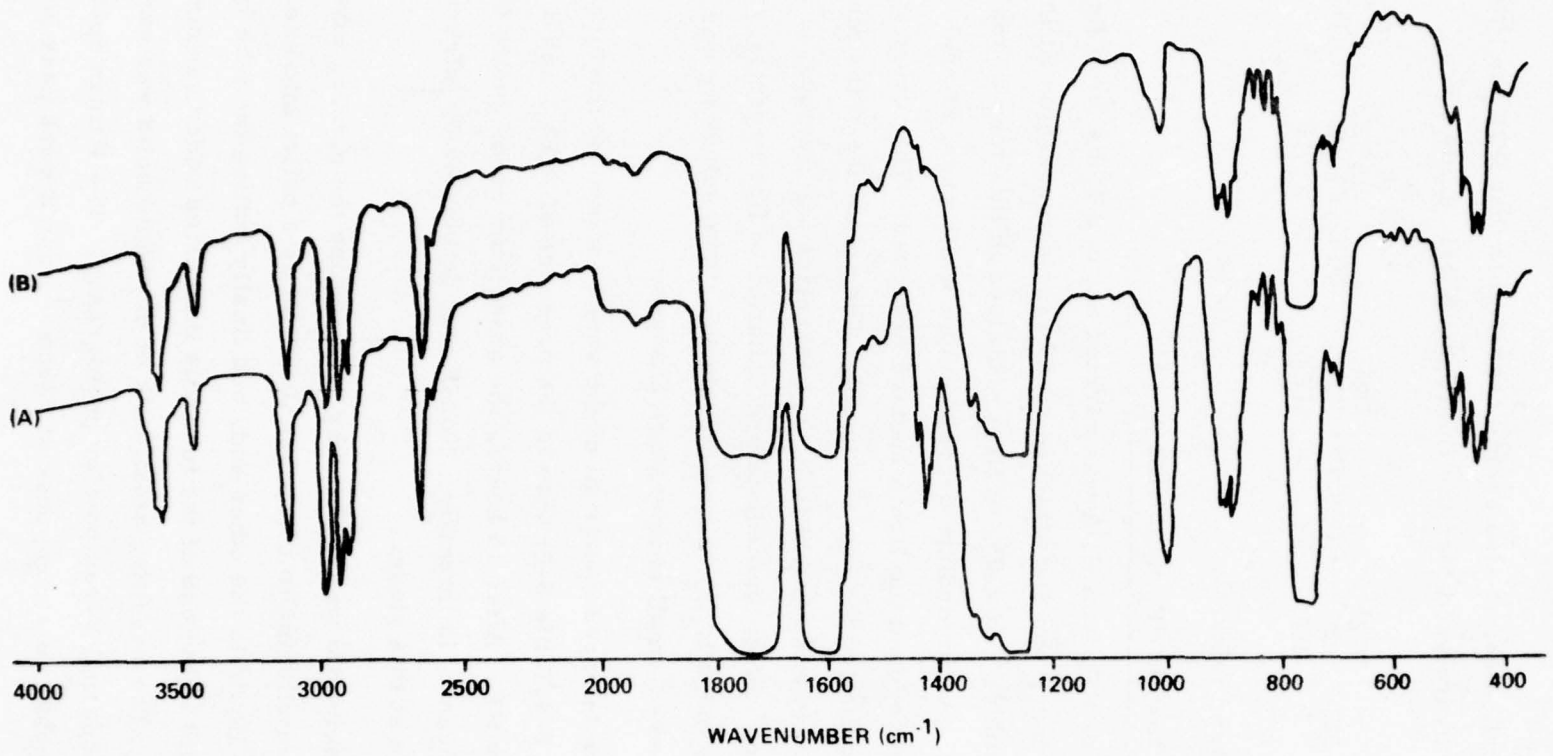


Figure 8-4. IR Spectrum of Atmosphere Over HDA/PF_5 Reaction (A)Immediate. (B)After 18 hr.

Table 8-3. Infrared Spectrum of Vapour Above PF_5/HDA Reaction Mixture

(only bands not resulting from HNO_3 or N_2O_4 shown)

Absorption Bands (cm^{-1})

Immediately		After 18 hr.		POF_3	
1415	s sp	1415	w sp	1415	ms
995	s sp	995	m sp	990	vs
876	s sh	875	m sh	873	ms
492	s vsp				
482	s vsp	482	w sp	485	ms

These absorbances are attributed to PF_6^- and NO^+ respectively[12,13]. The infrared spectrum was not recorded due to the strong likelihood that the material would react with the Nujol mulling agent. The X-ray powder photograph of the solid was found to be identical to that of $NOPF_6$[11] (Table 8-4).

Evacuation of the reaction mixture to dryness (20^oC, 10^{-3}mm) yielded a small bulk of white solid. The X-ray powder photograph of this solid (Table 8-4) contained lines attributable to both $NOPF_6$ and NO_2PF_6[11], though NO_2^+ peaks were not clearly observed in the Raman spectrum, implying that the solid contained only small quantities of NO_2PF_6.

From these observations, it seems likely that the initial product of the reaction of PF_5 with HDA is $NOPF_6$, which precipitates out of solution.

A cursory investigation of the solubility of NO_2PF_6 in 100% HNO_3 indicated that the solubility is very low, and the lack of co-precipitation of $NOPF_6$ and NO_2PF_6 from HDA when PF_5 is added implies that the two are not formed together in the initial reaction.

Evacuation of the solution, yielding a medium becoming steadily richer in HNO_3, probably converts the $NOPF_6$ to NO_2PF_6 via the cation exchange:

$$NOPF_6 + NO_2^+ \longrightarrow NO_2PF_6 + NO^+$$

This suggestion is consistent with the nature of species present in HNO_3/N_2O_4 mixtures, the large concentration of NO_3^- produced by ionisation of the N_2O_4 suppressing the formation of NO_2^+, and the correspondingly large concentration of NO^+ from N_2O_4 ionisation promoting the formation of $NOPF_6$. As N_2O_4 evaporates from solution, the HNO_3 self-ionisation will occur to a greater extent, and there will be a greater tendency to form NO_2PF_6.

Although precipitation of $NOPF_6$ was observed, it is not considered likely that at the low concentrations of inhibitor used in practice (0.6wt% PF_5) the solubility limits of $NOPF_6$ or NO_2PF_6 would be exceeded. These compounds are not therefore expected to be responsible for flow decay phenomena.

Table 8-4. X-ray Powder Patterns of PF_5/HDA Precipitate, Evaporate, $NOPF_6$ and NO_2PF_6

PF_5/HDA ppt		PF_5/HDA evap.		$NOPF_6$		NO_2PF_6	
d(nm)	I	d(nm)	I	d(nm)	I	d(nm)	I
0.462	100	0.462	100	0.455	s	0.467	s
		0.433	50			0.431	w
0.398	100	0.395	90	0.395	s	0.395	s
		0.375	80			0.374	s
		0.304	50			0.306	m
0.280	85	0.279	70	0.279	m	0.280	w
		0.269	5			0.272	w
		0.259	2			0.257	w
0.239	60	0.238	40	0.238	w		
0.228	55	0.229	50	0.227	w	0.229	m
		0.222	5				
		0.215	30			0.215	m
0.192	5	0.194	40			0.196	m
0.181	10	0.181	5			0.179	w
0.176	20	0.176	20	0.176	w	0.177	w
		0.164	5			0.163	w
0.161	30	0.161	30	0.161	w		

(c) ^{19}F n.m.r. studies of solution products

(i) PF_5/100% HNO_3 reaction

A sample of 100% HNO_3 in a small (3mm internal diameter) Kel-F n.m.r. tube was cooled to -196°C and 5wt.% PF_5 was added using the vacuum frame. On allowing the contents of the tube to liquify, some NO_2PF_6 was formed, which sank to the bottom of the tube, and the ^{19}F n.m.r. spectrum of the bulk liquid was recorded (Fig. 8-5) using $CFCl_3$ as an external reference standard. The spectrum shows three fluorine-containing species present in solution:

a) singlet δ_{CFCl_3} = 192.3ppm

b) doublet δ_{CFCl_3} = 82.8ppm J_{F-P} = 1023.5Hz

c) doublet δ_{CFCl_3} = 71.6ppm J_{F-P} = 745.5Hz

No integration of peak areas was attempted since solid NO_2PF_6 was present. The singlet at δ_{CFCl_3} = 192.3ppm was assigned to HF, and the doublets were assigned to species where the ^{19}F resonance was being split by coupling to ^{31}P. (For ^{31}P, I = 1/2, therefore each resonance for equivalent fluorines was split into (2nI + 1) peaks, in this case 2.) The species at δ_{CFCl_3} = 71.6ppm (J_{F-P} = 745.5Hz) was identified as PF_6^- from the known values[13] for this species of δ_{CFCl_3} = 72.2ppm (J_{F-P} = 710Hz) and the species at δ_{CFCl_3} = 82.8 ppm (J_{F-P} = 1023.5Hz) was thought to be either POF_3[13] (δ_{CFCl_3} = 95.7ppm) (J_{F-P} = 1060Hz) or HPO_2F_2[13] (δ_{CFCl_3} = 88.9ppm, J_{F-P} = 980 Hz). It seems more likely that it is HPO_2F_2 since the PF_6^- present gives a doublet with coupling constant (J_{F-P})30Hz higher than the literature value, and a 30Hz increase in the literature value of J_{F-P} for HPO_2F_2 brings it closer to the observed J_{F-P} = 1023.5Hz than the same increase in the literature value of J_{F-P} for POF_3. Also, other studies (Section 8-5) strongly suggest that HPO_2F_2 is formed when PF_5 reacts with HNO_3. These observed species would seem to be consistent with reactions (I) and (II).

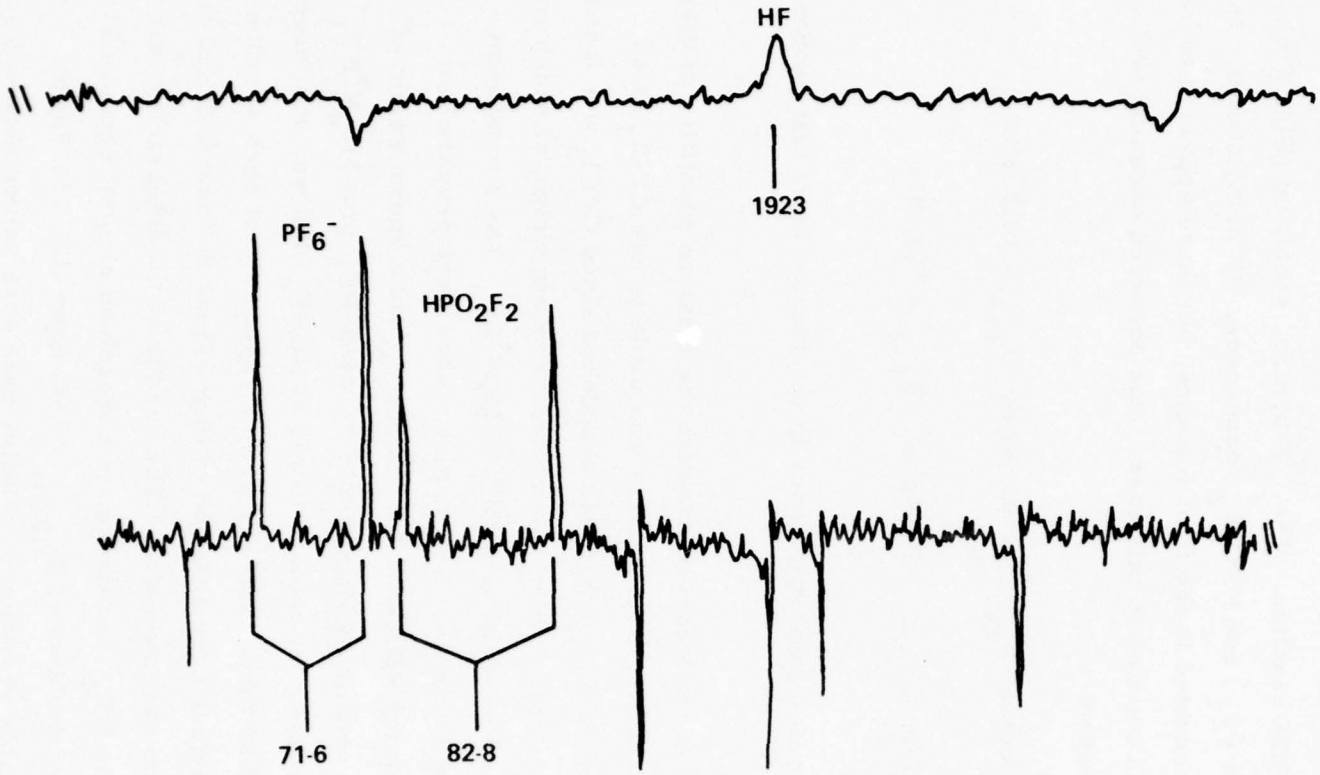


Figure 8-5. ^{19}F n.m.r. Spectrum of HNO_3/5wt% PF_5

(ii) PF_5/HDA reaction

An identical experiment to the one described above with 100% HNO_3 was conducted on the PF_5/HDA reaction. The ^{19}F n.m.r. spectrum (Fig. 8-6), however, only exhibited PF_6^- and HPO_2F_2 resonances, HF being absent. No peak integration was conducted in the first instance, but there appeared to be relatively more PF_6^- in solution in this case. The observed chemical shifts and coupling constants were:

a) HPO_2F_2 doublet δ_{CFCl_3} = 92.2ppm J_{F-P} = 1022.3Hz

b) PF_6^- doublet δ_{CFCl_3} = 78.4ppm J_{F-P} = 738.4Hz

The absence of HF indicates some difference in mechanism from that proposed for HNO_3/PF_5.

Further studies were conducted to evaluate the relative quantities of these two species present in solution. An attempt was made to use $CFCl_3$ as an internal quantitative standard, but this was abandoned since $CFCl_3$ was found to be immiscible with HDA. $Me_4N^+BF_4^-$ was tried, a known weight of which was dissolved in HDA before the addition of PF_5. $Me_4N^+BF_4^-$ has a maximum solubility of about 0.5wt% in HDA. Two n.m.r. tubes were prepared for examination, one containing HDA with 1.85wt.% PF_5 and a known weight of $Me_4N^+BF_4^-$, the other containing HDA with 6.80 wt.% PF_5 plus $Me_4N^+BF_4^-$. The second tube precipitated out some crystals of $NOPF_6$, but was still used for comparison with the other tube. The ^{19}F n.m.r. spectrum of each solution was recorded on three occasions over a period of time (Figs. 8-7 and 8-8) and the peak areas integrated on each occasion. The results of the integrations are given in Table 8-5. The BF_4^- resonance (an unresolved singlet) appears at higher field than the two doublets at δ_{CFCl_3} = 158.4ppm (lit. 150.9ppm). Because of the unavoidable variation of relative peak area values obtained using the Varian HA100 n.m.r. spectrometer, no attempt was made to calculate

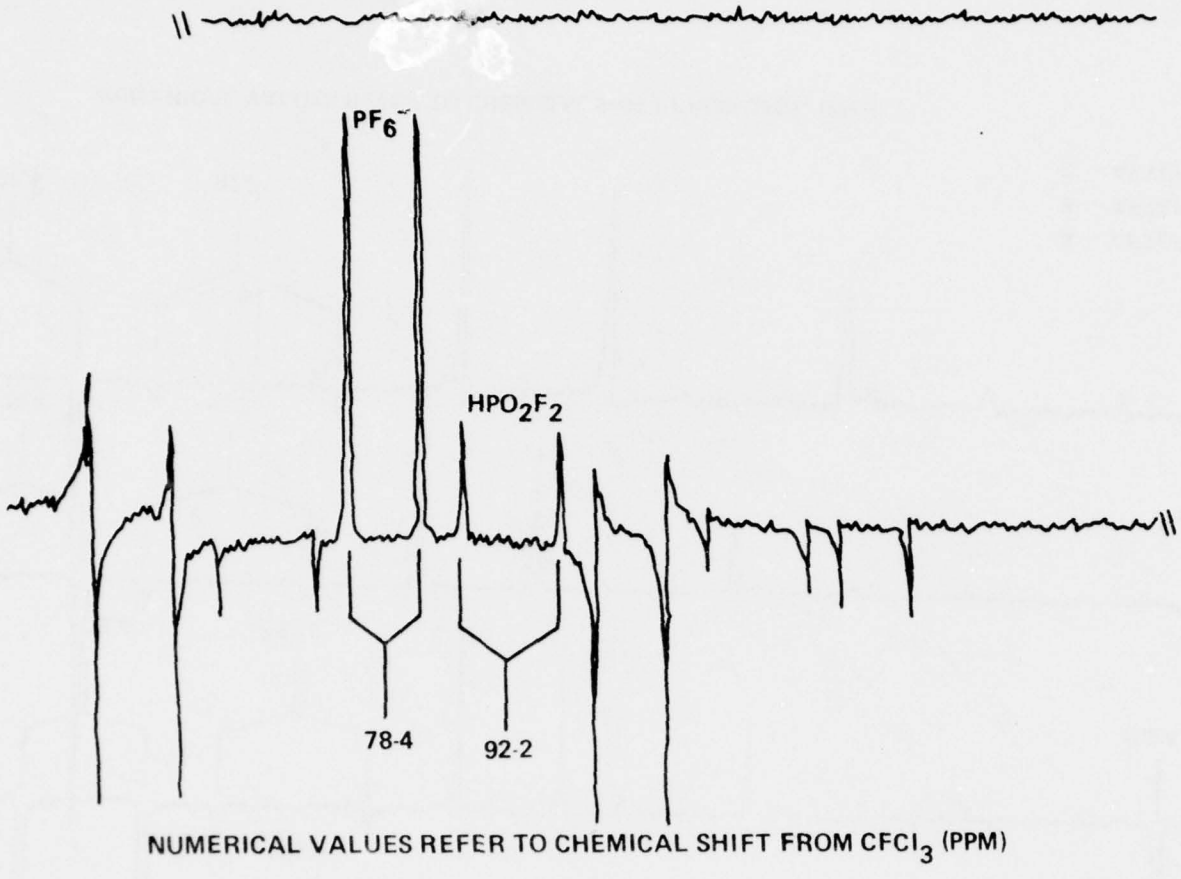


Figure 8-6. ^{19}F n.m.r. Spectrum of HDA/5wt% PF_5

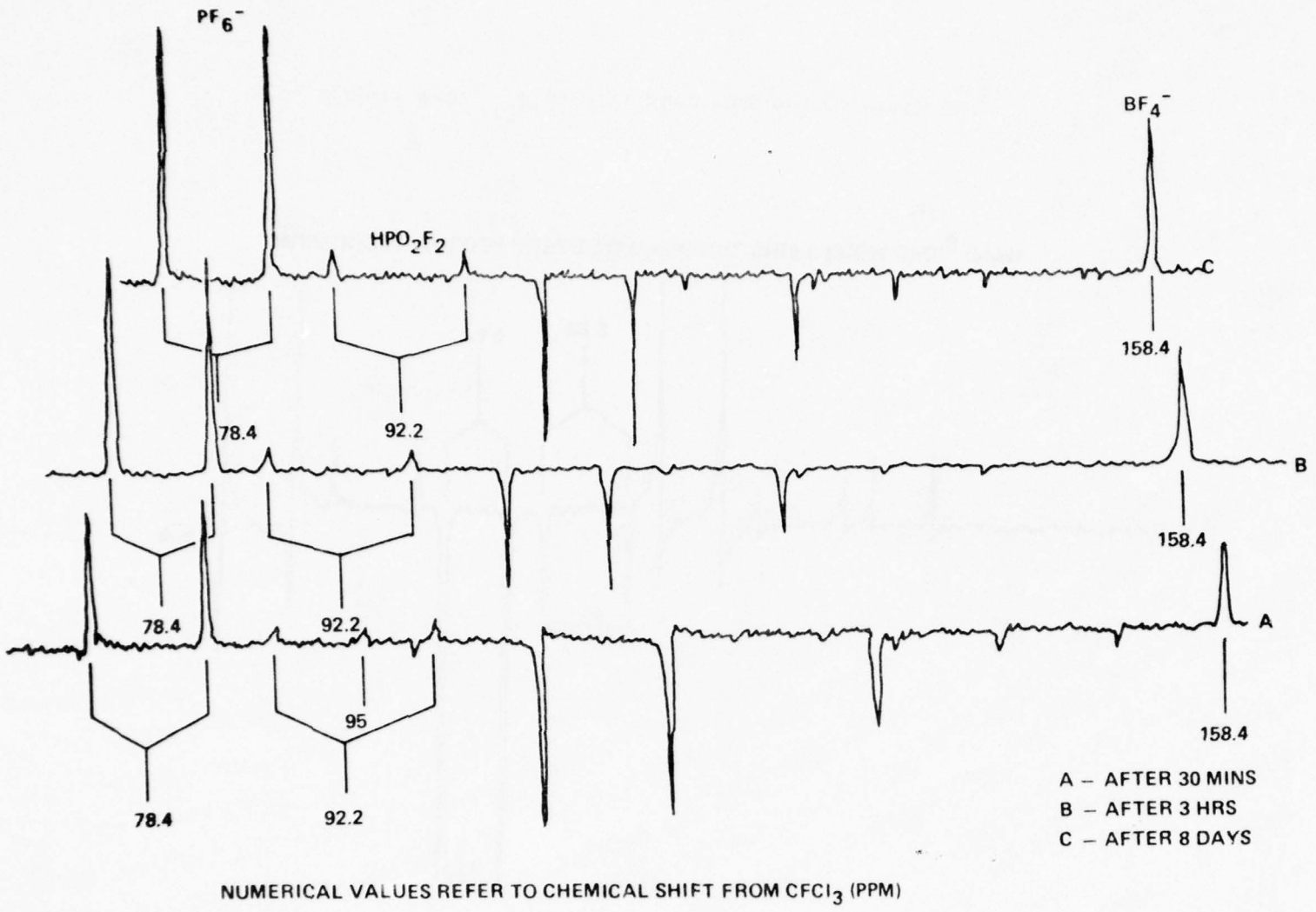


Figure 8-7. ^{19}F n.m.r. Spectra of HDA/1.85wt% PF_5

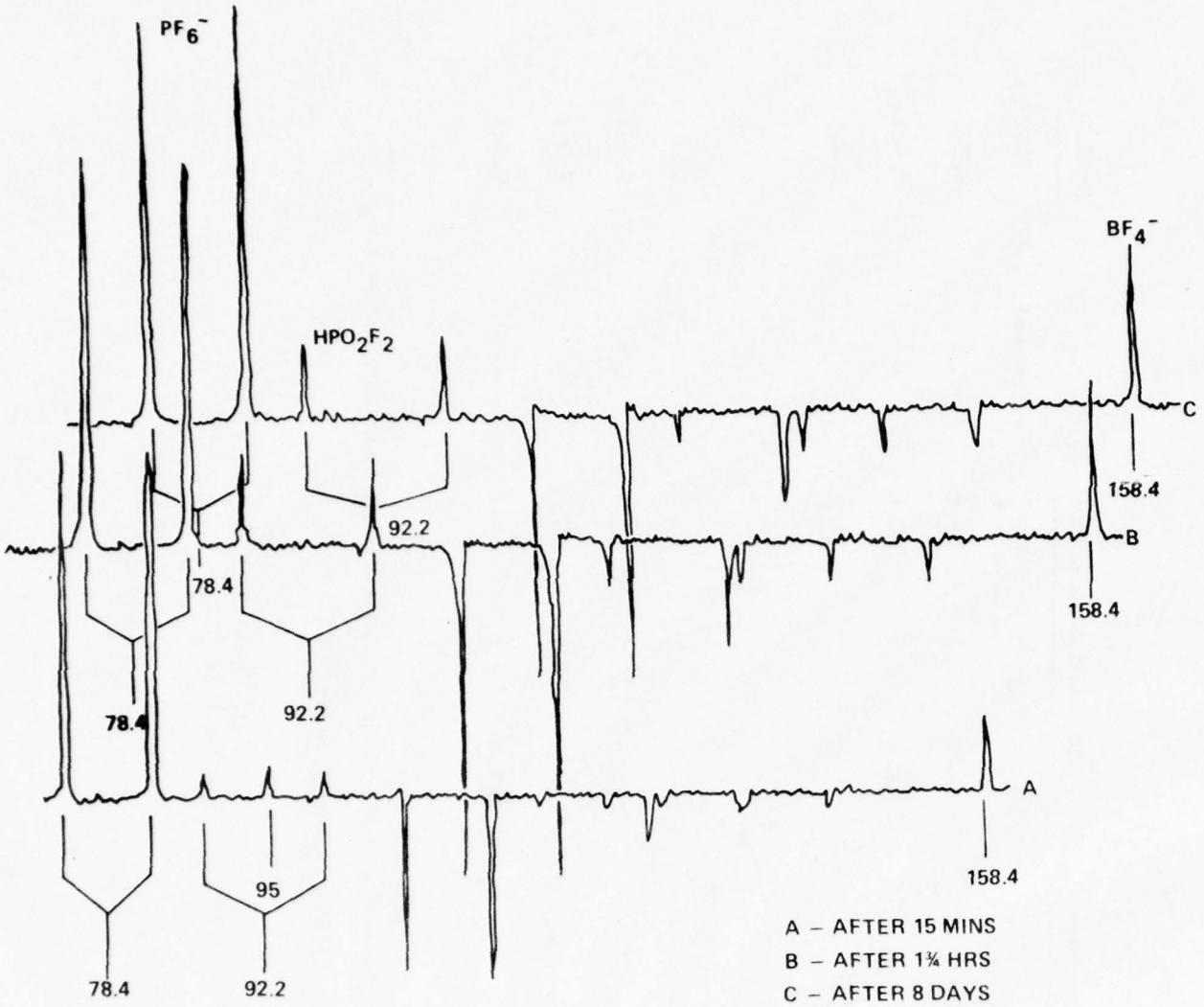


Figure 8-8. ^{19}F n.m.r. Spectra of HDA/6.80wt% PF_5

Table 8-5. Results of the Peak Area Integrations for ^{19}F n.m.r. Experiments with HDA/1.85 wt.% PF_5 and HDA/6.80wt.% PF_5

a) With 1.85 wt.% PF_5

Time after reaction	Relative peak areas				Ratios
	PF_6^-	HPO_2F_2	BF_4^-	extrapeak	PF_6^-:HPO_2F_2
30 mins.	115.5	13.3	38.4	1.6	8.7:1
3 hrs.	84.2	9.5	32.6	-	8.9:1
8 days	70.0	9.7	21.2	-	7.2:1

b) With 6.80 wt.% PF_5

15 mins.	127.3	13.3	13.7	3.5	9.6:1
1 3/4 hrs.	109.7	13.3	15.0	-	8.3:1
8 days	187.8	19.5	25.2	-	9.6:1

In this table, the extra peak mentioned is assumed to be due to the BF_4^-.
The mean PF_6^-:HPO_2F_2 ratio observed is 9:1.

actual quantities of the fluorine species present using the internal $Me_4N^+BF_4^-$ standard, but the mean ratio of peak areas for the two species PF_6^- and HPO_2F_2 was calculated and found to be approximately 9:1. This indicates that these products are formed in the molecular ratio 3:1 (since PF_6^- has three times as many fluorine atoms per molecule as HPO_2F_2). The overall conversion of PF_5 to these products in HDA, without a detectable residue of HF, can be explained by the reactions:

$$PF_5 + H_2O \longrightarrow POF_3 + 2HF$$

$$POF_3 + H_2O \longrightarrow HPO_2F_2 + HF$$

$$PF_5 + HF + NO^+ + NO_3^- \longrightarrow NO^+PF_6^- + HNO_3$$

The difference between the PF_5/HDA and PF_5/HNO_3 reactions seems to be that PF_5 does not leave HF as a product in HDA, but does leave HF as a product in HNO_3.

An interesting phenomenon observed during these experiments was the appearance of a transient extra peak near the middle of the HPO_2F_2 doublet. This was not connected with the HPO_2F_2 resonance since its disappearance had no effect on the existing doublet, and it appeared neither exactly in the centre of it nor with an acceptable peak area ratio, to be considered as part of a triplet for HPO_2F_2. This peak disappeared after the first spectrum for each tube had been run, and it must be concluded that it was associated with the presence of the BF_4^- anion, since it was only observed in the presence of this species. The chemical shift of this unknown species appears to be situated at δ_{CFCl_3} = ca. 95ppm.

8.3 Reactions of orthophosphoric acid with metal nitrate hydrates and metals in HDA

As mentioned above (*Section 8-2*) a possible product of the reaction of PF_5 with HDA is H_3PO_4. It was therefore decided to investigate the effects of H_3PO_4 in HDA solution with the metal nitrato-species likely to result from

corrosion of stainless steel and aluminium by HDA and to observe any inhibiting effects of H_3PO_4 on metal corrosion by HDA. The nature, solubility, and likelyhood of precipitation of metal phosphates was the principal concern.

The effect of the addition of H_3PO_4 to solutions of iron, nickel, chromium, and aluminium nitrate hydrates in HDA was investigated. In each case the experimental procedure was identical: an excess of H_3PO_4, dissolved in ca. 2ml. HDA to permit mixing with the metal nitrate solution, was added to ca. 25 ml of the metal nitrate hydrate/HDA solution, against a counter-current of argon. Iron nitrate solution for use in the above procedure was prepared by reaction of mild steel with HDA, and the reaction of mild steel with H_3PO_4/HDA solution was also studied (see below, Section 8-3(a) (i) and (ii)). Nickel and aluminium nitrate solutions were saturated with the nitrate hydrate at room temperature (i.e. ca. 2wt. % $Ni(NO_3)_2 \cdot 2H_2O$, and 1wt. % of $Al(NO_3)_3 \cdot 6H_2O$). A solution of similar concentration of chromium (III) nitrate hydrate in HDA was prepared by dissolving the appropriate weight of $Cr(CO)_6$ in the mixture.

With all 3 solutions, immediate precipitation of an almost colloidal solid occurred. Each solution was allowed to stand overnight to encourage settling, and the precipitate was then filtered off by suction on a grade 3 sinter mounted in a filter stick protected from atmospheric moisture. Filtration occurred in each case with relative ease. The precipitates were washed thoroughly with HDA to remove traces of H_3PO_4, and were dried under vacuum ($20^{o}C$, 10^{-3}mm). The solids dried rapidly to give free-flowing powders, and were examined by infrared spectroscopy, X-ray powder diffractometry, and elemental analysis. The filtrate was in each case evaporated in vacuum in order that the nature of any residues could be examined. The final stage of evacuation of the extremely tenacious gums obtained from the chromium and aluminium solutions was carried out at $20^{o}C$ and 10^{-5}mm.

(a) The reaction of mild steel/HDA corrosion products with H_3PO_4

(i) Reaction of iron/HDA solution with H_3PO_4/HDA solution

This reaction was carried out using a sample of iron-containing HDA prepared by allowing a sample of mild steel to react with HDA for five days.

A large amount of fine precipitate instantly formed on addition of the H_3PO_4/HDA solution. This was filtered off and dried under vacuum (10^{-3} mm) yielding a pale pink powder which was shown to be amorphous by X-ray powder photography. The infrared spectrum was recorded (Fig. 8-9, Table 8-6) and this indicated that the compound was an iron phosphate, although a trace of nitrate was indicated by weak bands in the 800cm^{-1} region, possibly assignable to the $\pi(NO_3)$ absorption. Elemental analysis of the compound was rendered difficult by its insolubility. It would only dissolve by boiling in concentrated H_2SO_4 and only remained soluble in fairly acid solution.
(Found: Fe, 13.1%; P, 27.8%; N, 0.7%). The observed Fe:P ratio is 1:3.8 which suggests that a possible formulation of this product is $FePO_4 \cdot 3H_3PO_4$.
(Requires: Fe, 12.6%; P, 27.9%).

(ii) Reaction of mild steel with H_3PO_4/HDA solution

To investigate the possibility of corrosion inhibition by phosphate, a piece of mild steel, cleaned and abraded, was immersed in a solution of H_3PO_4 in HDA. A dense gelatinous precipitate grew in strands on the metal surface overnight, incorporating bubbles of gas (possibly N_2O, see Section 5.3(d)). A series of experiments was then conducted, using small pieces of cleaned mild steel placed in solutions of HDA containing ranging concentrations of H_3PO_4. The concentrations used were 32, 10, 5, 2 and 0.2wt.% H_3PO_4 in HDA. All these solutions remained the normal brown HDA colour, except the 32 wt.% which had a paler colour. A precipitate of identical appearance to that previously observed was obtained in each case; the strands eventually filling most of the liquid volume and forming a crust on top of the liquid, but after different periods of time. The lower the concentration of H_3PO_4, the more rapidly was the resulting precipitate formed. The precipitate from the experiment involving 5wt.% H_3PO_4 was filtered off after two weeks and evacuated to dryness, leaving a pale pink amorphous powder. The infrared spectrum of this (Fig. 8-10, Table 8-7) was almost identical to that of the product described in 8-2(a)(i) above and formulated as $FePO_4 \cdot 3H_3PO_4$, except that less nitrate

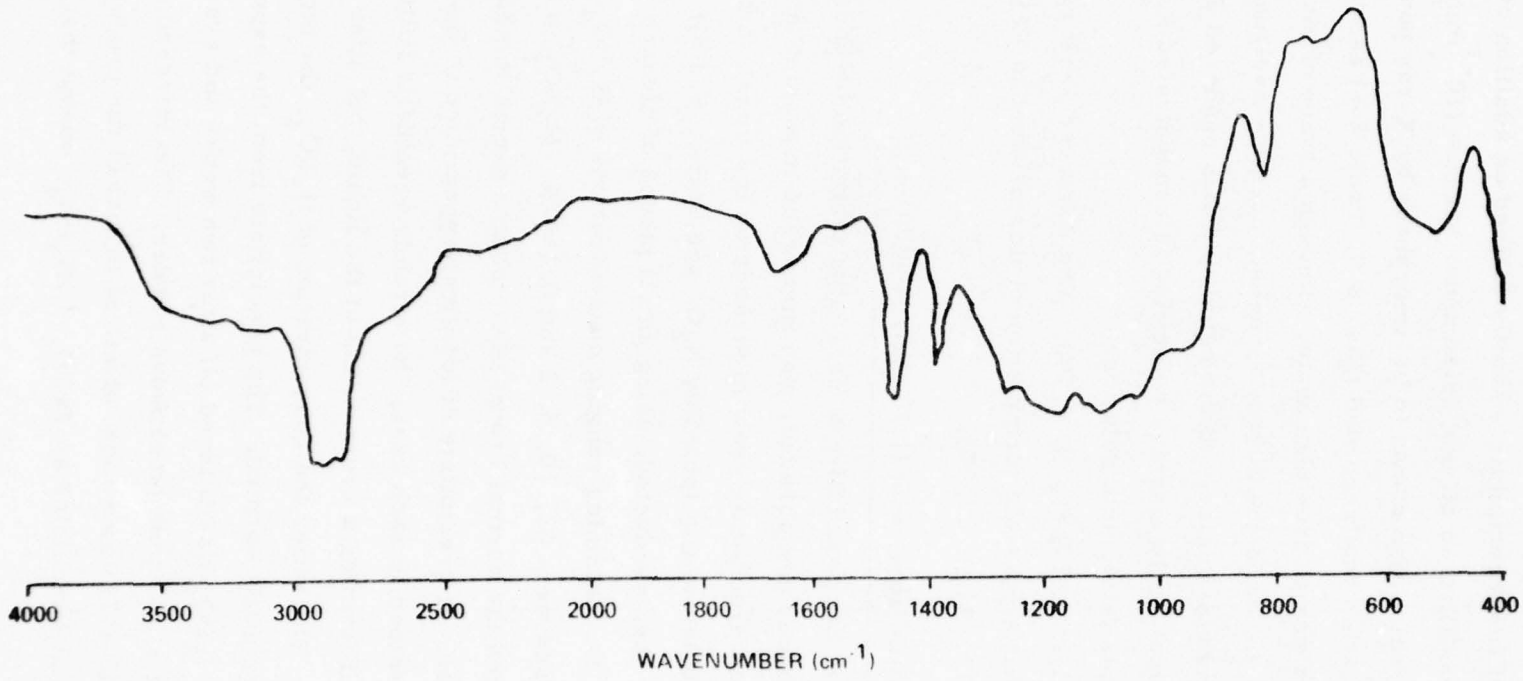


Figure 8-9. IR Spectrum of Solid Product from H_3PO_4/Iron in HDA Reaction

Table 8-6. Infrared Spectrum of Precipitate from (Mild Steel/HDA)/H_3PO_4 Reaction

Absorption band (cm^{-1})		Assignment
3300	m br	ν(OH)
1650	m br	$\delta(H_2O)$
1260-900	s vbr	ν(P-O) and ν(P=O)
800	m sp	$\pi(NO_3)$
500	m br	δ(OPO)

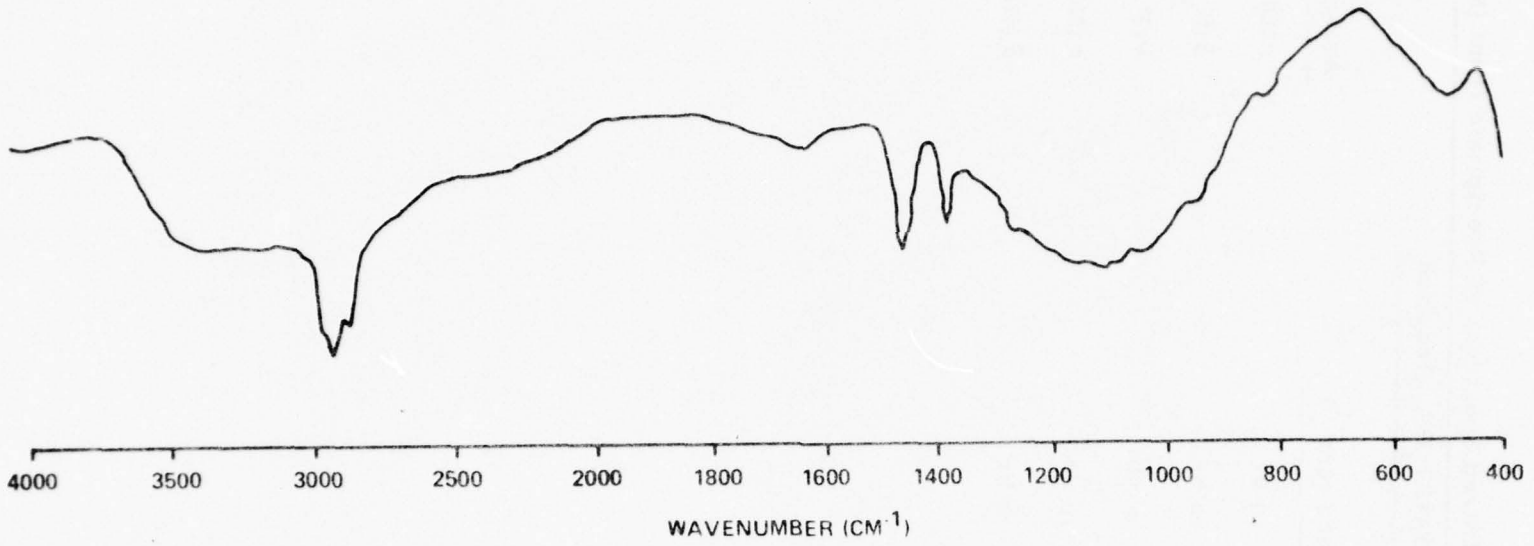


Figure 8-10. IR Spectrum of Solid Product from Mild Steel/H_3PO_4 in HDA Reaction

Table 8-7. Infrared Spectrum of Solid Product from Mild Steel/ H_3PO_4 in HDA Reaction

Absorption band (cm^{-1})		Assignment
3300	m br	ν(OH)
1630	w br	$\delta(H_2O)$
1260-900	s vbr	ν(P-O) and ν(P=O)
800	w sh	$\pi(NO_3)$
500	m br	δ(OPO)

appeared to be present, the 800cm^{-1} absorbance being much less intense. Analysis of the present product for iron was again consistent with the above formulation (Found: Fe, 13.0%; $FePO_4 \cdot 3H_3PO_4$ requires: Fe, 12.6%). It is thus concluded that the overall reaction between iron in HDA and H_3PO_4 gives the same product by either route (i) or (ii). The qualitative observation that faster precipitation occurs with less added H_3PO_4 may indicate that, the rate of corrosion of mild steel in HDA decreases with increasing H_3PO_4 concentration. An alternative explanation of the slower precipitation of material by greater concentrations of H_3PO_4 could be that a higher degree of complexing of corrosion product occurs in the more concentrated phosphate solutions.

(b) Reaction of $Ni(NO_3)_2 \cdot 2H_2O$/HDA solution with H_3PO_4/HDA solution

This reaction was carried out twice. In both cases a yellow-green amorphous solid was obtained. The infrared spectra of both products (Fig. 8-11, Table 8-8) showed intense, very broad, and relatively featureless bands assignable to PO_4^{3-} and co-ordinated water. A sharp band at 725cm^{-1}, and an associated shoulder at 770cm^{-1} may be due to residual nitrate. However, in the absence of any other distinct absorptions usually assigned to nitrate, in the heavily obscure 800cm^{-1} - 1400cm^{-1} region, it is difficult to confirm this assignment.

Analysis of the products of the two reactions gave conflicting results i.e. Ni, expt. 1, 21.1%, expt. 2, 18.0%; P, expt. 1, 15.3%, expt. 2, 17.8%. These figures do not correspond to a definite stoichiometry, but approximate to: expt. 1, $Ni_3(PO_4)_2 \cdot 2H_3PO_4 \cdot 16.44H_2O$; expt. 2, $Ni_3(PO_4)_2 \cdot 3.6H_3PO_4 \cdot 17H_2O$. The lack of definite stoichimetry, the apparently high degree of hydration, and the amorphous nature of these products suggests the structural possibility of a loosely bound matrix of hydrogen bonded H_2O, H_3PO_4, and PO_4^{3-} and coordinated Ni^{2+}. The shoulder in the O-H stretching absorbance at 3200cm^{-1} (IR) suggests two types of OH grouping in the system.

Evacuation of the filtrate to dryness gave a blue-green, dry solid. The X-ray powder photograph of this solid showed strong lines corresponding to

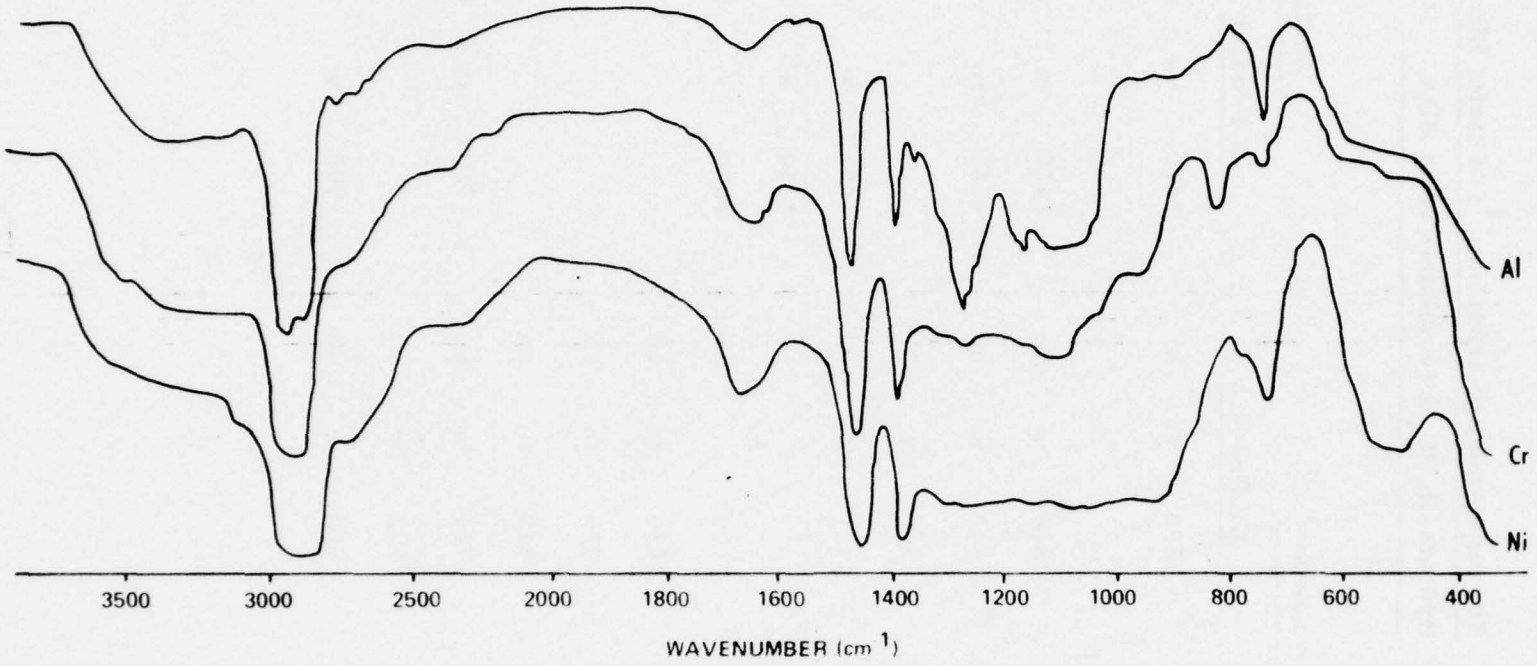


Figure 8-11. IR Spectra of Phosphate Precipitates from Ni, Cr, Al Nitrate Hydrate/HDA/H_3PO_4 Reactions

Table 8-8. The Infra-red Spectrum (cm^{-1}) of Metal Nitrate Hydrate/H_3PO_4 Precipitates from HDA

Absorption Bands									Assignment
Ni Products			Cr Product			Al Product			
3150	vs	sh	3200	vs	b	3400	vs	vb	ν(OH)
2900	vs	vb							
			2320	w	sh	2400	w	sh	
1670	m	b	1640	m	b	1650	m	sp	$\delta(H_2O)$
1300	s	b	1300	s	b				
1260	s	b	1265	s	sp	1265	s	vsp	ν(P=O)
						1150	s	sp	
1080	s	vb	1100	s	b	1070	s	b	
			1020	m	sh				ν(P-O)
930	s	b	935	m	sh				
770	m	sh	810	m	sp				$\pi(NO_3)$?
725	m	sp	725	w	sp	720	m	vsp	$\delta(NO_3)$?
			595	w	sh				δ(OPO)
500	s	b	500	w	sh	500	w	sh	

those of $Ni(NO_3)_2 \cdot 2H_2O$. The infrared spectrum was also similar to that of $Ni(NO_3)_2 \cdot 2H_2O$, but with evidence of residual H_3PO_4. The dry, free flowing nature of this evaporate suggests however, that only a small amount of H_3PO_4 was associated with it, and implies that an almost complete removal of H_3PO_4 occurs by solvation of $Ni_3(PO_4)_2$ when the latter is precipitated from HDA.

(c) Reaction of $Cr(CO)_6$/HDA solution with H_3PO_4/HDA solution

The reaction of chromium in solution in HDA with H_3PO_4 yielded a blue-green amorphous solid. The infrared spectrum (Fig. 8-11, Table 8-8) again showed intense, broad and somewhat featureless bands assignable to phosphate and co-ordinated water. Additional weak bands at 812cm^{-1}, 725cm^{-1}, and 1025cm^{-1} were possibly indicative of residual nitrate.

Analysis of the product (found: Cr, 24.4; P, 14.2%) corresponded well with $Cr(PO_4) \cdot 4H_2O$ (requires: Cr, 24.2; P, 14.4%). The existence of this hydrate is well established[15].

Evacuation of the filtrate ultimately yielded a green viscous gum, presumably containing residual H_3PO_4 and chromium. The quantity of this gum was very small relative to the quantity of solid precipitate isolated.

(d) Reaction of $Al(NO_3)_3 \cdot 6H_2O$/HDA solution with H_3PO_4/HDA solution

The product from the reaction of $Al(NO_3)_3 \cdot 6H_2O$ in HDA solution with H_3PO_4 was initially much more gelatinous than the products from nickel and chromium solutions, but dried to an amorphous white solid. The infrared spectrum again showed the intense, broad bands associated with phosphate and co-ordinated hydroxo-species. A weak, sharp band at 725cm^{-1} may correspond to a nitrate absorption, but well-defined confirmatory bands for nitrate at ca 800cm^{-1} or 1000-1050cm^{-1} are absent (Fig. 8-11, Table 8-8).

Analysis of this product (found: Al, 11.8; P, 28.5%) corresponded well with the formulation $Al(PO_4) \cdot H_3PO_4$ (requires: Al, 12.4; P, 28.2%). On the basis of this formulation, the sharp, strong absorbance at 1265cm^{-1} in the infrared spectrum could be assigned to $\nu(P=O)$ in the combined H_3PO_4, occurring

as a well-defined absorbance due to lack of hydrogen bonding with e.g. lattice or co-ordinated water.

Evacuation of the filtrate ultimately yielded a colourless viscous gum, presumably containing excess phosphoric acid.

(e) The reaction of 1% H_3PO_4 solution in HDA with aluminium metal

In connection with the studies described above, the effect of small concentrations of H_3PO_4 on the corrosion of aluminium by HDA was observed.

A strip of aluminium, 3cm x 1cm x 0.1cm was immersed in ca. $25cm^3$ of a 1% solution of H_3PO_4 in HDA. After 18 hr. traces of a flocculent colourless deposit had formed along edges and corners of the strip, presumably around the areas of high surface energy where corrosion would be maximised. After 2 weeks the metal appeared to be completely encased in a loose gelatinous shell of reaction products, which could be detached by agitation. At the end of 3 months the gelatious material was scraped from the surface, under the liquid, filtered, thoroughly washed with HDA and dried under vacuum ($20^{\circ}C$, 10^{-3}mm). The resulting white solid was found to be amorphous, and to give an infrared spectrum very similar to that of the $Al(NO_3)_3 \cdot 6H_2O + H_3PO_4 \xrightarrow{HDA}$ precipitate described above (Fig. 8-11, Table 8-8).

Analysis of the solid suggested the formulation $Al(PO_4) \cdot (H_3PO_4) \cdot 9H_2O$. (Found: Al, 7.34%; P, 15.9%. $Al(PO_4) \cdot (H_3PO_4) \cdot 9H_2O$ requires Al, 7.12%; P, 16.35%.) Although incorporating water molecules, this formulation is again consistent with the presence of 1 molecule of H_3PO_4 per $Al(PO_4)$ unit as indicated by the analysis of the product formed in (d) above. Variability of hydration number appears to be a common feature of aluminium phosphates[16] and incorporation of water is to be expected in the presence of excess H_3PO_4.

(f) The reaction of 1% H_3PO_4 solution in HDA with 321 stainless steel

A sample of 321 stainless steel rod 1.5cm. diam. x 1.0cm. long was immersed in ca. $25cm^3$ of a 1% solution of H_3PO_4 in HDA at room temperature in a sealed vessel. A control experiment was also set up in which an identical rod of 321 stainless steel was immersed in ca. $25cm^3$ of HDA.

After 3 weeks the control sample was black, and metal crystallites had broken off and fallen to the bottom of the vessel. Darkening of the HDA, as the concentration of dissolved metal ions had built up, had also occurred. The sample immersed in 1% H_3PO_4 had retained the original metallic lustre, indicating that no integranular corrosion had occurred. The metal was enclosed in a translucent sac of gelatinous material, extending some 1.5mm from the metal surface. This sac could be detached by gentle shaking, but possibly provided a sufficiently coherent diffusion barrier to inhibit corrosion.

Analysis of the metal content of the HDA solutions by atomic absorption spectrophotometry showed that considerable corrosion inhibition had occurred. The iron and chromium concentrations of the HDA containing H_3PO_4 were 39.7 and 18.6 ppm. respectively, whereas those of the control sample were 318 and 110 ppm. respectively.

(g) Conclusions

The experiments described in (a) to (e) of this Section show that iron, chromium, nickel, and aluminium phosphates have very low solubilities in HDA. Similar products appear to be formed whether H_3PO_4 is added to a solution of metal nitrate hydrate in HDA, or the metals are allowed to react with HDA containing a low concentration of H_3PO_4. These precipitates are gelatinous, and cause considerable difficulty in filtration. The formation of gelatinous sacs around the metal samples may be one of the factors responsible for corrosion inhibition, as diffusion of HDA to the metal surface is thereby hindered.

8.4 Reactions of phosphorus pentafluoride with metal nitrate hydrates and metals in HDA

(a) The reaction of mild steel/HDA corrosion products with PF_5

To examine the potential iron corrosion products in modified HDA, mild steel was used in these experiments. Although this has a high corrosion rate compared to stainless steel in HDA, it was thought that the rate of corrosion would be similarly influenced when PF_5 was added to HDA. The initial

experiment (i) was conducted by adding PF_5 to HDA already containing dissolved iron from mild steel, under the assumption that this would be a quicker, if synthetic, route to the corrosion products of iron in modified HDA. Later experiments (ii) were conducted by introducing mild steel directly into modified HDA.

(i) Reaction of iron/HDA solution with PF_5

Two identical experiments were conducted using HDA in which a piece of mild steel had been held for some weeks. About 8wt.% PF_5 was added by condensation in small portions at -196°C onto the iron/HDA solution in a 15mm. diameter Kel-F tube, allowing the mixture to warm and react after each addition. After leaving overnight at room temperature, the lower half of the HDA was seen to contain a very fine, mobile precipitate, with clear HDA above. This precipitate was isolated on a filter stick, washed in a little fresh HDA to remove any $NOPF_6$ and dried under vacuum, leaving a pale green powder, which was shown to be amorphous by X-ray powder photography. The infrared spectra of the products of both the experiments were recorded (Fig. 8-12, 8-13, Table 8-9). These were practically identical, showing broad bands attributable to the presence of phosphate and co-ordinated water. Only traces of co-ordinated nitrate appeared to be present, a weak band at 800cm^{-1} being visible. No bands corresponding to NO^+, NO_2^+, or PF_6^- were visible, suggesting that $NOPF_6$ and NO_2PF_6 were absent. Elemental analysis gave the following results:

Product 1: Fe, 23.5; F, 22.8; P, 19.4%.
Product 2: Fe, 26.5; F, 24.0; P, 13.2; N, 0.6%.

These analyses give a mean Fe:P:F ratio of about 1:1.2:2.8 which suggests that this product could be close to the formulation $FeF_3 \cdot H_3PO_4$ (requires: Fe, 26.5%; F, 27.0%; P, 14.7%). Alternatively, the product could be considered to contain $PO_2F_2^-$ because:

1. The infrared spectrum is very similar to that of the PF_5/mild steel/HDA reaction product (reaction 8-5(c)) which is assumed to contain $PO_2F_2^-$.

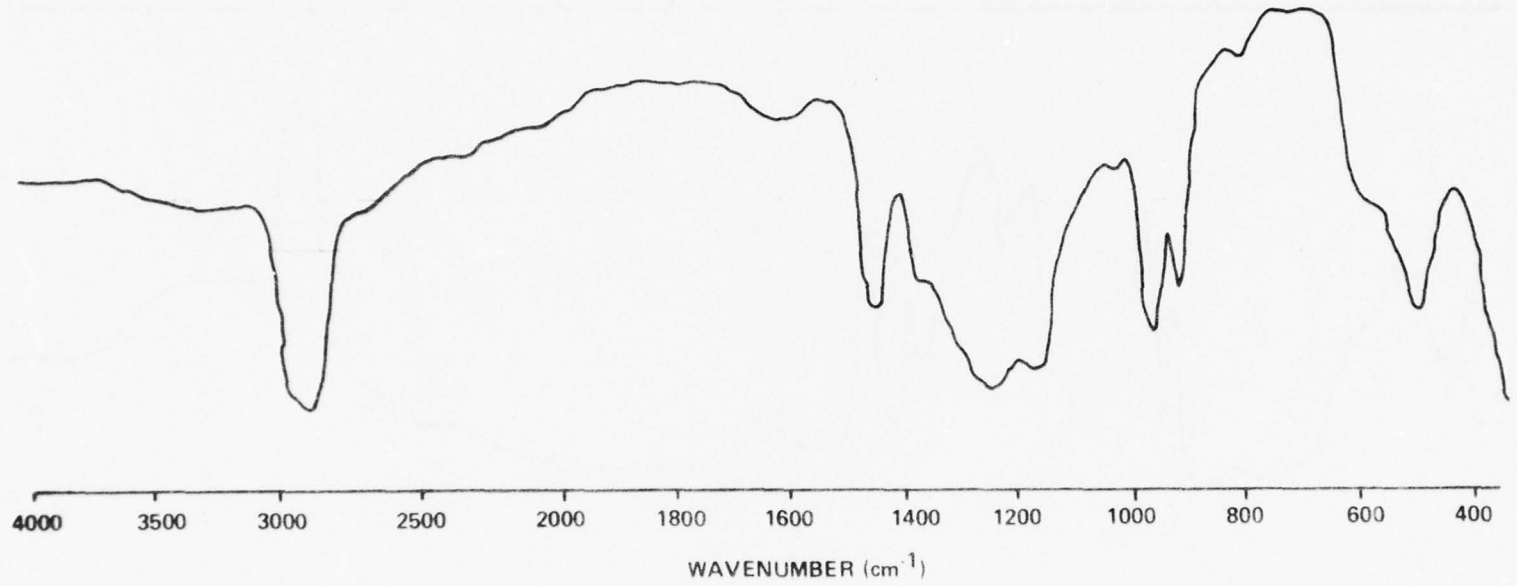


Figure 8-12. IR Spectum of Product 1 from Iron/PF_5 Reaction in HDA

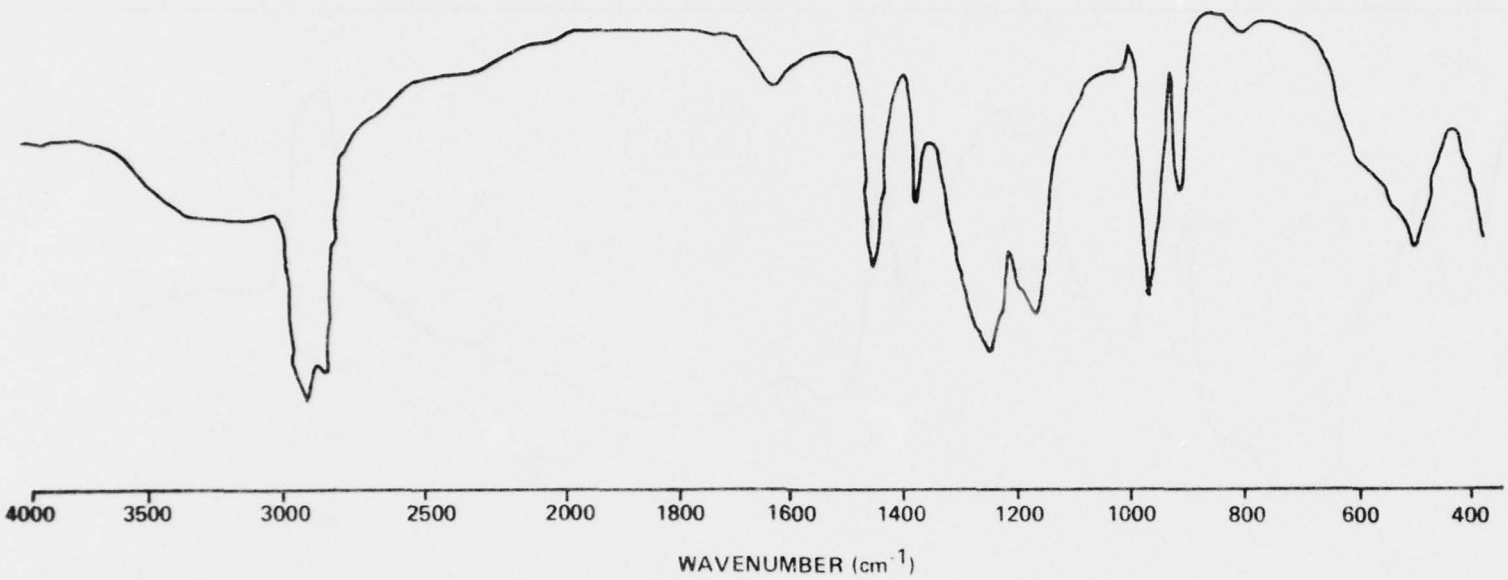


Figure 8-13. IR Spectrum of Product 2 from Iron/PF_5 Reaction in HDA

Table 8-9. Infrared Spectrum of Solid Products from Iron/PF_5 Reaction (8 wt. %) in HDA

Absorption band (cm^{-1})	Assignment
3300 w, br	ν(OH)
1620 m, br	$\delta(H_2O)$
1250 s, br	$\nu_{as}(PO_2)$
1170 s	$\nu_s(PO_2)$
960 s	$\nu_{as}(PF_2)$
910 s	$\nu_s(PF_2)$
800 w	$\pi(NO_3)$
500 s	ν(Fe-F) or δ(O-P-F)

2. The infrared spectrum has close similarities to that of KPO_2F_2[17], as indicated by the assignments (Table 8-9).

3. The Mössbauer spectrum (Fig. 8-14) of the first product gives two close singlet peaks, of different intensities, in the isomer shift region characteristic of $Fe^{III}(3d^5)$. These peaks are +0.6 (larger peak) and +0.3 (smaller peak) mm sec.$^{-1}$. This indicates that there are two types of Fe^{III} environment (probably octahedral) in the solid, in different proportions. The Mössbauer spectrum of FeF_3 is well characterised, and below 363K exhibits six-line magnetic hyperfine splitting, and three pairs of doublets[18] which are not observed in the spectrum of the product obtained.

4. The known fluorine species in modified HDA are PF_6^-, $PO_2F_2^-$ (see Section 8.2), and therefore the product precipitate could be $Fe(PF_6)_3$ or $Fe(PO_2F_2)_3$. Since, however, the very characteristic infrared band of PF_6^- at 840cm^{-1} is not observed in the infrared spectrum of the products, and the spectra do tend to indicate $PO_2F_2^-$, it is at present assumed that the product is some form of iron(III) difluorophosphate.

The analytical figures, however, do not fit those expected for $Fe(PO_2F_2)_3$, (requires: Fe, 15.5; F, 31.8; P, 25.9%,) although this might be partially explained by the great persistence (i.e. resistance to hydrolysis) of $PO_2F_2^-$ during analysis. Product 2 was therefore re-analysed for fluorine and phosphorus before and after autoclave hydrolysis (see also Appendix B.4(h)) and for iron before autoclave hydrolysis:

	Fe	'Free F'	'Resistant F'	'Free' P	'Resistant' P	0 (by difference)
found %	23.6	21.8	9.1	13.1	8.1	24.3
Atomic Ratio	1.0	2.7	1.1	1.0	0.6	3.6

These figures show that the F:P ratio in the "hydrolysis-resistant" component of the mixture was 2:1, consistent with the presence of $PO_2F_2^-$.

(ii) Reaction of mild steel with PF_5/HDA solution

An initial experiment was conducted to ascertain whether any reaction product between mild steel and modified HDA could be obtained, for comparison with the products described above. A small piece of degreased and abraded mild steel was immersed in HDA containing 2wt.% PF_5 in a 15mm. diameter

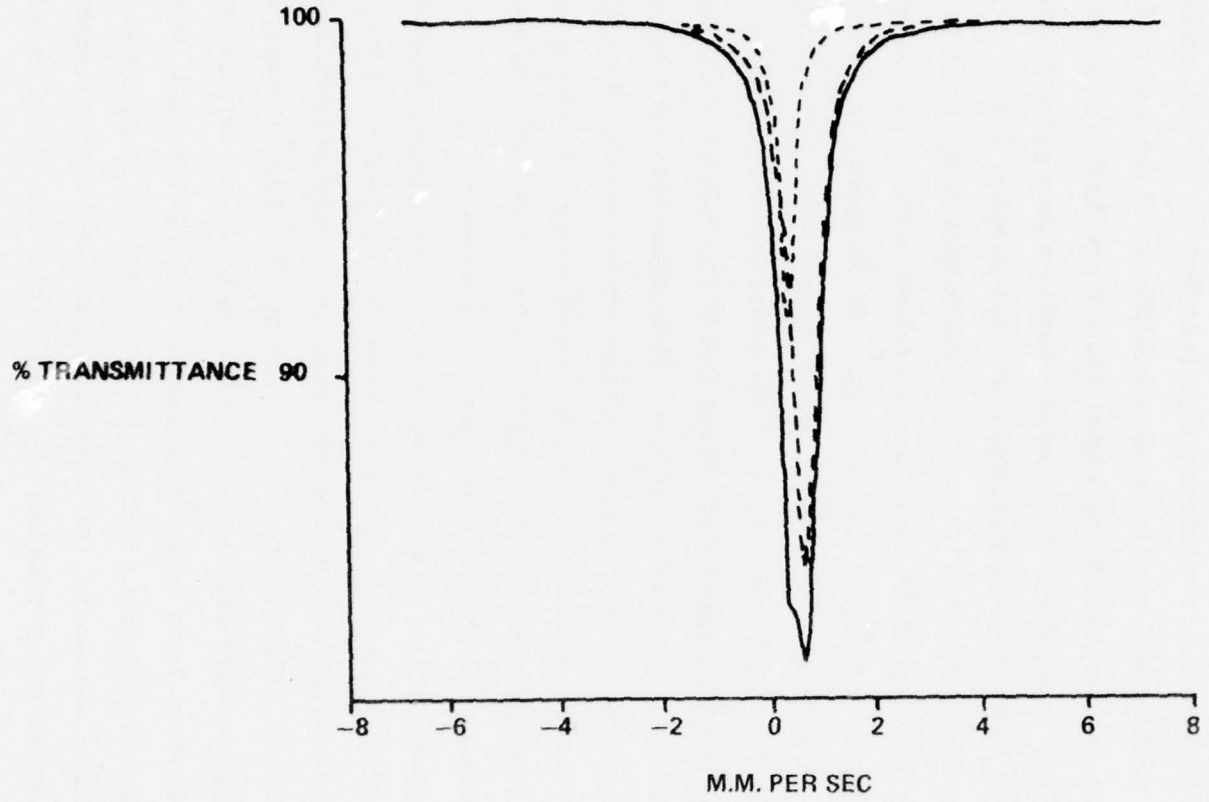


Figure 8-14. Mössbauer Spectrum of Product 1 from Iron/PF_5 Reaction in HDA

Kel-F tube. The edges of the mild steel turned black immediately (a phenomenon usually observed for mild steel only after reaction with HDA for several days), and after five minutes, the black areas had spread, becoming covered in bubbles of gas, presumably N_2O (see Section 5.3(d)), and a gelatinous precipitate was seen to be slowly falling from the side of the metal sample. The reaction was left overnight, and the precipitate was filtered off and evacuated (10^{-3}mm, 20°C) to dryness, leaving a pale green powder. This was shown to be amorphous by X-ray powder photography, and its infrared spectrum (Fig. 8-15, Table 8-10) was identical to that of the product formed from the above reaction of PF_5 with iron dissolved in HDA, except that the nitrate band was more intense. Analysis gave the following results: Fe, 21.4%; F, 19.8%; P, 18.1%; N, 0.5%. Again, these figures were given an approximate atomic ratio of Fe:P:F, 1:1.5:2.7. It is therefore presumed to be the same product as that from the experiment described in (i), validating the use of the 'synthetic' route to the corrosion product. This experiment was repeated using HDA containing 0.7wt.% PF_5, to give a closer representation of modified HDA. The mild steel turned completely black almost instantly, indicating an even faster rate of reaction than with 2wt. %PF_5. After 15 minutes the surface was covered in bubbles, and after 25 minutes the gelatinous precipitate had begun to form. (The appearance of the precipitate after a longer time, despite the initial observation of large rate increase compared to the 2 wt.% PF_5 HDA, is attributed to the smaller amounts of PF_5 solution species present in the 0.7 wt.% PF_5/HDA solution). This reaction was left to proceed without interruption. After two weeks, a phase separation was observed, a layer of clear brown-orange liquid of about 3mm depth had appeared on top of the HDA, which had become dark brown and opaque but was still presumed to contain the observed precipitate. After one month, the layer of liquid on the top had become about 10mm deep, and the Kel-F tube had become bent and covered in very fine cracks, leaking traces of N_2O_4. It was assumed at this stage that the upper liquid was N_2O_4, salted out of the modified HDA by iron species in solution. After a further two weeks, the tube was opened and the upper liquid layer

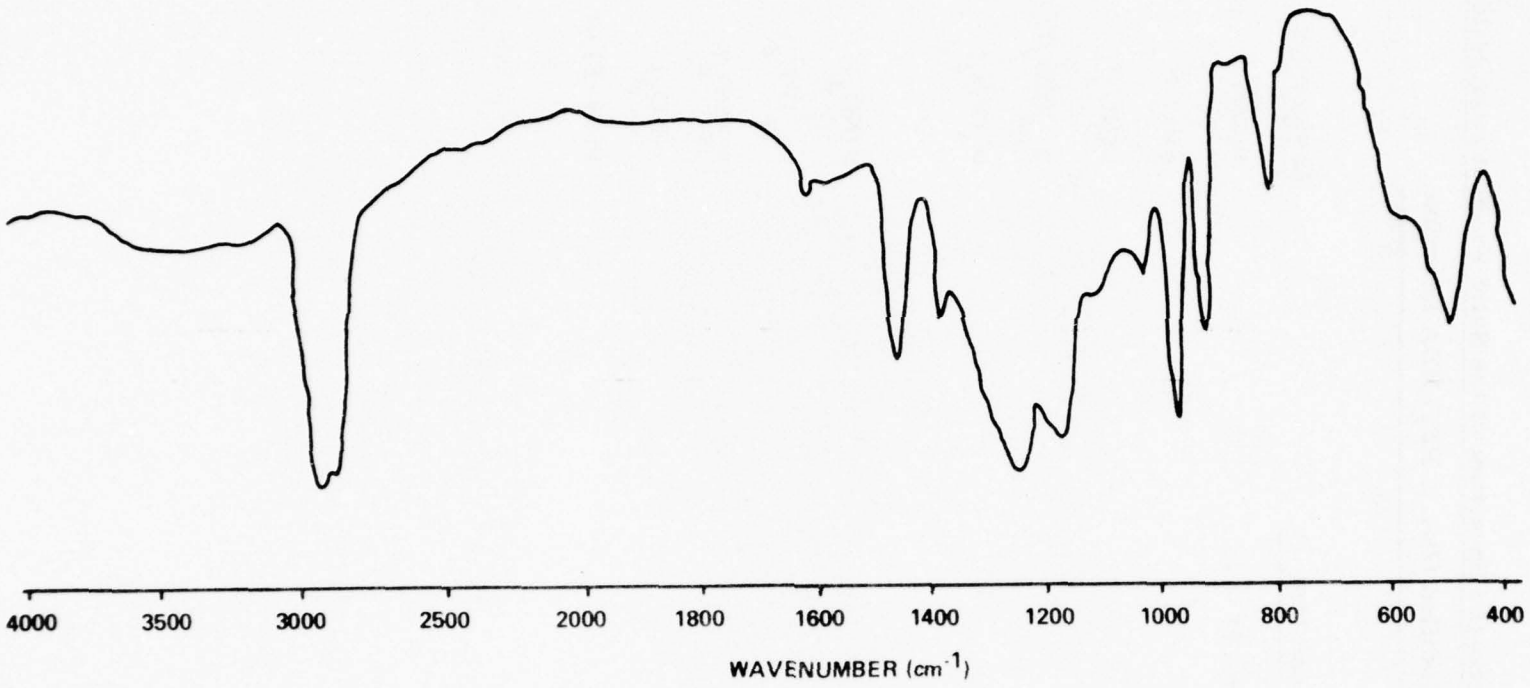


Figure 8-15. IR Spectum of Solid Product of Mild Steel/Modified (2wt% PF_5) HDA Reaction

Table 8-10. Infrared Spectrum of the Solid Product from Mild Steel/ Modified (2wt. % PF_5) HDA Reaction

Absorption band (cm^{-1})	Assignment
3600-3100 w, br	ν(OH)
1600 m, sp	$\delta(H_2O)$
1580 w, sh	$\nu(NO_3)$
1240 s, br	$\nu_{as}(PO_2)$
1160 s	$\nu_s(PO_2)$
1100 sh	
1020 m	$\nu(NO_3)$
960 s, sp	$\nu_{as}(PF_2)$
910 s, sp	$\nu_s(PF_2)$
800 m	$\pi(NO_3)$
600 sh	ν(Fe-F) or δ(O-P-F)
490 s	

decanted under an argon counter-current into a Schlenck tube, and evacuated to dryness. The liquid evaporated very rapidly and no solid residue remained after evacuation. It was therefore concluded that the upper layer was liquid N_2O_4. On filtration of the lower layer, no solid remained, and it was obvious that the original precipitate had redissolved. A sample of the lower liquid layer was diluted and analysed for iron content, and found to contain approximately 10^5 p.p.m. (i.e. 10wt.% Fe). This very high value, obtained after only one and a half months, confirmed the previous indication that the rate of corrosion of mild steel was very much increased in modified HDA compared to uninhibited HDA. The rest of the lower layer was evacuated to dryness, forming a brown gum, then a brown powder, similar to those obtained by evacuation of solutions of mild steel in uninhibited HDA. This powder was found to be amorphous by X-ray powder photography, and its infrared spectrum (Fig. 8-16, Table 8-11) was practically identical to that of the mild steel/HDA product (Fig. 8-17, see Section 5.3(c)), the only significant difference being a shoulder at $500cm^{-1}$ which could be attributable to an Fe-F stretch or O-P-F deformation. The material was analysed (found: Fe, 17.8%; P, 0.5%; F, 1.1%; N, 19.7%.) (Required for $Fe(NO_3)_3 \cdot 2H_2O$: Fe, 20.1%; N, 15.1%.) It was therefore concluded that the powder was simply the mild steel/HDA product containing small quantities of PF_5 reaction products and HNO_3 (as indicated by the higher nitrogen content.)

(b) Reaction of $Ni(NO_3)_2 \cdot 2H_2O$/HDA solution with PF_5

The experimental details of the addition of PF_5 to HDA solutions of the nitrate hydrates of nickel (this section), chromium (Section 8.4(c)) and aluminium (Section 8.4(d)) were essentially identical and will be described here. Solutions of the nitrate hydrates were transferred against an argon counter-current into 15 mm diam. Kel-F tubes, which were then fitted with adaptors and valve connectors. The liquids were then cooled to liquid nitrogen temperature (-196°C), evacuated to 10^{-5} mm, and then allowed to melt and de-gas. The degassed solutions were then refrozen and re-evacuated, and appropriate weights of PF_5, as calculated from the weight of solution, were condensed in, in a number of aliquots. In between each addition of PF_5, the solutions were allowed to melt, and the resulting changes in the solution were monitored.

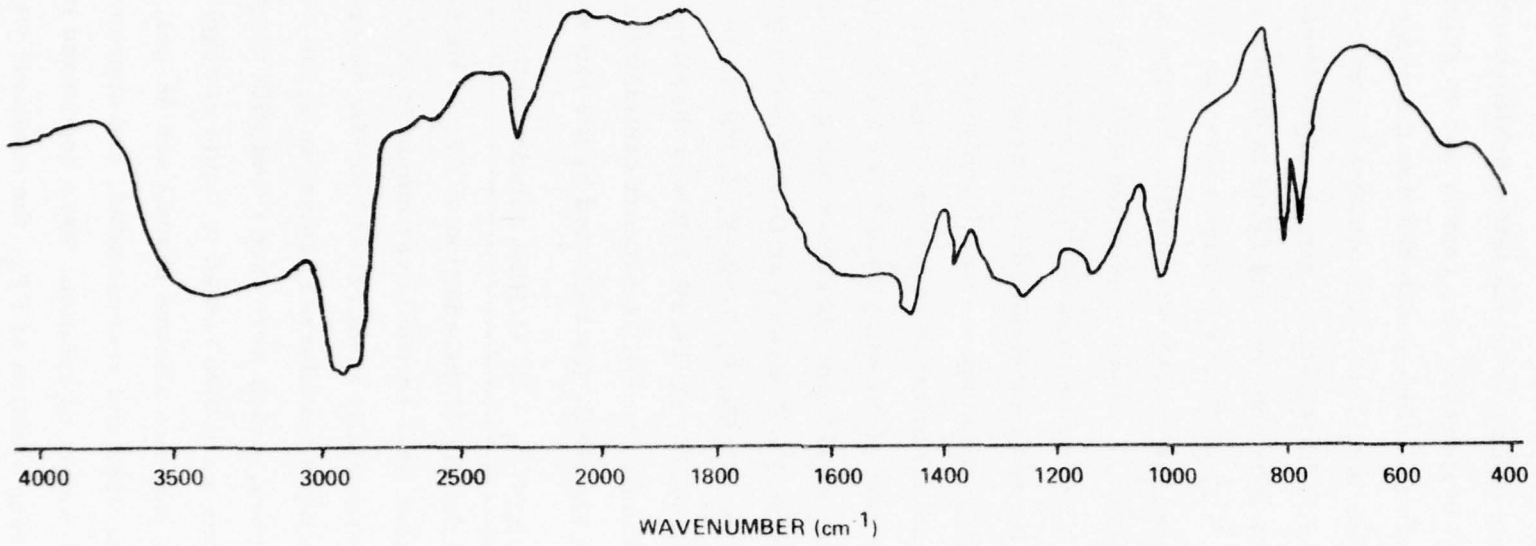


Figure 8-16. IR Spectrum of Product from Evacuation of Mild Steel/Modified HDA (0.7wt% PF_5) Reaction

Table 8-11. Infrared Spectrum of Product from Evaporation of Mild Steel/ Modified HDA(0.7 wt. % PF_5) Reaction

Absorption band (cm^{-1})		Assignment
3300	s, vbr	ν(OH)
2275	m	$\nu(NO^+)$
1550	s, vbr	$\nu(NO_3)$
1290	m, sh	
1260	m, sp	$\nu(NO_3)$
1140	m	
1010	s	$\nu(NO_3)$
800	s, sp	$\pi(NO_3)$
765	s, sp	$\delta(NO_3)$
720	w, sh	$\delta(NO_3)$
500	m, br	ν(Fe-F) or δ(O-P-F)

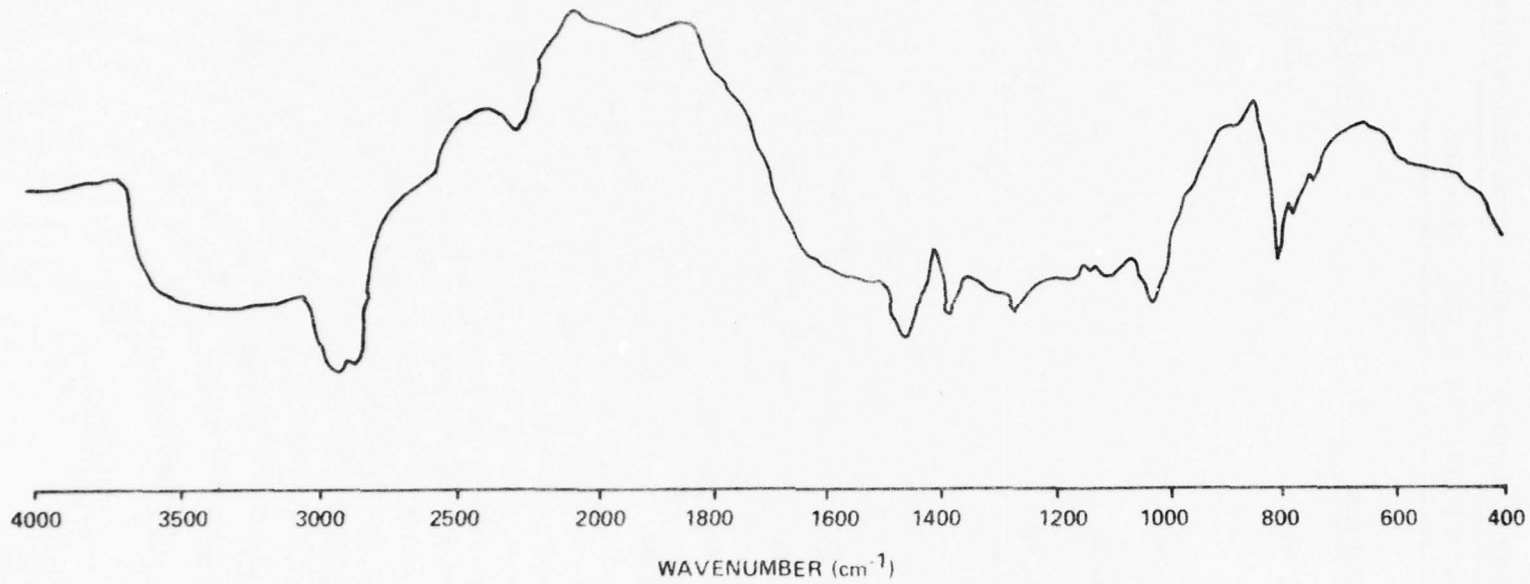


Figure 8-17. IR Spectrum of the Mild Steel/HDA Product

24.58g of a solution containing $Ni(NO_3)_2 \cdot 2H_2O$ (0.144g) was used in the case of nickel. To this was added a total of 0.49g PF_5 (i.e. ca. 2.0 wt%) in 6 aliquots.

On addition of each portion of PF_5, a crust of white solid (presumably $NOPF_6$) formed around the upper parts of the tube and around the liquid surface. This crust redissolved on shaking. No change in the green colour of the solution or frozen glassy solid was noticed over the entire addition of PF_5, implying that the octahedrally, oxygen co-ordinated nickel species was being maintained, and no precipitation occurred. The mixture was allowed to stand for three days, and was evacuated to dryness in situ ($20^{\circ}C$, 10^{-5}mm). After approximately three hours of evacuation, the solution had evaporated to give a large bulk of pale yellow, frothy solid. The X-ray powder photograph of the solid showed only $NOPF_6$, and it is therefore concluded that the solid consisted of a mixture of $NOPF_6$ and amorphous nickel-containing species.

The infrared spectrum (Fig. 8-18, Table 8-12) shows only bands probably assignable to phosphate in the 1400-450cm^{-1} region although bands in the lower part of this region (600-450cm^{-1}) may be due to metal-fluorine stretching modes. Bands associated with co-ordinated water are prominent, co-ordinated nitrate appears to be completely absent, unless the very weak shoulders at 805cm^{-1} and 1020cm^{-1} represent traces of nitrate. Analysis of the material similarly indicated a complex mixture; i.e.

	Ni	P	PF_6^-	'Free' F	N
% found	8.09	16.58	39.79	1.054	3.90
Atomic Ratio	1.00	3.87	1.99	0.39	2.02

both nickel phosphate and fluoride apparently being present in the solid. From the nickel to fluorine ratio, it would appear, on the basis that all 'free' fluorine is present as NiF_2, that the ratio of $Ni_3(PO_4)_2$ to NiF_2 is about 1.33:1. To account for the rest of the phosphate it is necessary to regard the solid as containing associated H_3PO_4.

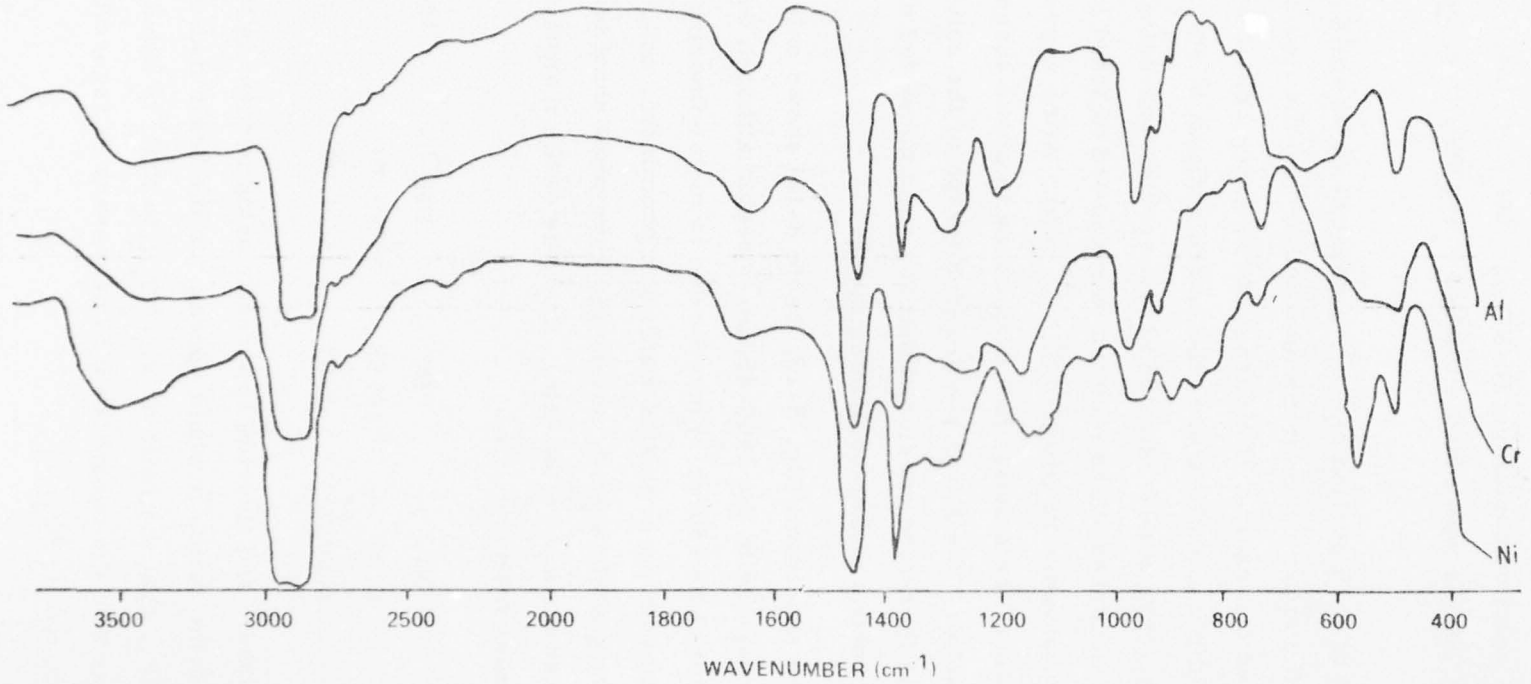


Figure 8-18. IR Spectra of Products of Ni, Cr, Al Nitrate Hydrate/HDA/PF_5 Reactions

Table 8-12. Infrared Spectrum of Metal Nitrate Hydrate $|HDA|PF_S$ Products

Absorption Bands (cm^{-1})

Ni	Cr	Al	Assignment
3480 s b	3000 vs vb	3200 s vb	ν(O-H)
2720 w sp			
2340 w sh	2340 w sh		$\nu_{as}(NO_2^+)$
1660 m b	1640 m b	1665 m b	$\delta(OH_2)$
1310 m b		1300 s b	ν(P=O)
	1255 s b	1210 s b	
1140 m sp	1155 s b		
1115 m sh			
1020 m sp	1020 w b	1020 w sp	$\nu(NO_3)$
960 m b	960 m sp	970 s sp	ν(P-O)
890 m sp	910 m sp	925 w sp	
		900 w sp	
835 w sh	800 w sh	800 w sp	PF_6^-
770 w sh			
725 m sp	723 m sp	720 v w sp	$\delta(NO_3)$
	600 m sh	670 m b	$\delta_d(NO_2^+)$
560 s sp	540 m sh		PF_6^-
495 s sp	490 m sp	500 m sp	δ(O-P-O)

It is difficult to account for the formation of nickel fluoride during the reaction, since the experiments described previously (Section 7.5) indicate that HF in HNO_3/N_2O_4 mixtures does not react with dissolved $Ni(NO_3)_2 \cdot 2H_2O$. It is possible that attack occurs via the phosphate formed, although the lack of reaction during the early stages of the addition of PF_5 would suggest that the reaction only occurs when the solution becomes more concentrated during evacuation to dryness, as the $NOPF_6$ hydrolyses in an HNO_3^- rich medium to give a more concentrated solution of HF. Fluoride from this hydrolysis would then provide NiF_2, rather than HF formed as a by-product of the PF_5/HDA reaction.

(c) Reaction of $Cr(CO)_6$/HDA solution with PF_5

A solution containing 0.36g Cr in 18.16g HDA was prepared by dissolving 1.53g of $Cr(CO)_6$ in the mixture. The solution was prepared in this way due to the great length of time necessary to prepare chromium solutions by the reaction of chromium metal and HDA. To this was added a total of 6wt.% PF_5, in a series of 6 aliquots. On addition of each aliquot a precipitate of white $NOPF_6$ formed, which subsequently redissolved. After the addition of 4wt.% PF_5 the mixture was allowed to stand overnight. At the end of this time large lumps of a gelatinous green precipitate had formed. A further 2 wt.% PF_5 was added without further change. On filtration of the mixture all but a minute amount of the precipitate passed through the porosity 3 sinter. The residual material on the walls of the Kel-F reaction vessel was found to be tenacious and insoluble in water. On evaporation of the filtrate to dryness (20^oC, 10^{-3}mm), a dark green solid was obtained after a short period of evacuation. This solid gave a completely blank X-ray powder photograph, indicating that only a small amount of $NOPF_6$ was present, since this compound has invariably been encountered previously in crystalline form.

The infrared spectrum (Fig. 8-18, Table 8-12) shows few bands except the absorptions associated with phosphate and perhaps metal-fluorine stretching vibrations. Bands due to co-ordinated water are prominent. Nitrate appears to be completely absent.

Chemical analysis again indicated a mixture of metal fluoride and phosphate:

	Cr	P	'Free' F	N
found %	15.2	16.1	14.2	2.0
Atomic Ratio	1	1.76	2.56	0.49

Assuming 'free' fluorine to be present in the form of CrF_3, the high F:Cr ratio suggests that the metal is mainly in the form of this fluoride. On the basis of these figures, the ratio of CrF_3:$CrPO_4$ is 1:0.15. Again the solid appears to be associated with H_3PO_4 and co-ordinated water.

(d) Reaction of $Al(NO_3)_3 \cdot 6H_2O$/HDA solution with PF_5

23.3g of a saturated solution of $Al(NO_3)_3 \cdot 6H_2O$ in HDA, prepared by the reaction of $AlCl_3$ and HDA, was used. To this was added 2 wt% of PF_5 in two aliquots. On addition of the first aliquot, deposits of $NOPF_6$ formed and subsequently redissolved. After ca. 10 minutes a gelatinous precipitate formed which increased in bulk over a period of two hrs. At the end of this time a second aliquot of one weight percent PF_5 was added. This appeared to cause no change in the system, some of the larger lumps of precipitate settling out. After 24 hours, the precipitate had apparently redissolved. The solution was therefore evacuated to dryness (20^oC, 10^{-5}mm), yielding a white solid. The powder photograph indicated that the solid contained $NOPF_6$ and amorphous material. The infrared spectrum (Fig. 8-18, Table 8-12) showed only bands attributable to phosphate, though a broad strong absorbance at $670cm^{-1}$ may be assignable to an Al-F stretching mode. Bands due to co-ordinated water were also prominent. Analysis indicated the same complex mixture of fluoride and phosphate as obtained for chromium and nickel:

	Al	P	'Free' F	PF_6^-
found %	6.38	13.8	4.50	0
Atomic Ratio	1	1.89	1	

No PF_6^- was detected analytically in the product, suggesting that only small amounts of $NOPF_6$ were present. On the basis of the Al:F ratio, it would appear that the aluminium is mainly in the form of the phosphate, the $AlPO_4$:AlF_3 ratio being 2:1.

The experiment was repeated using a second portion of the aluminium solution, but after one addition of ca. one weight percent PF_5, the mixture was allowed to stand for 2 hours after which time a substantial bulk of the transient precipitate had formed. This precipitate was then filtered off, washed well with HDA and dried under vacuum (20^oC, 10^{-3}mm). The filtrate was also evaporated to dryness under vacuum. The precipitate dried rapidly to give a white solid, shown by X-ray powder photography to be completely amorphous. The infrared spectrum of this material was found to be very similar to that of the residue from the evaporated solution, described above, only phosphate and water bands being readily assignable.

Analysis of the dried precipitate again suggested a complex mixture of $AlPO_4$, AlF_3 and additional H_3PO_4 and water:

	Al	P	'Free' F
found %	7.70	13.9	6.40
Atomic Ratio	1	1.58	1.19

Here again there was slightly more phosphate than fluoride, although the ratio of phosphate to fluoride is slightly different to that of the evaporated solution product, i.e. $AlPO_4$:AlF_3 = 1.52:1.

The similarity between the results of these two analyses suggest that the products are closely related, and it is possible that the precipitate encountered in the first reaction did not in fact go into solution, but became colloidal. Similar behaviour was encountered in the analogous chromium system described above, where the bulk of the precipitate passed through a porosity 3 sinter. These observations may throw some light on the nature of the precipitates

occasionally observed when HF is reacted with an $Al/HNO_3/N_2O_4$ system, where a precipitate formed initially appears to rapidly redissolve.

(e) Reaction of metallic nickel with a solution of PF_5 in HDA

In connection with the suggestion above that nickel fluorides and phosphates are only formed in the latter stages of solution evaporation rather than in the primary mixture, it was decided to react nickel metal with a 2.2 wt. % solution of PF_5 in the HDA to form $Ni(NO_3)_2 \cdot 2H_2O$ in situ, and to examine the nature of precipitating species when the concentration of $Ni(NO_3)_2 \cdot 2H_2O$ exceeded the solubility limits for the HNO_3/N_2O_4 mixture.

A solution containing 2.2wt. % PF_5 was prepared by adding 0.59g PF_5 to 26.8g of HDA at $-196^{o}C$ under vacuum. The mixture was allowed to melt, and was shaken to dissolve all the $NOPF_6$ formed.

The pressure in the vessel was restored to atmospheric pressure with argon, and the Kel-F tube was detached and rapidly fitted with a suitable glass adaptor to maintain an argon counter-current and blanket. 0.25g of previously degreased metallic nickel was then added to the solution. An immediate reaction began, with evolution of bubbles and formation of a green solution. After 24 hr. the metal had completely dissolved, leaving a blue-green precipitate below a green solution. The mixture was filtered, and the precipitate washed with cold HDA. On examination after vacuum drying, this precipitate was found to be qualitatively identical to $Ni(NO_3)_2 \cdot 2H_2O$, only lines characteristic of this material being seen on the X-ray powder photograph, and the infra-red spectrum was identical to that of $Ni(NO_3)_2 \cdot 2H_2O$. No bands attributable to phosphate were observed. The solution was evaporated under vacuum to give a pale green-yellow solid, the X-ray powder photograph of which showed only $NOPF_6$ and NO_2PF_6. The infra-red spectrum however indicated co-ordinated nitrate, phosphate and co-ordinated water.

Analysis of the residue from the evaporation suggested a complex mixed product, containing $Ni_3(PO_4)_2$, NiF_2, NO_2PF_6, $NOPF_6$, $Ni(NO_3)_2 \cdot 2H_2O$, and H_3PO_4:

	Ni	P	'Free' F	N	PF_6^-
found %	15.9	9.93	1.05	9.89	39.8
Atomic Ratio	1	1.18	0.203	2.60	1.01

The precipitation of $Ni(NO_3)_2 \cdot 2H_2O$ in this reaction lends weight to the suggestion that this compound is stable in the solutions of PF_5 of low concentration and that it decomposes only as the concentration of $NOPF_6$, HF, H_3PO_4 etc. increases.

(f) Conclusions

These experiments show that the chemistry involved when phosphorus pentafluoride is added to solutions of metal/HDA corrosion products is complex, and mixed products, containing metal phosphates, fluorides, and possible complex polyfluorophosphates are precipitated. In the case of iron (Section 8.4(a)) the precipitated corrosion product formed when mild steel reacts with modified HDA appears to be identical to the products obtained by addition of PF_5 to a mild steel/HDA solution, lending weight to the value of these complementary experiments. The formation of $Ni(NO_3)_2 \cdot 2H_2O$ as a precipitate when nickel reacts with modified HDA is significant, and shows that $Ni(NO_3)_2 \cdot 2H_2O$ is still an important compound in the corrosion of steels by this medium.

The enhancement of corrosion of mild steel by the presence of PF_5 in HDA, and the lack of inhibition in the corresponding nickel systems, is interesting, and possibly implies that the corrosion inhibition of stainless steels occur by the formation of a chromium-containing diffusion barrier of gelatinous material, consisting mainly of the fluoride (See Section 8.4(c)).

8.5 References

1. H. Moissan, Ann. Chim. Phys., 1887, 12(6), 472.
2. H. Moissan, Bull. Soc. Chim. Paris, 1891, 5(3), 880.
3. H. Moissan, Ann. Chim. Phys., 1891, 24(6), 224.
4. R. Linke and W. Rohtmann, Z. Phys. Chem., 1937, B35, 256.
5. S. Johnson, Ph. D. Thesis, Purdue University, 1953.
6. H. Moissan, Ann. Chim. Phys., 1906, 8(8), 84
7. H. S. Gutowsky and A. D. Liehr, J. Chem. Phys., 1952, 20, 1652.
8. S. J. Kuhn and G. A. Olah, J. Am. Chem. Soc., 1961, 83(4), 4564.
9. S. J. Kuhn, Canad. J. Chem., 1962, 40(2), 1660.
10. R. J. Gillespie and O. J. Millen, J. Chem. Soc., 1950, 1050.
11. R. D. Peacock and I. L. Wilson, J. Chem. Soc. (A), 1969, 2030.
12. L. A. Woodward and L. E. Anderson, J. Inorg. Nucl. Chem., 1956, 3, 326.
13. D. W. A. Sharp and J. Thorley, J. Chem. Soc., 1963, 3557.
14. J. W. Emsley, J. Feeney and L. H. Sutcliffe, 'High Resn. nmr. Spectroscopy,' 1966, 2, 951.
15. Gmelin, "Handbuch der Anorg. Chemie," 1966, Cr(B52), 440.
16. J. W. Mellor, "A Comprehensive Treatise on Inorganic and Theoretical Chemistry," 1925, 5, 362.
17. K. Bühler and W. Bues, Z. Anorg. Chem., 1961, 308, 62.
18. "Mössbauer Spectroscopy and its Applications," IAEA Vienna 1972, 283.

9. THE EFFECT OF PF_5 IN INCREASING THE CORROSION RATE OF MILD STEEL IN HDA

In Chapter 3, it was shown that corrosion of 321 steel is greatly reduced on addition of PF_5, and that the latter is a remarkably good inhibitor. However, in Chapter 8 (Section 8.4(a)(ii)), it was observed that the reaction of mild steel with HDA was increased considerably on addition of even small amounts of PF_5. This apparent conflict is important to the understanding of the mechanism of corrosion inhibition, and therefore a quantitative study of the mild steel-HDA-PF_5 system was made.

Identical pieces of degreased and abraded mild steel (approximate dimensions 50 x 8 x 1mm) were allowed to corrode in:

A) about $15cm^3$ of uninhibited HDA in a sealed Kel-F tube
B) the same volume of modified HDA in a Kel-F tube
C) the same volume of uninhibited HDA in a glass tube
D) the same volume of modified HDA in a glass tube

The surface to volume ratio for these experiments was constant at about $0.06cm^{-1}$. The solutions were sampled over periods of time, analysed for iron content, and the visible condition noted, (Table 9-1). The results of the iron analyses are plotted graphically (Fig. 9-1). It is clear that PF_5 increases the rate of corrosion of mild steel in HDA, which is quite the opposite of its effect on 321 steel. The graphs also indicate that there is a difference between the corrosion rates in glass and in fluoro-plastic tubes. This is no doubt real, but at present it is a side-issue and will not be discussed further. Phase separation also occurred in these experiments (see Table 9-1), brought about by iron concentrations in excess of 10^4 ppm Fe in the HDA.

As soon as the modified HDA containing mild steel in the glass tube (experiment D, Fig. 9-1) showed phase separation, the HDA was sampled, and the mild steel removed with tweezers, dried under argon, and added to $15cm^3$ of fresh HDA. Subsequent measurement of the corrosion rate, (curve D_a, Fig. 9-1)

Table 9-1. (1 of 2)

Iron analyses and visual condition of mild steel in HDA and modified HDA experiments

	on preparation	after 12 hours	after 24 hours	after 2 days	after 3 days	after 4 days	after 1 week
(A) Mild steel/ HDA in Kel-F	steel slowly blackening	steel black, few bubbles. HDA orange	steel black, yellow froth just appearing	steel black, froth and ppt. forming on liquid surface	steel black, HDA orange, no bubbles on surface but faint ppt.	steel grey, HDA orange, no bubbles, some gelat. material on liquid surface	steel grey, HDA orange, some bubbles on surface
|Fe| ppm							
(B) Mild Steel/ modified HDA in Kel-F	steel blackening instantly, yellow froth appearing	steel black, yellow froth on liquid surface, fine gelat. ppt. fills 1/2 tube	steel grey, otherwise as before	as before, froth going, ppt. 2.5cm thick	steel grey, HDA red/brown, no bubbles or froth but much ppt.	as before, possibly with phase separation	as before
|Fe| ppm							
(C) Mild steel/ HDA in glass	steel slowly blackening		steel black, HDA orange, few bubbles on surface	steel grey, few bubbles, some gelat. material		steel grey, HDA orange	
|Fe| ppm							
(D) Mild steel/ modified HDA in glass	steel blackened instantly, yellow froth, bubbles and ppt. after 5 mins.	steel black, yellow froth on liquid surface, fine gelat. ppt. fills 1/2 tube	as before, but froth absent	as before	steel grey, HDA red/brown, no bubbles or froth, much ppt, phase separation beginning		
|Fe| ppm					2.45×10^4		
(Da) Mild steel from experiment (D)/ fresh HDA in glass		steel black, HDA orange			steel grey, HDA orange		
|Fe| ppm							
(Db) Fresh mild steel/ modified HDA from experiment (D) in glass		steel still bright no ppt. HDA red/brown			as before		
|Fe| ppm							

Table 9-1. (2 of 2)

Iron analyses and visual condition of mild steel in HDA and modified HDA experiments

	after 11 days	after 14 days	after 22 days	after 28 days	after 30 days	after 57 days
(A)		as before	steel grey, HDA orange	as before	possible phase separation	as before
[Fe] ppm	3.04×10^3		6.67×10^3	8.34×10^3		
(B)		as before, with definite phase separation	as before, Kel-F tube distorting - experiment transferred to glass tube	as before	HDA opaque red/brown	much N_2O_4 separated. HDA solution black
[Fe] ppm	2.38×10^4		4.00×10^4	4.45×10^4		
(C)	after 9 days	after 12 days as before	after 20 days as before	after 26 days as before	after 28 days phase separation	after 55 days as before
[Fe] ppm	3.92×10^3		7.80×10^3	9.25×10^3		
(Da)	after 8 days from using fresh HDA	after 11 days as before	after 19 days as before with fine grey ppt. (metal?)	after 25 days as before, with possible phase separation	after 27 days as before, red/brown HDA, possible phase separation	after 54 days as before
[Fe] ppm	5.06×10^3		9.90×10^3	1.18×10^4		
(Db)	after 8 days from adding fresh mild steel, ∴ after 11 days of reaction of the modified HDA	after 11 days, steel grey, no ppt., HDA red/brown, distinct phase separation	after 19 days as before	after 25 days as before	after 27 days as before	after 54 days as before
[Fe] ppm	5.85×10^4		7.65×10^4	7.32×10^4		

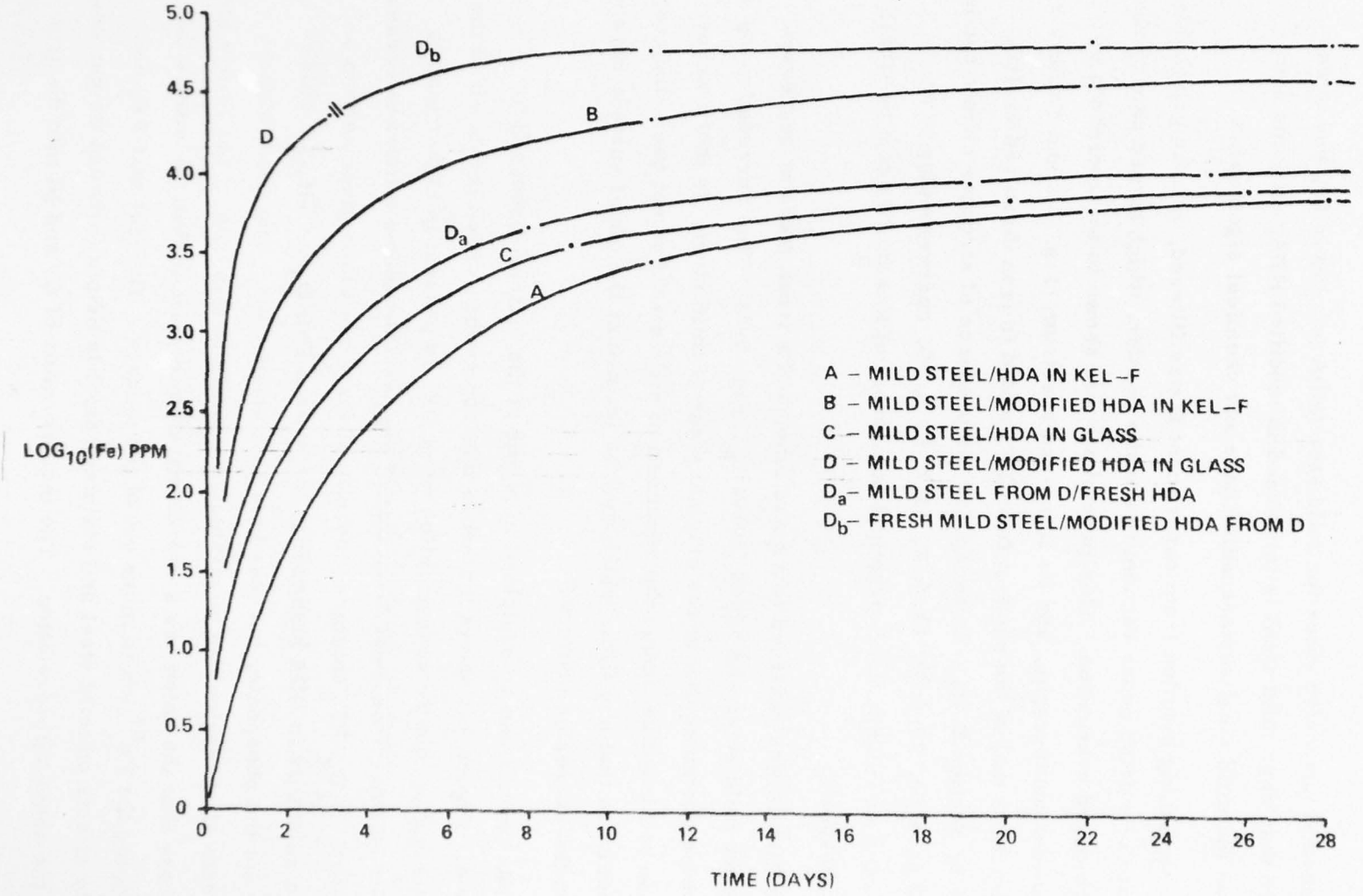


Figure 9-1. Iron Concentration vs Time for Mild Steel/HDA or Modified HDA Experiments

showed normal corrosion rates for mild steel/HDA (cf. curve C), and it was concluded that when mild steel is immersed in modified HDA, no films are formed on the mild steel surface which have any chemical significance.

The remaining solution from experiment D was filtered, and the gelatinous precipitate was dried under vacuum to a white powder, which turned pale brown under prolonged evacuation. This precipitate was shown to be amorphous by X-ray powder photography, and its infra-red spectrum (Fig. 9-2 and Table 9-2) was identical to that of the product from PF_5 added to iron dissolved in HDA (Chapter 8, Section 8.4(a)(i)), except for the presence of stronger nitrate bands. Analysis gave Fe, 25.4; P, 11.5; F, 13.3; N, 2.5%, corresponding to an Fe:P:F ratio of 1:0.8:1.5. A principal component of this could again be iron(III) difluorophosphate.

The filtrate was returned to a glass tube, and a fresh piece of degreased and abraded mild steel was added (curve D_b, Fig. 9-1). This corroded along a curve which continued that of the original piece of mild steel. In other words, corrosion continued as though the specimen of mild steel had not been changed, which indicates that any films which may be formed at the metal surface have no effect on the corrosion process.

These results can be explained in terms of the factors discussed in Chapter 4. Figure 9-1 shows that when the iron concentration levels off to the saturation value, the Fe concentration when PF_5 is present is higher than in uninhibited HDA. This must mean that of the possible anions which are present in the HNO_3-N_2O_4-PF_5 mixture, there is at least one which gives an iron salt having a solubility in HDA higher than the nitrate $Fe(NO_3)_3 \cdot 2H_2O$. This is clearly not the phosphate, but may be a fluorophosphate. The much higher initial rate of corrosion can be attributed entirely to this factor, but it may also be the case that the anion has a coordinating power higher than the nitrate ion, thus helping the Fe^{n+} ion to move out of the surface. The fact that PF_5 has opposite effects on mild steel and stainless steel is helpful because we can now extend the above interpretation. The incorporation of Cr and Ni into the iron

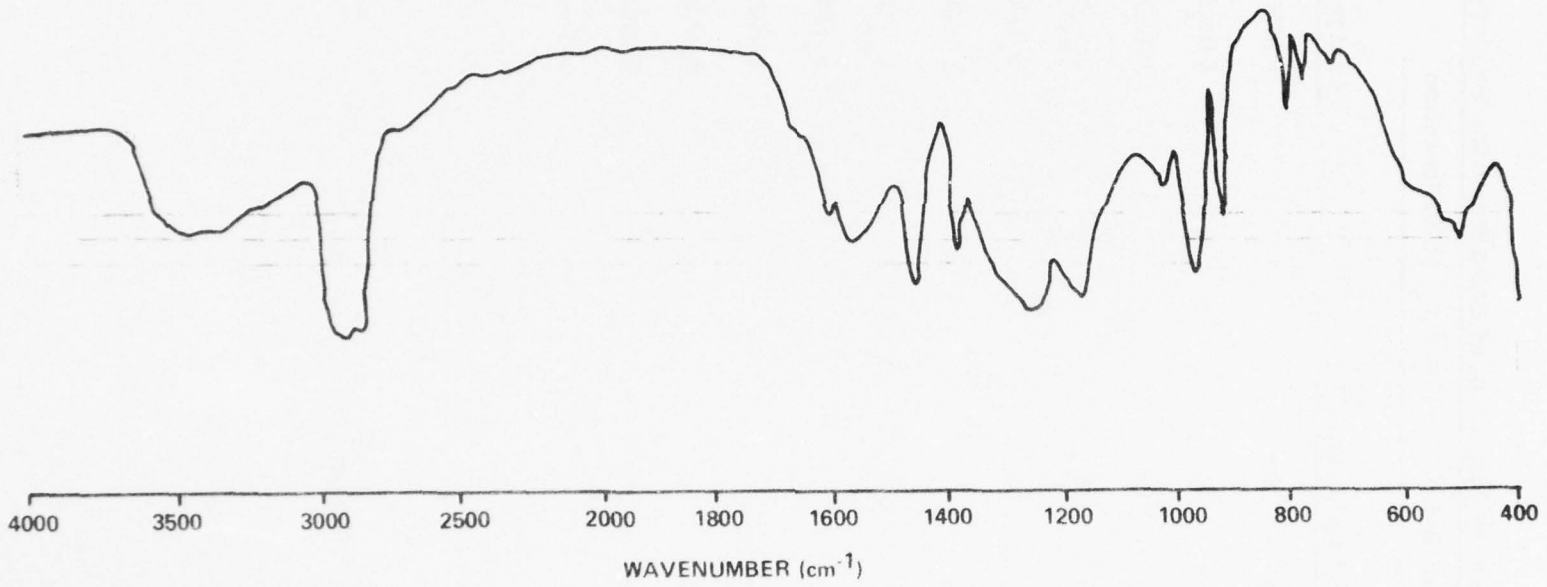


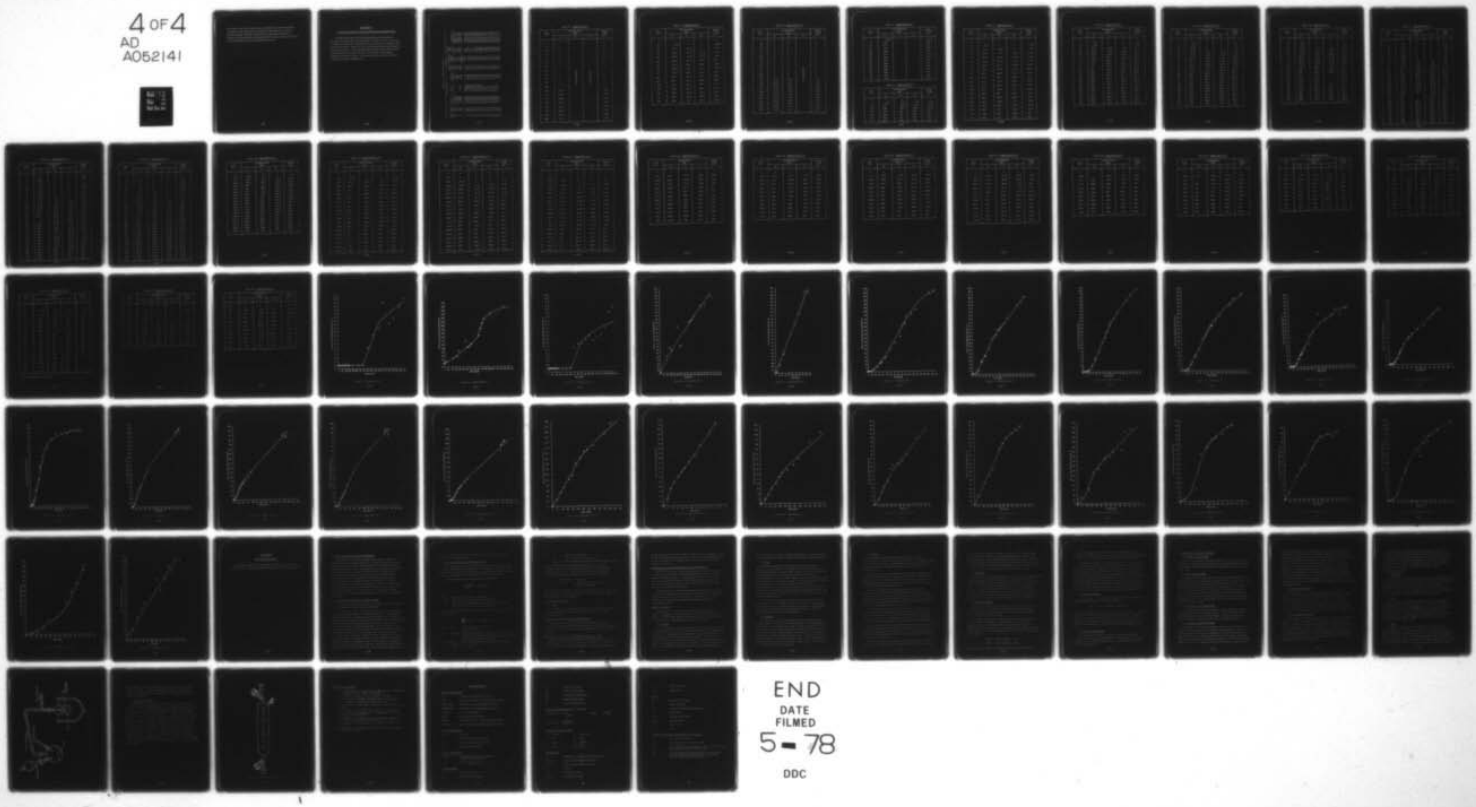
Figure 9-2. IR Spectrum of Solid Product of Mild Steel/Modified (0.6wt% PF_5) HDA Reaction

Table 9-2. Infrared Spectrum of Solid Reaction Products of Mild Steel/ Modified (0.6 wt.% PF_5) HDA Reaction

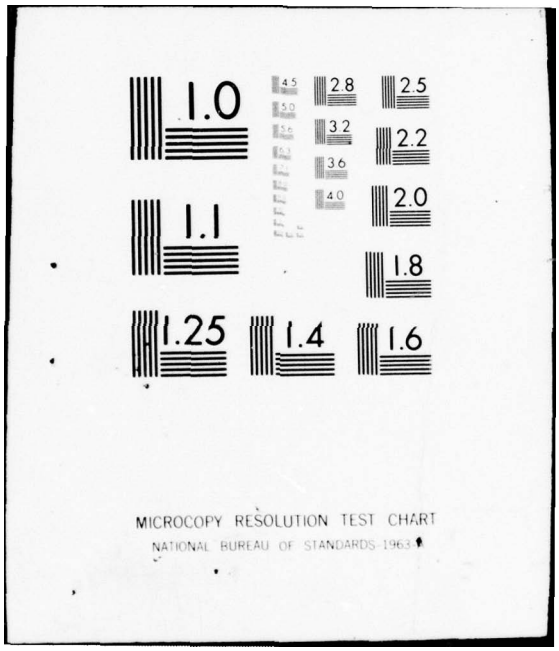
Absorption bands (cm^{-1})			Assignment
3400	m,	vbr	ν(OH)
1600	m,	sp	$\delta(H_2O)$
1570	m,	br	$\nu(NO_3)$
1260	s,	br	$\nu_{as}(PO_2)$ or $\nu(NO_3)$
1160	s,	br	$\nu_s(PO_2)$
1015	m		$\nu(NO_3)$
960	s		$\nu_{as}(PF_2)$
910	s		$\nu_s(PF_2)$
800	m		$\pi(NO_3)$
770	m		$\delta(NO_3)$
720	w		$\delta(NO_3)$
500	s		ν(Fe-F) or δ(O-P-F)

AD-A052 141 NOTTINGHAM UNIV (ENGLAND) DEPT OF INORGANIC CHEMISTRY F/G 7/2
HDA CORROSION CHEMISTRY.(U)
DEC 77 C C ADDISON, N LOGAN AFOSR-74-2709
UNCLASSIFIED AFRPL-TR-77-65 NL

4 OF 4
AD
A052141



END
DATE
FILMED
5-78
DDC


1.0
1.1
1.25
1.4
1.6
1.8
2.0
2.2
2.5
2.8
3.2
3.6
4.0
4.5
5.0
5.6
6.3
MICROCOPY RESOLUTION TEST CHART
NATIONAL BUREAU OF STANDARDS-1963-A

matrix gives very low corrosion rates, so that there is an anion produced by the addition of PF_5 which gives a salt with Cr or Ni which has a very low solubility in HDA. This general point has been discussed in Chapter 4; Chapter 8 has indicated some of the species which can be present in the mixture, so that the pattern for future solubility studies is clear.

APPENDIX A

Concentration Data from Corrosion Studies with Uninhibited HDA

This appendix contains the tables and graphs of the results for the corrosion rate studies described in Chapter 3. Table A-1 forms a key to the remainder of the appendix. Experiments are given numbers according to their position in this table. References are to the description of the experiments in the body of the report. The remaining tables give the relation between metal concentration in the solution, and time. This relation is also depicted graphically following the tables. Concentration values are measured by the techniques described in Appendix B.3.

Table A-1. Experimental Details

Expt No.	Temp. °C	Specimen Details: Initial wt. g	Specimen Details: final wt. g	Specimen Details: Surface Area cm^2	Liquid Details: Initial volume cm^3	Liquid Details: Composition % N_2O_4 in HNO_3	Surface to volume ratio cm^{-1}	Reference
1	0.0	31.18322	-	13.952	100.0	44.2	0.139	Section 3.1(a)
2	22.0	30.43512	-	14.207	99.0	44.0	0.143	Section 3.1(b)
3	0.0	31.24700	-	12.852	100.0	44.2	0.128	Section 3.1(c)
4	22.0	5.33404	2.82012	5.733	100.0	44.0	0.0573	Section 3.1(d)
5	0.0	31.17520	-	13.880	100.0	25% N_2O_5 in HNO_3	0.139	Section 3.1(e)
6	20.5	30.30510	28.88815	14.170	122.3	HNO_3	0.116	Section 3.2(a)
7	20.5	30.43630	29.17918	14.169	134.0	3.51	0.106	Section 3.2(a)
8	20.5	30.07075	29.26801	14.049	157.0	14.36	0.0895	Section 3.2(a)
9	20.5	30.45510	29.95822	14.192	128.0	23.21	0.111	Section 3.2(a)
10	20.5	29.18331	28.79652	13.279	117.0	34.64	0.113	Section 3.2(a)
11	20.5	29.15977	29.01049	13.258	107.0	44.82	0.124	Section 3.2(a)
12	20.5	30.36602	30.32559	14.128	120.0	51.05	0.118	Section 3.2(a)
13	14.9	30.69081	26.25724	13.760	145.6	HNO_3	0.0945	Section 3.2(a)
14	14.9	30.75105	28.50465	13.782	146.8	15.44	0.0939	Section 3.2(a)
15	14.9	30.64784	29.80783	13.193	152.3	32.63	0.0866	Section 3.2(a)
16	14.9	29.70163	29.44613	13.919	150.3	46.37	0.0926	Section 3.2(a)
17	27.3	30.75364	25.686	14.260	139.5	HNO_3	0.102	Section 3.2(a)
18	27.3	30.28701	27.425	13.627	143.0	14.21	0.0953	Section 3.2(a)
19	27.3	30.70952	29.310	13.757	152.3	31.04	0.0903	Section 3.2(a)
20	27.3	29.97669	29.662	13.490	143.7	42.91	0.0939	Section 3.2(a)
21	31.0	30.78935	25.130	13.790	141.1	HNO_3	0.0977	Section 3.2(a)
22	31.0	30.35949	27.080	13.635	145.4	15.20	0.0938	Section 3.2(a)
23	31.0	29.02296	27.511	13.239	144.8	29.61	0.0914	Section 3.2(a)
24	31.0	30.94914	30.383	13.837	148.4	43.44	0.0932	Section 3.2(a)
25	20.0	25.32397	17.47840	13.053	400.1	HNO_3	0.0326	Section 3.3(e)
26	20.0	28.30707	-	13.607	150.0	48.78	0.0907	Section 3.3(b)
27	20.0	-	-	13.607	150.3	48.78	0.0905	Section 3.3(b)

Table A-2. Experiment No. 1

Time hrs.	Concentrations ppm			Weight Loss $g.m.^{-2}$
	Fe	Cr	Ni	
0	0	Not measurable	Not measurable	0
24	0			0
48	0			0
72	0			0
96	0			0
120	0			0
144	0			0
168	0			0
192	0			0
240	0			0
336	0			0
408	0			0
504	16.60			2.39
576	28.37			4.09
672	34.45			4.99
744	58.63			8.47
840	38.64			5.58
912	44.14			6.37
1008	54.57			7.88
1080	62.10			8.97

Table A-3. Experiment No. 2

Time hrs.	Concentrations ppm			Weight Loss $g.m.^{-2}$
	Fe	Cr	Ni	
0	0	0	0	0
24	71.24	0	0	8.048
120	187.6	37.77	0	25.11
168	197.4	71.51	56.74	36.07
192	452.8	76.19	62.35	65.02
288	846.6	131.2	112.9	118.7
312	541.0	120.6	109.0	84.67
336	580.0	134.3	113.7	90.77
360	677.9	130.6	125.0	101.7
456	1032	140.4	181.1	144.9
480	1383	153.9	186.0	182.6
504	1659	151.4	197.7	211.3
528	1852	170.0	205.6	233.2
624	2088	176.5	232.6	259.7
696	2039	186.6	233.9	256.0
792	2354	191.1	251.0	288.4

Table A-4. Experiment No. 3

Time hrs.	Concentrations ppm			Weight Loss $g.m.^{-2}$
	Fe	Cr	Ni	
0	0	0	Not measurable	0
24	0	0		0
48	0	0		0
72	0	0		0
96	0	0		0
120	0	0		0
144	0	0		0
168	0	0		0
192	0	0		0
216	0	0		0
312	0	0		0
384	0	0		0
480	0	0		0
552	23.42	3.69		2.77
648	26.17	6.67		3.35
720	27.96	6.07		3.47
816	30.94	7.33		3.89
888	36.15	7.41		4.40
984	30.90	6.16		3.78
1056	34.17	7.98		4.26
1152	40.92	4.30		4.55
1224	51.48	4.70		5.57
1320	72.42	6.18		7.63
1392	79.26	6.19		8.32

Table A-5. Experiment No. 4

Time hrs.	Concentrations ppm			Weight Loss $g.m.^{-2}$
	Fe	Cr	Ni	
0	64.62			18.56
96	1408			400.6
144	2115			599.7
168	1901			540.0
264	3920			1096
288	2143			611.9
312	2270			646.2
432	4341			1193
456	4464			1225
480	4580			1254
504	4856			1324
600	5859			1575
672	5979			1604
768	6780			1800

Table A-6. Experiment No. 5

Time hrs.	*Concentrations* ppm			Weight Loss $g.m.^{-2}$
	Fe	Cr	Ni	
0	0	0	0	0
4	72.00	36.71	77.40	22.00
24	1153	258.8	176.5	186.1
48	3098	389.1	408.2	453.4
120	7368	1270	1257	1141
144	8849	1651	1618	1394
168	13580	1546	1667	1919
192	13420	1605	1733	1915

Table A-7. Experiment No. 6

Time hrs.	Concentrations ppm			Weight Loss $g.m.^{-2}$
	Fe	Cr	Ni	
0	0	0	0	0
5	4.20	0	0	0.550
18	35.61	4.44	0	5.21
31	147.4	31.75	23.96	26.22
43	304.2	72.29	47.65	54.48
49	356.8	86.56	61.57	64.71
66	647.6	162.1	90.02	114.3
73	727.2	179.9	97.21	127.3
91	1034	248.9	136.9	178.6
97	1114	281.1	188.6	198.7
121	1716	397.8	265.8	295.2
146	2114	623.6	322.3	377.0
174	2661	770.7	377.6	465.9
187	3521	1057	359.1	597.9
198	3887	947.9	493.2	643.2
209	4482	985.6	613.1	730.0
235	4658	1064	632.8	762.9
259	5073	1147	670.4	821.3
331	6450	1504	889.9	1039
355	6489	1633	982.9	1068

Table A-8. Experiment No. 7

Time hrs.	Concentrations ppm			Weight Loss $g.m.^{-2}$
	Fe	Cr	Ni	
0	0	0	0	0
5	4.24	0	0	0.611
18	13.34	0	0	1.91
31	102.8	10.84	9.65	17.51
43	204.9	37.96	31.36	38.79
49	277.8	46.01	59.92	54.11
66	870.0	156.8	78.46	154.2
73	735.9	182.5	109.7	143.5
91	1123	220.5	146.9	207.0
97	1167	230.9	154.0	215.0
121	1661	310.5	217.9	300.7
146	2284	418.5	292.9	408.2
163	2442	447.8	323.6	437.1
174	2530	491.8	337.5	456.2
187	2835	515.6	390.4	505.8
198	2879	524.0	396.2	513.3
209	3038	560.9	414.3	540.7
235	3278	615.3	464.6	584.4
259	3626	679.9	507.4	641.7
331	4564	822.4	648.3	794.0
355	4814	854.7	678.3	836.3
406	5206	894.4	734.5	892.4

Table A-9. Experiment No. 8

Time hrs.	Concentrations ppm			Weight Loss $g.m.^{-2}$
	Fe	Cr	Ni	
0	0	0	0	0
5	9.40	0	0	1.61
18	21.82	0	0	3.73
31	19.02	0	0	3.26
43	35.88	4.59	5.18	7.75
49	53.28	8.74	9.14	12.03
66	201.6	32.00	17.92	42.05
73	251.1	43.51	31.58	54.38
91	451.3	68.95	49.30	94.35
97	459.3	76.12	50.91	97.09
121	675.2	110.7	81.22	142.5
146	1063	192.4	103.3	221.6
163	1208	228.9	125.5	254.2
174	1363	255.3	175.4	290.9
187	1417	255.6	188.7	301.6
198	1622	291.2	255.6	345.0
209	1717	298.9	232.1	362.0
235	1859	333.0	244.8	391.1
259	2090	363.7	277.2	436.2
331	2550	455.3	340.7	529.7
355	2751	490.1	371.0	569.9
406	2980	510.4	393.4	610.6

Table A-10. Experiment No. 9

Time hrs.	Concentrations ppm			Weight Loss $g.m.^{-2}$
	Fe	Cr	Ni	
0	0	0	0	0
18	8.09	0	0	1.16
31	14.10	0	0	2.01
43	36.40	6.72	4.96	6.80
49	51.40	8.70	9.20	9.77
66	182.8	26.26	24.50	32.60
73	256.2	37.24	29.68	44.92
91	425.6	64.43	52.30	74.85
97	474.4	76.05	53.94	83.26
121	632.1	108.0	76.34	111.7
146	1006	172.8	98.17	173.0
163	1090	190.6	108.5	187.8
174	1191	211.5	-	205.8
187	1303	218.4	-	223.3
198	1307	239.9	-	236.6
209	1370	242.7	172.2	239.1
235	1593	265.5	195.4	273.1
259	1675	301.4	221.5	291.1
331	2046	363.7	268.6	350.0
355	2247	392.4	295.4	382.2
406	2420	411.4	321.2	408.8

Table A-11. Experiment No. 10

Time hrs.	Concentrations ppm			Weight Loss $g.m.^{-2}$
	Fe	Cr	Ni	
0	0	0	0	0
5	7.66	0	0	0.811
18	5.86	0	0	0.832
43	7.70	0	0	1.08
49	10.58	0	0	1.48
66	24.52	0	0	3.40
73	32.88	0	0	4.53
91	62.99	8.23	7.41	10.69
97	67.19	10.67	8.58	11.74
121	118.1	21.28	18.47	21.19
146	257.7	34.05	26.39	42.17
163	326.0	43.16	33.26	44.25
174	380.8	51.49	38.79	61.85
187	410.8	56.62	46.07	67.25
198	433.8	62.89	50.84	71.54
209	461.2	75.00	56.44	77.17
235	541.9	87.95	67.60	90.12
259	600.8	102.3	77.38	100.3
331	757.1	-	99.47	125.4
355	1095	-	108.4	170.6
406	1169	206.2	142.8	188.7
502	1438	230.1	191.1	288.8
624	1602	307.4	210.6	259.1
723	1708	282.8	232.9	279.2
789	2024	306.5	243.9	310.9
885	1779	329.2	264.2	288.2
962	1948	346.7	294.2	316.3
984	1980	360.1	296.2	317.6

Table A-12. Experiment No. 11

Time hrs.	Concentrations ppm			Weight Loss $g.m.^{-2}$
	Fe	Cr	Ni	
0	0	0	0	0
5	3.71	0	0	0.488
18	14.90	0	0	1.94
31	9.07	0	0	1.19
43	4.76	0	0	0.644
49	6.74	0	0	0.895
66	13.24	0	0	1.71
73	16.08	0	0	2.06
91	32.00	5.66	0	4.72
97	35.67	5.66	4.86	5.76
121	57.40	11.32	7.98	9.44
146	85.46	14.87	11.74	13.66
163	101.4	16.91	12.71	15.89
174	160.2	22.49	16.28	23.84
187	176.5	22.81	18.83	26.06
198	[illegible].4	27.72	20.58	29.90
209	211.4	30.28	21.67	31.21
235	260.9	35.67	27.30	37.99
259	305.5	42.86	34.08	44.47
331	402.1	56.61	45.92	57.84
355	428.6	61.97	48.57	61.58
406	469.0	64.84	57.78	67.18
502	540.9	75.90	72.65	77.52
624	608.0	85.51	80.15	86.32
723	730.5	97.27	91.34	101.3
789	817.4	105.1	96.03	111.4
885	875.5	120.2	109.8	120.1
962	912.7	157.6	110.6	127.7
984	918.0	159.5	127.9	130.1

Table A-13. Experiment No. 12

Time hrs.	Concentrations ppm			Weight Loss $g.m.^{-2}$
	Fe	Cr	Ni	
0	0	0	0	0
5	0	0	0	0
18	4.19	0	0	0.574
31	7.61	0	0	1.04
43	3.77	0	0	0.521
49	6.23	0	0	0.850
66	16.12	4.44	0	2.74
73	16.59	3.67	0	2.70
91	26.23	5.48	0	4.19
97	47.73	6.70	6.55	7.96
121	48.60	7.44	5.86	8.08
146	60.94	11.65	7.66	10.40
163	74.80	12.87	8.07	12.35
174	78.12	14.55	8.87	13.07
187	113.9	15.93	12.30	18.07
198	116.6	17.67	13.59	18.80
209	123.3	20.15	11.76	19.65
235	135.9	21.82	13.37	21.46
259	149.7	24.55	16.35	23.86
331	178.1	28.06	17.58	27.51
355	189.2	26.65	21.85	29.37
406	210.3	30.16	24.87	32.54
502	244.2	32.71	26.80	34.63
624	225.4	33.50	28.30	35.03
723	223.9	34.77	29.40	35.12
789	230.4	36.71	30.31	36.15
885	233.5	37.19	30.67	36.58
862	230.6	37.52	31.23	36.37
984	224.1	36.46	30.35	35.47

Table A-14. Experiment No. 13

Time hrs.	Concentrations ppm			Weight Loss $g.m.^{-2}$
	Fe	Cr	Ni	
0	0	0	0	0
49.5	44.86	6.31	0	8.23
122.5	595.2	114.9	79.74	126.2
168.0	884.3	183.3	129.0	190.8
218.5	1898	377.6	176.2	388.6
287.5	2586	494.9	329.2	538.5
340.5	3171	632.0	425.6	665.7
383.5	3619	735.1	482.4	759.5
455.5	4108	1166	579.4	915.2
503.5	4336	1305	604.4	974.8
552.0	4695	1410	663.2	1053
628.0	5133	1505	721.9	1142
796.5	6881	1862	862.5	1476
959.0	8290	1992	900.0	1708
2688.0	18158	3829	1209	3469
2713.0	18170	4809	1267	3622
2736.0	18269	4976	1189	3649
2831.5	18653	5245	1326	3762
2858.0	18648	5296	1241	3756
2879.5	18655	5732	1260	3539

Table A-15. Experiment No. 14

Time hrs.	Concentrations ppm			Weight Loss $g.m.^{-2}$
	Fe	Cr	Ni	
0	0	0	0	0
49.5	19.33	0	0	3.24
122.5	355.2	64.59	47.13	77.91
168.0	603.6	110.2	80.19	132.0
218.5	1079	243.7	110.8	237.3
287.5	1577	349.0	153.9	342.8
340.5	1889	375.2	253.9	413.9
383.5	2115	441.4	284.7	466.0
455.5	2474	455.9	328.4	535.9
503.5	2505	541.3	314.4	549.0
552.0	2762	552.8	359.1	598.3
628.0	2958	638.6	412.9	650.8
796.5	3526	746.0	482.8	766.6
959.0	4029	1134	558.6	915.6
2688.0	9510	2563	1243	2079
2713.0	9511	2860	1265	2128
2736.0	9169	2712	1226	2048
2831.5	9757	2968	1340	2191
2858.0	9565	2151	1309	2037
2879.5	9688	2046	1306	2039

Table A-16. Experiment No. 15

Time hrs.	Concentrations ppm			Weight Loss $g.m.^{-2}$
	Fe	Cr	Ni	
0	0	0	0	0
49.5	0	0	0	0
122.5	30.91	0	0	5.76
168.0	74.28	9.91	9.88	17.47
218.5	168.5	34.36	21.28	41.41
287.5	320.3	67.32	41.31	78.85
340.5	391.9	87.11	52.15	97.41
383.5	444.9	107.4	62.95	112.6
455.5	557.5	132.6	78.97	140.1
503.5	643.5	127.0	84.57	155.4
552.0	692.8	184.6	93.83	175.9
628.0	986.7	208.0	104.8	233.5
796.5	1238	268.7	168.7	298.9
959.0	1466	311.1	213.5	353.4
2688.0	2078	1023	418.8	787.5
2713.0	3177	1164	414.9	827.8
2736.0	3044	1233	430.4	819.6
2831.5	3078	1229	447.3	827.4
2858.0	3063	883.5	430.5	764.6
2879.5	3178	877.8	439.6	785.8

Table A-17. Experiment No. 16

Time hrs.	Concentrations ppm			Weight Loss $g.m.^{-2}$
	Fe	Cr	Ni	
0	0	0	0	0
49.5	0	0	0	0
122.5	15.53	0	0	2.73
168.0	33.14	0	0	5.80
218.5	59.53	11.61	10.49	14.19
287.5	109.2	20.57	13.01	24.71
340.5	138.4	28.02	19.55	32.09
383.5	174.7	32.85	20.34	39.20
455.5	216.6	41.48	26.57	48.70
503.5	237.6	36.80	29.57	51.99
552.0	264.0	40.35	38.81	58.50
628.0	294.8	47.90	38.00	64.60
796.5	368.1	61.06	45.20	79.80
959.0	420.4	70.23	51.19	90.51
2688.0	934.1	196.2	141.2	206.7
2713.0	1084	201.2	138.4	230.7
2736.0	1074	233.2	134.2	233.5
2831.5	1123	229.8	148.8	242.8
2858.0	1163	1485	144.8	251.3
2879.5	1129	248.1	149.1	246.7

Table A-18. Experiment No. 17

Time hrs.	Concentrations ppm			Weight Loss $g.m.^{-2}$
	Fe	Cr	Ni	
0	0	0	0	0
72.5	1311	311.1	143.6	262.5
122.0	2644	610.9	343.9	533.1
172.5	3727	729.4	514.8	734.2
240.5	4877	1307	705.3	1013
293.5	5516	1556	824.9	1159
336.5	8245	1829	926.7	1603
408.5	9190	1948	1388	1820
456.5	10569	2364	1342	2067
506.0	10886	2406	1429	2130
581.0	11650	2652	1514	2282
749.5	14232	3058	1808	2735
912.0	16325	3307	2137	3100

Table A-19. Experiment No. 18

Time hrs.	Concentrations ppm			Weight Loss $g.m.^{-2}$
	Fe	Cr	Ni	
0	0	0	0	0
72.5	712.0	111.9	96.99	152.0
122.0	1630	381.8	206.5	364.5
172.5	2263	475.0	294.5	497.0
240.5	2687	578.4	415.8	601.6
293.5	3227	659.7	494.8	714.1
336.5	3443	776.5	541.5	774.5
408.5	3835	1151	610.9	906.6
506.0	4475	1295	652.7	1035
581.0	5681	1444	714.5	1254
749.5	7046	1675	801.2	1512
912.0	7715	1906	1143	1701

Table A-20. Experiment No. 19

Time hrs.	Concentrations ppm			Weight Loss $g.m.^{-2}$
	Fe	Cr	Ni	
0	0	0	0	0
72.5	302.8	39.04	42.34	69.12
122.0	586.5	117.1	81.36	140.7
172.5	979.9	239.1	113.0	237.9
240.5	1308	299.8	147.3	312.5
293.5	1672	368.6	241.4	404.8
336.5	1981	393.1	264.0	466.7
408.5	2172	422.3	304.2	511.7
506.0	2478	517.5	337.6	586.0
581.0	2889	610.3	404.7	682.6
749.5	3752	1073	542.4	928.5
912.0	4365	1273	640.6	1080

Table A-21. Experiment No. 20

Time hrs.	Concentrations ppm			Weight Loss $g.m.^{-2}$
	Fe	Cr	Ni	
0	0	0	0	0
72.5	112.9	15.82	18.18	26.57
122.0	319.5	48.87	42.20	73.93
172.5	426.9	98.96	57.36	104.7
240.5	579.0	137.4	77.00	141.9
293.5	940.7	167.7	91.42	213.4
336.5	1017	210.1	96.25	235.0
408.5	1104	187.0	100.1	246.7
456.5	1058	194.0	94.85	239.1
506.0	1144	211.9	104.4	258.4
581.0	1315	237.0	117.1	293.8
749.5	1743	325.9	206.5	395.8
912.0	1998	363.9	259.3	453.5

Table A-22. Experiment No. 21

Time hrs.	Concentrations ppm			Weight Loss $g.m.^{-2}$
	Fe	Cr	Ni	
0	0	0	0	0
48.5	-	332.1	151.1	308.2
121.5	3684	870.7	504.7	782.9
170.5	4884	1244	692.7	1052
221.0	5609	1542	867.7	1234
294.5	9530	2041	1443	1989
341.5	10560	2242	1578	2193
385.0	11860	2225	1742	2409
457.0	12480	2411	1962	2560
509.5	12970	2882	1820	2680
554.5	13690	2918	1938	2807

Table A-23. Experiment No. 22

Time hrs.	Concentrations ppm			Weight Loss $g.m.^{-2}$
	Fe	Cr	Ni	
0	0	0	0	0
48.5	621.9	106.8	83.04	136.5
121.5	-	499.1	312.2	303.4
170.5	2795	661.5	375.4	638.5
221.0	3191	717.1	455.4	726.0
294.5	3942	1201	577.8	947.9
341.5	4151	1222	631.5	994.0
385.0	4495	1293	708.5	1073
475.0	4629	1409	744.3	1119
509.5	6713	1539	949.0	1503
554.5	7031	1688	923.4	1572

Table A-24. Experiment No. 23

Time hrs.	Concentrations ppm			Weight Loss $g.m.^{-2}$
	Fe	Cr	Ni	
0	0	0	0	0
48.5	113.9	18.51	17.40	26.57
170.5	552.6	99.58	77.93	128.1
221.0	1996	553.3	282.2	493.0
294.5	2374	527.2	344.5	564.4
341.5	2645	710.5	389.9	649.9
385.0	2778	676.0	411.0	670.2
457.0	2976	665.7	446.8	707.9
509.5	3355	689.6	470.9	779.4
554.5	3349	739.8	513.8	793.9

Table A-25. Experiment No. 24

Time hrs.	Concentrations ppm			Weight Loss $g.m.^{-2}$
	Fe	Cr	Ni	
0	0	0	0	0
48.5	116.3	18.75	15.80	26.50
121.5	438.0	75.68	59.91	100.0
170.5	548.1	99.85	75.07	126.1
221.0	587.2	145.9	84.08	142.3
294.5	893.9	234.4	103.7	213.2
341.5	1021	275.2	109.6	242.7
385.0	1121	282.8	117.5	262.1
457.0	1162	310.5	123.0	274.5
509.5	1148	249.4	116.4	261.0
554.5	1238	257.8	162.3	284.8

Table A-26. Experiment No. 25

Time hrs.	Concentrations ppm			Weight Loss $g.m.^{-2}$
	Fe	Cr	Ni	
0	0	0	0	0
24	49.20	17.54	15.26	38.37
48	592.0	98.38	68.15	354.2
72	1963	353.4	148.7	1148
94	2589	489.4	292.4	1569
164	4444	659.7	531.4	2618
170	4754	715.7	563.4	2354
191	6937	1474	628.9	3022
194	7157	1489	623.4	3344
212	7914	1423	682.6	3086
217	8053	1688	703.4	3404
264	9227	1931	938.8	3684
336	9351	2078	1020	4126
360	10160	2953	1693	
384	10620	1056	1431	
408	11110	2457	1654	
432	11320	2381	1676	

Stirring commenced after 187 hours.

Table A-27. Experiment No. 26

Time hrs.	Concentrations ppm			Weight Loss $g.m.^{-2}$
	Fe	Cr	Ni	
0	0	0	0	0
24	3.92	0	0	0.707
48	7.39	0	0	1.33
72	14.24	0	0	2.55
94	19.35	5.77	7.75	5.84
168	52.83	12.10	6.48	12.60
192	72.71	17.03	9.29	17.42
216	87.57	18.54	12.18	20.75
240	110.3	25.21	13.85	26.09
264	134.2	32.40	17.37	32.00

Table A-28. Experiment No. 27

Time hrs.	Concentrations ppm			Weight Loss $g.m.^{-2}$
	Fe	Cr	Ni	
264	0	0	0	32.00
288	38.76	7.40	5.57	41.36
312	179.0	21.49	18.40	71.39
336	292.9	31.65	26.61	95.00
360	341.5	41.11	35.28	106.8
432	589.3	86.49	61.43	163.0
456	473.0	50.16	66.11	137.2
480	638.3	72.75	42.67	165.7
504	760.7	97.47	66.70	195.2
528	694.2	133.2	74.71	183.6
600	799.4	126.5	81.96	209.2

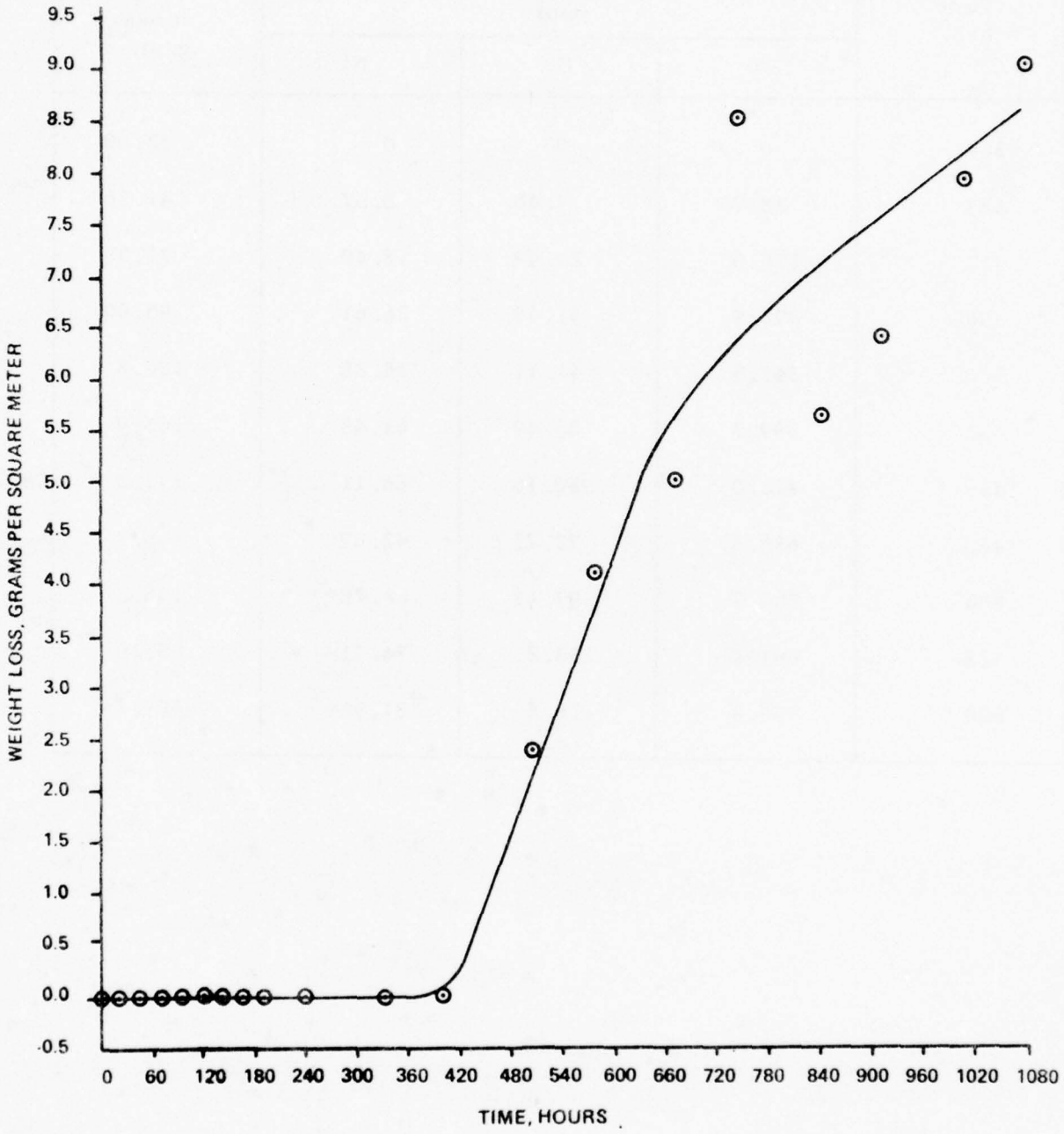


Figure A-1. Experiment No. 1

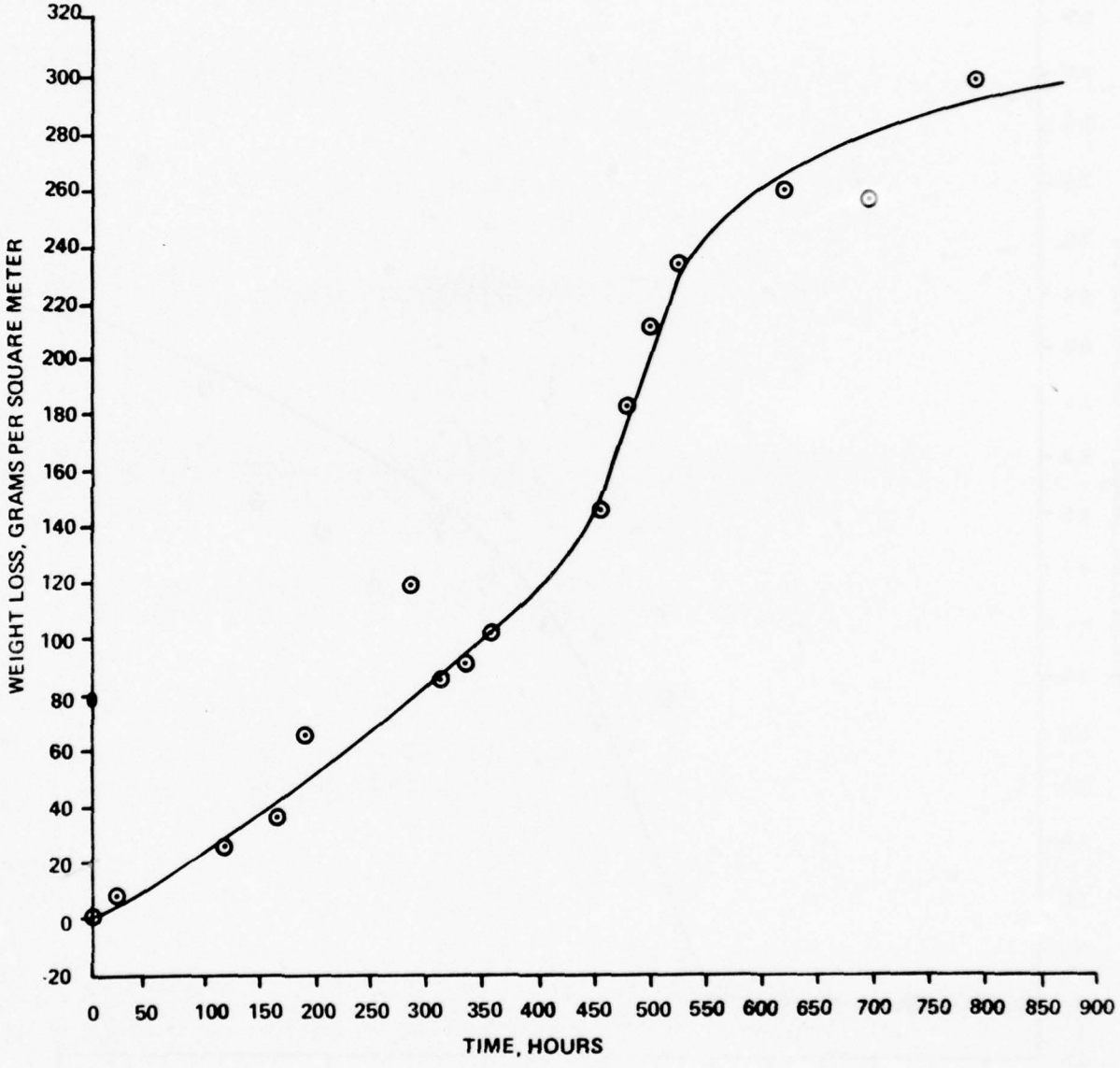


Figure A-2. Experiment No. 2

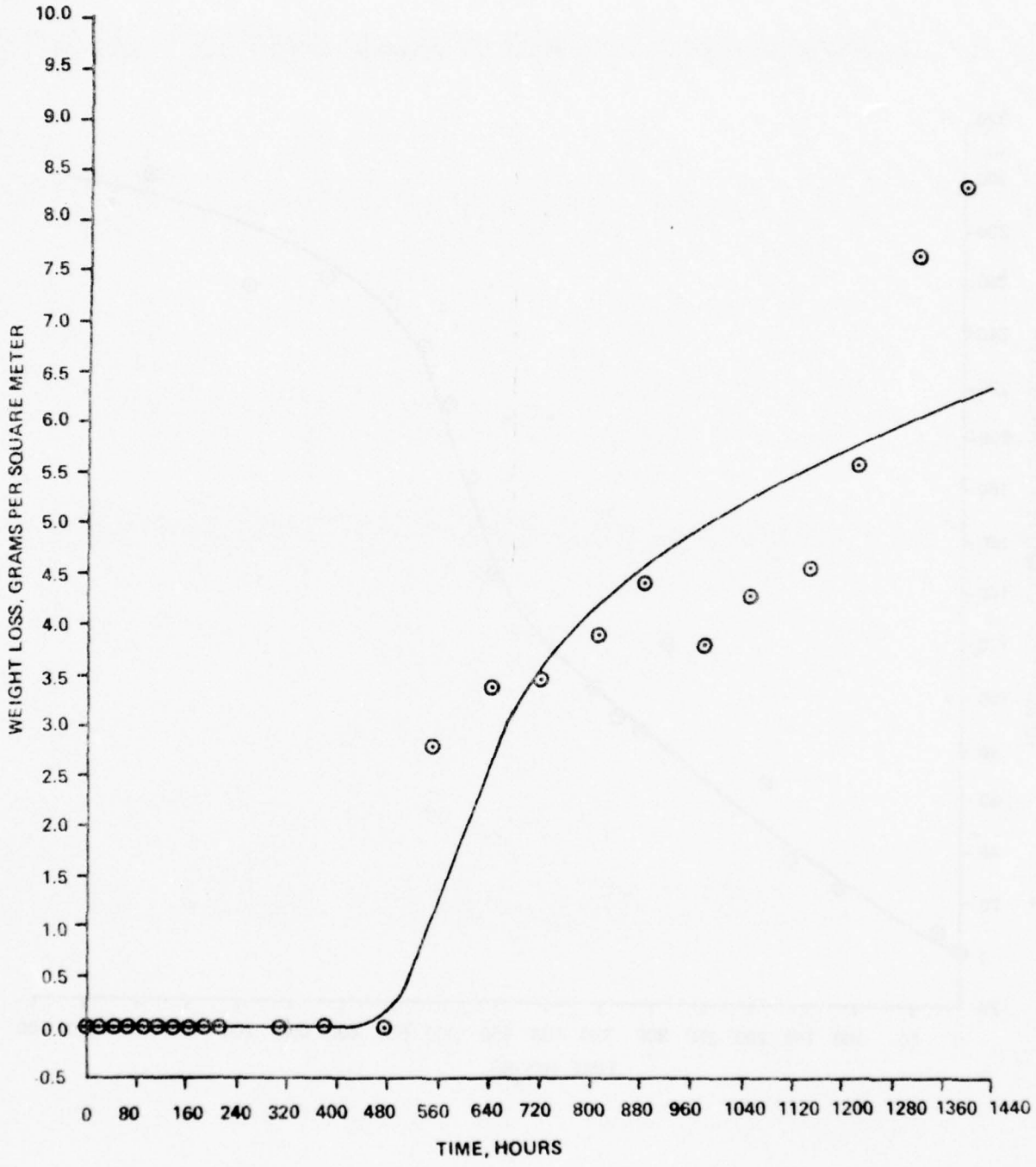


Figure A-3. Experiment No. 3

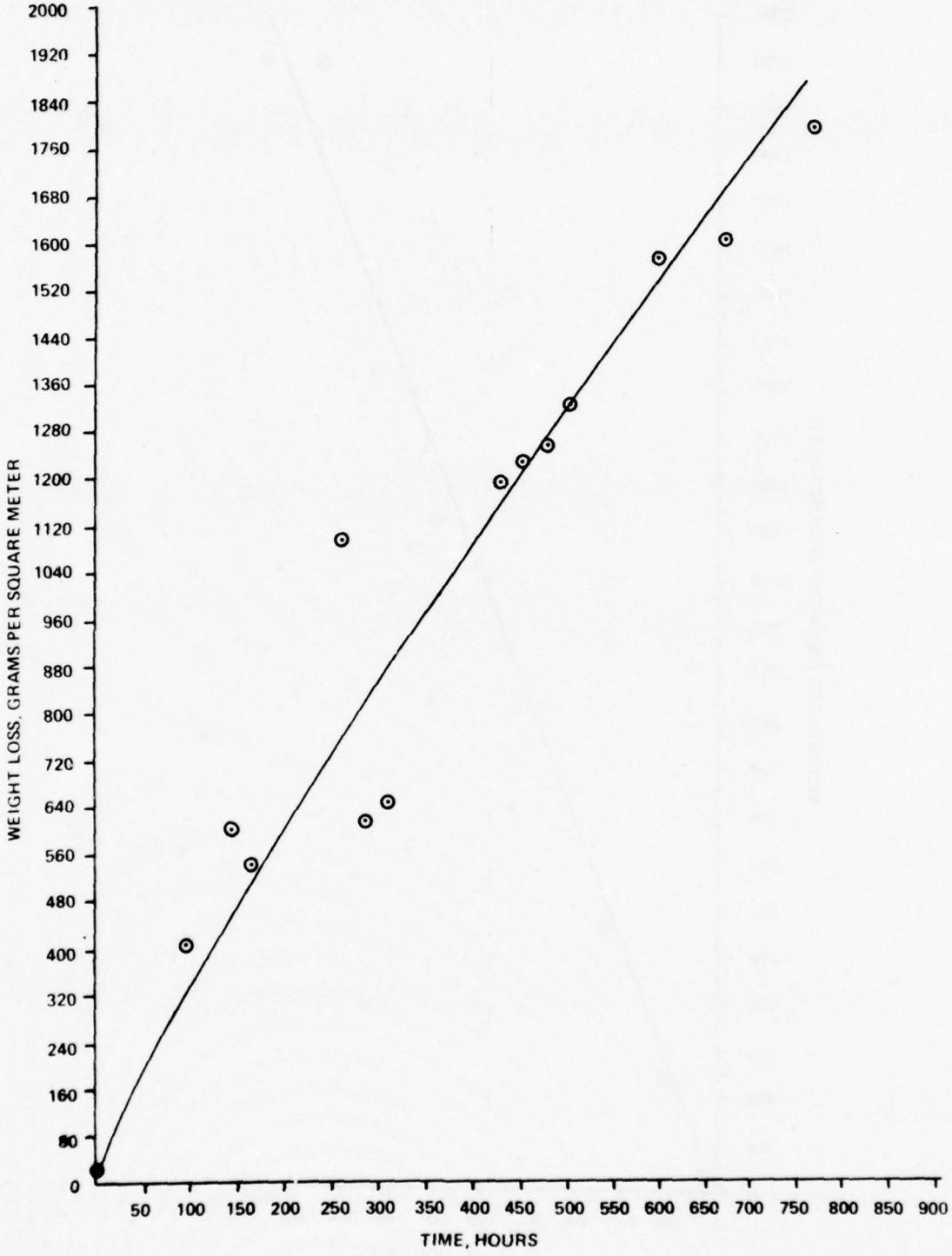


Figure A-4. Experiment No. 4

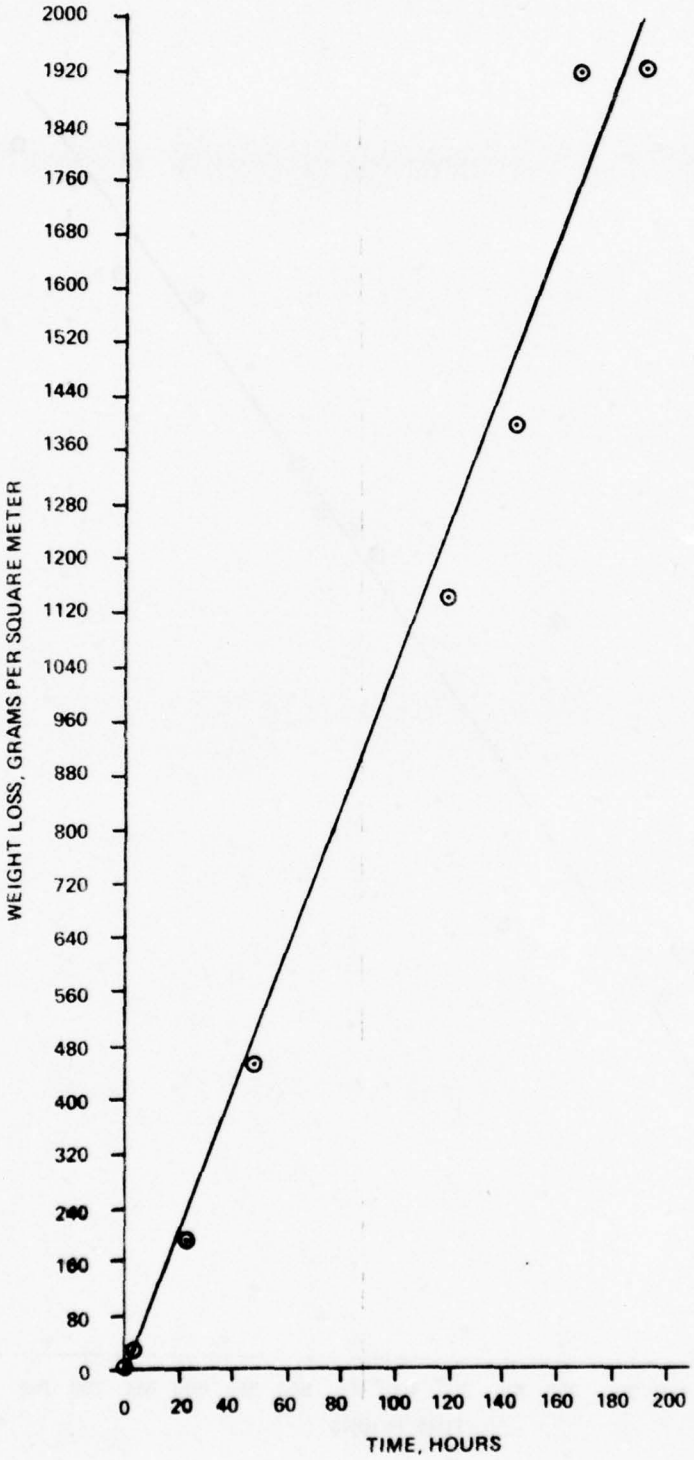


Figure A-5. Experiment No. 5

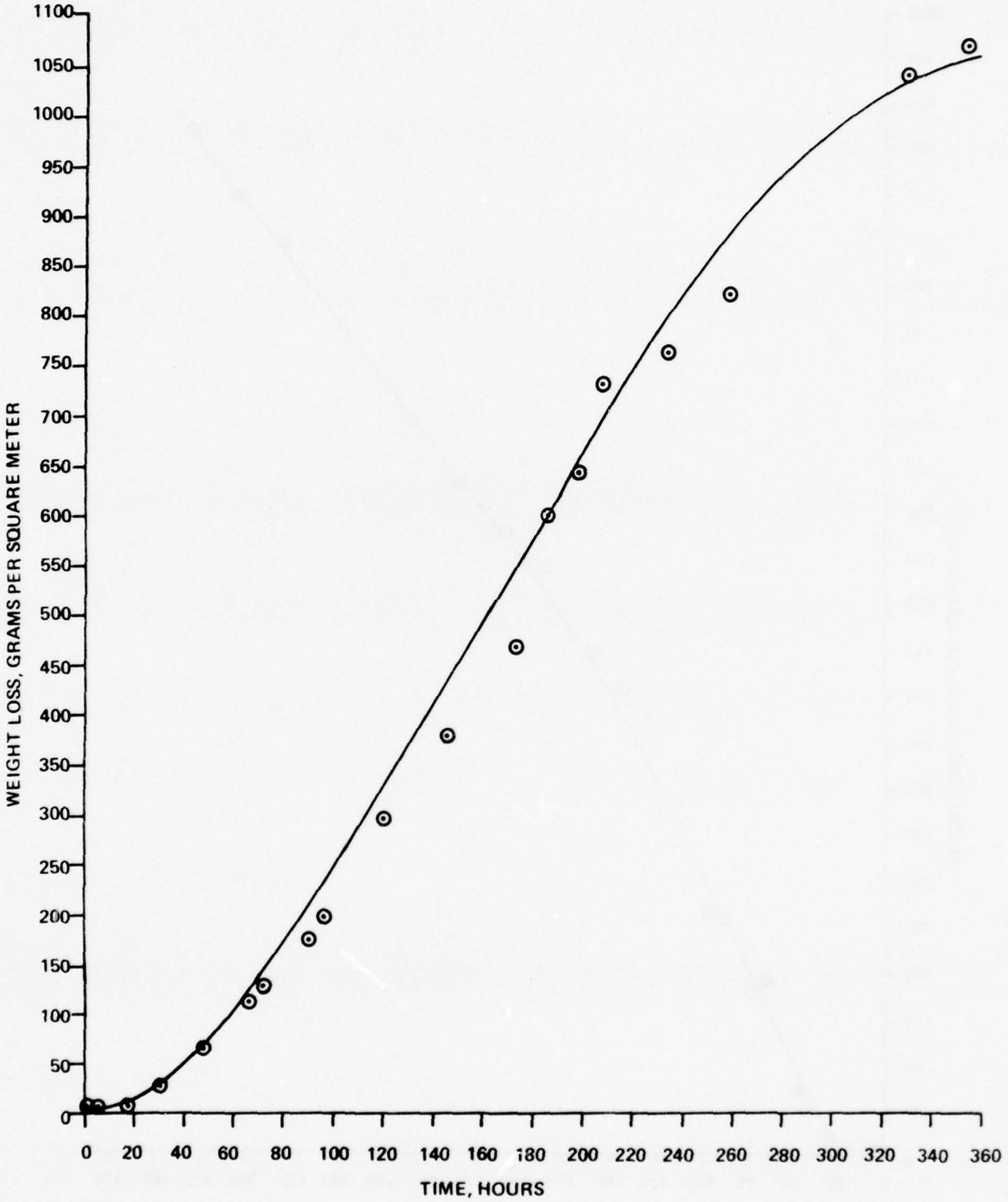


Figure A-6. Experiment No. 6

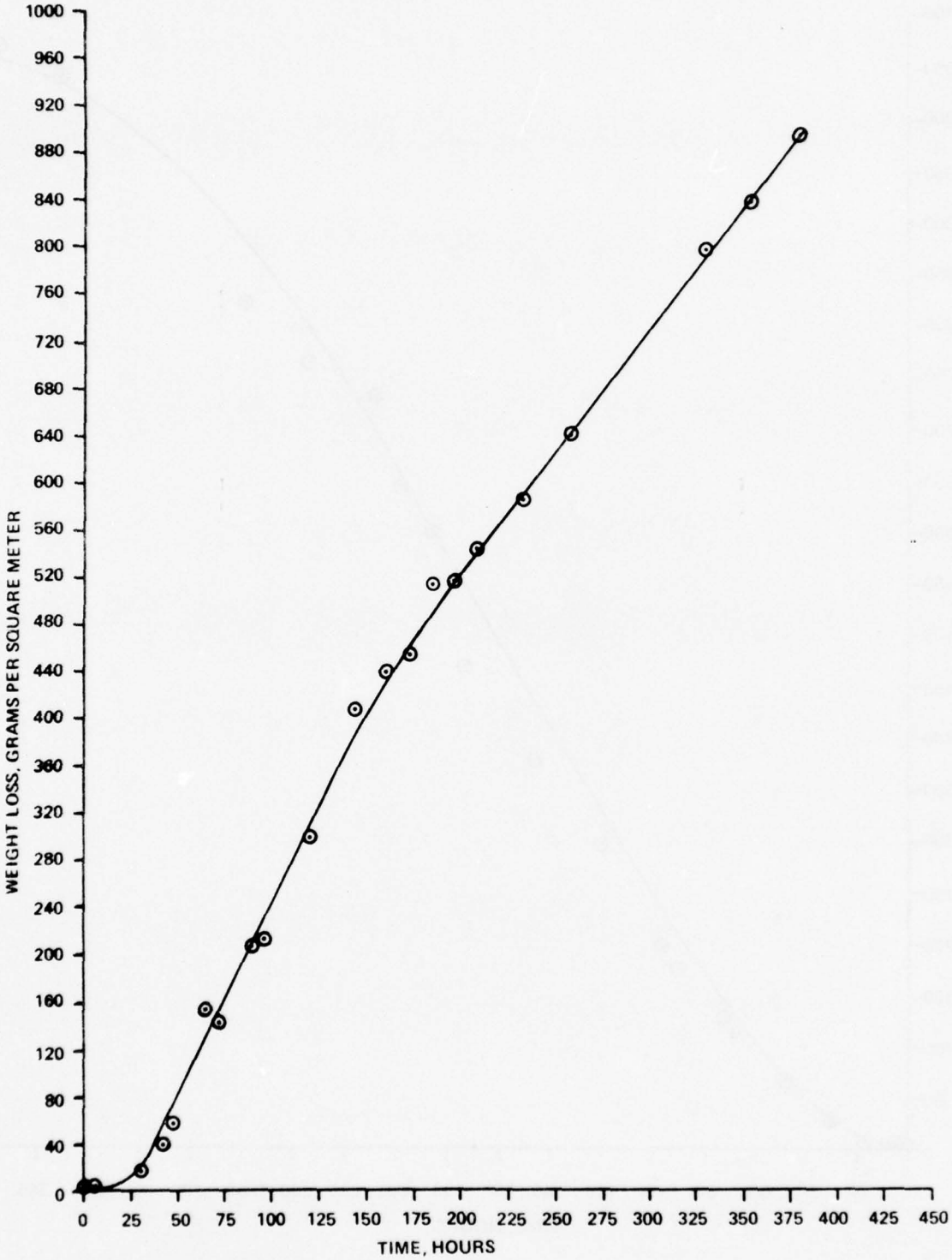


Figure A-7. Experiment No. 7

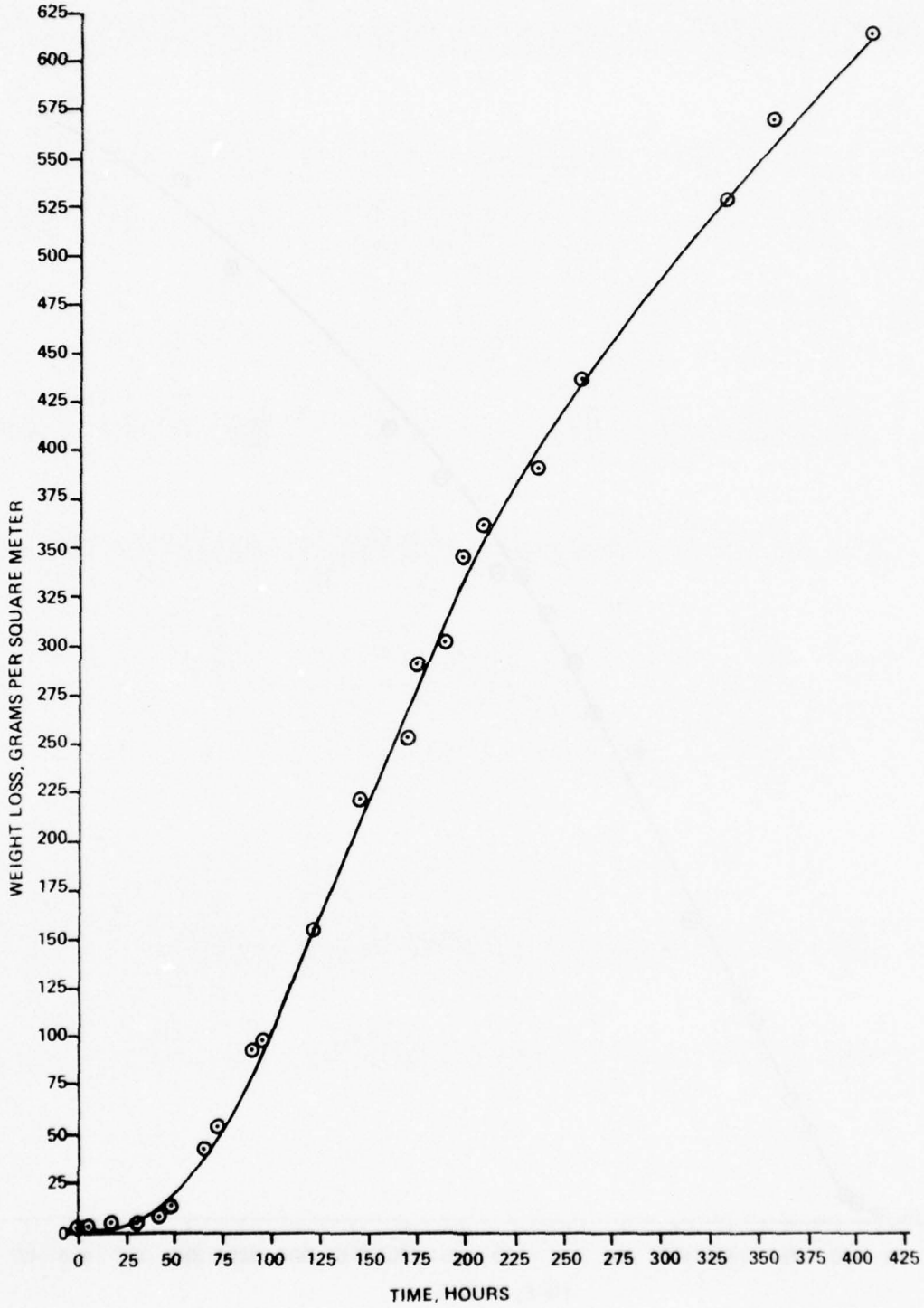


Figure A-8. Experiment No. 8

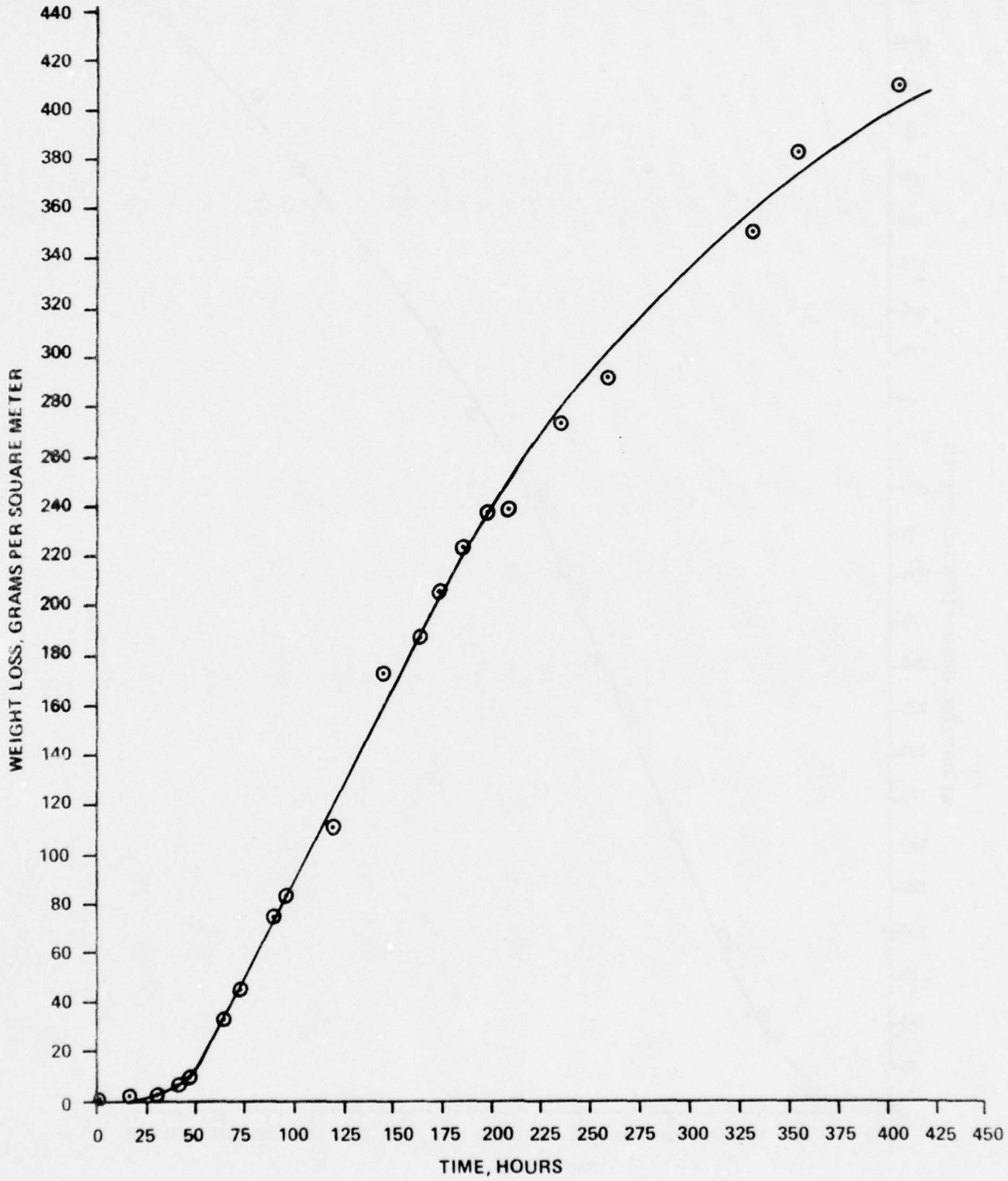


Figure A-9. Experiment No. 9

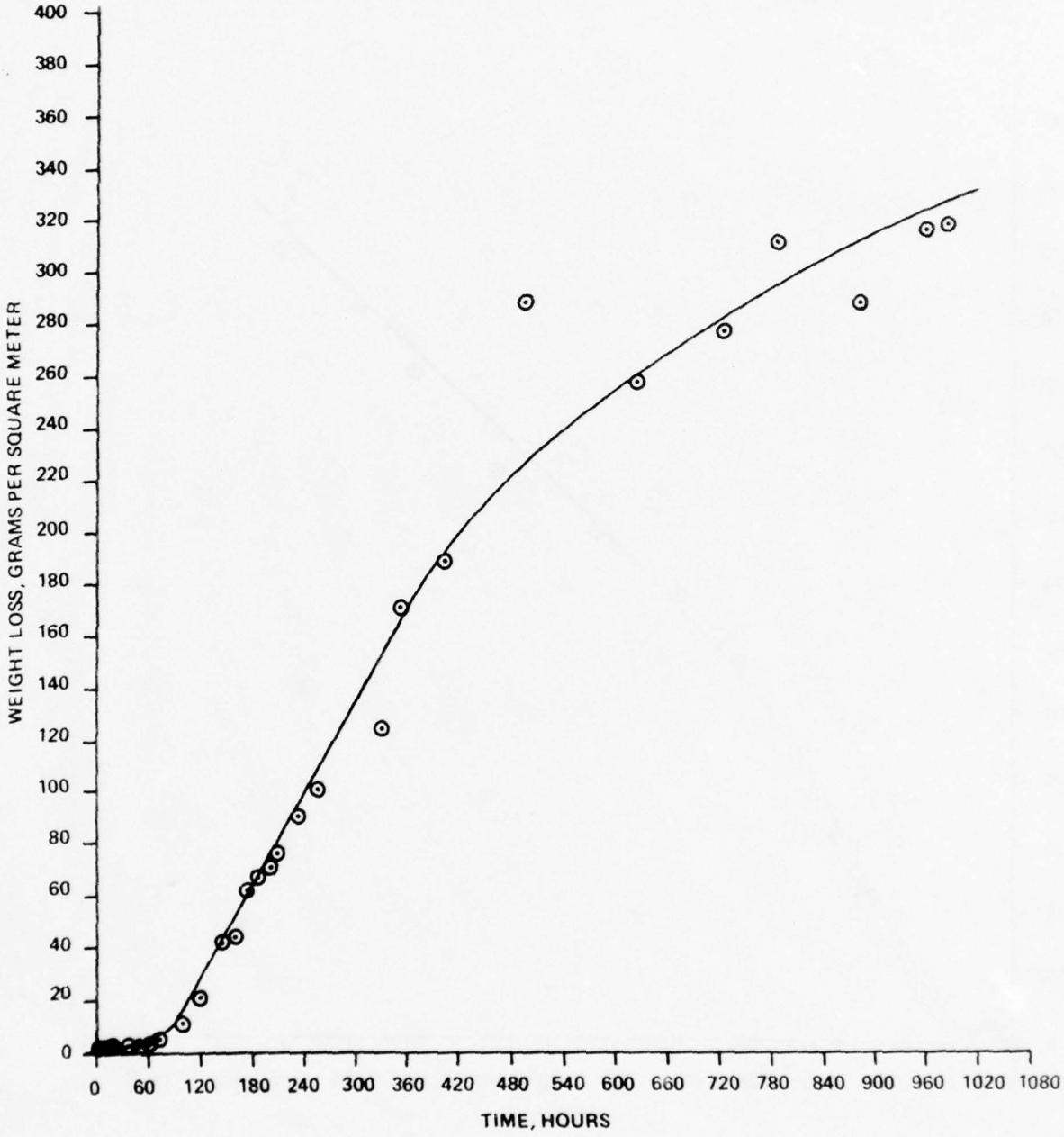


Figure A-10. Experiment No. 10

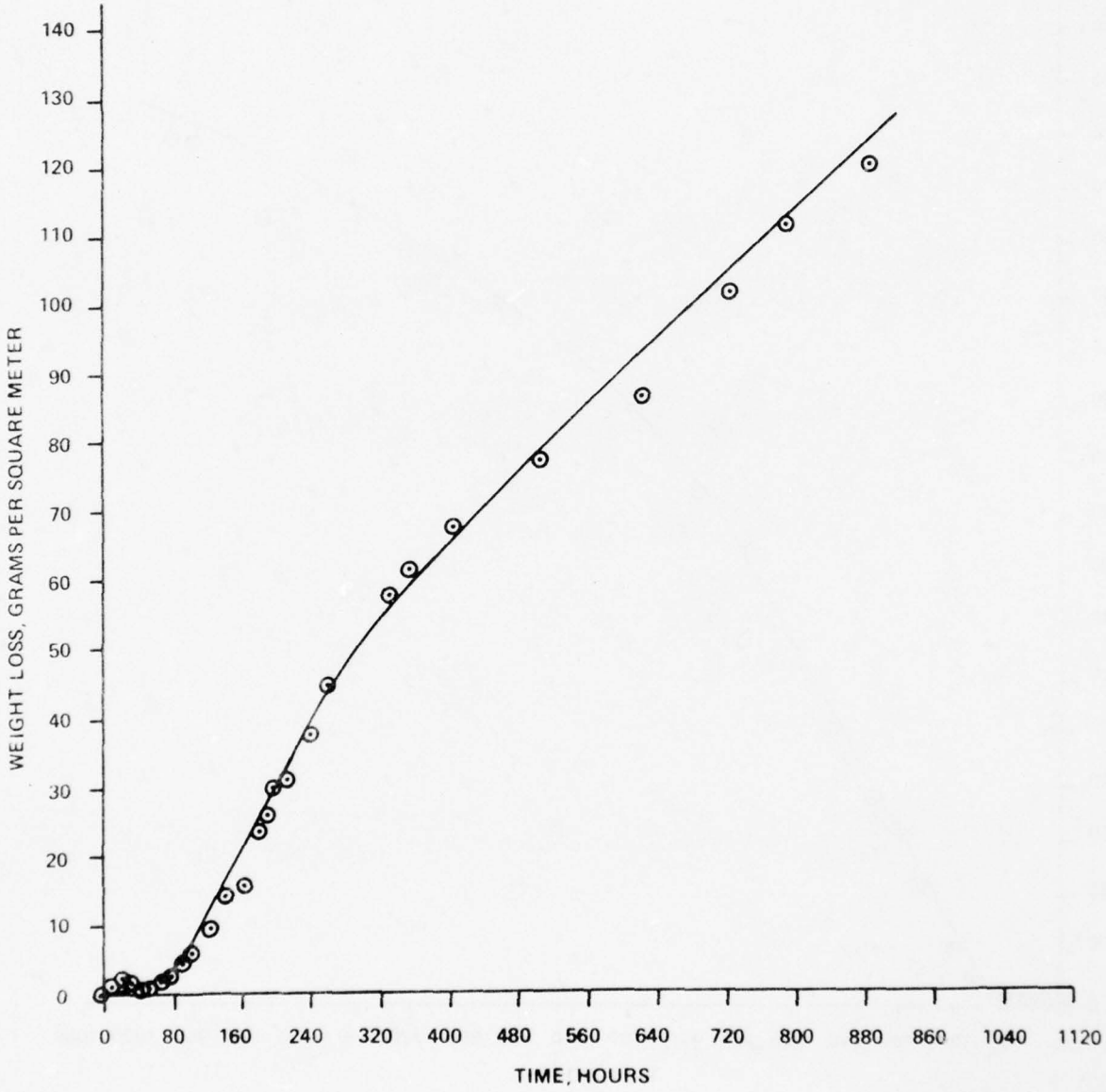


Figure A-11. Experiment No. 11

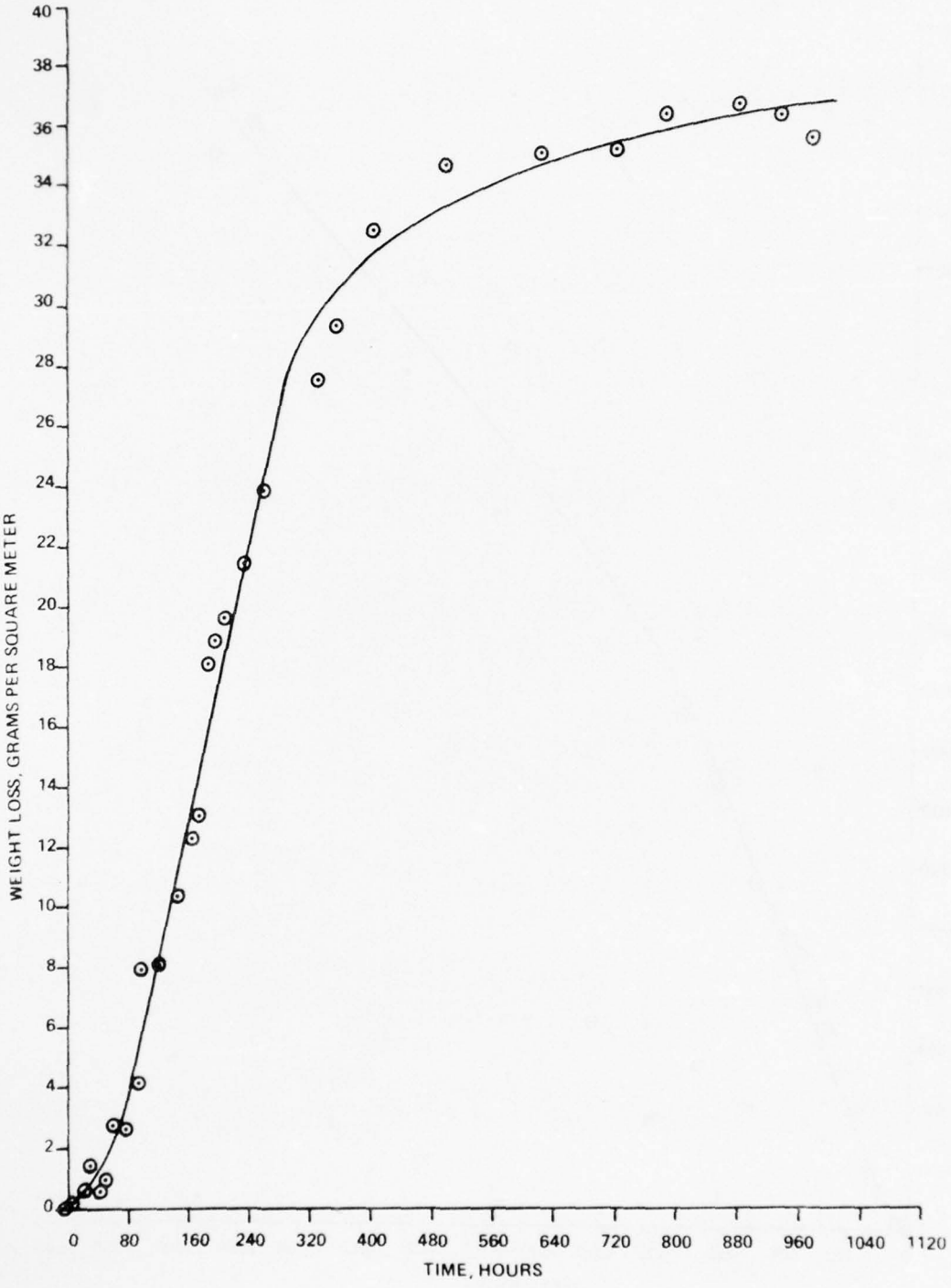


Figure A-12. Experiment No. 12

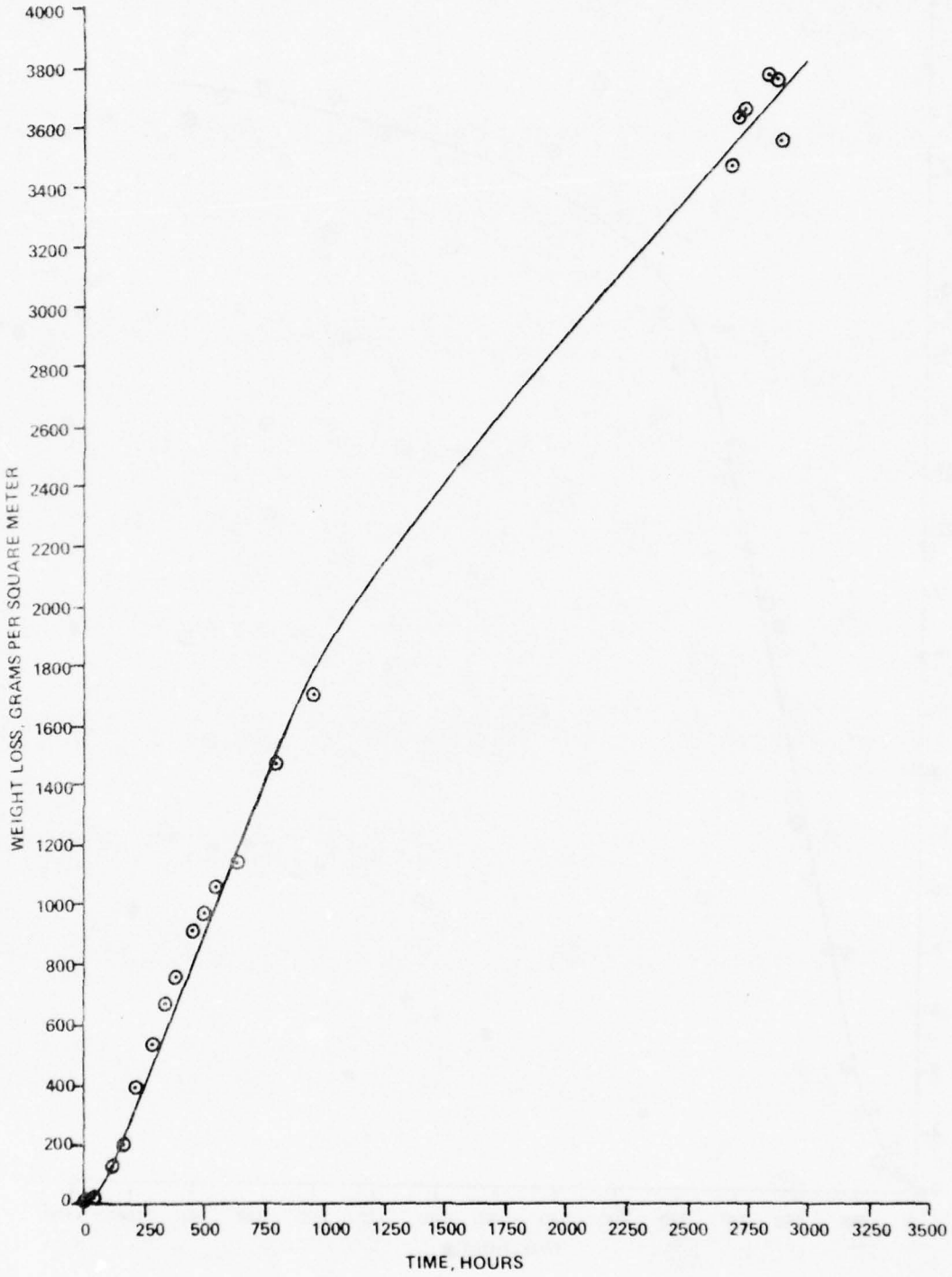


Figure A-13. Experiment No. 13

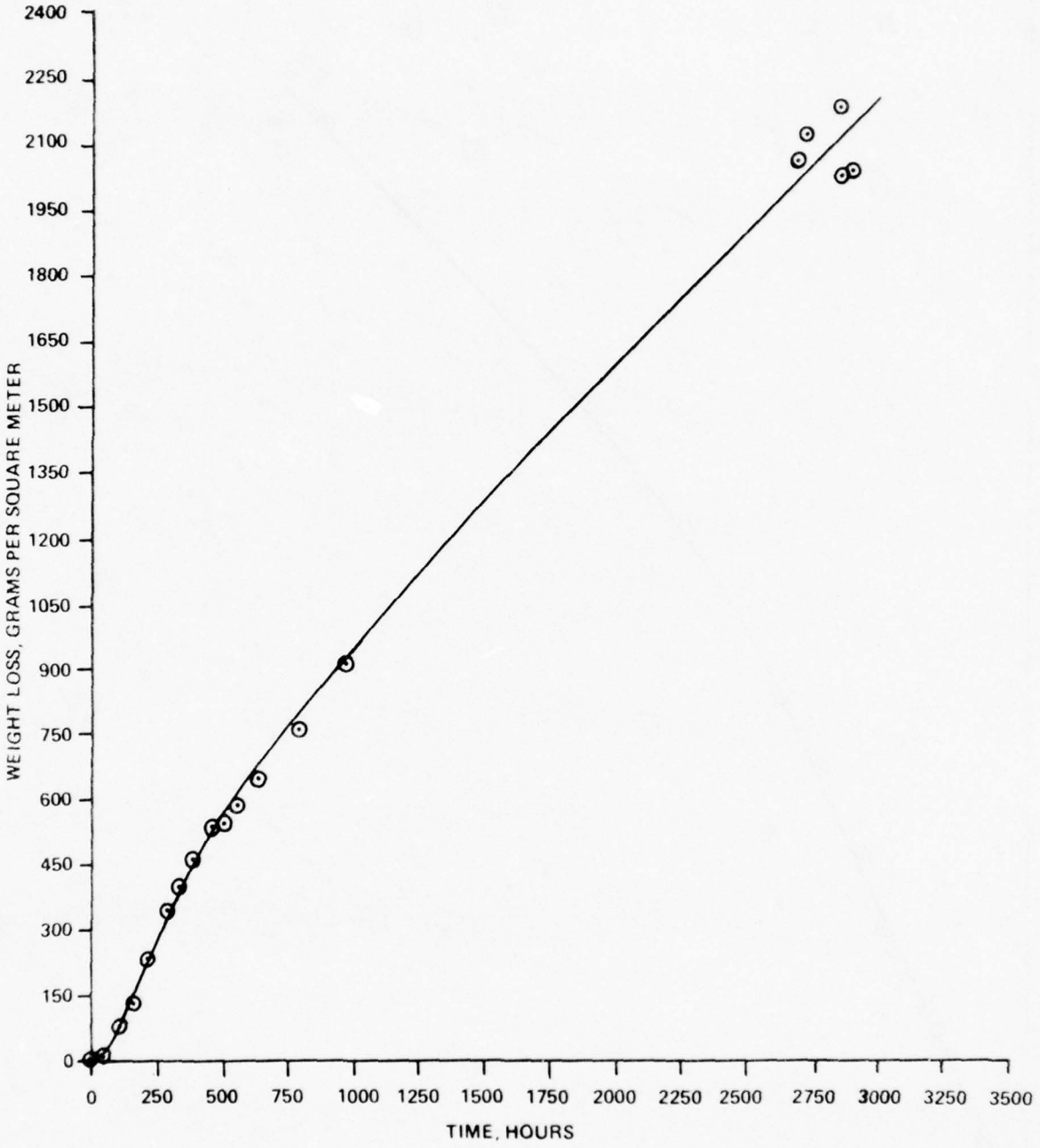


Figure A-14. Experiment No. 14

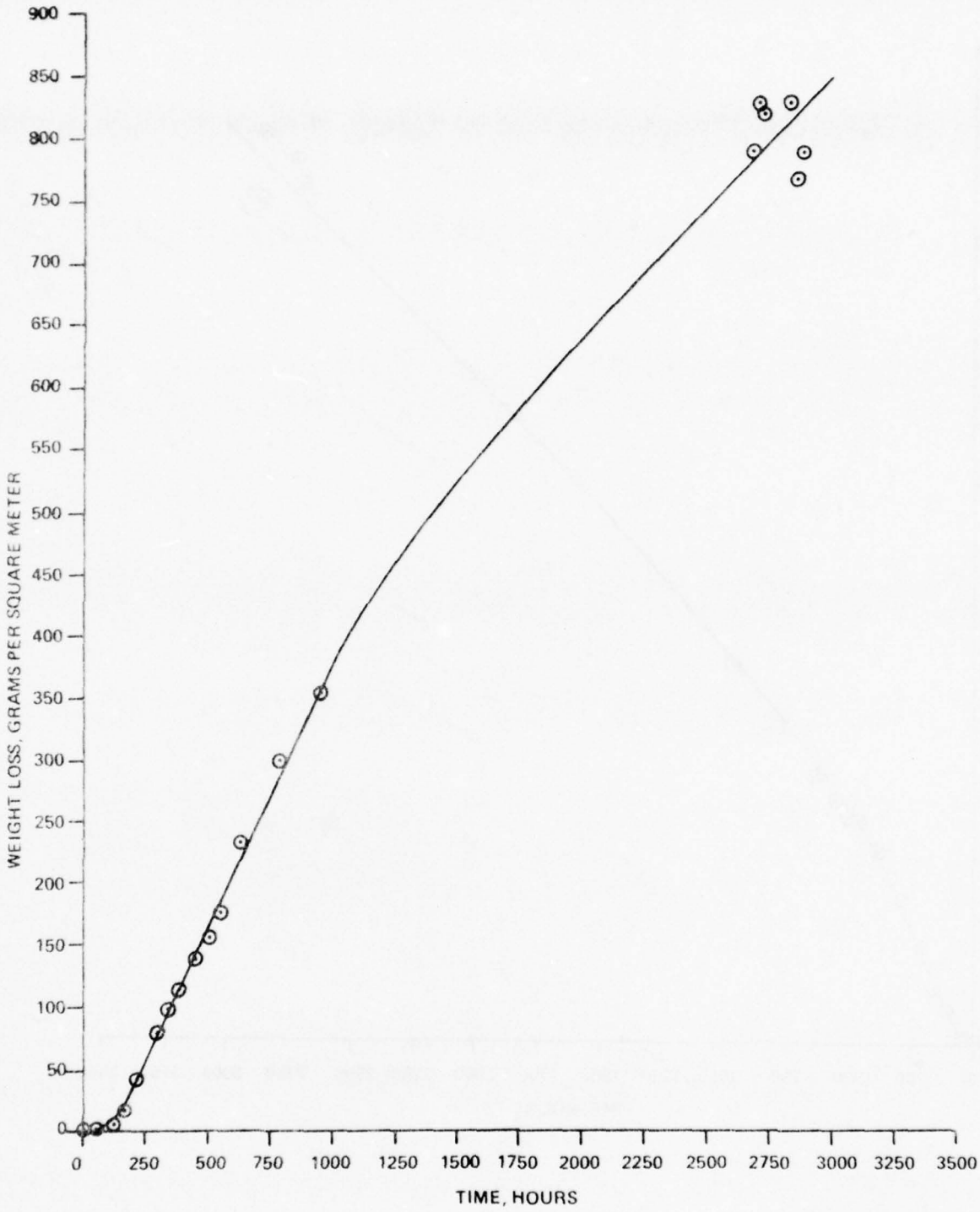


Figure A-15. Experiment No. 15

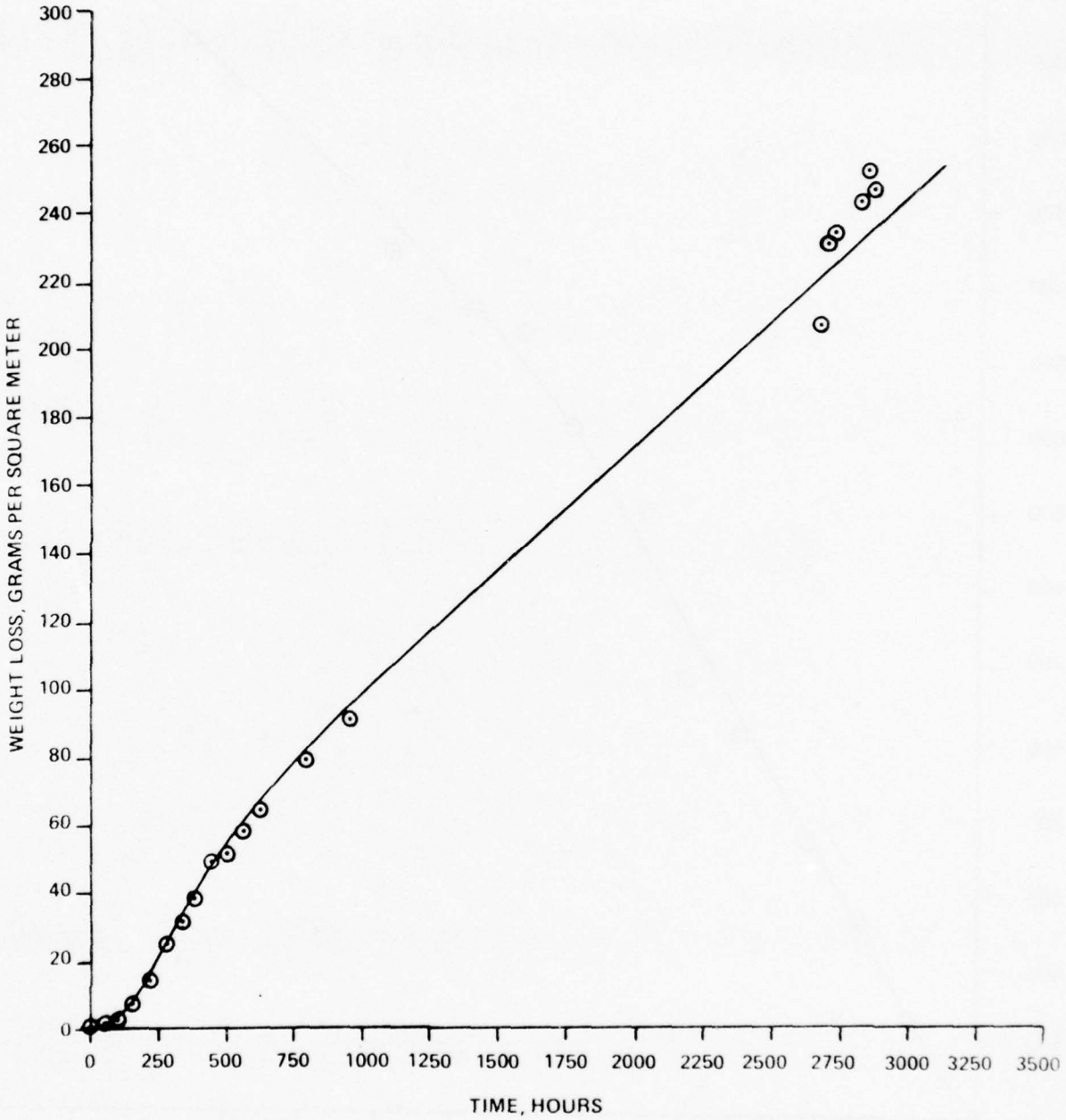


Figure A-16. Experiment No. 16

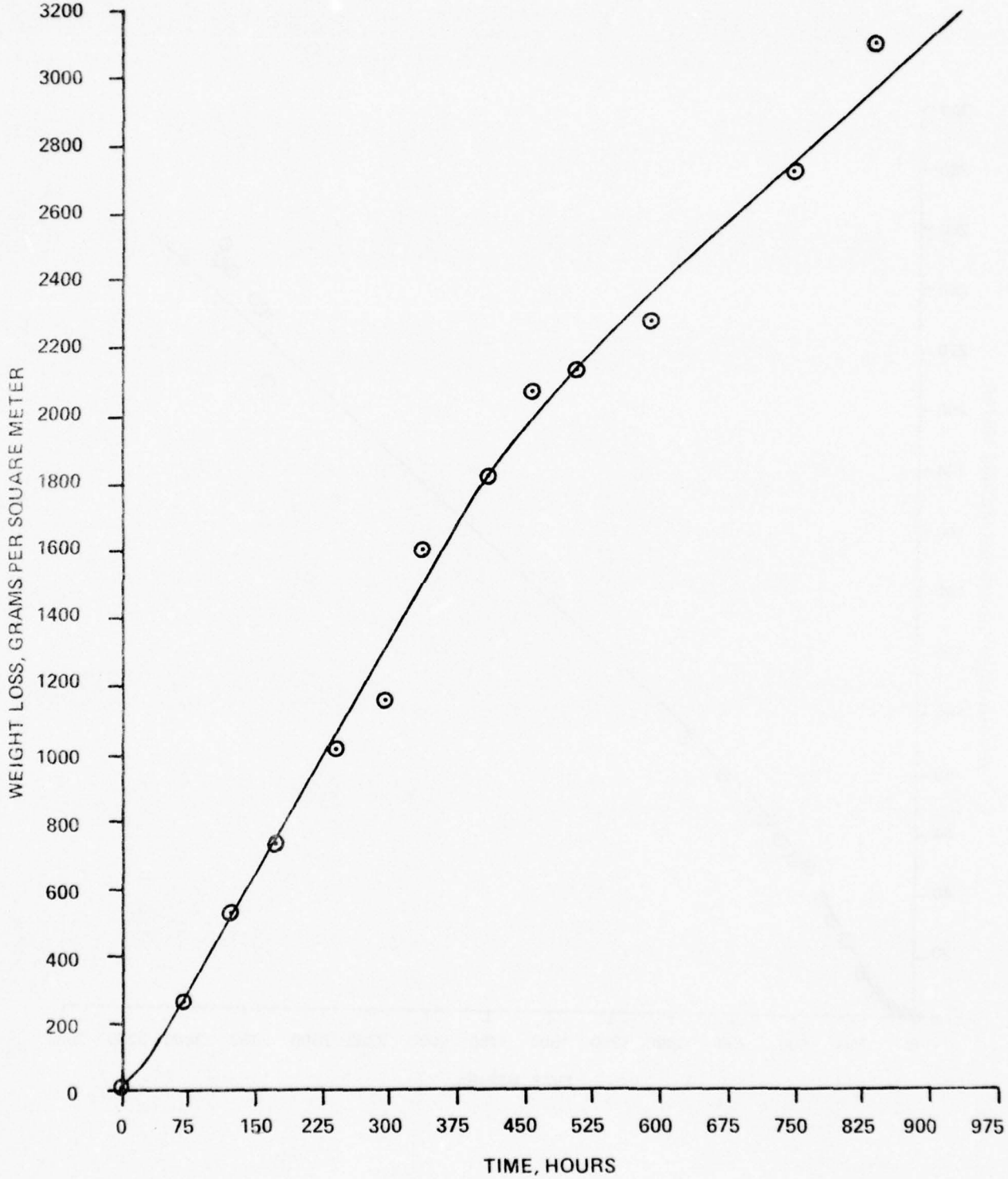


Figure A-17. Experiment No. 17

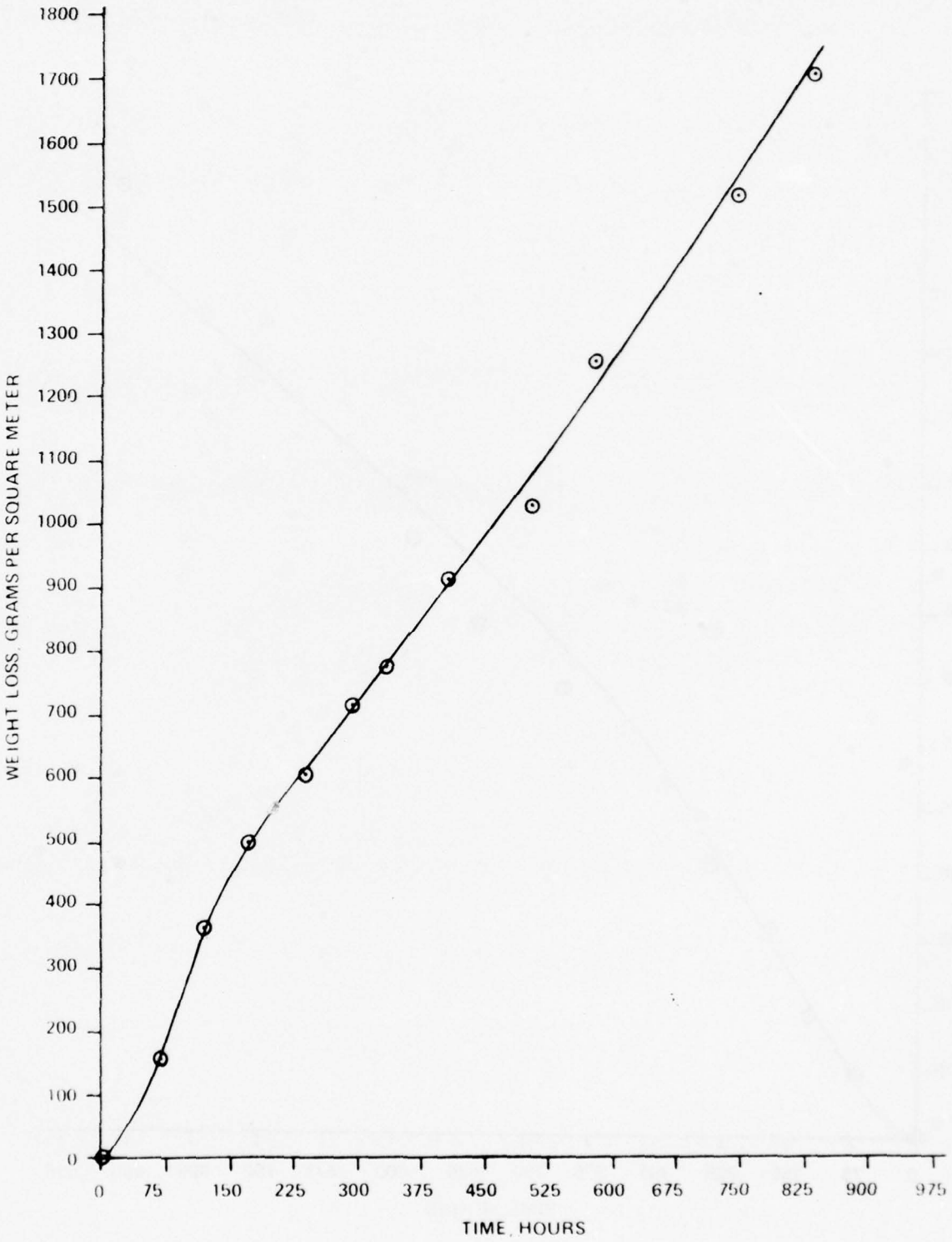


Figure A-18. Experiment No. 18

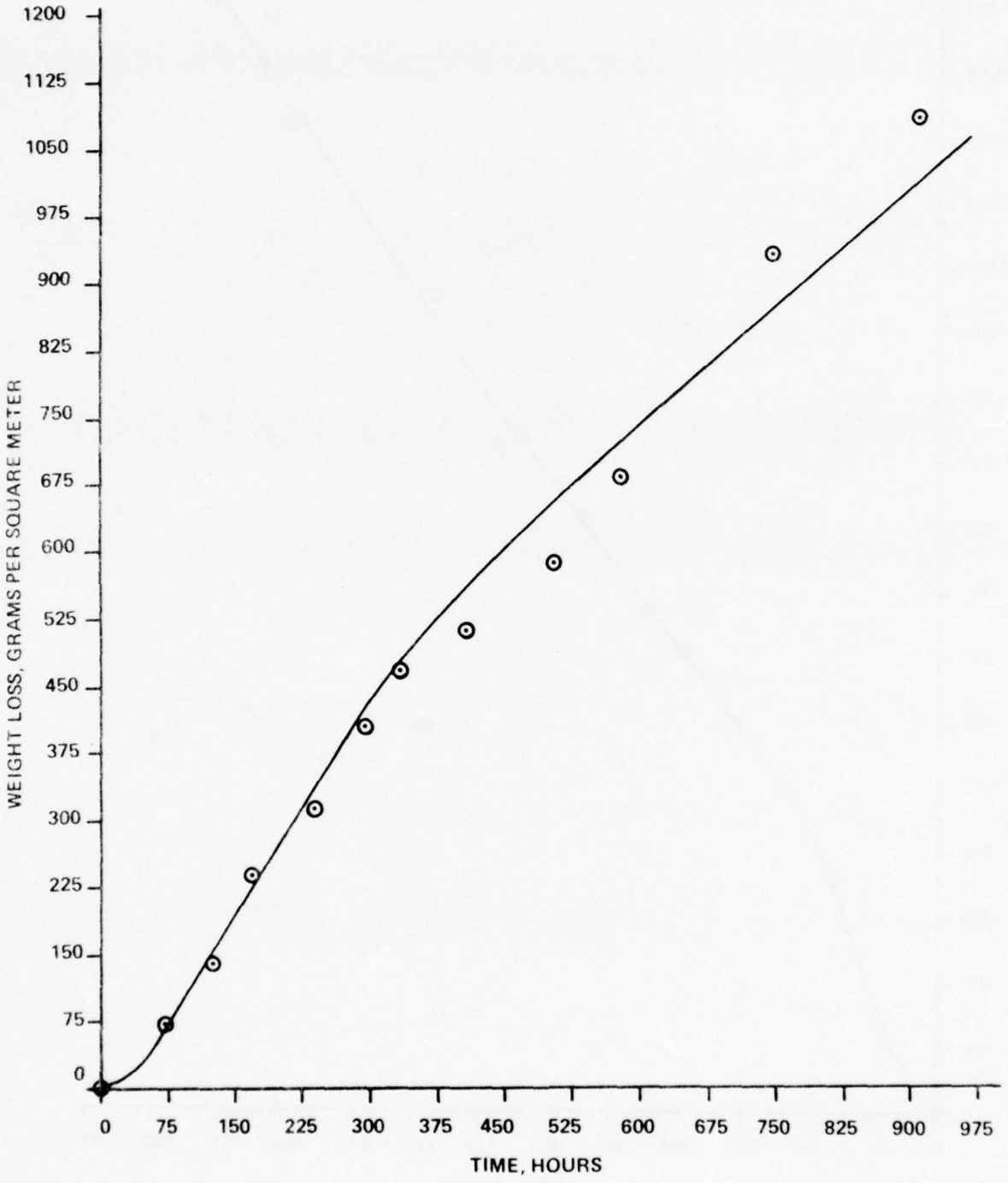


Figure A-19. Experiment No. 19

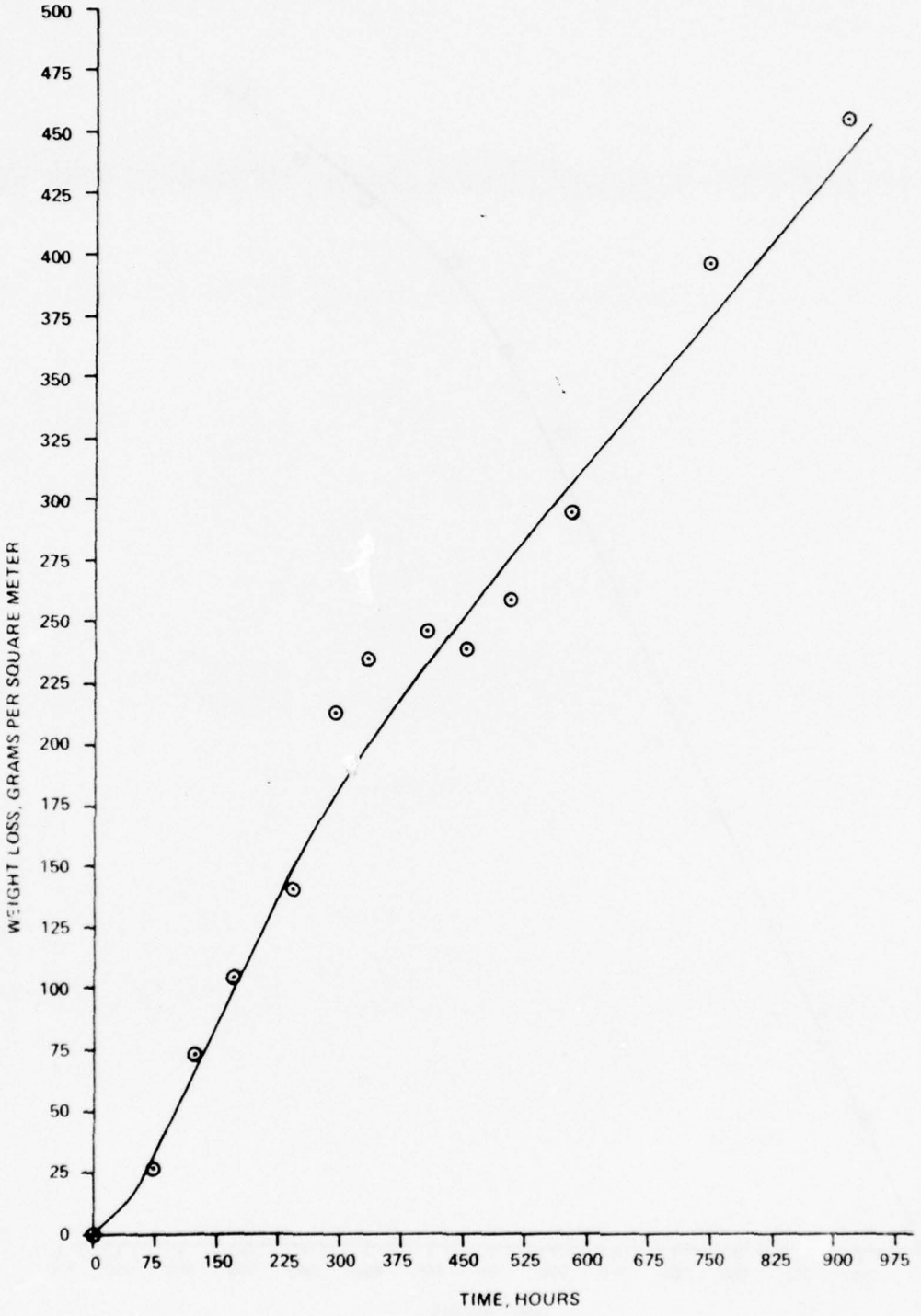


Figure A-20. Experiment No. 20

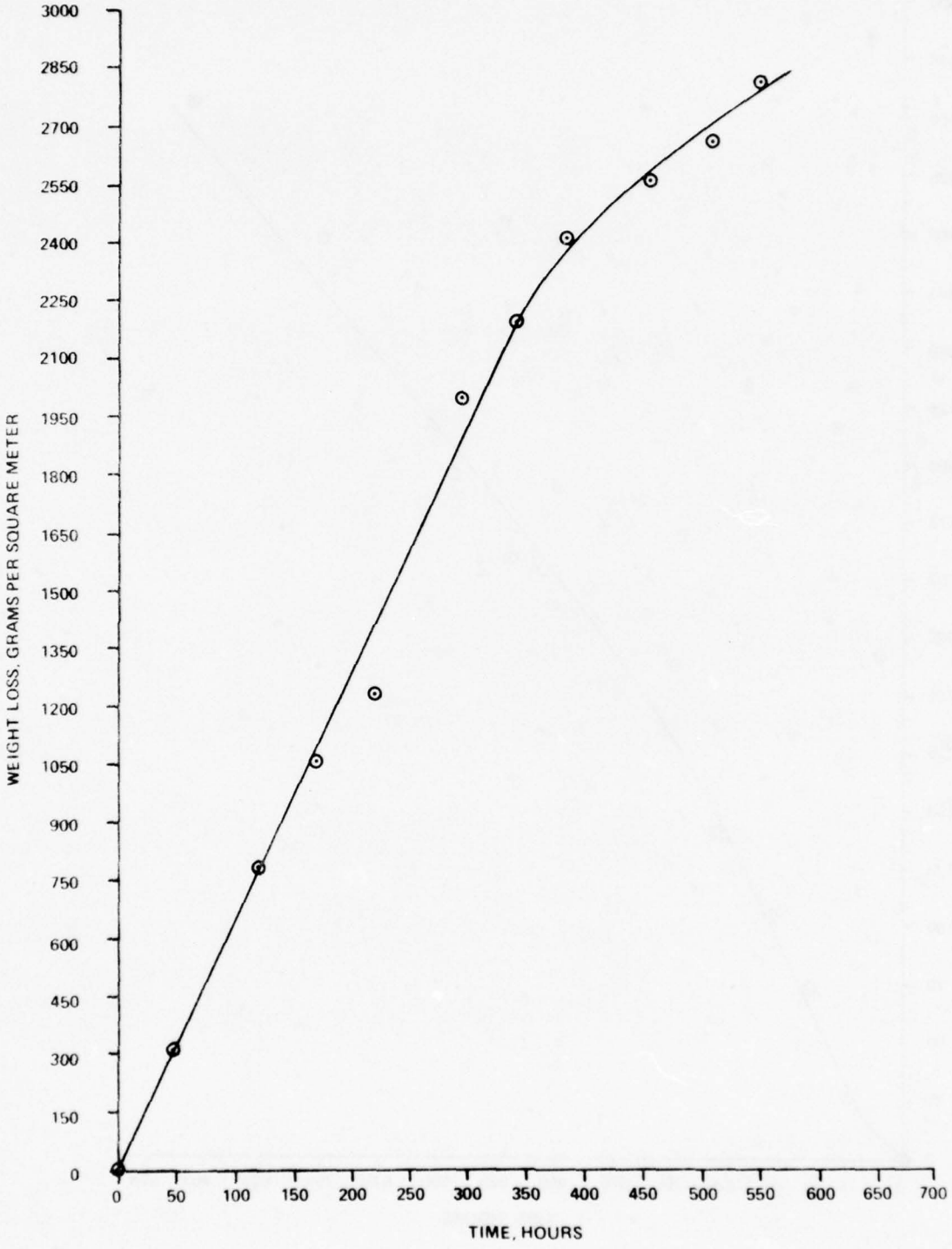


Figure A-21. Experiment No. 21

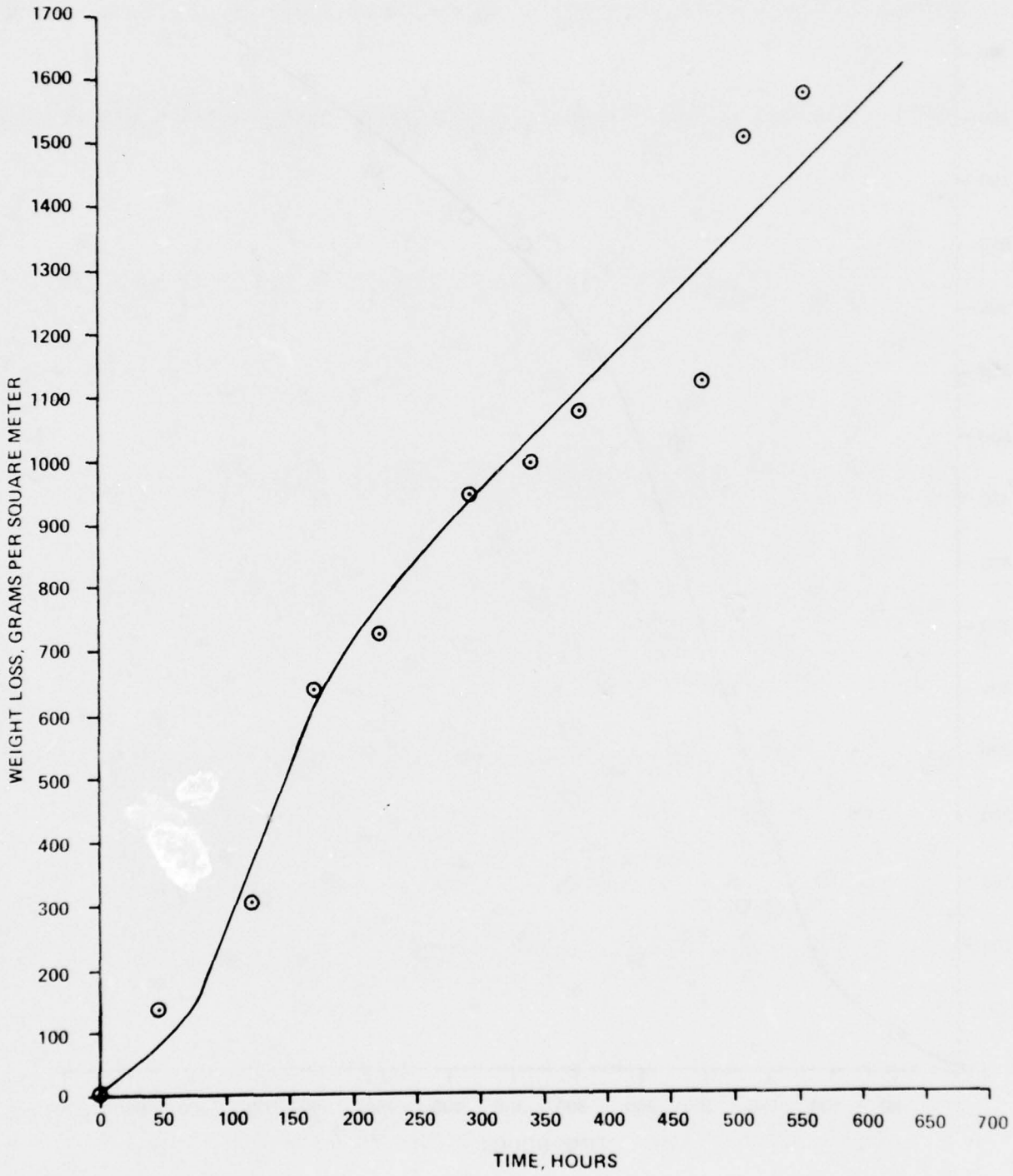


Figure A-22. Experiment No. 22

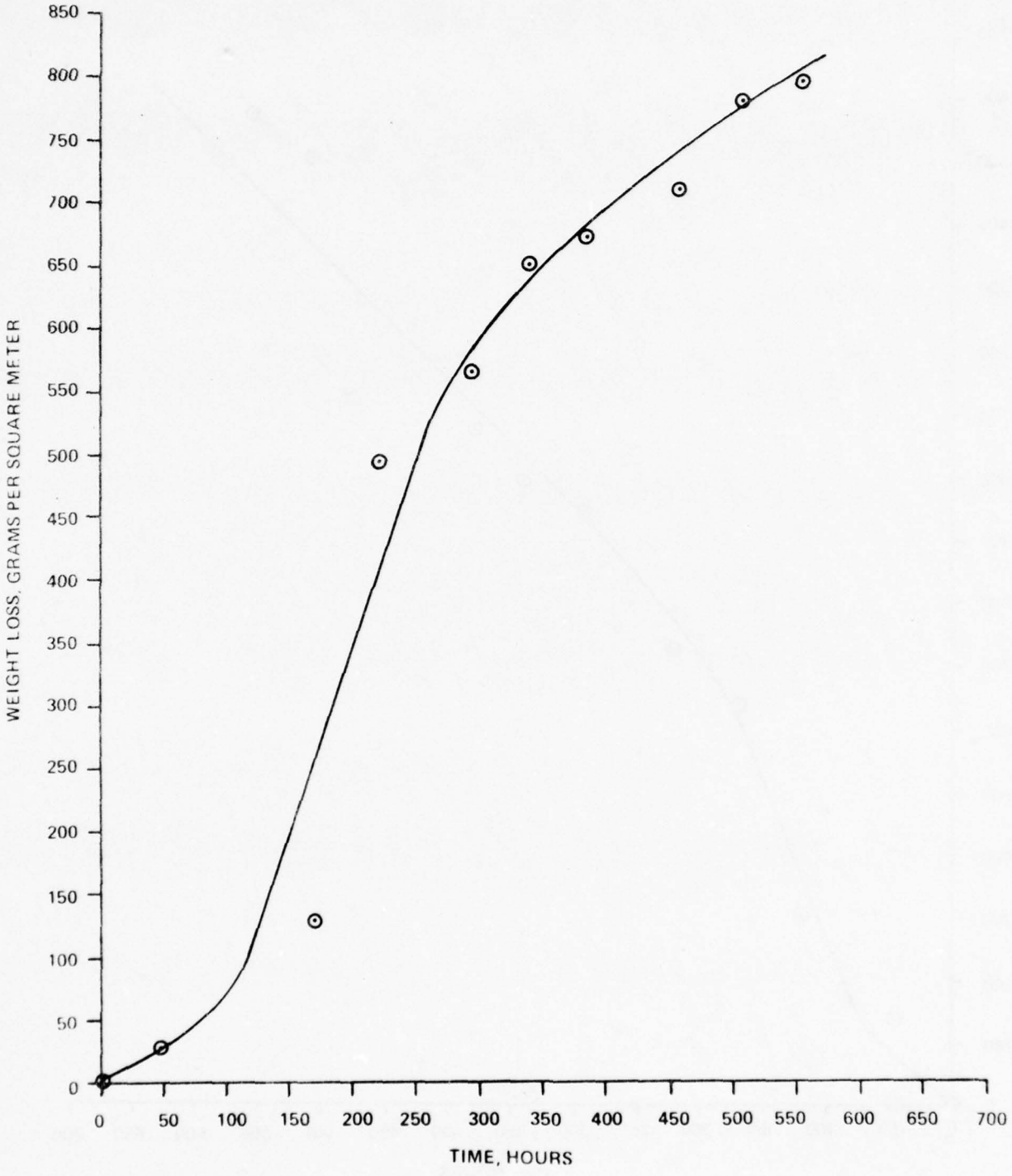


Figure A-23. Experiment No. 23

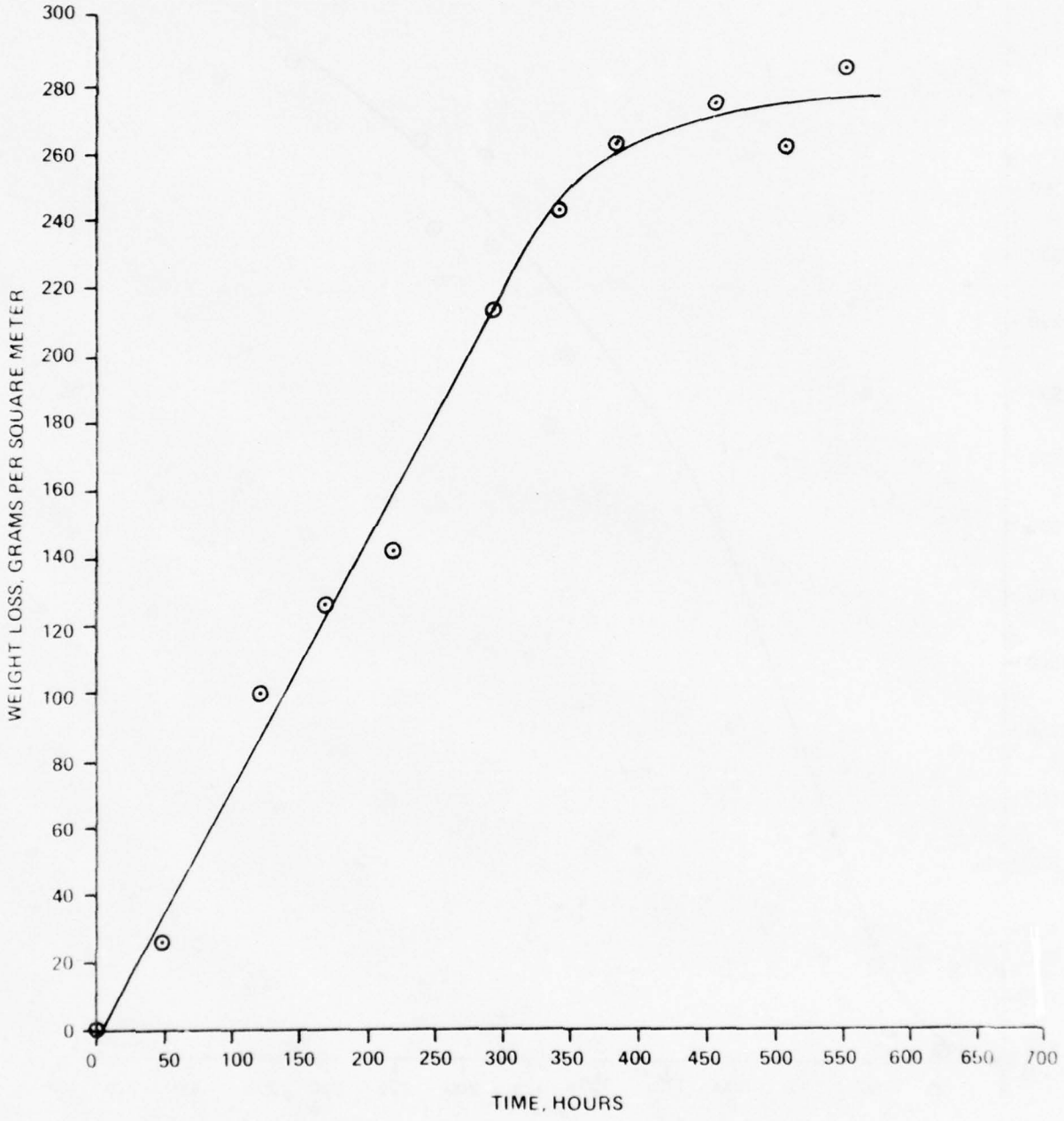


Figure A-24. Experiment No. 24

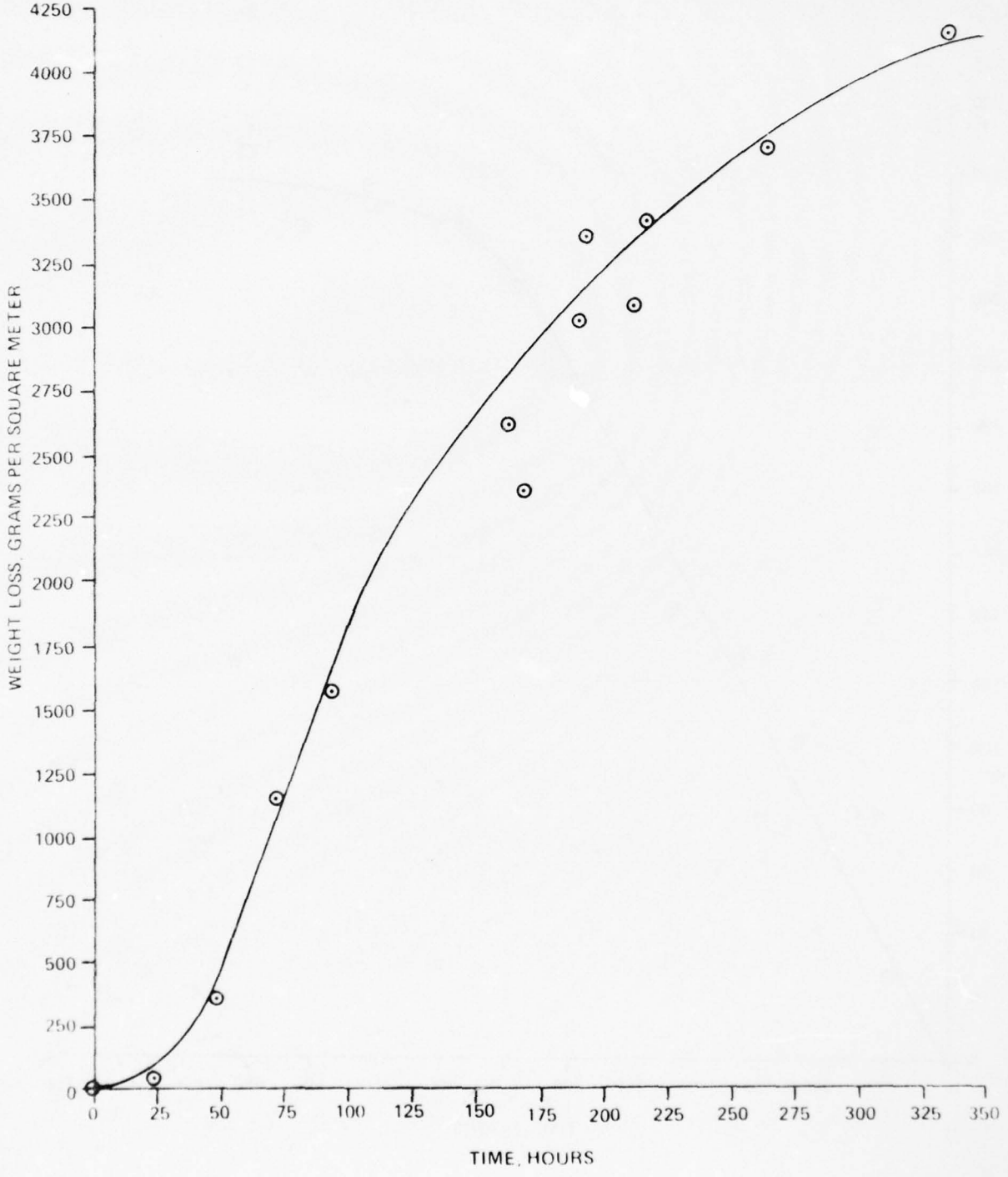


Figure A-25. Experiment No. 25

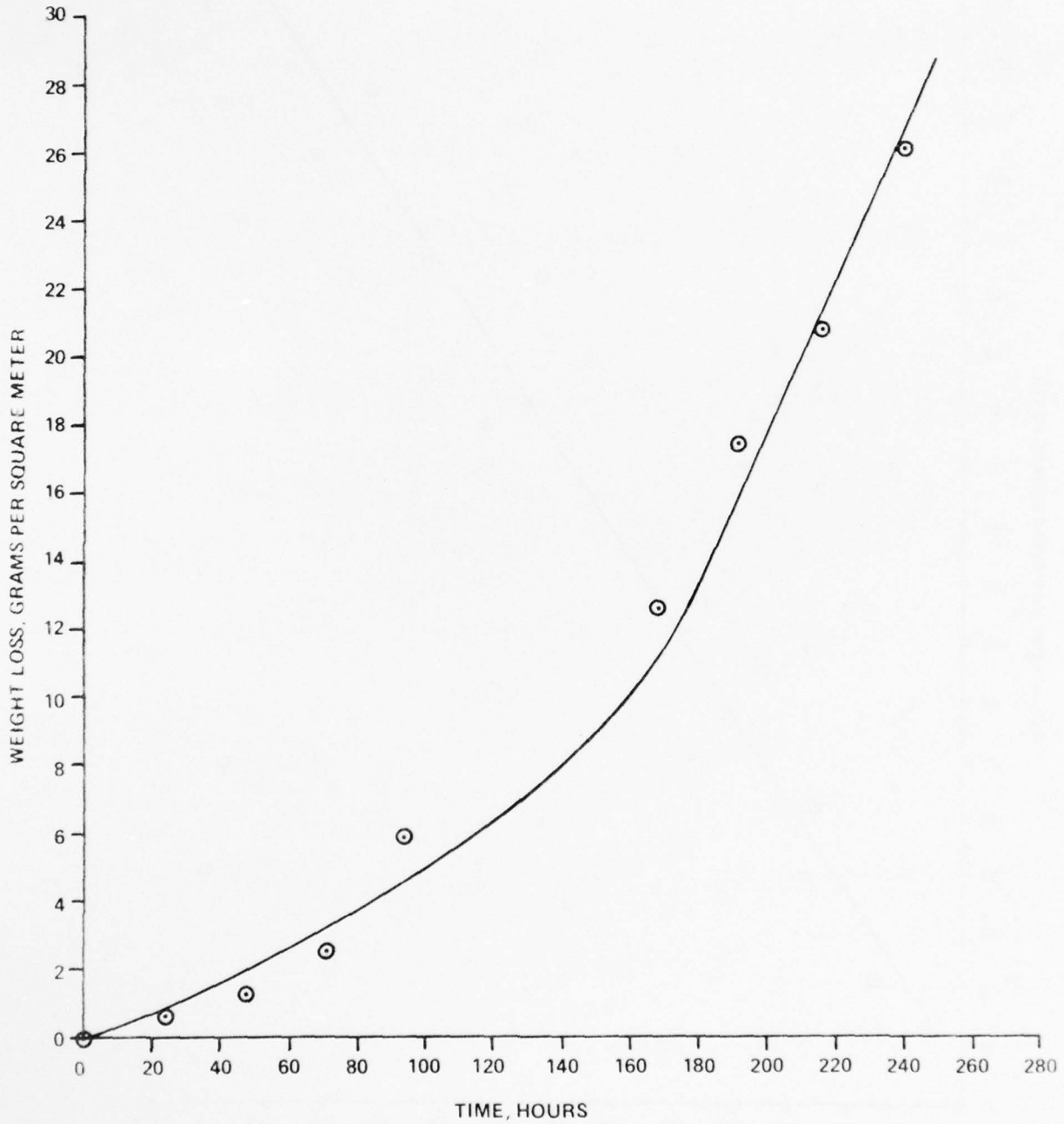


Figure A-26. Experiment No. 26

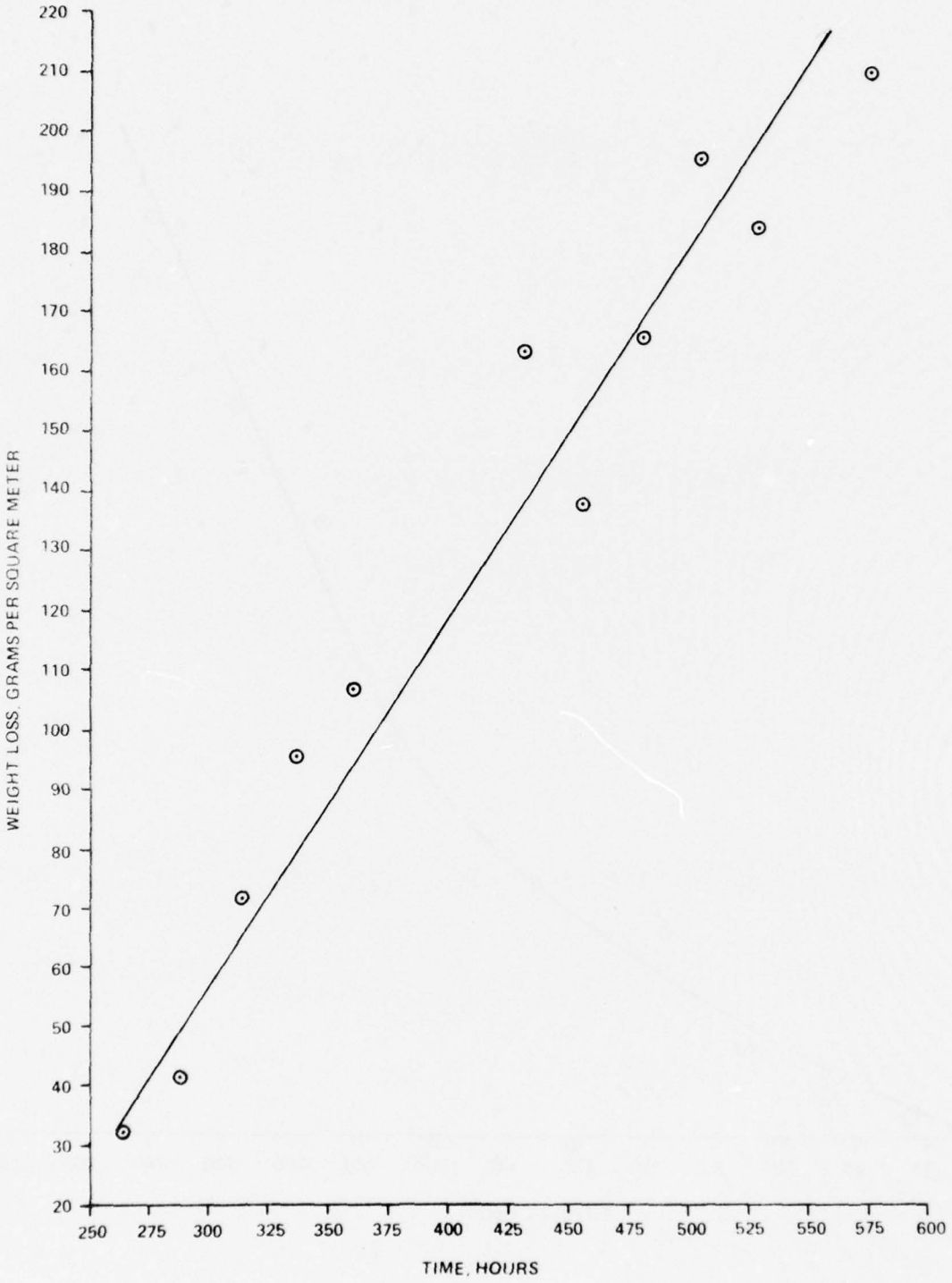


Figure A-27. Experiment No. 27

APPENDIX B

Experimental Techniques

This appendix contains the manipulative, analytical, and spectroscopic techniques, etc., employed throughout the studies of HDA corrosion chemistry.

B.1 Hydrogen Fluoride Manipulation Techniques

Liquid hydrogen fluoride was obtained commercially from Imperial Smelting Ltd., and purified by distillation in a metal and fluoroplastic (Kel F and Teflon FEP) vacuum system (glass sections of the pumping system were protected by soda lime traps). The system was first pumped out, the primary HF collection vessel was cooled to -78°C, and HF was allowed to distil into it from the cylinder under static vacuum. Any non-condensibles in the HF were removed by pumping very briefly on the vessel at the start of this distillation, and periodically during the distillation. To remove some of the less volatile impurities, the primary collection vessel was warmed to room temperature, and the HF was allowed to distill into a second vessel at 0°C containing K_2NiF_6 [1] as a scavenger for oxygen and water. A further purification was achieved by cooling the second vessel to -96°C and pumping to remove SiF_4.

B.2 Corrosion Rate Studies; Run Sampling Technique

During the course of the research, several sampling methods were tried, the most rapid and convenient being described below.

A one cubic centimeter (1 cm^3) sample was taken from the reaction flask using a glass graduated pipette and a rubber pipette filler. This sample was quickly transferred to a weighed sample tube with stopper and the sample was left open to the atmosphere overnight in a fume cupboard. The samples were taken from the reaction flask quickly and without the use of a countercurrent of nitrogen to avoid loss of N_2O_4 during sampling. Ingress of moisture to the system during sampling was prevented by the slightly positive pressure of N_2O_4 in the flask. Sampling was also carried out after removal of the reaction vessel from the thermostat bath in order to facilitate shaking of the vessel to ensure homogeneity of the reaction mixture. After standing overnight, each sample was diluted by the addition of 5cm^3 of de-ionised water. (Addition of water, immediately after sampling, produced a violent reaction which resulted in expulsion of tube contents, particularly in the case of HNO_3/N_2O_4 mixtures.)

The tubes were then stoppered, the contents were mixed thoroughly, and then they were weighed before analysis.

B.3 *Corrosion Rate Studies; Calculation of Results*

All calculations were performed on the University of Nottingham ICL 1906A computer and are described in detail here. Iron, chromium, and nickel content was determined by atomic absorption spectroscopy (see below, Appendix B.5 (d)) and data were obtained in the usual way by the use of calibration curves.

The initial dilution was calculated from the equation below:

$$\frac{W_f - W_i}{W_s} = \text{initial dilution}$$

where:

W_i = initial weight of sample tube and stopper.

W_f = final weight of tube, stopper and diluted sample.

W_s = weight of original HDA sample, i.e. weight of $1 cm^3$ of mixture. (Density values were taken from the literature[2, 3]).

The weight lost by the metal specimen at any time was then calculated using the following equation.

$$\sum_{1 \rightarrow n} W_{soln}(n) + W_{cum}(n-1)$$

where: W_{soln} = the weight of metal in solution

$= [M]\ (ppm) \times V_r \times d$

and: $[M]\ (ppm)$ = measured concentration in solution in parts per million.

V_r = volume of HDA remaining in reaction flask before sampling.

d = density of HDA (literature values[2, 3])

and where; W_{cum} = the cumulative weight loss from solution by sampling.

$W_{cum}(n) = W_m + W_{cum}(n-1)$

where n = number of samples taken

W_m = weight of metal in the sample ($1 cm^3$).

$W_{cum}(n-1)$ = the cumulative weight loss before the nth sample was taken.

The weight loss in terms of each separate metal (Fe, Cr, Ni) was first calculated, and then the three values were added together and then plotted. (See Figures A-1 to A-12). The surface area of the steel specimen was calculated using the standard formula for the surface area of a cylinder.

$$\text{Surface area} = 2\pi r(r + l)$$

where; r = radius of the circular section.

l = length of the cylinder.

both of these were measured accurately before the experiment was started. Thus the weight loss per unit area ($g.m^{-2}$) could be calculated, from which the rate of reaction ($g.m^{-2}\ hr^{-1}$) was deduced.

B.4 Analytical Procedures

(a) Iron

Two methods for iron analysis were used, viz. (i) titration with mercury (I) nitrate and (ii) analysis by atomic absorption spectroscopy. This section describes the former.

Preparation of ca 0.1M Mercury (I) Nitrate Solution

Slightly more than the theoretical amount of $Hg_2(NO_3)_2 \cdot 2H_2O$ was dissolved in 0.5M HNO_3 and the solution was diluted to 1 litre with 0.5M HNO_3. The mercury (I) nitrate solution was then standardised by one of the following methods.

Standardisation Using A. R. Iron (III) Alum, $KFe(SO_4)_2 \cdot 12H_2O$

Analytical reagent grade iron (III) alum (1.0g), was dissolved in 0.5M HNO_3 and diluted to ca $60 cm^3$ with acid of the same concentration. $15 cm^3$ of 40% ammonium thiocyanate solution was then added. The intensely red solution was

titrated with mercury (I) nitrate solution, shaking well after each addition. When the solution changed colour from deep red to orange, it was subsequently shaken well for 15 seconds after the addition of each drop, until at the end point the solution was colourless.

Standardisation Using Standard Potassium Dichromate Solution

$25cm^3$ of $^M/_{60}$ $K_2Cr_2O_7$ solution was transferred to a $250cm^3$ conical flask and a known volume (excess) of an approximately $^M/_{10}$ solution of iron (II) ammonium sulphate was added. Sufficient HNO_3 to make the solution 0.5M in this acid was then added followed by $15cm^3$ of 40% NH_4 NCS solution, and if necessary the solution was diluted to $60cm^3$ with 0.5 M HNO_3. The titration was then carried out as described above.

Iron (II) ammonium sulphate solution inevitably contained some iron (III). The amount of Fe (III) present in the volume of iron (II) solution taken in excess was determined by direct titration with mercury (I) nitrate (i.e. a "blank" titration was performed and the necessary correction was made to the standardisation result).

Analysis of Products

Samples (ca 0.1g) were dissolved in 0.5M HNO_3 solution (ca $25cm^3$). Sulphamic acid (ca 0.5g) was added to destroy traces of HNO_2 or NO_2^- which interfere, followed by 40% NH_4NCS solution ($15cm^3$), and the resulting solution was titrated with the standardised mercury (I) nitrate solution.

(b) Chromium

Chromium was determined volumetrically as Cr (VI). Samples for analysis were weighted out in dry, airtight vials, and dissolved in $50cm^3$ of 4M H_2SO_4 in a conical flask. Solid potassium peroxydisulphate, $K_2S_2O_8$, (10g) was then added, followed by $10cm^3$ of 10% silver nitrate solution. The mixture was boiled for 20 minutes whereupon all the chromium present was oxidised to Cr (VI), and any excess $K_2S_2O_8$ was destroyed by hydrolysis. A funnel was inserted into the neck of the flask during boiling to prevent loss of liquid by splashing or as

spray. The solution was then titrated with standard iron (II) ammonium sulphate solution using Ferroin O-Phenanthroline iron (II) sulphate complex as indicator.

(c) Nickel

Nickel was determined gravimetrically as the dimethylglyoximate $Ni(C_4H_7O_2N_2)_2$. Solid samples for analysis were each weighed out in a dry, airtight vial and dissolved in about 200cm^3 of water containing 3cm^3 conc. HCl. The solution was heated to 60-80^{o}C, and 30cm^3 of a 1% solution of dimethylglyoxime in ethanol was added. Dilute ammonia was then added dropwise until precipitation occurred. The precipitate was allowed to settle, and complete precipitation tested for by addition of 2cm^3 of ammonia and 2cm^3 of dimethylglyoxime. The mixture was then heated for 1 hour on the steam bath, allowed to cool, and filtered through a porosity 4 sintered glass crucible. The precipitate was washed well with water, dried at 110^{o}C to constant weight, and weighed as $Ni(C_4H_7O_2N_2)_2$.

The complex products obtained from the PF_5 reaction gave rise to some interference and co-precipitation. In these cases, nickel was precipitated as the hydroxide, $Ni(OH)_2$, by addition of NaOH to the solution. This precipitate was then filtered off, washed, and redissolved in dilute HCl. The above determination was then carried out as described.

(d) Aluminium

Aluminium was determined gravimetrically as the 8-hydroxy-quinoline ("oxine") complex. Portions of material for analysis were weighed out in dry, airtight vials, and dissolved in about 150cm^3 of water containing 1cm^3 of 0.1M hydrochloric acid. The solution was heated to 60-80^{o}C, and 30cm^3 of 2% oxine in 2M acetic acid added. 2M ammonium acetate solution was then added until precipitation occurred, followed by a further 50cm^3. The mixture was then allowed to stand for 1 hour with occasional stirring. The precipitate was then filtered through a porosity 4 sintered glass crucible, dried to constant weight at 140-150^{o}C and weighed as $Al(C_9H_6NO)_3$.

(e) Fluorine

Fluorine was determined electrochemically using an 'Activion' fluoride-sensitive electrode, used in conjunction with an Ag/AgCl/1M KCl/1M KNO_3 standard reference electrode. The EMF generated by these electrodes when immersed in a solution containing fluoride ions is dependant only on the concentration of F^-.

Solutions for analysis were prepared using a technique to avoid contact of fluorine-containing solutions with glassware. Samples were weighed out in a dry box into a 2" x 1/4" (50 x 7mm) Kel-F tube (sealed at one end) which was closed by a small rubber bung, pushed in just sufficiently to make the tube air-tight and prevent premature hydrolysis.

The bung was dislodged by vigorously shaking the tube in a 200 ml. polypropylene jar, fitted with a screw cap, and containing accurately 100cm^3 of a 1:1 mixture of water and a total ionic strength adjustment buffer (TISAB). TISAB consisted of a solution containing H_2O (500 ml.), A. R. glacial acetic acid (57 cm^3), A. R. sodium chloride (58g) and sodium citrate (0.30g), titrated to pH 5.0-5.5 with 5M NaOH, and made up to 1000 cm^3.

The EMF generated from the electrodes immersed in the hydrolysed solution containing fluoride was then measured, and from this the fluoride concentration determined using a calibration graph obtained by making EMF measurements on a series of TISAB buffered NaF solutions (1:1 TISAB:NaF solution). A fresh calibration graph was prepared for each fluoride determination.

It was found that the weakly acidic TISAB buffered solutions did not hydrolyse the stable hexafluorophosphate anion PF_6^-, and this method was thus used as a measure of the amount of 'free' fluoride, e.g. HF or simple metal fluorides. Fluoride contained in hexafluorophosphate was determined indirectly as $NOPF_6$ or NO_2PF_6 as described below.

In the case of mixtures containing aluminium, which formed extremely tenacious fluoro-complexes, a prior precipitation of the aluminium as $Al(OH)_3$

was carried out using aqueous ammonia at a pH of about 5[8]. This precipitate was filtered off and used for a gravimetric determination of aluminium as the 8-hydroxyquinolinate, after dissolution in dilute hydrochloric acid. The filtered fluoride containing solution was then made up to an appropriate volume with water and TISAB, and the electrochemical determination carried out as above. The precipitation and filtration were carried out in polypropylene vessels.

(f) Phosphorus

Phosphorus was determined gravimetrically as ammonium 12-molybdophosphate $(NH_4)_3[PMo_{12}O_{40}]$. Samples for analysis were weighed out in a dry box into airtight vials and dissolved in hot dilute nitric acid ($150cm^3$). This solution was heated to 60^oC, and $100cm^3$ of ammonium molybdate reagent was added with stirring. The mixture was heated to 60^oC for 1 hour, and was then filtered through a porosity 4 sintered crucible. The precipitate was washed well with 2% ammonium nitrate solution, and dried at 280^oC. It was anticipated that this treatment with hot, acid solution would break down any PF_6^- to phosphate.

(g) Hexafluorophosphate

Early experience of fluoride determination using the fluoride ion sensitive electrode indicated that PF_6^- did not break down in the weakly acid TISAB (see (e) above) buffered solutions used. This necessitated the determination of PF_6^- separately from 'free' fluoride.

The method employed was the hitherto unreported determination as the nitron (4, 5-dihydro-1, 4-diphenyl-3, 5-phenylimino-1, 2, 4-triazole) salt, $C_{20}H_{16}N_4 \cdot HPF_6$, which readily forms a crystalline precipitate of low solubility[9]. It was assumed that PF_6^- was present solely as NO_2PF_6 or $NOPF_6$, as determined by X-ray powder photography, and that hydrolysis of these would occur as below:

$$NO_2PF_6 + H_2O \longrightarrow HNO_3 + HPF_6$$

$$NOPF_6 + H_2O \longrightarrow HNO_2 + HPF_6$$

HNO_2 in the second reaction being ultimately completely converted to HNO_3.

Reaction of NO_2PF_6 with a solution of nitron would therefore give a precipitate consisting of a mixture of nitron nitrate and nitron hexafluorophosphate in a 1:1 ratio. The resulting precipitate would hence contain 17.41% PF_6^-.

The sample was weighed out for analysis, in a dry box, into a Kel-F tube (as used for fluoride analysis), closed by a bung. The bung was loosened, and the tube opened by shaking in ca 50cm^3 of 2% acetic acid in a sealed plastic jar, hence ensuring that no nitrogen was lost as NO, NO_2, etc. The tube and bung were then removed from the jar using tongs, and the tube, bung, tongs, and lid were rinsed, the washings being collected in the jar. The jar and contents were then heated to about 70°C on a water bath, and 10 cm^3 of a 10% nitron solution in 5% acetic acid was added. A bulky white precipitate formed rapidly, and the mixture was then set aside at 0°C for 2 hr. The precipitate was filtered off on a porosity 4 sinter, washed with a little ice cold water and dried at 105°C.

(h) Autoclave Hydrolysis

The anion $PO_2F_2^-$ is resistant to hydrolysis under normal conditions but can be hydrolysed quantiatively according to the equation

$$PO_2F_2^- + 4OH^- \longrightarrow PO_4^{3-} + 2H_2O + 2F^-$$

at elevated temperature and pressure[10]. Accordingly, about 0.3g of a sample of solid product suspected to contain this anion was heated in 4cm^3 of 0.4M NaOH solution in a small, sealed nickel autoclave (bomb) at 160°C for 3 hours. After cooling and careful opening of the autoclave, the resulting hydrolysate was washed out and submitted to F^- and PO_4^{3-} analysis as described in (e) and (f) above.

(i) Nitrite and Total Nitrogen

After hydrolysis of samples in a sealed vessel containing 2M sodium hydroxide solution, nitrite was determined by titration against cerium (IV) and total nitrogen by a modified Kjeldahl method. These techniques have already been described in detail[4].

B.5 Spectroscopic and X-ray Techniques

(a) ^{19}F n.m.r. Spectroscopy

^{19}F n.m.r. spectra were recorded at 34°C using a Varian H.A. 100 n.m.r. spectrometer and $CFCl_3$ as an external standard. Liquid samples were sealed into FEP tubing which was mounted inside a conventional 5m.m. diameter glass n.m.r. tube.

(b) Infra-red Spectroscopy

Infra-red spectra were recorded on a Perkin-Elmer 457 spectrometer. For solids, nujol mulls were prepared in a dry box, and AgCl cell windows were used. Liquid films were also prepared between AgCl windows in a mull cell. The spectra of gaseous phases containing HNO_3 or N_2O_4 vapour were recorded in a gas cell fitted with AgCl windows. The spectra of vapours containing HF or other fluorine-containing volatiles were recorded by condensing a little of the vapour in a 4mm diameter Kel-F tube sealed at one end, freezing the gas down, and sealing off the tube at a suitable length. Spectra were then compared with the spectrum of Kel-F itself.

(c) Ultra-violet/visible Spectroscopy

U.V./visible spectra were recorded using a Unicam SP800 spectrometer, and silica cells were fitted with teflon stoppers. Diffuse reflectance spectra were recorded on a Unicam SP700 spectrometer. Moisture sensitive solid samples for diffuse reflectance spectroscopy were loaded in a dry box.

(d) Atomic Absorption Spectroscopy

Analyses for iron, chromium, and nickel were carried out by means of a Southern Analytical A3000 atomic absorption spectrophotometer. Solutions were prepared in the manner described in Appendix B.2 and diluted appropriately. Calibration curves were obtained using solutions of known metal concentrations. These were prepared by the method given by Belcher et. al[5,6] to give a nominally 100ppm Fe, Cr, Ni stock solution which was then diluted with dilute nitric acid

to give standards in the concentration range required for optimum sensitivity (0⟶30ppm). Mutual interference by the three metals can be overcome by the preparation of calibration series which contain approximately the same proportions of metals as the solutions being analysed. However the interference under optimum conditions was not considered significant and the results obtained in this way were considered accurate to better than 1% from an interference standpoint. Activion (GB) single element, hollow cathode lamps were used throughout the determinations. The detection limits obtained were 1ppm for both Cr and Fe and 2ppm for Ni. Thus in view of the fact that it was necessary in all cases to dilute the neat HDA solution by a factor of approximately 3.5, the practical limits for the original HDA solutions were ca 4ppm for iron and chromium and ca 8ppm for nickel.

(e) Mössbauer Spectroscopy

Mössbauer measurements were performed at room temperature and -196°C against a $^{57}Co/^{57}Fe$ source using a Harwell Mössbauer spectrometer system equipped with a 256 multichannel analyser. All spectra were allowed to accumulate a minimum of 2×10^5 counts per channel. The resultant data were then fitted to Lorentzian line shapes by usual least squares methods. Isomer shifts are quoted relative to the source $^{57}Co/^{57}Fe$. Samples were prepared in a dry box as nujol mulls and were mounted using a lead spacer and aluminium foil.

(f) X-ray Powder Photography

Powder patterns were obtained using a Philips X-ray powder diffractometer with an 11cm. camera and either CuKα or FeKα (iron-containing samples) radiation. Samples were loaded into 0.5mm Lindemann glass (lithium beryllium borate) capillaries in a dry box. The capillaries were sealed with grease in the box, withdrawn and flame sealed. None of the previously reported difficulty[4] in sealing was experienced. X-ray powder photography was used principally as a "fingerprint" technique, to permit rapid comparison of patterns for reaction products with those of known compounds.

The introduction of the NRC crystallographic program NRC-21 "The d-spacings", which generated indices and computed the d-spacings for all the non-equivalent reflections within a selected sphere, or part of asphere, in reciprocal space, enabled powder photographs to be computed from known crystal parameters such as cell dimensions and angles. This program was employed in the examination of aluminium nitrate/H_2O systems.

B.6 Preparative Methods

(a) 100% HNO_3

100% nitric acid was prepared by the previously described method[4] involving vacuum distillation of a 1:2v:v mixture of fuming HNO_3 and concentrated H_2SO_4. A modified form of the apparatus illustrated in ref. 4 was employed. The distillation temperature was altered to 50°C, at which temperature the acid distilled more rapidly, and the condenser and receiver were cooled to ca -30°C. The rate of disillation was controlled by the tap on the air bleed.

(b) N_2O_4

Pure, dry N_2O_4 was prepared from cylinder grade N_2O_4 by distillation from P_4O_{10} through a column of P_4O_{10}, into a receiver cooled to -78°C in methcol/CO_2 and fitted with a P_4O_{10} guard tube. Pure N_2O_4 condensed as a white solid. Any NO present, in the form of blue N_2O_3, was removed by allowing the solid to melt completely in a vented system when the more volatile N_2O_3 evaporated out. The dry liquid was always transferred against a counter-current of nitrogen or argon.

(c) N_2O_5

The technique described here is a modification of that described in Inorganic Syntheses[7] and the apparatus currently in use in these laboratories is shown in Figure B-1. Fuming nitric acid (S.G. 1.5) is dehydrated by dropwise addition to phosphoric oxide. The dinitrogen pentoxide vapour is carried over into the receiving vessel in a slow stream of dry ozonised oxygen, which converts any contaminating dinitrogen tetroxide to the pentoxide. The column of loosely

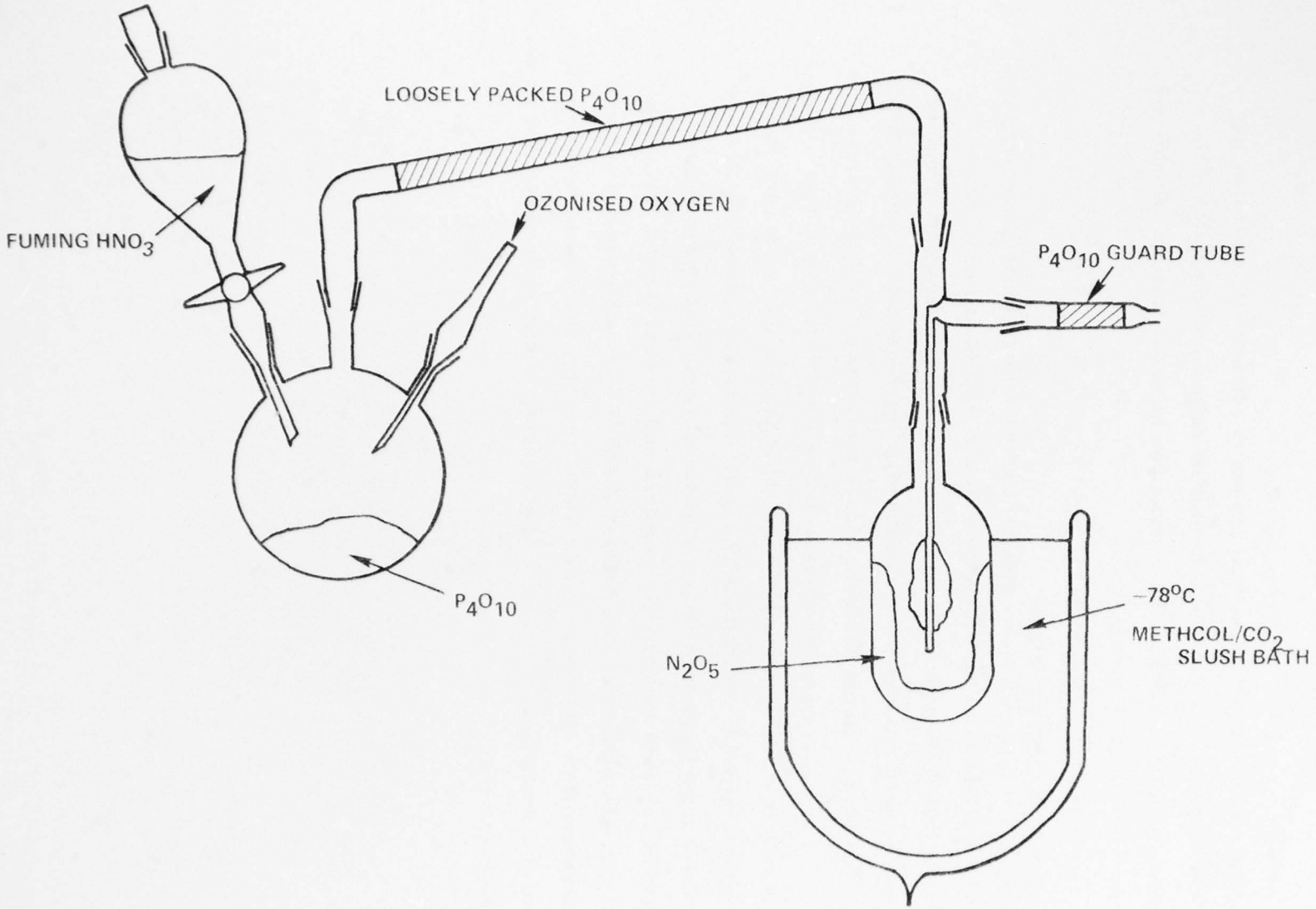


Figure B-1. Apparatus for Preparing N_2O_5

packed phosphoric oxide and glass wool serves to remove nitric acid vapour from the gas stream. The dinitrogen pentoxide collects on the walls of the Schlenk tube as white crystals. The product can be resublimed in vacuum and stored at or below $0^{o}C$.

(d) HNO_3/N_2O_4 Mixtures

Preparation of these mixtures was carried out using reagents prepared in the manner described in (a) and (b) above, in dry conditions using counter current techniques. First the weights and volumes of the separate reagents required to make up a desired mixture were calculated. The required volume of 100% nitric acid was measured out using the closed measuring cylinder illustrated in Figure B-2. The liquid was then transferred to a weighed flask and the contents checked by weighing. The required volume of N_2O_4 was then added and the contents again checked by weighing. The final composition of the mixture was then calculated from these weighings. A physical method of checking the composition of any such mixture was required and several methods have been attempted e.g. chemical analysis, infra-red and U.V./visible spectroscopy, density measurements and proton n.m.r. spectroscopy, but none of these methods has proved successful and ^{14}N n.m.r. spectroscopy is currently under investigation for this purpose.

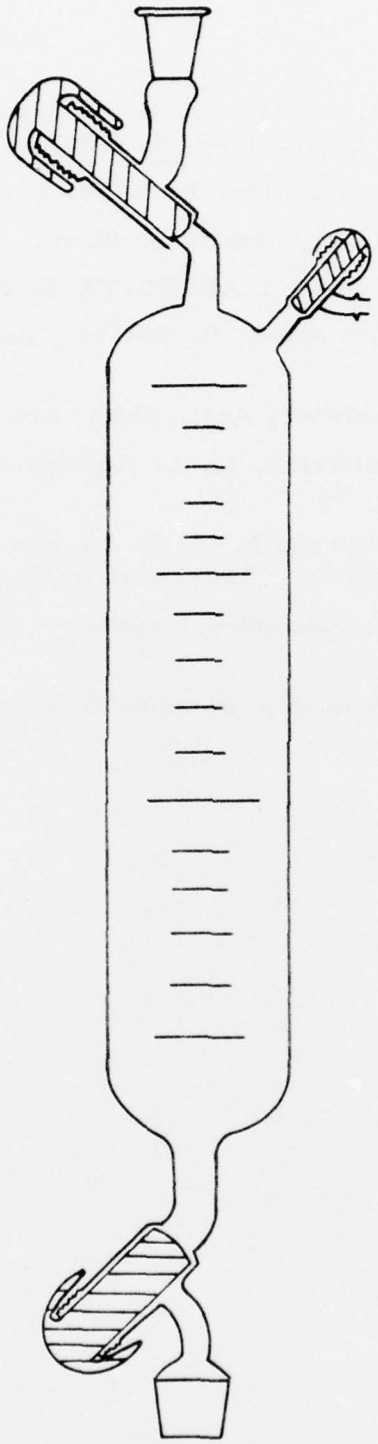


Figure B-2. Measuring Cylinder

References to Appendix B

1. N. A. Matwiyoff, L. B. Asprey, W. E. Wageman, M. J. Reisfeld and E. Fukushima, Inorg. Chem. 1969, 8, 750.
2. A. Poitier, Ann. Fac. Sci. Univ. Toulouse, 1956, 20, 1.
3. E. Berl and H. H. Saenger, Monatsch. Chem., 1929, 53, 1036.
4. C. C. Addison, "Flow Decay", AFRPL-TR-72-84.
5. K. Kinson, R. J. Hodges and C. B. Belcher, Anal. Chim. Acta. 1963, 29, 134.
6. K. Kinson and C. B. Belcher, Anal. Chim. Acta, 1964, 30, 64.
7. N. S. Gruenhut, M. Goldfrank, M. L. Cushing and G. V. Caesar, Inorg. Synth., 1950, 3, 78.
8. R. Belcher, A. J. Nutten and A. M. G. Macdonald, 'Quantitative Inorganic Analysis', 3rd Ed., Butterworths, 1970, p. 73.
9. W. Lange, in 'Fluorine Chemistry,' Academic Press, 1950, Vol. 1, p. 165.
10. R. Schmutzler, in 'Advances in Fluorine Chemistry,' Butterworths, 1965, Vol. 5, p. 192.

NOMENCLATURE

Reagents and materials

A.R.	analytical reagent (grade of chemical)
HDA	high density acid (i.e. 56wt.% HNO_3, 44wt.% N_2O_4).
Standard HDA	high density acid containing ca 0.6wt.% HF
Modified HDA	high density acid containing ca 0.6wt.% PF_5
Inhibisol	1,1,1 Trichloroethane.
Kel-F	poly-trifluorochloroethylene
Methcol	methylated spirit i.e. 97% ethanol + 3% methanol.
Teflon/FEP	mixture of fluorinated ethylene propylene polymers.

Infra-red spectroscopy

I.R.	infra-red
ν	bond stretching vibrational mode
δ	angle deformation vibrational mode
mlt	multiple absorption bands

N.m.r. spectroscopy

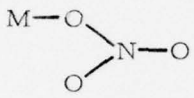
δ_{CFCl_3}	^{19}F chemical shift (parts per million) relative to $CFCl_3$ as standard
J_{F-P}	^{19}F-^{31}p coupling constant

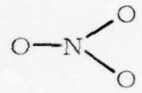
Vibration modes

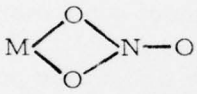
ν_s	symmetric stretching
ν_{as}	antisymmetric stretching

ν_d	degenerate stretching
δ_s	symmetric deformation
δ_{as}	antisymmetric deformation
δ_d	degenerate deformation
π	out-of-plane deformation

Nitrate coordination modes (M = metal atom)

unidentate (C_s) 

ion(D_{3h}) 

bidentate (C_{2v}) 

Intensities of absorption bands

vw	very weak	vs	very strong
w	weak	b	broad
m	medium	sh	shoulder
s	strong	sp	sharp

Miscellaneous

d	perpendicular spacing between crystal planes
^{19}F n.m.r.	fluorine nuclear magnetic resonance
^{1}H n.m.r.	proton nuclear magnetic resonance
I	intensity
K_{eq}	equilibrium constant
r.p.m.	revolutions per minute

v/v	volume in volume
wt. %	weight percent

Units

$\mathring{A}$	angstrom (10^{-10} metre)
^{o}C	degree centigrade
cm^{-1}	reciprocal centrimetre (wavenumber)
K	degree Kelvin
nm	nanometre (10^{-9} metre)
p. p. m.	parts per million
eV	electron volt
J	joule

Schoenflies point group symbols (molecular symmetry)

C_s	one symmetry plane only.
C_{2v}	two-fold axis and two symmetry planes.
D_{3h}	three-fold axis, three two-fold axes, three vertical symmetry planes and one horizontal symmetry plane.
D_{4h}	four-fold axis, four two-fold axes, two vertical symmetry planes, two dihedral symmetry planes, one horizontal symmetry plane and an inversion centre.